

AD-A243 061



AFOSR-89-01-0418

AIR FORCE OF SWITZERLAND
NOTICE OF
This text is
approved
Distribution in
Gle
STINFO Program Manager



Approved for public release,
distribution unlimited

DTIC
ELECTE
DEC 6 1991

USE OF BLOCKS BY BIOPOLYMERS

PROPERTY RELATIONSHIPS IN BLOCKS

Best Available Copy

Final Report

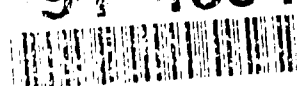
Submitted to

AFOSR-88-0133 and AFOSR-89-0490

James A. Staley, and John A. Aron

October 1991

91-16540



91-1126-49

UNIVERSITY OF WASHINGTON

Approved for public release

REPORT DOCUMENTATION PAGEForm Approved
OMB No. 0704-0188

Public reporting burden for this collection of information is estimated to average 1 hour per response, including the time for reviewing instructions, searching existing data sources, gathering and maintaining the data needed, and completing and reviewing the collection of information. Send comments regarding this burden estimate or any other aspect of the collection of information, including suggestions for reducing this burden, to Washington Headquarters Services, Directorate for Information Operations and Reports, 1215 Jefferson Davis Highway, Suite 1204, Arlington, VA 22202-4302, and to the Office of Management and Budget, Paperwork Reduction Project (0704-0188), Washington, DC 20503.

1. AGENCY USE ONLY (Leave blank)		2. REPORT DATE October 1991	3. REPORT TYPE AND DATES COVERED Final Report 15 Aug 89 to 14 Feb 91	
4. TITLE AND SUBTITLE Ultrastructure-Property Relationships in Biocrystals			5. FUNDING NUMBERS 61102F 2303/B2	
6. AUTHOR(S) Mehmet Sarikaya, James T. Staley, and Ilhan A. Aksay				
7. PERFORMING ORGANIZATION NAME(S) AND ADDRESS(ES) University of Washington Department of Ceramics Engineering Seattle, WA 98195			8. PERFORMING ORGANIZATION REPORT NUMBER	
9. SPONSORING/MONITORING AGENCY NAME(S) AND ADDRESS(ES) AFOSR/NC Bolling AFB, DC 20332-6448			10. SPONSORING/MONITORING AGENCY REPORT NUMBER AFOSR-89-0496	
11. SUPPLEMENTARY NOTES				
12a. DISTRIBUTION/AVAILABILITY STATEMENT Approved for public release; distribution is unlimited			12b. DISTRIBUTION CODE	
13. ABSTRACT (Maximum 200 words) <p>The intracellular growth of magnetite crystals in <i>Aquaspirillum magnetotacticum</i> was studied with respect to morphology, size, shape, defects, and crystal structures. A model was developed to describe the alignment of magnetite crystals in the bacteria. It was determined that the particles formed in a sequential manner along the chain, and that each particle was enclosed by a membrane. Fracture strength and fracture toughness were evaluated for the transverse direction to the shell plane for the nacre of red abalone shell and of pearl oyster shell. A unique "brick and mortar" arrangement consisting of - 95% CaCO₃ and - 5% biopolymer. The CaCO₃ was found to exist as aragonite platelets in a twinned hierarchical structure. Crack propagation was found to occur by a tortuous pathway. Toughening methods found included crack blunting, branching, microcrack formation, layer pull-out, sliding of CaCO₃ layers, and bridging of organic ligaments, with the last two being the most effective.</p>				
14. SUBJECT TERMS			15. NUMBER OF PAGES 297	
			16. PRICE CODE	
17. SECURITY CLASSIFICATION OF REPORT UNCLASSIFIED	18. SECURITY CLASSIFICATION OF THIS PAGE UNCLASSIFIED	19. SECURITY CLASSIFICATION OF ABSTRACT UNCLASSIFIED	20. LIMITATION OF ABSTRACT SAR	

FINAL REPORT
on
PROCESSING OF CERAMICS BY BIOPOLYMERS
February 1, 1990 - January 31, 1991
(Third and Final Year)
and
ULTRASTRUCTURE-PROPERTY RELATIONSHIPS
IN BIOCRYSTALS

February 1, 1990 - January 31, 1991

Submitted to

*Air Force Office of Scientific Research
Bolling Air Force Base
Washington, D.C.
Attn: Dr. Frederick L. Hedberg*

by

M. Sarikaya, J. T. Staley,† and I. A. Aksay**

Department of Materials Science and Engineering,
Department of Microbiology;†
Advanced Materials Technology Center,
Washington Technology Center,
University of Washington
Seattle, WA 98195*

October 9, 1991



Accession For	
NTIS GRA&I	<input checked="" type="checkbox"/>
DTIC TAB	<input type="checkbox"/>
Unannounced	<input type="checkbox"/>
Justification	
By	
Distribution/	
Availability Codes	
(Avail and/or	
Dist	Special
A-1	

Contents

1. Summary	1
2. Brief Description of Research Accomplishments	3
2.1 Use of Acidic Biopolymers in Ceramic Processing	6
2.1.1 Processing of Ceramic Suspensions with Biologically Produced Polymers G. L. Graff and I. A. Aksay	6
2.1.2 Use of Acidic Biopolymers as Dispersants for Processing of Ceramics J. T. Staley, N. B. Pellerin, T. Ren, G. L. Graff, D. R. Treadwell, and I. A. Aksay	7
2.1.3 Acidic Biopolymers as Dispersants for Ceramic Processing J. T. Staley, N. B. Pellerin, and T. Ren	8
2.2 The Use of Alginate in Ceramic Processing	9
2.2.1 The Use of Biopolymers (Alginates) in the Preparation of Highly Concentrated Suspensions of Al_2O_3 Powder G. L. Graff, I. A. Aksay, N. B. Pellerin, and J. T. Staley	9
2.2.2 Use of Alginate as an Aid in Ceramics Processing N. B. Pellerin, T. Ren, G. L. Graff, I. A. Aksay, and J. T. Staley	9
2.2.3 Processing of Ceramic Particles with <i>Azotobacter vinelandii</i> T. Ren, N. B. Pellerin, J. T. Staley, G. L. Graff, and I. A. Aksay	10
2.3 Mechanical Structural-Property Relationships in a Biological Composites	11
2.3.1 Structure-Mechanical Property Relationships in a Biological Ceramic-Polymer Composite: Nacre of Red Abalone <i>Haliotis rufescens</i> K. E. Gunnison, M. Sarikaya, and I. A. Aksay	11
2.3.2 Structure-Property Relationships in Nacre of <i>Pinctada margaritifera</i> S. Sawyer, M. Sarikaya, and I. A. Aksay	12
2.4 Structural Characterization of Biocomposites	13
2.4.1 Hierarchical Twin Structures and Multiple Tilings in the Nacre of Abalone Shell M. Sarikaya, J. Liu, and I. A. Aksay	13
2.4.2 Studies on the Understanding of the "Single Crystalline" Structure of Sea Urchin Spine J. Liu, M. Sarikaya, and I. A. Aksay	14

2.4.3 Atomic Resolution Electron Microscopy Studies of Defect Structures of Biocrystals	
M. Sarikaya, J. Liu, and I. A. Aksay	15
2.5. Ultrafine Magnetic Particles in Magnetotactic Bacteria	16
2.5.1 Formation of Magnetite Particles in <i>Aquaspirillum magnetotacticum</i>	
J. T. Staley, N. B. Pellerin, J. Liu, M. Sarikaya, and I. A. Aksay	16
2.5.2 Geometrical Alignment of Magnetosomes in Magnetotactic Bacteria	
W.-H. Shih, W. Y. Shih, M. Sarikaya, and I. A. Aksay	17
3. Publications/Presentations	18
3.1 Publications	18
3.1.1 Papers	18
3.1.2 Extended Abstracts	19
3.1.3 Undergraduate Project Reports and Graduate Theses	20
3.2 Presentations: Invited Talks, Conferences, Workshops	20
3.3 Patents	24
3.4 News Clippings	24
4. Personnel	25
5. APPENDICES	26

1. Summary

This is the combined final report for the two grants entitled "Processing of Ceramics by Biopolymers," and "Structure-Property Relationships in Biocrystals," monitored under grant numbers AFOSR-88-0135 and AFOSR-89-0496, respectively. This report summarizes the research accomplishments during the period February 1, 1990, to January 31, 1991, for both projects. The research plans presented for the second three-year-project proposal entitled "Materials Processing by Biomimicking," were submitted October 1990 and the first year of support officially started on July 1, 1991, under grant number AFOSR-91-0281.

The research activities, undertaken by our collaborative groups (Figure 1), for the present reporting period were divided into five categories. These are: (i) selection and characterization of existing biopolymers for use in ceramic processing, (ii) the use of alginic acid as a processing aid, (iii) *in situ* processing of ceramics with bacteria, (iv) synthesis and characterization of ultrafine magnetite particles by bacteria, and (v) microstructure-property correlations in biocrystals. The research results will be highlighted in the following sections.

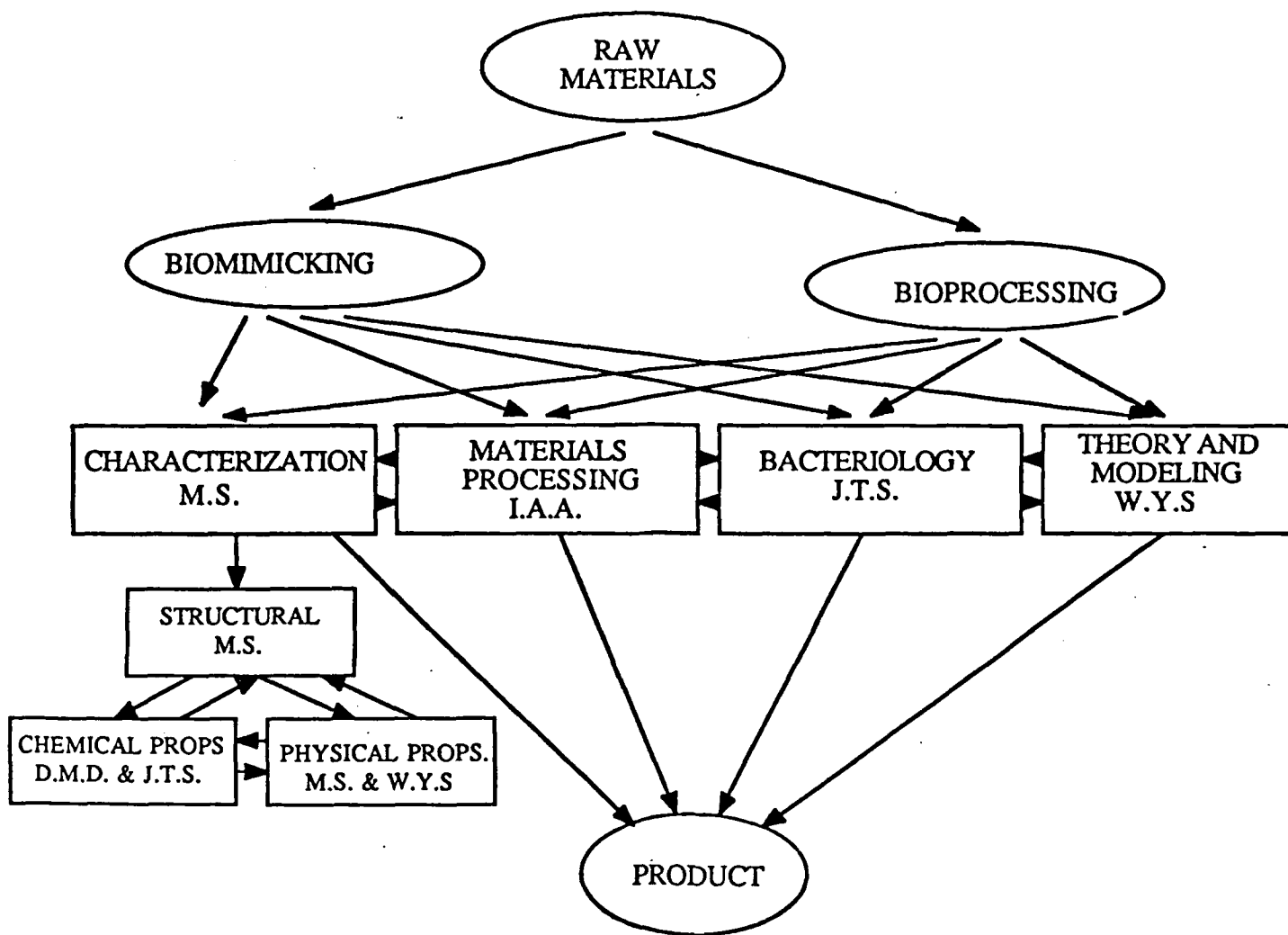


Figure 1. A chart showing the categories of research and division of work among the collaborating groups in Bioprocessing and Biomimicking. See Section 4, Personnel, for abbreviation of names.

2. *Brief Description of Research Accomplishments*

In this section, a brief description is given of each of the research accomplishments achieved during the last year of the project, with a summary of previous accomplishments. Detailed results of the studies are described in the Appendices, which include copies of the papers that have been published, are in review, or in preparation. These individual publications will be referred to specifically in each section.

Some of the highlights of our findings are as follows:

(i) Use of Biopolymers as Processing Aids:

- Biopolymers obtained from bacterial sources were shown to be effective processing aids in the preparation of aqueous suspensions of submicron-sized ceramic powders. Biopolymers are an infinitely large, diverse, inexpensive, nontoxic source of additives for powder processing. (Over 20 commercially available biopolymers have been screened using sedimentation and consolidation experiments.)
- By comparing dextran and dextran sulfate directly, the existence of charged functional groups on the polysaccharide were shown to be necessary to achieve suspension stability in aqueous systems. This finding could greatly facilitate polysaccharide selection when considering potentially useful molecules of biological origin.
- The production and isolation of potentially useful native bacterial polysaccharides in our laboratories have been accomplished. These internally isolated polymers were evaluated for effectiveness as dispersants.
- We have shown that alginate obtained from the marine alga, *Macrocystis pyrifera*, (kelp) is nearly as effective as PMAA, and has the advantage of being biogenic.
- Alginate is a copolymer of the isomers D-mannuronic (M) and L-guluronic (G) acids. Its biosynthesis is thought to involve the initial formation of polymannuronic acid, followed by the epimerization of D-mannurosyl residues to L-guluronic acid.
- A similar polymer is produced extracellularly by several bacteria including *Azotobacter vinlandii* and various pseudomonas species.

- It was demonstrated that *Azotobacter vinelandii* could be used to develop an *in situ* process for coating ceramic particles. It was shown that the organism could be grown in the presence of ceramic particles and produces alginate during growth and metabolism. The organism grew at concentrations of alumina between 5 and 15 vol%. In addition, the viscosities of the suspensions were reduced accordingly.

(ii) Synthesis and Characterization of Ultrafine Ceramic Particles by Bacteria

- A strain of *Aquaspirillum magnetotacticum* was obtained and kept fresh in our laboratory; growth curves were produced for the strain under various conditions.
- Ultramicrotome preparation of thin sections for transmission electron microscopy (TEM) studies was established.
- The nature of magnetite crystallites, which form intracellularly, was determined in terms of morphology, size/shape, and defect and crystal structures.
- From the presence of particles in decreasing sizes as the end of a chain is approached, it is assumed that the particles form in a sequential manner. Since even the smallest particle at the end of the chain shows a crystalline structure, the precursor material may or may not be amorphous (the former was claimed to be the case).
- A model was developed to describe the alignment of magnetite crystals in the bacteria.
- Magnetite particles with intact membranes, magnetosomes, were isolated from whole cells and it was established that the membranes have "lubrication" properties. Magnetosomes form closed packed clusters. This is opposite to systems where, in the absence of surfactants, nano-sized (10-30 nm) ceramic or metal particles form open (porous) structures that are usually fractals. In the present system, the magnetosome membrane covers the particles and stays intact as the particles are packed. The separation between particles is, therefore, consistent with the presence of a membrane around each particle.

(iii) Structure-Property Correlations in Biocomposites:

- Fracture strength, σ_f , and fracture toughness, K_{IC} , properties have been evaluated for the nacre of red abalone shell in the transverse direction (perpendicular) to the shell plane on single notched, 3-point, and 4-point bending samples. Typical σ_f and K_{IC} values are 180 MPa and about 8 MPa-m^{1/2}, respectively. These properties are superior to monolithic high-technology ceramics, with an increase of over 40 times that of monolithic CaCO₃.
- Similarly the K_{IC} and σ_f properties of the nacre of pearl oyster were also established.
- The crack propagation behavior on the nacre of red abalone shell reveals a high degree of tortuosity not seen in more traditional brittle ceramics (such as Al₂O₃) and high-toughness ceramics (such as ZrO₂). Certain toughening mechanisms such as crack blunting, branching, microcrack formation, and "layer pull-out" all operate in the shell.
- It was revealed by fractographic analyses that the cracks mostly advance through the organic layer with difficulty since this process is accompanied by sliding of CaCO₃ layers (when there is a resolved shear component of the applied stress on the layer planes) and by bridging of the organic ligaments (when there is a normal stress component). It is believed that it is these two mechanisms that increase the toughness most effectively.
- The microstructure of nacre was studied by TEM. The superior properties of the nacre, compared to those of more traditional ceramics and their components, come from the unique "brick and mortar" microstructure. The aragonite crystals, which form the hard component, are 0.2-0.5 μ m thick, and the thin film (10-50 nm) organic substance between (proteins and macromolecules) provides the ductile component.
- From the research accomplished to date, design guidelines can be drawn for the development of laminated composite structures involving hard and soft phases. These are:
 - a laminate thickness for the hard component of less than 1 μ m, for the soft component of less than 100 nm;
 - a highly ductile soft phase;

- strong interfaces between the soft and hard layers; and
 - the ability of the soft phase to form ligaments.
- One of the major findings in the present study is the crystallography of the inorganic component and its relationship with the organic matrix in nacre. It was found that aragonite platelets form a structure of hierarchical twins, covering a size scale from the nanometer to the submillimeter levels (five orders of magnitude in dimension). Although it was known that soft tissues in biological systems can be hierarchical, this is the first time a hard tissue was found to be hierarchical.
 - Crystallographic relationships among the inorganic layers (transverse and longitudinal) suggest a "single crystalline" organization of the organic "template" (another significant finding).
 - The morphology of the organic matrix was established and the organic films were found to be present, including a chitin layer between the aragonite platelets on all sides.

2.1 Use of Acidic Biopolymers in Ceramic Processing

2.1.1 Processing of Ceramic Suspensions with Biologically Produced Polymers

G. L. Graff and I. A. Aksay

The primary objectives of this research were, first, to determine whether a biologically produced macromolecule could be found that would compare favorably to the best synthetic polymers as a suspension stabilizer. If such a molecule were located, our second goal was then to determine the stability mechanisms operative in the system. The specific molecules we tested were the polysaccharides dextran, dextran sulfate, alginate, polyguluronic acid, and polymannuronic acid.

Detailed studies on the solution and rheological behavior of dextran sulfate and polyguluronic acid have conclusively shown that these molecules function as polymeric stabilizers in aqueous α - Al_2O_3 suspensions. By optimization of the polyguluronic acid- Al_2O_3 system, we prepared low viscosity (110 mPa·s at a shear rate of 9.3 s^{-1}), stable suspensions with solids loadings of 50 vol%. This rivals values obtained using the best synthetic polyelectrolyte dispersants.

We have also determined that the electrostatic stabilization resulting from highly charged electric layers is the dominant stability mechanism operating in the systems tested. High affinity adsorption of the anionic polyelectrolytes creates a sufficient repulsive surface charge on the individual particles to provide suspension stability. By measuring polymer adsorption isotherms, we also determined that the polysaccharides in a flat conformation (polymer segments in trains) adsorbed on the alumina surface, thus limiting the possibility of steric interactions in the suspension.

In addition, we found that the existence of highly charged functional groups (SO_3^- , COO^-) on each monomer was required before effective suspension stability could be attained, and that the viscosity of the concentrated Al_2O_3 suspensions was extremely pH sensitive, even when the polymer dissociation behavior changed only slightly with pH. Finally, the polymeric stabilizer, polyguluronic acid, had no adverse effects on the consolidation and densification behavior of the alumina compacts and monoliths.

These findings suggest that biologically produced molecules, in addition to synthetic polymers, should be considered an important source of potentially useful additives for powder dispersion and consolidation.

2.1.2 Use of Acidic Biopolymers as Dispersants for Processing of Ceramics

***J. T. Staley, N. B. Pellen, T. Ren, G. L. Graff, D. R. Treadwell,
and I. A. Aksay***

Three types of acidic biopolymers have been found to be satisfactory dispersants of alumina particles for ceramics processing. Dextran sulfate, modified chemically from dextran; kelp and bacterial alginate; and polypeptides of the dicarboxylic acids, glutamic and aspartic acids all serve as good ceramics dispersants.

In situ processing of alumina particles was examined by growing the alginate-producing bacterium, *Azotobacter vinelandii*, in the presence of alumina particles. Results from these studies indicate that *Azotobacter vinelandii* can grow and produce alginate in the presence of 15 vol% alumina (0.4 μm diameter) particles. The alginate produced adheres strongly to the particles and is not removed by successive washing with water. In contrast, the bacterial cells are readily removed. It is also possible to use nongrowing cultures of *Azotobacter vinelandii* for alginate production. Under nongrowing conditions, a single bacterial cell produces enough alginate to coat 250,000 alumina particles.

Tests are now under way to determine whether polypeptides can be produced by *in situ* processes using the poly D-glutamic acid-producing bacterium, *B. licheniformis*.

2.1.3 Acidic Biopolymers as Dispersants for Ceramic Processing

J. T. Staley, N. B. Pellerin, and T. Ren

Some acidic biopolymers serve as dispersants for colloidal processing of ceramics (e.g., 400-nm-diameter Al_2O_3). We tested one bipolar alginate, a heteropolysaccharide, comprising two carboxylic sugar acids, D-mannuronic and D-guluronic acids. This kelp alginate was a suitable dispersant provided that its viscosity was reduced by partial acid hydrolysis. Low molecular weight polymers rich in guluronic acid proved to be better dispersants than those rich in mannuronic acid, perhaps due to their charge density caused by their buckled molecular configuration.

In situ processing of ceramic materials was tested by growing the alginate-producing bacterium, *Azotobacter vinelandii*, in the presence of alumina particles. Growth occurred at 15% alumina in the medium. Alumina particles, which were exposed to such a treatment, showed high packing density comparable to that with purified polymer.

Polypeptide polymers of the dicarboxylic amino acids, glutamate and aspartate, also served as excellent dispersants for small alumina particles. *In situ* growth experiments are now in progress with *Basillicus spp.* that produce D-glutamic acid.

These results, coupled with the previous finding from our laboratories that dextran-sulfate (but not dextran) serves as a satisfactory dispersant for alumina particles, indicate that several acidic biopolymers can be used as effective dispersants in colloidal processing of ceramics.

2.2 The Use of Alginate in Ceramic Processing

2.2.1 The Use of Biopolymers (Alginates) in the Preparation of Highly Concentrated Suspensions of Al_2O_3 Powder

G. L. Graff, I. A. Aksay, N. B. Pellerin, and J. T. Staley

A naturally occurring polysaccharide (alginate) derived from kelp has been used as an effective dispersant in the preparation of concentrated suspensions of submicron-sized Al_2O_3 powder. Due to the gelling behavior of the polysaccharide, the preparation of fluid suspensions was initially prevented. Gelation was subsequently avoided by hydrolysis of the native high MW, block copolymer into oligomeric units of polymannuronic acid and polyguluronic acid. The oligomers provided suspension stability without the adverse gelling tendencies. In addition, the polyguluronic acid oligomer proved to be a more effective polyelectrolyte than the polymannuronic acid fraction. The higher charge density resulting from the tertiary structure of the polyguluronic acid is believed to be the cause of this difference.

2.2.2 Use of Alginate as an Aid in Ceramics Processing

N. B. Pellerin, T. Ren, G. L. Graff, I. A. Aksay, and J. T. Staley

The high charge associated with small ceramic particles prevents them from evenly dispersing during processing. Organic molecules, in particular lipids and polymers of acrylic acids, are currently used to coat the particles to alleviate this problem. We have tested the use of alginate as a processing aid for the packing of 400-nm-sized alumina particles. High molecular weight (75,000-100,000) kelp alginate results in a reduction of cake height to 50% of the theoretical maximum in sedimentation experiments using 2 vol% alumina. Alginate produced by *Azotobacter vinelandii* showed similar characteristics. Viscosity measurements of high-solids-loaded (30 vol%) alumina suspensions show that the suspension is unstable. Low molecular weight fractions of alginate were obtained by hydrolysis. Sedimentation experiments show that mannuronic acid-rich and guluronic acid acid-rich fractions produce cake height reductions similar to the intact polymer. However, these fractions produce stable suspension.

2.2.3 Processing of Ceramic Particles with *Azotobacter vinelandii*

T. Ren, N. B. Pellerin, J. T. Staley, G. L. Graff, and I. A. Aksay

Alginate from the bacterium, *Azotobacter vinelandii*, was an effective dispersant for small ceramic particles (400-nm-diameter alumina). Furthermore *Azotobacter vinelandii* grew and produced alginate in the presence of up to 15 vol% alumina particles, indicating that an *in situ* process might be developed to use this bacterium to coat ceramic particles with its alginate dispersant. In *in situ* processing experiments, the sedimentation heights of alumina suspensions were significantly reduced and the viscosities of 5 and 10 vol% suspensions were reduced four- and 60-fold over controls, respectively. The bacteria could be readily removed from the ceramic particles by washing. However, the dispersant was bound firmly to the particles and could not be removed by repeated washing in distilled water. 3.22 mg of the polyronic acid bound to 1g of alumina particles. By calculation, the polymer produced by a single *Azotobacter vinelandii* cell under *in situ* nongrowth conditions coated approximately 2.5×10^5 alumina particles.

2.3 Mechanical Structural-Property Relationships in a Biological Composites

2.3.1 Structure-Mechanical Property Relationships in a Biological Ceramic-Polymer

Composite: Nacre of Red Abalone Haliotis rufescens

K. E. Gunnison, M. Sarikaya, and I. A. Aksay

The objective of this work was to study nacre, a biological ceramic-polymer composite, to determine structure-property relationships. Nacre is a naturally occurring laminated composite found in mollusk shells. The structure contains calcium carbonate crystals in the form of aragonite and an organic matrix material. The mechanical properties of nacre are better than those of monolithic calcium carbonate, which makes up 95-98% of the composite. The highly ordered microarchitecture incorporating thin films (100 Å thick) of organic matrix makes nacre both a tough and a strong composite. The engineering significance of the nacre structure has been noted by biologists and zoologists and, although some models have been proposed, the structure-property relationships have not been fully understood. Therefore, this study was undertaken (i) to evaluate the mechanical properties with respect to the microarchitecture and (ii) to better understand the structure of the organic matrix and its morphological relationship with the inorganic component.

In this work, 4-point bending strength and 3-point bend fracture toughness tests were performed and the results averaged 180 MPa and 8 MPa-m^{1/2}, respectively. Fractographic studies with scanning electron microscopy (SEM) identified two significant toughening mechanisms: (i) ligament formation in the organic matrix and (ii) sliding of the aragonite platelets upon each other. The unique "brick and mortar" microstructure of the nacre allows for high energy absorption, damage tolerance, and the prevention of catastrophic failure.

The structure of the organic matrix was studied in ultramicrotomed sections with and without the aragonite platelets intact. We found that the organic matrix is indeed a multilayered laminated composite at the nanometer level, but thinner than previously thought. The morphology of the interface between the organic and the inorganic regions suggests the presence of an "interphase" region.

2.3.2 Structure-Property Relationships in Nacre of *Pinctada margaritifera*

S. Sawyer, M. Sarikaya, and I. A. Aksay

Nacre is a microstructure found in many seashells. It is a two-phase structure, with one phase being calcium carbonate crystallite and the other phase being an organic fibrous protein. The two phases form a brick-and-mortar-type structure. The calcium carbonate comprises 95% of the entire structure. This structure shows incredible mechanical properties when its constituent components are considered. The correlation between the microstructure and the mechanical properties was investigated. The nacre structure was tested for strength and toughness. The average strength was found to be 220 MPa and the average toughness was found to be 10 MPa-m^{1/2}. These values are comparable to high performance ceramics like tungsten carbide and boron carbide. Two reasons for the better mechanical properties in nacre of pinctada compared to nacre of abalone, may be (i) there are no growth layers in pinctada, hence eliminating easy crack propagation; (ii) samples from pinctada are considerably smaller than those from abalone, giving effectively higher toughness; (iii) in pinctada, the vol% of organic material is slightly higher than that in abalone. Photomicrographs were taken with SEM to investigate the fracture behavior. It seems that the crystallites or plates in the structure pull away from each other. This means that the cracks have to change paths and go around the plates, thus hindering crack propagation. It was also observed that the organic matrix and the crystallites have a strong bond which also contributes to the superior mechanical properties. Therefore, essentially, the toughening mechanisms observed in the nacre of abalone were also observed in pinctada.

2.4 Structural Characterization of Biocomposites

2.4.1 Hierarchical Twin Structures and Multiple Tilings in the Nacre of Abalone Shell

M. Sarikaya, J. Liu, and I. A. Aksay

The nacre has the form of a "brick and mortar" microarchitecture with 0.5- μm -thick aragonite platelets and a 20-nm-thick organic matrix between them. An analysis performed by TEM imaging and diffraction has revealed that, in the face-on configuration, the structure can be described by twinning on three different length scales: (i) first generation, incoherent twinning between platelets; (ii) second generation, coherent twinning between domains within platelets; and (iii) the third generation, nanoscale twins within domains. Both 60° and 90° twin boundaries were observed at different length scales, a phenomenon which has never been encountered in natural mineral aragonite. The structures of biological soft tissues, such as tendon, are known to be hierarchical. To our knowledge, this is the first time that an inorganic component of a biological material has been shown to have a hierarchical structure. In this case, the hierarchical twin structure covers a length scale of six orders of magnitude, from the nanometer to millimeter scale.

Further studies indicate that aragonite platelets can be regarded as space filling tiles at each layer. Since each tile, i.e., a platelet, is twin related with the neighboring one on the same layer, this suggests that the underlying organic matrix must have a superstructure that perfectly fits all variants of twins in both 60°- and 90°-symmetry platelets. This allows, as observed, platelets to have 3-, 4-, 5-, and 6-sided edges, hence, multiple tilings. A model for a lattice structure of the organic matrix is forwarded that satisfies all the experimentally observed crystallographic and space filling requirements for the longitudinal and transverse directions.

2.4.2 Studies on the Understanding of the "Single Crystalline" Structure of Sea Urchin Spine

J. Liu, M. Sarikaya, and I. A. Aksay

Previous studies performed by x-ray diffraction (XRD) and SEM imaging indicated that sea urchin spine has (i) a porous morphology with pores at the 10 nm scale, (ii) a single crystalline structure, (iii) and that it is single-phase calcite (with little organic component), and (iv) that the proteins are possibly occluded in calcite in the form of a domained structure. Sea urchin spine has a conical shape with a cone diameter of about 1.5 mm at the base and a length of about 2-4 cm. The finding that the spine is a single crystalline containing organic molecules is significant and could have important implications in terms of producing biomimetic materials. This is because the inorganic crystal forms on organic templates but also because of its connection with an organic matter in a bulk form to produce highly organized and regulated materials, structures, and shapes.

We studied sea urchin spines by TEM diffraction, imaging, and energy dispersive x-ray spectroscopy (EDS). These provided more detailed and nanostructural information for some of the unanswered questions related to the structure and its morphological and crystallographic features. It was found that the spine is not a single crystal but is polycrystal. The crystals of calcite are $> 5 \mu\text{m}$ in size and they have low angle boundaries (hence, in the x-ray diffraction pattern they produce broadening of the peaks but may appear to be a "single" crystalline pattern. The calcite matrix has small (50-200 Å dia.) crystalline Mg-containing precipitates which are coherent with the matrix; hence, they produce coherency strains matrix-precipitate interface. There is a high density of dislocations within the matrix. The earlier claims that proteins might be occluded within the crystals has not been proven or disputed from the results of the experiment performed so far. Further studies are being planned to analyze (i) the structure of the precipitate and its crystallographic (and structural) relationship with the matrix (strain contrast and high-resolution imaging experiments), (ii) possible involvement of proteins with the precipitates, (iii) analysis of the calcite lattice in terms of protein occlusion (atomic resolution electron microscopy and electron energy loss spectroscopy), and (iv) the nature of the interfaces between the calcite grains. In the quest for structural design rules for producing synthetic materials via biomimicking, these studies are essential from the point of a fundamental understanding of a biological composite where the major portion of the volume ($> 99\%$) is occupied by an inorganic matrix.

2.4.3 Atomic Resolution Electron Microscopy Studies of Defect Structures of Biocrystals

M. Sarikaya, J. Liu, and I. A. Aksay

Biocrystal products such as seashells and bacterial magnetite have highly organized architecture at all spatial levels down to the nanometer scale. This is probably due to control by the organism of both the nucleation and growth of these crystals in or on a matrix of organic matter. The control by the organisms takes place not only in regard to shape, size, and spatial organization of the crystallites but also in the crystallography in the lattice defects within the atomic structure. The objective of this work is to gain some insight into organism-controlled structural evolution during biocrystallization by studying ultrastructural features.

The first of two examples studied is aragonite (CaCO_3 , Pmnc) crystallites in the nacre section of the red abalone shell, *Haliotis refuscens*. It was found, by electron microdiffraction, that aragonite crystallites have definite crystallographic orientation relationships on the "in-layer" and "through-thickness" directions. In addition, analysis of the lattice structure at atomic resolution indicates that there are various types of dislocations, twins, and stacking faults not usually encountered in nonbiological aragonite crystals. The second example, magnetite, which is intracytoplasmically produced by *Aquaspirillum magnetotacticum*, is known to have defect-free single crystalline particles with sizes in the single magnetic domain region (about 50-60 nm in diameter). Atomic resolution transmission electron microscopy (ARTEM) studies of the growing crystals indicate that magnetite crystallites do, in fact, have a defect structure, comprising several ultrafine domains, which may eventually become a single domain. In both examples, the structural evolution of the crystals will be described in the context of biomineralization.

2.5. Ultrafine Magnetic Particles in Magnetotactic Bacteria

2.5.1 Formation of Magnetite Particles in *Aquaspirillum magnetotacticum*

J. T. Staley, N. B. Pellerin, J. Liu, M. Sarikaya, and I. A. Aksay

We have established conditions for the growth and reproduction of healthy *Aquaspirillum magnetotacticum* bacteria which were originally received in pure cultures. The goal of this research has been to study the formation and growth of ultrafine magnetite, which grows in the form of a string of particles 500 Å in diameter. The presence of these particles is believed to help bacteria navigate in swamp waters having a relatively low oxygen content.

The purpose of this study was to grow healthy *Aquaspirillum magnetotacticum* and to establish the growth curves for further studies. In addition to the number of bacteria, the number of magnetite particles formed at each time period was also a concern. The curves are for bacteria grown in two media, (i) 1319-medium and (ii) 1319-medium with pyruvate (see Appendix IV for details). It was found that bacterial growth attains a steady-state after four to five days.

Initially, the bacteria samples were suspended in carbon grids for TEM observation. TEM analysis performed on samples prepared from these cultures after four days usually indicated strings of magnetosomes, numbering in excess of the average of 22 that is generally quoted in earlier studies. In fact, individual bacteria containing more than 50 magnetosomes (sometimes up to 150 particles) were not uncommon. An interesting observation is that often bacteria have double, and very occasionally triple, chains. The analysis of the relative configuration and crystallography of the chains was important in identifying the mechanism of formation of the magnetite particles. Therefore, a section is included to describe the physics of double chain formation.

A more detailed analysis of the bacteria was accomplished on samples prepared by microtomes. Techniques were developed for the preparation of this section by ultramicrotoming through centrifugation and filtration methods. These methods will be applied for the preparation of magnetosomes separately on whole cells for the study of (i) magnetosome membranes and (ii) the initial stages of particle formation.

2.5.2 Geometrical Alignment of Magnetosomes in Magnetotactic Bacteria

W.-H. Shih, W. Y. Shih, M. Sarikaya, and I. A. Aksay

The magnetotactic bacterium *Aquaspirillum magnetotacticum* contains magnetosomes, which are particles of magnetite (Fe_3O_4) bound to the intracytoplasmic membrane. These magnetosomes are often arranged in one chain with the chain axis more or less parallel to the axis of the motility of the cell. In this paper, we report on the study of the alignment of the less often encountered double chains of magnetosomes and the onset of double chain formation. We adopted the chains of spheres model by Jacobs and Bean, and calculated the stable magnetic moment configuration for each geometrical alignment of magnetosomes.

For the square-lattice alignment, two neighboring chains have an opposite magnetic orientation, whereas for the close-packed alignment, two neighboring chains have the same magnetic orientation. To navigate along a magnetic field, the bacterium prefers the close-packed arrangement of magnetosomes as this configuration maximizes the net magnetic moment. TEM micrographs indeed show that most of the double chains have the close-packed arrangement. It was further shown that the symmetric fanning mode has an even lower energy than the parallel rotation.

For double chain formation to occur, we found that there exists a critical number N_c for the number of particles N in a chain. If $N > N_c$, then a new particle will be added to the end of the chain. This indicates that doubling of the chains occurs for those cases where there are large numbers of particles, which agrees with our TEM observations.

3. Publications/Presentations

3.1 Publications

3.1.1 Papers

1. M. Sarikaya, K. E. Gunnison, M. Yasrebi, and I. A. Aksay, "Mechanical Property-Microstructural Relationships in Abalone Shell," in *Materials Synthesis Utilizing Biological Processes, MRS Symp. Proc.*, Vol. 174, edited by P. C. Rieke, P. D. Calvert, and M. Alper (Materials Research Society, Pittsburgh, Pennsylvania, 1990), pp. 109-16.
2. M. Sarikaya, K. E. Gunnison, M. Yasrebi, D. L. Milius, and I. A. Aksay, "Seashells as a Natural Model to Study Laminated Composites," in *Proc. American Society Composites, Fifth Technical Conference* (Technomic Publ., Lancaster, Pennsylvania, 1990), pp. 176-83.
3. M. Yasrebi, G. H. Kim, D. L. Milius, M. Sarikaya, and I. A. Aksay, "Biomimetic Processing of Ceramics and Ceramic-Metal Composites," in *Better Ceramics through Chemistry IV, MRS Symp. Proc.*, Vol. 180, edited by C. J. Brinker, D. E. Clark, D. R. Ulrich, and B. J. J. Zelinksi (Materials Research Society, Pittsburgh, Pennsylvania, 1990), pp. 625-35.
4. N. B. Pellerin, G. L. Graff, D. R. Treadwell, J. T. Staley, and I. A. Aksay, "Alignate as a Ceramic Processing Aid," submitted for publication in *J. Indus. Microbiol.* (1991).
5. W.-H. Shih, W. Y. Shih, M. Sarikaya, and I. A. Aksay, "Geometrical Arrangement of Magnetosomes in Magnetotactic Bacteria," accepted for publication in *Materials Synthesis Based on Biological Processes, MRS Symp. Proc.*, edited by M. Alper, P. C. Rieke, R. Frankel, P. A. Calvert, and D. A. Tirrell (Materials Research Society, Pittsburgh, Pennsylvania, 1991), pp. 109-114.
6. M. Sarikaya, J. Liu, and I. A. Aksay, "Morphology, Crystallography, and Defect Structures in Biocomposites," submitted for publication in *Proc. of a Workshop on Design and Processing of Materials by Biomimicking*, edited by M. Sarikaya and I. A. Aksay (Seattle, Washington, 1991).

7. N. B. Pellerin, J. T. Staley, T. Ren, G. L. Graff, D. R. Treadwell, and I. A. Aksay, "Acidic Biopolymers as Dispersants for Ceramics Processing," submitted for publication in *Materials Synthesis Based on Biological Processes, MRS Symp. Proc.*, Vol. 218, edited by M. Alper, P. D. Calvert, P. C. Rieke, D. A. Tirrell, and R. Frankel (Materials Research Society, Pittsburgh, Pennsylvania, 1991), pp. 123-128.
8. M. Sarikaya, J. Liu, and I. A. Aksay, "Multiple Tilings with Hierarchical Twin Structures in the Nacre of Red Abalone," to be submitted to *Physical Review B* (1991).
9. J. Liu, M. Sarikaya, and I. A. Aksay, "Multiple Tilings with Hierarchical Twins: A TEM Study of the Nacre Structure of Red Abalone Shell," to be submitted to *Science* (1991).
10. I. A. Aksay and M. Sarikaya, "The Nacre of Abalone Shell: A Natural Multifunctional Nanolaminated Ceramic-Polymer Composite Material," to be submitted to *Structure, Cellular Synthesis, and Assembly of Biopolymers*, edited by S. T. Case (Springer-Verlag, New York, 1992), in preparation.
11. I. A. Aksay and M. Sarikaya, "Bioinspired Processing of Composite Materials," *Proc. Centennial Int'l. Symp. on Ceramics* (Japanese Ceramic Society, Tokyo, Japan, 1991).
12. M. Sarikaya and I. A. Aksay, "Synthetic and Biological Nanocomposites," accepted for publication in *Proc. 5th Int'l. Conf. on Ultrastructure Processing*, edited by L. L. Hench and J. K. West (Wiley, New York, 1991).

3.1.2 Extended Abstracts

1. I. A. Aksay and M. Sarikaya, "Microstructure-Property Relationships in Biocomposites," in *Biostructures as Composite Materials, Proceedings of ARO Workshop*, edited by E. Baer and I. Ahmed (U. S. Army Research Office, Research Triangle Park, North Carolina, 1990) pp. 171-74.
2. K. E. Gunnison, M. Sarikaya, and I. A. Aksay, "Toughening Mechanisms in Abalone Shell," in *Proc. XIIth International Congress for Electron Microscopy* (San Francisco Press, San Francisco, 1990), pp. 196-97.

3. M. Sarikaya, K. E. Gunnison, and I. A. Aksay, "Seashells as a Natural Model to Study Ceramic-Polymer Composites," in *Proc. 47th Ann. Meeting EMSA*, edited by G. W. Bailey (San Francisco Press, San Francisco, 1989), pp. 558-59.
4. J. Liu, M. Sarikaya, and I. A. Aksay, "Hierarchical Twin Structures in Nacre of Red Abalone Shell," in *Proc. 49th Ann. Meeting EMSA*, edited by G. W. Bailey (San Francisco Press, San Francisco, 1991) pp. 946-47.

3.1.3 Undergraduate Project Reports and Graduate Theses

1. Katie E. Gunnison, "Structure-Property Correlation in Abalone Shell" (May 1989).
2. Karen Reidel, "Growth of *Aquaspirillum Magnetotacticum*: Magnetite-Making Bacteria" (May 1989).
3. Jin Lee, "Sample Preparation and Cutting for TEM" (May 10, 1991).
4. Susan Sawyer, "The Correlation Between the Microstructure and Mechanical Properties of the Nacre of Pinctada Shell," U. G. Project Report (June 1991).
5. Hugh Denham, "Self-Healing in Abalone Shells," U. G. Project Report (June 1991).
6. Katie E. Gunnison, "Structure-Mechanical Property Correlations in a Biological Composite: Nacre," M.S. Thesis (June 1991).
7. Gordon L. Graff, "Processing of Ceramic Suspensions with Biologically Produced Polymers," M.S. Thesis (June 1991).

3.2 Presentations: Invited Talks, Conferences, Workshops

1. I. A. Aksay and M. Sarikaya, "Structure-Property Relationships in Biocomposites," 3rd Technical Conference on Composite Materials, American Society for Composites, Seattle, WA, September 26-29, 1988.

2. M. Sarikaya, "Microstructure-Mechanical Property Correlation in Seashells," and "Biomineralization in Seashells," Wright Patterson Air Force Base, Dayton, OH, July 24-25, 1989.
3. I. A. Aksay, "Microstructure-Property Relationships in Biocomposites," ARO Workshop on Bio-Structures as Composite Materials Systems, Cleveland, OH, October 23-25, 1989.
4. M. Sarikaya, "Mechanical Property-Microstructural Relationships in Nacre of Abalone Shell," Fall Meeting, Materials Research Society, Boston, November 27-December 2, 1989.
5. I. A. Aksay, "Biomimetic Processing of Ceramics and Ceramic-Metal Composites," Seminar Center of Excellence for Advanced Materials, University of California, San Diego, La Jolla, CA, February 5, 1990.
6. K. E. Gunnison, M. Sarikaya, and I. A. Aksay, "Ductile/Laminate Modeling with Abalone," American Ceramic Society 92nd Annual Meeting, Dallas, TX, April 20-26, 1990.
7. I. A. Aksay, M. Yasrebi, and M. Sarikaya, "Biomimetic Processing of Ceramics and Ceramic-Metal Composites," Spring Meeting Materials Research Society 1990, San Francisco, CA, April 16-20, 1990.
8. I. A. Aksay, "Biomimetic Processing of Ceramics and Ceramic-Metal Composites," Self-Assembling Molecular Materials Conference, Princeton University, Princeton, NJ, May 14-16, 1990.
9. I. A. Aksay, "Biomimetic Processing of Ceramics and Ceramic-Metal Composites," Colloquium, Department of Materials Science and Engineering, Ohio State University, Columbus, OH, May 18, 1990.
10. M. Sarikaya and I. A. Aksay, "Seashells as a Natural Model to Study Laminated Composites," Vth Annual Meeting of Composite Materials, East Lansing, MI, June 1990.
11. I. A. Aksay, "Biomimetic Processing of Ceramics and Ceramic-Metal Composites," Japan-U.S. Cooperative Science Program, "Processing, Microstructure Development, and Properties of Advanced Ceramics and Their Composites," Tokyo, Japan, August 22-24, 1990.

12. I. A. Aksay, "Biomimetic Processing of Ceramics and Ceramic-Metal Composites," Acta Metallurgica Conference on "Materials with Ultrafine Microstructures," Atlantic City, NJ, October 1-5, 1990.
13. I. A. Aksay and M. Sarikaya, "Biomimetic Processing of Ceramics and Ceramic-Metal Composites," National Science Foundation "Biomolecular Materials Workshop," Washington D.C., October 10-12, 1990.
14. I. A. Aksay, "Biological Structures for Multifunctional Applications," American Ceramic Society 43rd Pacific Coast Regional Meeting, Symposium J, "Technology for Tomorrow," Seattle, WA, October 25-27, 1990.
15. I. A. Aksay, J. T. Staley, W.-H. Shih, and M. Sarikaya, "Biological Structures for Multifunctional Applications," American Ceramic Society 43rd Pacific Coast Regional Meeting, Seattle, WA, October 25-27, 1990.
16. M. Sarikaya, Workshop on "Aerospace Applications of Bionics," NASA, Kiawah Island, Charleston, SC, November 12-14, 1990.
17. I. A. Aksay and M. Sarikaya, "Ceramic-Polymer and Ceramic-Metal Composites through a Biomimicking Approach," Ceramic Science and Technology Congress of the American Ceramic Society, Orlando, FL, November 12-14, 1990.
18. I. A. Aksay, "Biomimetic Processing," Princeton University, NJ, November 30, 1990.
19. J. T. Staley, N. B. Pellerin, T. Ren, G. L. Graff, D. R. Treadwell, and I. A. Aksay, "Use of Acidic Biopolymers as Dispersants for Processing of Ceramics," Fall Meeting of Materials Research Society Meeting, Boston, MA, November 26, 1990.
20. M. Sarikaya, J. Liu, and I. A. Aksay, "Atomic Resolution Electron Microscopy Studies of Defect Structures of Biocrystals," Fall Meeting of the Materials Research Society, Boston, MA, November 26 - December 1, 1990.

21. J. T. Staley, N. B. Pellerin, T. Ren, G. L. Graff, D. R. Treadwell, and I. A. Aksay, "Acidic Biopolymers as Dispersants for Ceramic Processing," Fall Meeting of the Materials Research Society, Boston, MA, November 26-December 1, 1990.
22. H. Liu, G. L. Graff, M. Sarikaya, and I. A. Aksay, "Synthesis of Ultrafine Multicomponent Particles Using Phospholipid Vesicles," Fall Meeting of the Materials Research Society, Boston, MA, November 26-December 1, 1990.
23. W.-H. Shih, M. Sarikaya, W. Y. Shih, and I. A. Aksay, "Geometrical Alignment of Magnetosomes in Magnetotactic Bacteria," Fall Meeting of the Materials Research Society, Boston, MA, November 26-December 1, 1990.
24. M. Sarikaya, "Morphology, Crystallography, and Defect Structures in Biocomposites," "Design and Processing of Materials by Biomimicking" Workshop, Air Force Office of Scientific Research, Seattle, WA, April 2-4, 1991.
25. I. A. Aksay, M. Sarikaya, and J. T. Staley, "Processing of Ceramics by Biomimicking," at "Design and Processing of Materials by Biomimicking" Workshop, Air Force Office of Scientific Research, Seattle, WA, April 2-4, 1991.
26. M. Sarikaya, "Biomimetics with the Nacre of Red Abalone Shell: A Natural Ceramic-Polymer Composite," Exxon Research Labs, Amundale, NJ, May 7, 1991.
27. M. Sarikaya, "Nano-and Micro-Structural," Princeton Research Institute, Princeton University, Princeton, NJ, May 9, 1991.
28. K. E. Gunnison, J. Liu, M. Sarikaya, and I. A. Aksay, "Mechanical Properties of the Organic Component of Abalone Shell," 93rd Annual Meeting of American Ceramic Society, Indianapolis, IN, May 1991.
29. J. Liu, M. Sarikaya, and I. A. Aksay, "Hierarchical Twin Structures in the Nacre of Red Abalone Shell," 49th Annual Meeting of EMSA, San Jose, CA, August 4-9, 1991.

3.3 Patents

1. Process for Suspensions of Ceramic on Metal Particles Using Biologically Moduled Polymers. Inventors: J. T. Staley et al., filed May 14, 1991, reference: WTCC-1-5589.

3.4 News Clippings

The following is a list of national and international news clippings on biomimetic research performed in this group under the sponsorship of the Air Force Office of Scientific Research. Copies of these are included in Appendix XXIV.

1. "Mollusk Teaches Ceramics to Scientists," *Science News*, December 9, 1989, Vol. 136, No. 24, p. 383.
2. "Chemical Processing of Ceramics," *Chemical and Engineering News*, January 1, 1990, pp. 28-40.
3. "Nanostructured Materials," *Nature*, November 1990, Vol. 348, pp. 389-390.
4. "Biomimetics: Creating Materials from Nature's Blueprints," *The Scientist*, July 8, 1991, p. 14.
5. "The New Alchemy: How Science is Molding Molecules into Miracle Materials," *Business Week*, July 29, 1991, pp. 48-55.
6. "Heeding the Call of the Wild," *Science*, August 30, 1991, Vol. 253, issue 5023, pp. 966-968.

4. Personnel

Principal Investigators

Mehmet Sarikaya

James T. Staley

Ilhan A. Aksay

Research Scientists

Daniel M. Dabbs

Jun Liu

Nancy B. Pellerin

Wei-Heng Shih

David R. Treadwell

Graduate Students

Gordon L. Graff

Katie E. Gunnison

Tau Ren

Undergraduate Students

Hugh Denham

Katie E. Gunnison

Michael Hyde

Jin M. Lee

Susan Sawyer

Karen Reidel

5. *APPENDICES*

APPENDIX I

Mechanical Property-Microstructural Relationships in Abalone Shell

by

M. Sarikaya, K. E. Gunnison, M. Yasrebi, and I. A. Aksay

Materials Synthesis Utilizing Biological Processes

Materials Research Society Symposium Proceedings, Vol. 174

edited by P. C. Rieke, P. D. Calvert, and M. Alper

(Materials Research Society, Pittsburgh, Pennsylvania, 1990) pp. 109-16.

MECHANICAL PROPERTY-MICROSTRUCTURAL RELATIONSHIPS IN ABALONE SHELL*

M. SARIKAYA, K. E. GUNNISON, M. YASREBI, and I. A. AKSAY

Department of Materials Science and Engineering, and
Advanced Materials Technology Program, The Washington Technology Center,
University of Washington, Seattle, WA 98195

The microstructure and mechanical properties of abalone shell were studied. It was found that fracture strength, σ_f , is 180 MPa, and fracture toughness, K_{IC} , is $7 \pm 3 \text{ MPa}\cdot\text{m}^{1/2}$; these values are comparable with or better than most "high technology" ceramic materials. The microarchitecture of the nacre section of the red abalone shell is similar to a "brick and mortar" structure, where CaCO_3 is the brick and organic matter is the mortar, constituting 95% and 5% of the microstructure by volume, respectively. This impressive combination of σ_f and K_{IC} values is attributed to the laminated structure of the shell with hard and thick ($0.25 \pm 0.5 \mu\text{m}$) CaCO_3 and superplastic and thin (20-30 nm) organic components. Although there are several toughening mechanisms operating in the shell, fractographic studies identified sliding of CaCO_3 layers and bridging by the organic layers to be the most effective ones. These phases also have a strong interface. The results of our experiments are discussed in the context of using abalone shell as a model for the design of synthetic laminates such as cermet (ceramic-metal) and cerpoly (ceramic-polymer) composites.

INTRODUCTION

In the quest to develop tailor-made materials that possess certain physical properties, novel processing techniques are developed to control the complete microstructural evolution down to the nanometer scale. Some recent studies indicate that materials with controlled microstructural variations at this ultrastructural level exhibit unprecedented mechanical, electrical, superconductive, and optical properties [2-5]. The most notable of these properties are (i) the supermodulus effect (i.e., increase in modulus of elasticity) [2] in laminated materials where the laminate thickness is in the 1.5-5 nm range; and (ii) high temperature superconducting materials (e.g., $\text{YBa}_2\text{Cu}_3\text{O}_{7-x}$) [6], where the correlation length is 1.0-1.5 nm. The processing of these synthetic materials is based on the additive principle, in which the component phases with different properties are fused together in an ordered manner to form a multiphase system. Traditionally, the microstructures of these synthetic materials can be achieved by (i) phase transformations, such as those seen in eutectic and eutectoid systems (e.g., Al-Cu₂Al and Fe-Fe₃C, respectively) [7]; (ii) mechanical mixing of component phases (e.g., metal and ceramic matrix composites); and (iii) tape casting and infiltration (e.g., in cermet and cerpoly systems). However, in these cases, microstructural control is difficult. Other, more advanced processing involves ion beam techniques (such as molecular beam epitaxy) and liquid and vapor infiltration/deposition. With these techniques, the microstructure is controlled at the nanometer level, but the size of the materials that could be produced is extremely limited, and therefore, they do not have widespread application, except for electronic materials. In order to meet the demands of modern technology for materials with better properties, larger materials with complex shapes have to be developed through more intricate and energy-efficient strategies.

The approach used by living organisms in processing composites is in many ways more controlled than the synthetic methods. In the formation of biological composites, living or-

* Summary of a paper to be submitted to *J. Mater. Res.* (1990).

ganisms can efficiently design and produce more complex microstructures with unique properties at many spatial levels (down to the nanometer scale) and with greater control [8-11]. Such examples include magnetite (Fe_3O_4), produced by the freshwater magnetotactic bacteria, *Aquaspirillum magnetotacticum* [12]. Magnetite has an average size of 500 Å, well in the single domain region [13], with a perfect lattice structure, thereby enhancing its magnetic property (discussed elsewhere in these proceedings). Other examples include the complex structures of organic/inorganic composite mixtures, such as exoskeletons of invertebrates and the skeleton and teeth of vertebrates, which possess excellent mechanical properties [8,11].

It is desirable, therefore, to produce manmade materials by using the processing approaches and design principles similar to those used by living organisms, i.e., biomimicking. The present research has been initiated to study the principles inherent in the processing methods used by living organisms in producing composites and the physical properties of the composites as related to their microstructures.

The objectives of this paper are (i) to summarize some of the findings regarding microstructure-property relationships in an abalone shell, (ii) discuss possible toughening mechanisms for these composites on the basis of fractographic studies, and (iii) derive guidelines from this study for the design of synthetically laminated materials.

EXPERIMENTAL

The *Haliotis rufescens* (red abalone) was collected in the Pacific Ocean west of Baja California, and all studies discussed here were performed on adult (~10 years of age) specimens. The shells were 25-30 cm in diameter, with a thickness in the nacre layer of 0.5-1.0 cm. The mechanical tests were performed within 5 weeks following the removal of the abalone from the ocean.

Mechanical tests were conducted by using bar specimens with square cross-sections. Fracture strength, σ_f , and fracture toughness, K_{IC} , tests were performed on single straight notched samples in 4-point and 3-point bending modes, respectively. Similar tests were also done on polycrystalline $\alpha\text{-Al}_2\text{O}_3$ samples and plotted in Fig. 1 as a comparison.

Fractographic studies were done either on the fractured samples or on microhardness indented samples (to study crack propagation) using a scanning electron microscope (SEM). Ultramicrostructural analysis of the shell was performed by transmission electron microscopy (TEM) (Philips 430T) on ion-milled samples (details of the sample preparation are discussed in Ref. 1).

RESULTS

(a) Microstructure

A longitudinal cross-section of the red abalone shell (*Haliotis rufescens*) displays two types of microstructures: an outer prismatic layer and inner nacreous layer. Two forms of CaCO_3 , calcite (rhombohedral, $R\bar{3}c$) and aragonite (orthorhombic, $Pnnc$), constitute the inorganic component of the composite in the prismatic and nacreous layers, respectively. The structure and properties of the nacreous layer are described here, since it is this part of the shell that displays a good combination of mechanical properties as a result of its unique laminated microstructure.

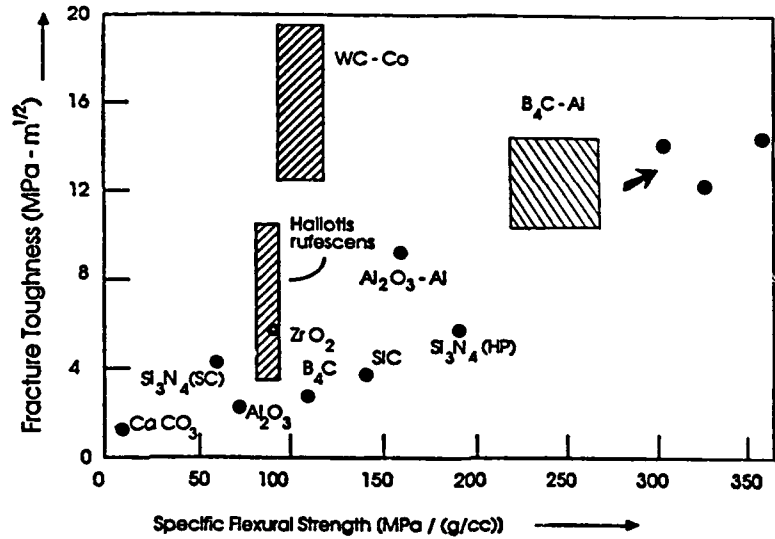


Fig. 1. Fracture toughness versus fracture strength (specific) of the nacre section of the abalone shell compared to some high technology ceramic and cermet materials.

Figure 2, a TEM bright-field image, shows the microstructure of the nacreous layer in which the CaCO_3 layer is about $0.25\text{--}0.5\text{ }\mu\text{m}$ and the organic layer is $20\text{--}50\text{ nm}$. The CaCO_3 "bricks" are single crystals, and there are specific orientation relationships among the crystals in the same layer, as well as among crystals in successive layers. The organic layer, the molecular composition of which is not well understood, is continuous between the CaCO_3 layers.

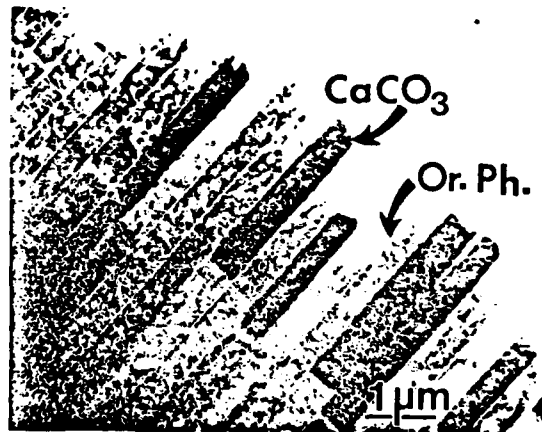


Fig. 2. Bright field image (TEM) of the cross-section of nacre (end-on orientation) showing aragonite "bricks" and organic phase "mortar".

(b) Mechanical Properties and Fractography

Both the fracture strength, σ_f , and fracture toughness, K_{IC} , values have been evaluated in the transverse direction, i.e., perpendicular to the shell plane. The average σ_f value is 185 ± 20 MPa and K_{IC} is 8 ± 3 MPa-m^{1/2}. As indicated, both the strength and the toughness values show a scatter, especially in the latter case. This is due to natural defects in the nacre and the somewhat curved shape of the layers. Nonetheless, the combination of these properties qualifies abalone shell as a high performance material, as shown in the toughness-strength diagram (Fig. 1).

The observation of the crack propagation behavior reveals a high degree of tortuosity not seen in the more traditional brittle ceramics (such as Al₂O₃) or the high toughness ceramics (such as ZrO₂) [14]. A microstructure showing the tortuous crack propagation of the abalone shell is displayed in Fig. 3. The most apparent feature of the crack propagation seen in the SEM micrographs is crack blunting/branching and microcrack formation. A closer examination of the fractographs reveals, however, that the microcracks advance both on planes parallel to the CaCO₃ layers and across those layers. However, it is not clear whether the cracks propagate inside the organic layer or through the interface plane between the organic and inorganic components.

The surface of the fractured sample (seen in Fig. 4) indicates that the major crack has meandered around the CaCO₃ layers, passing through the organic layers, and has resulted in a highly rough surface with partially exposed plates.

In micrographs taken at much higher magnification, separation of the CaCO₃ layers in both \vec{x} and \vec{y} directions (in the layer plane) is clearly seen (Fig. 5). The "bricks" have been left intact, which may indicate that they "slide" on the organic layer. The higher magnification micrograph in Fig. 6, on the other hand, displays organic ligaments which are stretched (in the perpendicular direction, i.e., the \vec{z} direction) between the CaCO₃ layers. This stretching indicates that the interface between the organic and inorganic phases is strong and that the organic phase acts as a strong binder.

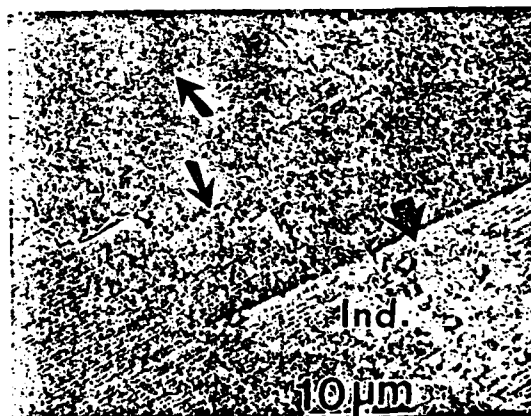


Fig. 3. Scanning electron image (SEM) of the polished surface of the shell showing the crack propagation behavior around a micro-indentation (Ind.). High tortuosity and microcrack formations are clearly revealed.

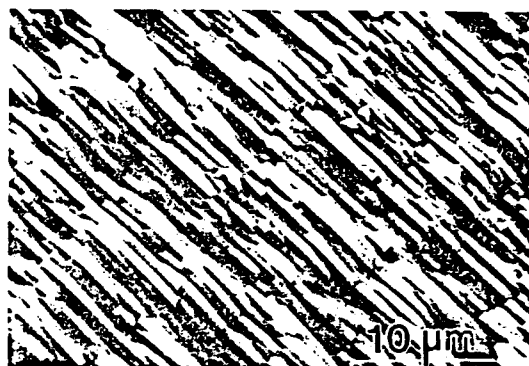


Fig. 4. SEM micrograph (SE) of the fractured surface of a test sample showing "plate pull-out" and resulting high tortuosity.

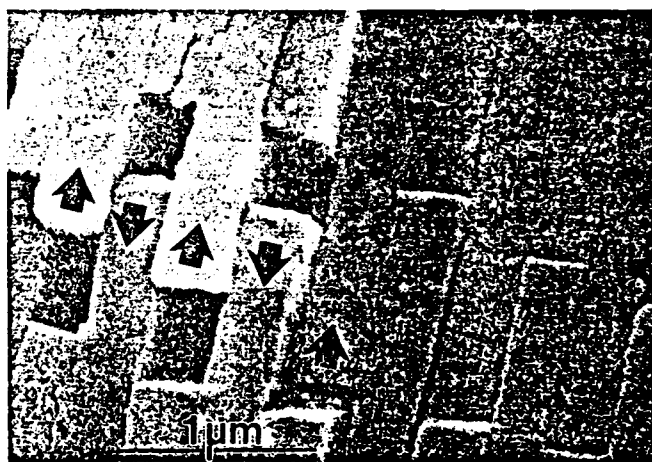


Fig. 5. SEM micrograph (SEM) clearly reveals sliding in the direction of the arrows (i.e., in the plane of the layers).

Preliminary results [15] on the mechanical properties of B_4C -Al (35 vol%) laminated cermets designed and processed on the basis of the above observations indicate a 30% increase in the fracture toughness of the composite (Fig. 1). An SEM image of the fracture surface of the B_4C -Al laminate is shown in Fig. 7. The increase in the cermet toughness is attributed to the same toughening mechanisms observed in abalone shell. Further improvement in both strength and toughness is expected with a decrease in the thickness to submicrometer levels of the composite layers; in the present case, the minimum thickness of the layers in the cermet laminate is about 10 μm , far too thick to benefit from the effects of the type of lamination seen in abalone shell. Consequently, our present research is directed to the processing of cermets with submicrometer-layer thicknesses in conjunction with studies of the quantitative effects of the organic layer in sea shells.

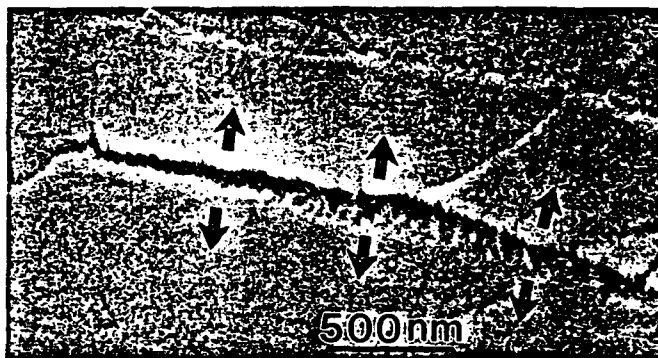


Fig. 6. SEM micrograph (SE) showing the organic ligament formation between the CaCO_3 layers when resolved stresses are in the direction shown by the arrows.

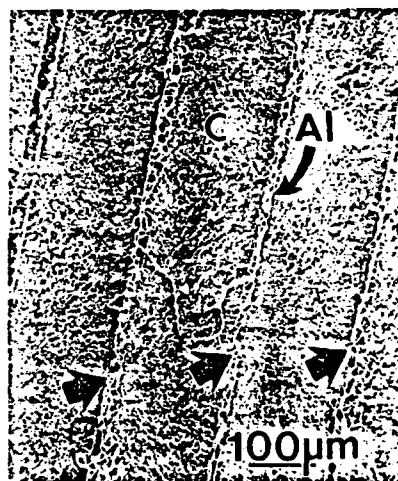


Fig. 7. SEM image of the fractured surface of the $\text{B}_4\text{C-Al/Al}$ composite. $\text{B}_4\text{C-Al}$ is indicated by C. Broad arrows show strong interfaces, open arrow shows weak interface.

DISCUSSION AND SUMMARY

The fracture behavior of the abalone shell and that of commonly used monolithic ceramic materials have been compared in terms of crack propagation. An indentation experiment (for example, the Vickers hardness test) performed in polycrystals of alumina and partially stabilized zirconia show that these ceramics exhibit straight cracks extending radially from the corners of the indentation, indicating brittle behavior. Indentation in the transverse direction in the nacreous layers in abalone shell indicates that cracks do not extend from the corners of the

indentation, but from regions close to the corners in various directions (Fig. 3). These directions are probably the high strain regions formed by the complex stress distribution in the shell structure. The formation of tortuous cracks and microcracks (Figs. 3-5) is an indication of a high degree of energy absorption in the form of deformation during crack propagation, resulting in a higher fracture toughness compared to monolithic ceramics.

Fractographic analysis of the fracture surfaces and indentation cracks reveals several possible toughening mechanisms. These are (i) crack blunting/branching, (ii) microcrack formation, (iii) pull-outs (plates), (iv) crack bridging (ligament formation), and (v) sliding of layers. It would be desirable for all of these mechanisms to be operative in a composite in order to increase fracture toughness and strength. The high tortuosity seen here in crack propagation is due mainly to crack blunting and branching. However, tortuosity is not the major toughening mechanism in these composites. The linear tortuosity, determined from a number of indentation cracks, indicates a 30-50% value. Although linear tortuosity may contribute, it cannot be the major mechanism for the more than 20-fold increase in toughness.

There are similarities between the deformation of a nacreous sea shell and a metal. These may be stated as follows:

(i) Around the periphery of the indentation (as seen in Fig. 3), the material exhibits deformation features, such as sliding of CaCO_3 layers to accommodate the strain caused by the indenter. These deformation features are similar to the Lüders bands (or slip bands) seen in metals (such as in face-centered cubic Cu and Ni) caused by the dislocation slip which accommodates the applied stress on high atomic density planes (such as {111}). It is also noted that the degree of sliding near the indentation is higher and it decreases with distance from the indentation.

(ii) As the sliding takes place to accommodate deformation, there is no cracking through the layers except for microcrack formation. This indicates that the biocomposite is not brittle and the strain accommodation mostly takes place between CaCO_3 layers, not through the ceramic layers. At this stage, however, it is not known whether the biopolymer layer at the interface between the ceramic and biopolymer is ruptured. Nonetheless, this complex deformation mode increases the toughness of the composite.

Sliding takes place, probably, when there is a resolved shear stress acting in the plane of the layers. However, if the resolved stress has a tensile component (normal to the layers) then the CaCO_3 layers are forced to separate. This separation is resisted by the formation of organic ligaments which are stretched across the organic layers and form bridges between the CaCO_3 plates. It should be noted here that the organic matrix has a plywood-like structure [11]. The fact that there is a 1000% deformation of the organic layer and that the organic layer is still intact is due to the strong interface between the organic and inorganic phases in the shell and the ultrastructure of the organic layer.

In order to aid the design of future synthetic laminated materials, three guidelines may be drawn from the present analysis: (i) lamination of the component phases should form a highly ordered microarchitecture; (ii) mechanical properties of the component phases should be such that the thick phase should be hard, and the thin phase should be soft; (iii) interfaces should be strong. Therefore, the property requirements for soft phase imply that it be highly plastic, while the thick phase should have a high hardness.

In the design of synthetic laminates, high hardness ceramics, such as BN, B_4C , TiC, etc., can be taken as the hard component. Highly plastic (superplastic) metals and alloys, such as

Al or Cu (and their alloys) may be good candidates for the soft component, provided that they can be processed and would result in strong interfaces. These requirements are met to a certain degree in the B_4C -Al laminate system (Fig. 7), but further modifications are necessary in processing to obtain finer layers with stronger interfaces.

ACKNOWLEDGMENTS

This research was supported by the Air Force Office of Scientific Research under Grant Nos. AFOSR-87-0114 and AFOSR-89-0496. The assistance of D. L. Milius in the mechanical property measurements is gratefully acknowledged.

REFERENCES

1. M. Sarikaya, K. E. Gunnison, and I. A. Aksay, "Sea-Shells as a Natural Model to Study Laminated Materials," to be submitted to *J. Mater. Res.* (1990).
2. F. Spaen, "The Art and Science of Microstructural Control," *Science*, **235**, 1010 (1987).
3. R. C. Cammarata, "The Supermodulus Effect in Composition Modulated Thin Films," *Scripta Met.*, **20**, 883 (1980).
4. M. S. Dresselhaus, "Intercalation of Layered Materials," *Mater. Res. Bull.*, **12** [3] 24 (1987).
5. *Metallic Superlattices: Artificially Strong Materials*, edited by T. Sinjo and T. Takada (Elsevier, Amsterdam, 1987).
6. See, for instance, J. D. Jorgensen et al., "Structural and Superconducting Properties of Orthorhombic and Tetragonal $YBa_2Cu_3O_{7-x}$: The Effect of Oxygen Stoichiometry and Ordering on Superconductivity," *Phys. Rev. B*, **36**, 5731 (1987).
7. A. Kelly and R. L. Nicholson, *Strengthening Methods in Crystals* (Wiley, New York, 1971).
8. a. H. A. Lowenstam, "Minerals Formed by Organisms," *Science*, **211**, 1126 (1981); b. H. A. Lowenstam and S. Weiner, *On Biomineralization* (Oxford University Press, Oxford, 1989).
9. a. S. Mann, "Mineralization in Biological Systems," *Structure and Bonding*, **54**, 124 (1983); b. *Biomineralization: Chemical and Biochemical Perspectives*, edited by S. Mann, J. Webb, and R. J. Williams (VCH Publishers, Weinheim, 1989).
10. S. Weiner, "Organization of Extracellularly Mineralized Tissues: A Comparative Study of Biological Crystal Growth," *CRC Critical Reviews in Biochemistry*, **20** [4] 365 (1986).
11. a. *The Mechanical Properties of Biological Materials*, edited by J. A. Currey and J. F. V. Vincent (Cambridge Univ. Press, Cambridge, 1980); b. J. D. Currey, "Biological Composites," *J. Materials Educ.*, **9** [1-2] 118 (1987).
12. R. P. D. Blakemore and R. S. Wolfe, "Isolation and Fine Culture of a Freshwater Magnetic *Spirillum* in Chemically Defined Medium," *J. Bacteriol.*, **140**, 720 (1979).
13. I. S. Jacobs and C. P. Bean, "An Approach to Elongated Fine Particle Magnets," *Phys. Rev.*, **100**, 1060 (1955).
14. *Deformation of Ceramic Materials II*, edited by R. C. Tressler and R. C. Bradt (Plenum, New York, 1984).
15. M. Yasrebi and I. A. Aksay, "Processing of Laminated B_4C -Al Cermets," unpublished results, University of Washington, Seattle (1989).

APPENDIX II

Seashells as a Natural Model to Study Laminated Composites

by

M. Sarikaya, K. E. Gunnison, M. Yasrebi, D. L. Milius, and I. A. Aksay

Proceedings of American Society Composites

Fifth Technical Conference

(Technomic Publishers, Lancaster, Pennsylvania, 1990) pp. 176-83

Seashells as a Natural Model to Study Laminated Composites

M. SARIKAYA, K. E. GUNNISON, M. YASREBI, D. L. MILIUS AND I. A. AKSAY

Department of Materials Science and Engineering

Advanced Materials Technology Center

Washington Technology Centers

University of Washington

Seattle, WA 98195

1. Abstract

The microstructure and mechanical properties of the nacre section of abalone shell were studied as a model for the fabrication of laminated ceramic-metal (cermet) composites. The shell consists of laminated CaCO_3 (aragonite) and organic layers with thicknesses of $0.25\ \mu\text{m}$ and $20\ \text{nm}$, respectively. The unusually high fracture toughness and fracture strength values of the shell are attributed to this unique microstructure. Laminated cermets ($\text{B}_4\text{C-Al}$) have been designed and processed to mimic the abalone shell. The fracture toughness and strength values of these cermets increase approximately 40% compared to the monolithic form of the same phase mixtures.

2. Introduction

In materials processing, progress is being made in controlling the microstructure of composites at the nanometer scale, resulting in the formation of materials that exhibit unprecedented mechanical, electrical, superconductive, or optical properties.¹⁻⁴ The processing of these synthetic materials is based on the additive principle, in which component phases with varying properties are fused together in an ordered manner to form a multiphase system. Conventionally, these structures can be achieved by phase transformations (precipitation-hardened alloys) or by mechanical mixtures at the microscale level (metal and ceramic matrix composites).⁵ More advanced processing involves ion beam techniques (such as molecular beam epitaxy and liquid and vapor deposition)^{3,4} in which the microstructure is controlled at the nanometer level. In order to meet the demands of modern technology for composites with better properties, more complex systems have to be developed through more intricate and energy-efficient processing strategies.

Methods used by living organisms in processing composites are in many ways more controlled than synthetic methods. In the formation of biological composites, living organisms can design and produce, efficiently, complex microstructures having unique properties at all spatial levels (down to the nanometer scale), and in more controlled ways at the

molecular level.⁶⁻⁸ It is desirable, therefore, to produce manmade materials by using processing approaches similar to those used by living organisms, i.e., by biomimicking. This present research has been initiated to study the principles inherent in the processing methods used by organisms in producing composites and the physical properties of those composites as related to their microstructures. In this paper, we summarize the results of a recent study on the microstructures of the red abalone shell (*Haliotis rufescens*) in relation to its mechanical properties.

3. Microstructure and Properties of the Nacre Section of Abalone Shell

A longitudinal cross section of the abalone shell displays two types of microstructures: an outer prismatic layer and an inner nacreous layer. Two forms of CaCO_3 , calcite (rhombohedral, $R\bar{3}c$) and aragonite (orthorhombic, $Pmnc$) constitute the inorganic component of the organic-inorganic composites in the prismatic and the nacreous layers, respectively. The structure and the properties of the nacreous layer are described here, as this is the portion of the shell which displays a good combination of mechanical properties.⁹

Mechanical properties, i.e., σ_f (fracture strength) and K_{IC} (fracture toughness), have been evaluated in the transverse direction (perpendicular) to the shell plane. Typical σ_f and K_{IC} values are 180 MPa and about $8 \text{ MPa}\cdot\text{m}^{1/2}$, respectively. The study of the crack propagation behavior reveals a high degree of tortuosity not seen in the more traditional brittle (such as Al_2O_3) and high toughness (ZrO_2) ceramics,¹⁰ indicating that certain toughening mechanisms such as crack blunting, branching, and "layer pull-out" are operating in the shell (Figure 1). A closer examination of the microstructure reveals that cracks mostly

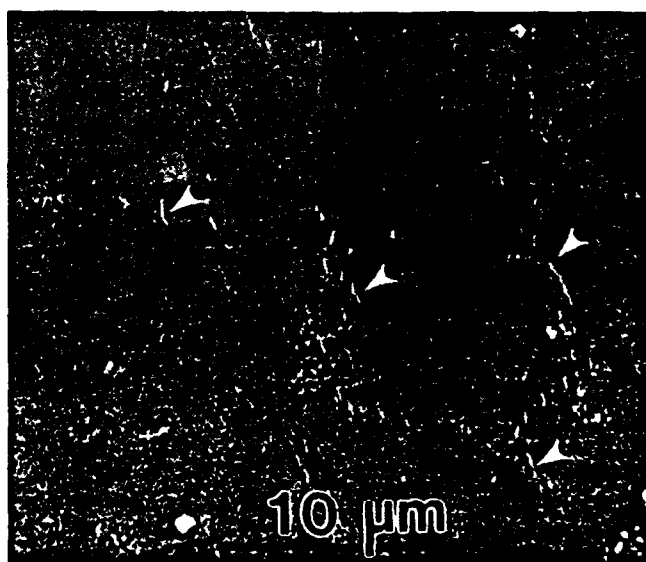
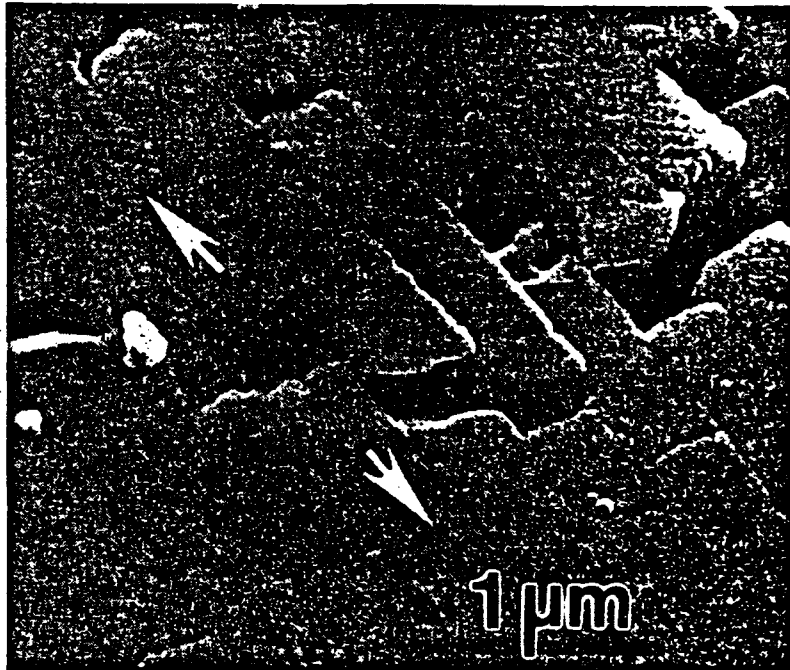


Figure 1. Scanning Electron Microscopy (SEM) image of multiple crack formation emanating from a microindentation.

deposition of the organic phase, and the subsequent deposition of the inorganic phase.

The organic phase is deposited first, and the inorganic phase is deposited subsequently. The organic phase is deposited in the form of a thin layer, and the inorganic phase is deposited in the form of a thicker layer.

The organic phase is deposited in the form of a thin layer, and the inorganic phase is deposited in the form of a thicker layer. The organic phase is deposited in the form of a thin layer, and the inorganic phase is deposited in the form of a thicker layer.



The organic phase is deposited first, and the inorganic phase is deposited subsequently. The organic phase is deposited in the form of a thin layer, and the inorganic phase is deposited in the form of a thicker layer.

The organic phase is deposited in the form of a thin layer, and the inorganic phase is deposited in the form of a thicker layer. The organic phase is deposited in the form of a thin layer, and the inorganic phase is deposited in the form of a thicker layer.

Figure 2. High resolution SEM image of the abalone shell exhibiting the sliding of the CaCO_3 layers.

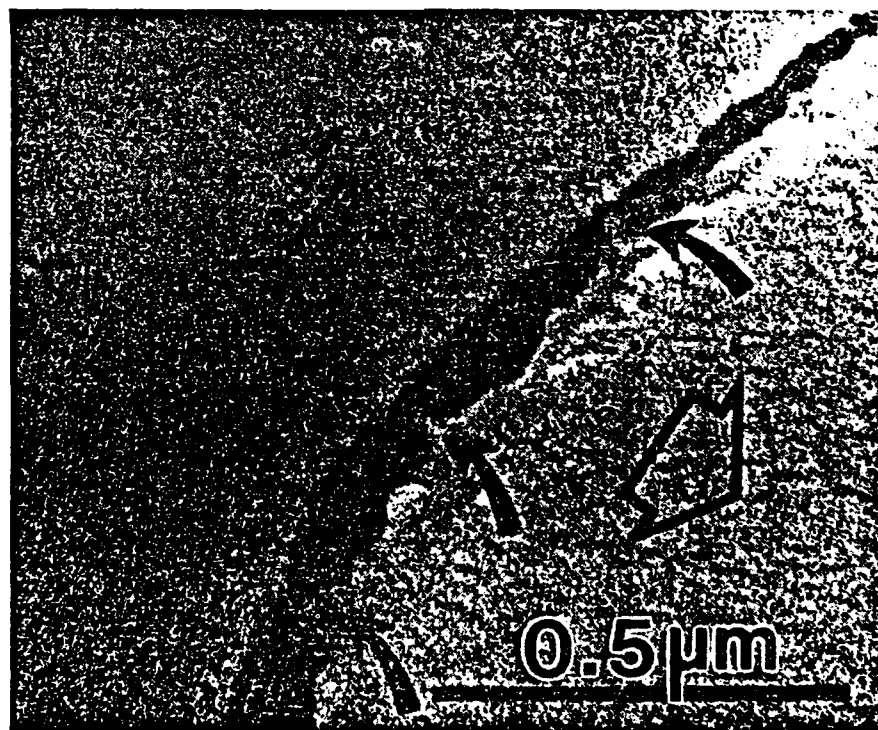


Figure 3. High magnification SEM image of abalone shell near a microindentation exhibiting the ligament formation of the organic phase bridging the CaCO_3 platelets.

advance through the organic layer and with difficulty, as this process is accompanied by sliding of the CaCO_3 layers (when there is a shear component of the resolved stress) and by the bridging of the organic ligaments (when there is a normal stress component), as shown in Figures 2 and 3, respectively. It is these last two mechanisms which contribute to the toughening of the shell.

The superior mechanical properties of abalone shell compared to those of more traditional ceramics and their composites (Table I) come from the unique "brick and mortar" microstructure. A Transmission Electron Microscope (TEM) image (Figure 4) recorded in the transverse direction shows the alternating layers of hexagonal-shaped 0.2-0.5 μm thick aragonite crystals which form the hard component and the thin (20-50 nm) organic substance in between (mainly proteins) which provides the ductile component of the composite.

Table I. Mechanical Properties of Ceramics, Cermets, and Abalone Shell

	σ_f MPa	K_{IC} $\text{MPa}\cdot\text{m}^{1/2}$	Hardness	
			Mohs	KHN (kg/mm^2)
SiC	450	3.5	8.0	2750-3000
Si_3N_4	200 (SC)†	4.0	---	1500
	650 (HP)†	5.5	---	2000
ZrO_2	500	5.5	6.5	1300
Al_2O_3	270	2.0	9.0	2100
	258*	2.1*	---	---
B_4C	285	3.1-6.0	9.5	4950
CaCO_3	< 10	< 1.0	3.0	135
$\text{Al}_2\text{O}_3\text{-Al}$	500-1300	8.0	---	---
$\text{B}_4\text{C-Al}$	600	12.0	---	---
Abalone shell	183*	5.8*	---	240*
	(165-204)	(3.6-10.4)		

†SC - Slip Cast and HP - Hot Pressed; *this study

4. Some Microstructural Design Guidelines for Laminated Composites

The unique combination of mechanical properties of the nacre comes from both the sliding of the CaCO_3 layers over the organic matrix (Figure 2) and the organic ligaments that form between the layers (Figure 3). The amount of strain in sliding is as much as

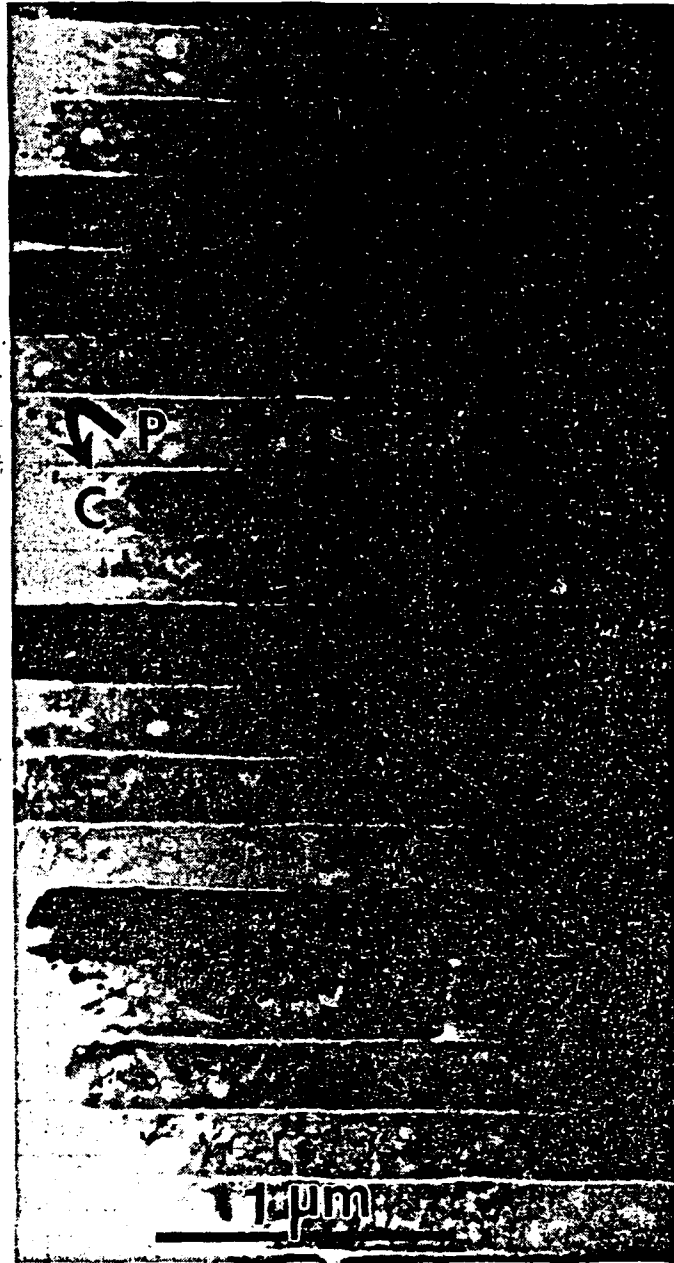


Figure 4. Bright field transmission electron microscopy image of the nacre section of the abalone shell revealing the CaCO_3 (C) and organic (P) layers. The image was recorded with the electron beam parallel to the laminate plane.

10% without a catastrophic failure. This is similar to plastic deformation in metals caused by the gliding motion of dislocation on slip planes. Similarly, in the formation of ligaments, the organic phase elongates as much as 1000%. This is similar to superplastic deformation of metals. Both of the above processes require that the interfaces between the organic matrix and the inorganic layers do not prematurely fail. Based on these observations, the

following guidelines can be drawn for the design of laminated composites consisting of a thick, hard, and strong component and a thin, ductile, and tough component. These design guidelines are:

- (i) Laminate thickness for the hard component of less than $1\ \mu\text{m}$ and for the soft component of less than $100\ \text{nm}$;
- (ii) Soft superplastic phase;
- (iii) The ability of the soft phase to form ligaments;
- (iv) Strong interfaces between the soft and hard layers.

In drawing these guidelines, the detailed microstructures of the soft and hard phases have yet to be taken into account. This subject will be dealt with in the future when more detailed microstructural and nanostructural information is available.

These guidelines can be followed to process laminated ceramic-metal and ceramic-polymer composites. In this section, we give some preliminary results from our ceramic-metal (cermet) research.¹¹ B_4C -Al is the system selected for processing the laminated cermets. By taking advantage of the limited reaction that takes place between B_4C and Al, fully dense monolithic composites with a good combination of mechanical properties have been fabricated. Figure 5 illustrates the first laminates of this cermet.¹¹⁻¹³ The fabrication of these

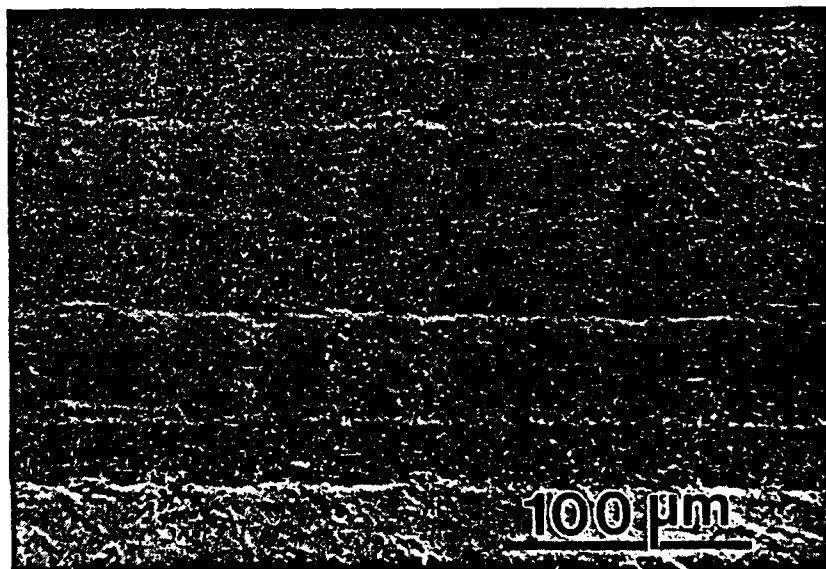


Figure 5. SEM image of B_4C -Al/Al cermet showing the fully dense microstructure.

laminates involves the infiltration of molten Al into preformed B_4C sponges of controlled porosity. The laminated composite is formed either by metal infiltration from the Al layers sandwiched between B_4C tapes or by lamination of B_4C tapes of different porosity and

then metal infiltration of the laminated body. Nearly dense laminates obtained this way show an average of 40% improvement in fracture strength (950 MPa) and fracture toughness ($K_{IC} = 19 \text{ MPa}\cdot\text{m}^{1/2}$).¹¹ The toughening is attributed to a similar mechanism observed in abalone shell. One of the functions of the soft phase Al, which is to "arrest" cracks, is illustrated in Figure 6 where two cracks emanating from an indentation in B_4C -Al layer

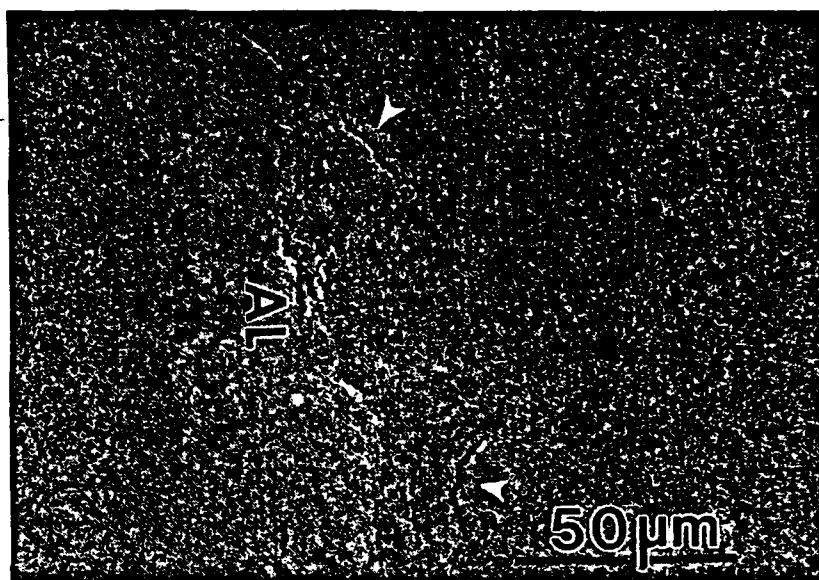


Figure 6. SEM micrographs of B_4C -Al/Al cermet revealing the effect of the soft Al layer in deflecting the microcracks (arrows) formed by a microindentation.

deviate in their normal propagation path in the vicinity of the interface. An advantage of the fabrication process described above is the ability to process graded microstructures of B_4C -Al laminates with properties that can be tailored to meet requirements which may vary along the transverse direction of the finished part, similar to abalone shell. However, in order to take full advantage of lamination in the present system, laminates of less than 10 μm thickness need to be processed. Further improvements, both in fracture toughness and strength, can be expected with decreases in the thickness of the laminates down to the submicrometer scale.

5. Summary

Preliminary results on the mechanical properties of B_4C -Al (35%) laminated cermets designed on the basis of the above observations, indicate a 40% increase in the fracture toughness and the strength of the composite. The increase in the fracture toughness is attributed to the same toughening mechanisms observed in abalone shell. Further improve-

ment in both strength and toughness is expected with the decrease in the thickness of the composite layers (to submicrometer levels); in the present case, the thinnest of the layers in the cermet laminate is about 10 μm , far too thick to benefit the effects of the lamination. Consequently, the present research is directed to the processing of cermets with submicrometer-layer thicknesses in conjunction with quantitative studies of the effects of the organic layer in seashells.

6. Acknowledgments

This research was supported by the Air Force Office of Scientific Research (AFOSR) under Grants Nos. AFOSR-87-0114 and AFOSR-89-0496.

7. References

1. Spaen, F., "The Art and Science of Microstructural Control," *Science*, 235, 1010 (1987).
2. Cammarata, R. C., "The Supermodulus Effect in Composition Modulated Thin Films," *Scripta Metallurgica*, 20, 883 (1980).
3. Dresselhaus, M. S., "Intercalation of Layered Materials," *Materials Research Society Bulletin*, 12 (3) 24 (1987).
4. *Metallic Superlattices: Artificially Strong Materials*, edited by T. Sinjo and T. Takada (Elsevier, Amsterdam, 1987).
5. *Strengthening Methods in Crystals*, edited by A. Kelly and R. B. Nicholson (Applied Science Publishers, Ltd., London, 1971).
6. Lowenstam, H. A., "Minerals Formed by Organisms," *Science*, 211, 1126 (1981).
7. Mann, S., "Mineralization in Biological Systems," *Structure and Bonding*, 54, 124 (1983).
8. Weiner, S., "Organization of Extracellularly Mineralized Tissues: A Comparative Study of Biological Crystal Growth," *CRC Critical Reviews in Biochemistry*, 20 (4) 365 (1986).
9. Currey, J. D., "Biological Composites," *Journal of Materials Education*, 9 (1-2) 118 (1987).
10. *Deformation of Ceramic Materials II*, edited by R. C. Tressler and R. C. Bradt (Plenum, New York, 1984).
11. Aksay, I. A., Yasrehi, M., and Milius, D. L., "Boron Carbide-Aluminum Laminates," Invention Disclosure, submitted to Washington Technology Centers, February 14, 1990.
12. Halverson, D. C., Pyzik, A. J., Aksay, I. A., and Snowden, W. E., "Processing of Boron Carbide-Aluminum Composites," *Journal of the American Ceramic Society*, 72 (5) 775 (1989).
13. Pyzik, A. J., Aksay, I. A., and Sarikaya, M., "Microdesigning of Ceramic-Metal Composites," *Ceramic Microstructures '86: Role of Interfaces*, edited by J. A. Pask and A. G. Evans (Plenum, New York, 1987), pp. 45.

APPENDIX III

Biomimetic Processing of Ceramics and Ceramic-Metal Composites

by

M. Yasrebi, G. H. Kim, D. L. Milius, M. Sarikaya, and I. A. Aksay

Better Ceramics Through Chemistry IV

Materials Research Society Symposium Proceedings, Vol. 180

edited by C. J. Brinker, D. E. Clark, D. R. Ulrich and B. J. J. Zelinski
(Materials Research Society, Pittsburgh, Pennsylvania, 1990) pp. 625-35

BIOMIMETIC PROCESSING OF CERAMICS AND CERAMIC-METAL COMPOSITES

M. YASREBI, G. H. KIM, K. E. GUNNISON, D. L. MILIUS, M. SARIKAYA, and I. A. AKSAY

Department of Materials Science and Engineering; and
Advanced Materials Technology Center, Washington Technology Centers,
University of Washington, Seattle, Washington 98195 USA

ABSTRACT

Biomimetic design and processing of laminated B_4C -Al cermets, based on knowledge gained from the microstructure-property characterization of abalone shells, is described. In the nacre section of the shell, the microstructure is highly organized as $CaCO_3$ (aragonite) crystals, with a thickness of $0.25\ \mu m$, separated by a layer of organic matter $300\text{--}500\ \text{\AA}$ thick. This organization forms a miniature "brick and mortar" microstructure. The resultant strength and fracture toughness of the nacre, i.e., $180\ \text{MPa}$ and $7\ \text{MPa}\cdot m^{1/2}$, are many orders of magnitude higher than those of monolithic $CaCO_3$. The processing of laminated B_4C -Al cermets, based on the microstructure of the nacre, was performed by a combination of tape casting of the ceramic and infiltration of the metal. The resultant cermets displayed a 40% increase in both fracture toughness and strength over monolithic B_4C -Al cermets.

INTRODUCTION

The use of composite materials has become popular and frequently necessary to meet the requirements of technology. The employment of composites is well appreciated from the fact that unique arrangements of constituent materials not only satisfy specific requirements but also exhibit properties superior to the sum of each component.

Laminated composites which have planar geometry are one example and can be found both in nature and early civilizations. Examples are seashells, glued woods, and metallic armor. Even though exotic techniques and materials are introduced in the processing of laminated composites for modern applications, the flexibility of offering specific anisotropic properties, such as a specific strength, toughness, and stiffness, makes laminated composites attractive and provides an edge over single-phase materials.

The discovery that modern laminates formed from composites with a nanoscale architecture have enhanced properties has drawn much attention. It has led to the reexamination of the structure-property relationship in composites with different scales of size. Eutectic composites, frequently known as *in situ* composites, exhibit a well-aligned fibrous or platelet-reinforcing phase by directional solidification or by phase transformation, the classical example being the pearlite structure. A wide range of materials belongs to this group such as metal-metal,¹ metal-ceramic,² intermetallic-intermetallic,¹ metal-intermetallic,³ and ceramic-ceramic^{4,6} systems. In all cases, the size dependency of properties was observed and is known as the Hall-Petch relationship, $\sigma = \sigma_0 + kd^{-1/2}$, for ductile phases and the Orowan relationship, $\sigma_f = YK_{IC}d^{-1/2}$, for brittle phases. Although directional solidification is a thermodynamically-driven process, precise control of the interfacial characteristics and composition of the composites was possible even when the size was reduced to a few microns. Similar microstructures can be obtained at the nanometer range through the use of physical or chemical deposition techniques which are not limited by thermodynamic parameters. The subsequent enhancement

of properties results in unique behavior which is not only size dependent^{7,8} but also dependent on the nature of the interface,^{9,10} a phenomenon known as the supermodulus effect.¹¹

A laminated architecture is especially useful in naturally-occurring composites such as seashells where it maximizes strength and toughness, sometimes exceeding the properties of the constituent materials by more than 20 times.^{12,13} It should be noted that the biologically-produced laminates are formed *in situ* as are eutectic-like composites and have the same nanometer scale as superlattices. The classical work of Cook and Gordon¹⁴ on the importance of interfacial bond strength in determining toughness can be seen in the enhancement of toughness in laminates as well. Refined models^{15,16} are found in brittle matrix composites with all necessary microstructural dependencies. Our interpretation of the enhanced strength of biological laminates requires that a ductile-phase reinforcement be present so that the strength of the composite exceeds that of the strength of the component phases. This behavior has been observed in ceramic-metal composites which have been processed under the presence of strong wetting conditions where a liquid phase has formed between the molten metal and the ceramic phase such as in sintered WC-Co¹⁷⁻¹⁹ and liquid metal-infiltrated B₄C-Al composites.²⁰⁻²³

It is therefore apparent that further enhancement of strength and toughness is possible by employing a laminated microstructure with a smaller size scale while keeping the ductile-phase reinforcement, as in B₄C-Al cermet. It will be shown in this study that the properties of laminated B₄C-Al composites indeed exhibit a size dependency in producing desirable enhancements but do so without sacrificing density of the composite. In the following section, therefore, we give a summary of the possible strengthening and toughening mechanisms in the nacre section of the abalone shell and draw certain design guidelines for ductile-brittle laminate materials. This will be followed by a section on the preliminary studies of B₄C-Al laminated structures which already exhibit superior mechanical properties over other existing cermet structures.

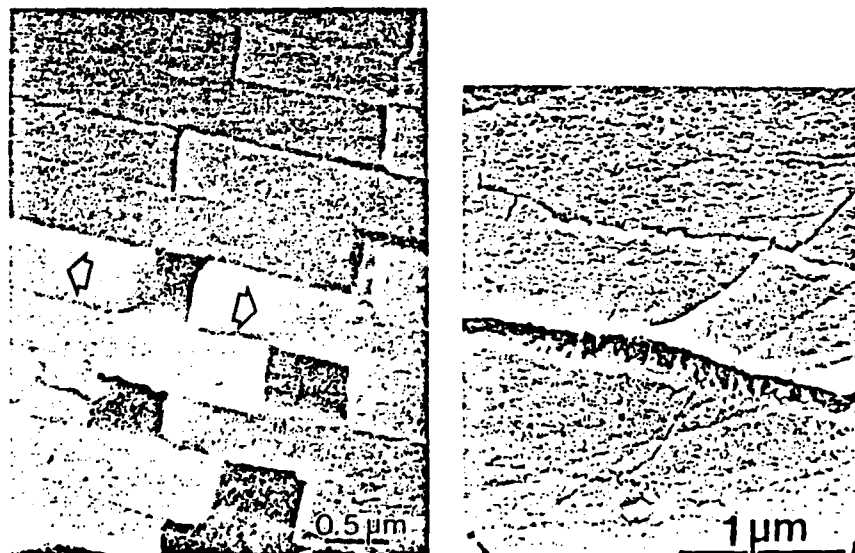


Figure 1. SEM images showing the two possible toughening mechanisms that significantly contribute to the toughening of the nacre section of the abalone shell: (a) sections, (b) ligament formation.

POSSIBLE TOUGHENING MECHANISMS IN LAMINATED MICROSTRUCTURES IN SEASHELL: EXAMPLE, NACRE

Structural components in biological systems such as load-carrying skeletons, grinding components such as teeth, and impact resistant "coats" like seashells, all have highly organized microstructures composed of an organic matrix and an inorganic major phase. In processing these structural components, the organism has full control so that the composite is tailor-made to fulfill certain functions in the body. In all these cases, because of the highly organized microstructures, biological composites have unique properties not yet achieved in synthetic materials. Therefore, it is imperative to examine biological composites to understand the relationship between microstructure and properties. Here we summarize mechanical property-microstructure relations in the nacre of abalone shell, draw some guidelines for laminated materials design, and subsequently apply these to the design and processing of laminated B_4C -Al cermets.

In general, seashells have various microstructures, each designed and processed to have optimum mechanical properties, such as adequate toughness, strength, hardness, or wear-resistance depending on the living environment of the animal. Nacre is a common structure found in many seashells and it primarily provides "toughness" to the shell. In the case of red abalone (*Haliotis refuscens*), the shell in the transverse direction (through thickness) consists of an outer prismatic layer and an inner nacre layer.^{12,13} Two forms of $CaCO_3$, calcite and aragonite, constitute the inorganic component of the composite in the prismatic and nacreous layers, respectively.¹² The microstructure and mechanical properties of the nacreous layer are described here only when relevant to the present work.

The nacreous layer is composed of 95% $CaCO_3$ by volume and is organized in a "brick and mortar" configuration with the remaining organic matrix (proteins, macromolecules, and chitin). The $CaCO_3$ layers are individually composed of hexagonal shaped crystallites with a thickness of 0.25 μm . The organic layer between the $CaCO_3$ layers has a total thickness of about 20-50 nm and is composed of several layers of different organic components, the detailed structure of which is still not well understood.¹³

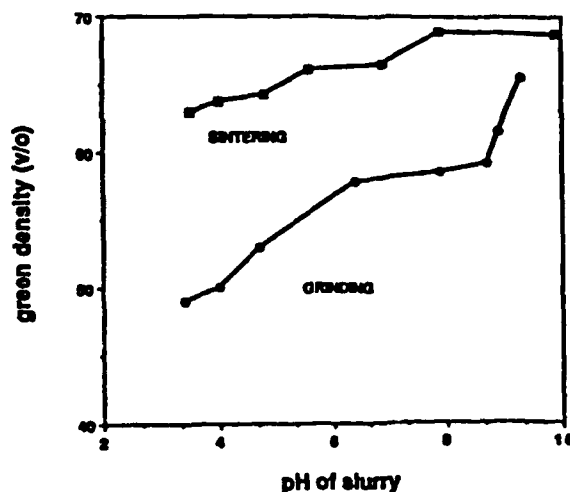


Figure 2. A plot of green-density vs. pH value of the slurry.

The mechanical properties in terms of fracture toughness (a straight notched three-point bend) and fracture strength (four-point bend) have been evaluated in the transverse direction. Typical values of σ_f and K_{IC} are 180 MPa and $7.0 \text{ MPa}\cdot\text{m}^{1/2}$, respectively. These high values for mechanical properties may be explained based on the behavior of crack propagation during failure. The study of crack propagation features reveals a high degree of tortuosity not seen in monolithic ceramics such as brittle Al_2O_3 or ZrO_2 . Certain toughening mechanisms such as microcrack formation, crack branching and blunting, and plate "pull-out" all operate in the nacre. However, the more than 20-fold increase in fracture toughness of the shell, which consists of 95% CaCO_3 and 5% organic matrix, compared to monolithic CaCO_3 , cannot be explained by any of these mechanisms. However, two other mechanisms not usually seen in synthetic composites probably are the causes of the extensive toughness and strength increase. Both sliding of CaCO_3 layers on each other and organic "ligament" formation between layers occur when the resolved applied stresses are parallel and perpendicular to the layers, respectively (Figures 1(a) and (b)). The sliding mechanism in the nacre is reminiscent of plastic deformation by the movement of dislocation on slip planes in metals. Therefore, the propagating crack can only advance under constrained crack opening conditions, and only after considerable energy absorption, which results in a toughness increase. Both of these toughening mechanisms require that the organic phase be highly plastic and that the interface between the CaCO_3 and the organic phase be "strong."¹³ In the above qualitative analysis neither the crystallographic configuration of the individual CaCO_3 plates nor the organization of the macromolecules (which are in the liquid crystalline form) is considered.

DESIGN GUIDELINES ON LAMINATED MATERIALS

The unusual combination of mechanical properties in the nacre as compared to synthetic ceramics and composites comes from (i) the intrinsic properties of the component phases (inorganic-brittle and organic-soft), (ii) the unique and highly ordered microstructure, and (iii) the size of the layers. Therefore, a number of design guidelines can be drawn from the study of the seashells. Based on the study of nacre, synthetic composites should possess:

- (i) a laminate thickness of the hard-brittle component of less than $1 \mu\text{m}$ and a soft component of less than 1000 \AA ;
- (ii) a highly plastic soft phase;
- (iii) strong interfaces between the soft and the hard phases;
- (iv) the ability of the soft phase to bind to the hard phase (strong interfacial bonding) and provide either plasticity to the whole composite (for sliding) or form ligaments to constrain crack opening, depending upon the resolved applied stresses

In practical processing, these guidelines may be difficult to apply. However, they are useful in the sense that they serve as ultimate conditions to be achieved for submicron laminate design. In the present study with B_4C -Al, mimicking lamination even with laminate thicknesses larger than $10 \mu\text{m}$ resulted in both fracture toughness and fracture strength improvements of more than 40%, as discussed in the next section.

PROCESSING OF LAMINATED B_4C -Al COMPOSITES

Materials

Two types of B_4C powders (supplied by the ESK Company) were used as starting powders. The main difference between the two powders that is of interest for this work was their packing behavior as a function of pH, as shown in Figure 2. ESK 1500 B_4C shows a lower packing green density compared to ESK sintering powder at all pH values.²⁴ The pH was adjusted with reagent grade HCl or NH_4OH . Rhoplex 11A-8, a polyacrylic-based emulsion from Rhom and Haas, was used as a binder. DF-160L foamaster from Henkle was used as a defoamer agent. Finally, aluminum alloy 1100 was used as the source of the metal phase.

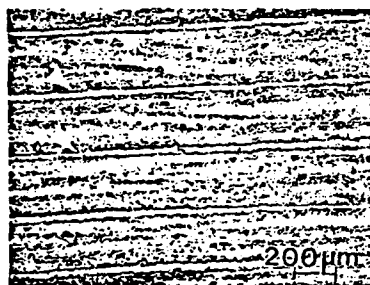


Figure 3. Laminated B_4C -Al composites processed by the first method. Arrows show Al-rich regions.

Fabrication of the Laminated Structure

The laminated composites were formed by three basic methods: (i) Partially sintered B_4C tapes were sandwiched with Al sheets and then heated to induce infiltration. (ii) Green B_4C tapes were stacked, partially sintered, and then metal infiltrated. (iii) Green B_4C tapes of different porosity were laminated (stacked and pressed), partially sintered, and then metal infiltrated.

In the first method, after B_4C tapes were cast, each tape was individually sintered to the desired density between polished graphite discs in order to prevent curling. Sintered tapes were then stacked with Al sheets and the whole stack was then heated to induce infiltration. The resulting structure was a B_4C -Al composite with Al interlayers (Figure 3). In the second method, B_4C tapes were stacked and the entire stack was then sintered. The resulting sintered body was composed of individual tapes of known density which were tightly sintered together but had almost a continuous thin gap between the tapes. The body was then infiltrated with aluminum. The resulting structure was a B_4C -Al composite with a thin ($\sim 5 \mu m$) Al interlayer (Figure 4). This method was used when B_4C tapes were thinner than $90 \mu m$. At these thicknesses, tapes could not be sintered by the first method without introducing defects into them. In the third method, tapes of B_4C with different green densities were stacked and laminated under pressure and temperature. The laminated body was then sintered and subsequently infiltrated with Al. The resulting structure is a B_4C -Al composite with graded morphology (Figure 5).

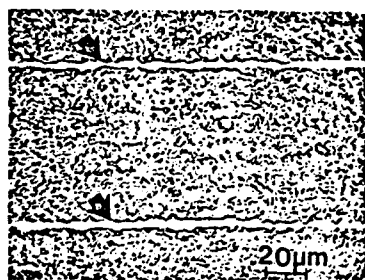


Figure 4. Laminated B_4C -Al composites processed by the second method. Arrows show Al-rich regions.

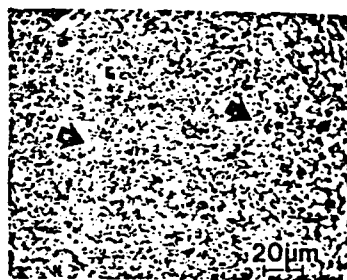


Figure 5. Laminated B_4C -Al composites processed by the third method. Arrows show Al-rich regions.

RESULTS: MICROSTRUCTURES VERSUS MECHANICAL PROPERTIES IN B_4C -Al MICROLAMINATES

The fracture strengths of the B_4C -Al composites were evaluated with four-point bend specimens, having a size of approximately 3 mm × 3 mm × 55 mm with a 1 μm surface finish. The test conditions were as follows: minor span size 12.7 mm, major span size 38.1 mm, and crosshead speed 0.05 mm/min. Fracture toughness was measured using approximately the same size bars with a single straight notch. The notch was cut by a diamond wheel saw with a 250-micrometer width. The tip of the notch was damaged by using 1/4 micrometer diamond paste and a razor blade. The ratio of the notch size to the sample height was 0.33. A three-point bend fixture and a crosshead speed of 0.05 mm/min were used.

Mechanical property testing of laminated B_4C -Al cermets showed an increase in fracture strength and toughness over the same Al-content materials processed with a monolithic morphology. Both the laminated structures with continuous Al layers (methods i and ii) or with graded structures (method iii) showed significant increases in fracture strength over monolithic material (Figure 6). However, the fracture toughness of the structures with continuous Al layers was found to be lower than the monolithic material. Further, as the Al content increased, the value of fracture toughness decreased. This is due to regions in the microstructure where Al is depleted, as shown in the scanning electron microscope (SEM) image (Figure 7). This depleted Al region is partially due to the precipitation of AlB_2 in the Al layers as well as processing defects caused by the infiltration of thin, sintered boron carbide tapes. In a fully dense composite without interfacial reaction products, the Al layers act as effective barrier against crack propagation (Figure 8).

The Al content of laminated samples in Figure 7 was altered by changing the ratio between the Al-rich and B_4C -rich layers in the microstructure. In Figure 9, the fracture strength and fracture toughness values are plotted versus the thickness ratios for laminated samples of Figure 6. It was revealed that a ratio of 6 to 1 of high boron carbide content tape to low boron carbide tape (and hence the Al-rich region in the post infiltration microstructures) with a 33.3 vol. % Al content (Figure 6) results in the highest fracture strength (945 MPa). Samples with a continuous Al layer do not show a maximum in fracture strength and the trend on fracture toughness is the opposite compared to graded samples.

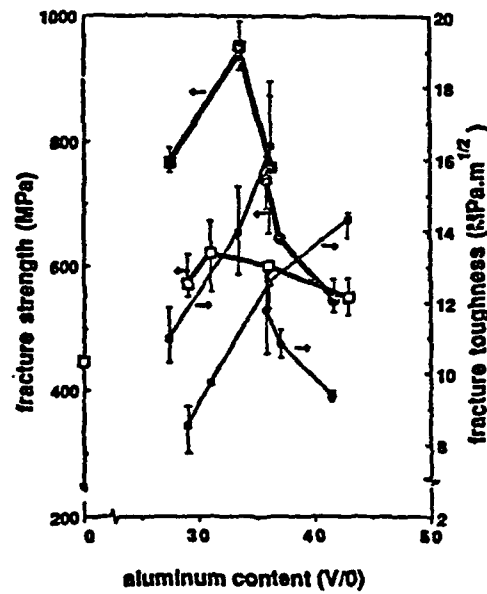


Figure 6. Fracture strength and fracture toughness of B_4C -Al composites. (□) monolith, (●) laminate with continuous Al layers, (■) laminate with graded layers.

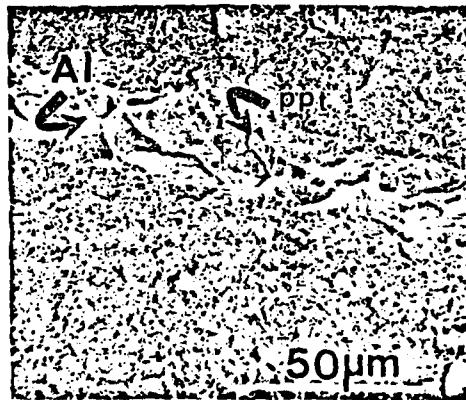


Figure 7. An example of depleted Al region.

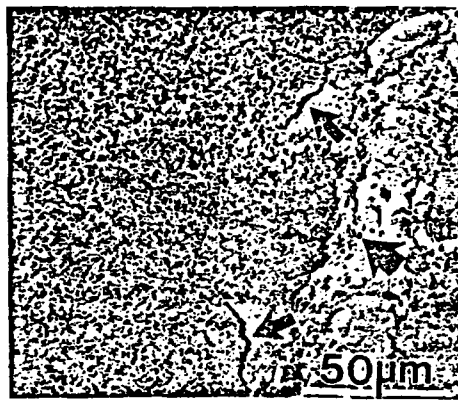


Figure 8. Blunting of a crack at the Al-rich region (SEM image).

After the proper ratio of high B_4C content to low B_4C content (or Al-rich laminae) was determined to be 6 to 1, simultaneous changes in the size of both laminae were made while maintaining the ratio.

The effect of changing the thickness of the laminae on both fracture strength and fracture toughness is shown in Figure 10. As expected from the Hall-Petch relation, the coarsening of the microstructure by increasing the tape thicknesses degraded the mechanical properties, with values approaching those for monolithic samples. Finer 6 to 1 ratio graded laminate structures have not been processed at this time due to the difficulty in casting and handling tapes thinner than 15 μm.

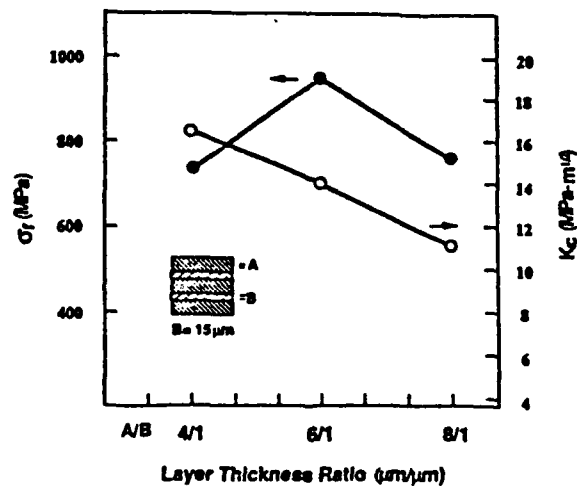


Figure 9. Fracture strength and fracture toughness plotted against B_4C thickness ratios.

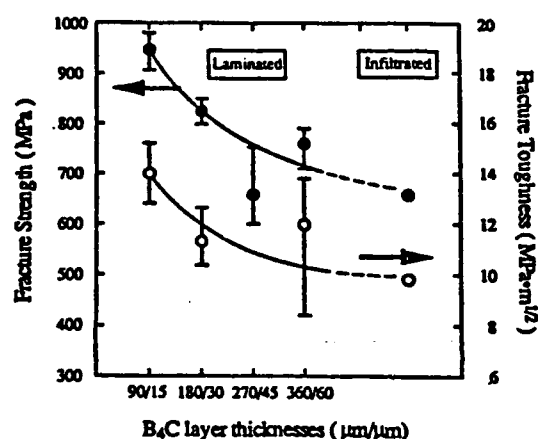


Figure 10. Fracture strength and fracture toughness vs. B₄C thickness plots.

SUMMARY AND CONCLUDING REMARKS

It was illustrated in this work that by processing materials based on the microstructures in biological systems, it is possible to significantly improve their properties. In biological systems, such as in the nacre section of the abalone shell, the microstructure is highly controlled, down to the nanometer scale. In the nacre shell structure, the component phases, CaCO₃ (aragonite) and organic matrix (a composite of chitin and macromolecules) form laminates 0.25 μm and 0.05 μm thick, respectively, stacked together to form an overall thickness up to a centimeter. Because of this unique microarchitecture, and also due to the properties of interfaces and the organic layer, unusual toughening and strengthening mechanisms operate, resulting in unexpectedly high mechanical strength and toughness values.

The processed B₄C-Al laminated cermets, based on the design principles outlined in the nacre, also show improvement in mechanical properties, both in fracture toughness and strength. These laminates were processed by tape casting of the B₄C layers which were then infiltrated with molten Al. The resulting microstructure produces layers of B₄C and Al, which are both continuous (unlike in the nacre) and have minimal reaction products at metal-ceramic contacts but still ensures a highly strong interface (like in the nacre).

Neither the fracture toughness nor the fracture strength of the nacre can be predicted based on the known relationships between the fracture toughness and critical flaw size (as in the Griffith relation), nor between the strength and the grain (or laminate) size (as in the Hall-Petch relationship). It should be noted that seashells have many different shapes with different microstructures, but all are based on the same basic components, i.e., CaCO₃ and the organic component.¹² Their microstructures have widely varying properties. The organic component can have its own unique "microstructure" in each of these cases. These issues have not been addressed in this paper. Only the gross microstructural features of the nacre have been mimicked in B₄C-Al laminates. In addition, in the case of B₄C-Al cermets, the size of the laminated layer is far from what might be required to achieve the unusual increases in mechanical properties as seen in the nacre. These issues, therefore, call for further detailed

studies in the biomimicking area in order to process highly ordered and tailored microstructures to achieve specific, non-isotropic properties in materials.

ACKNOWLEDGMENTS

This work was supported by the Air Force Office of Scientific Research (AFOSR) and was monitored under Grant Nos. AFOSR-87-0114 and AFOSR-89-0496.

REFERENCES

1. F. D. Lemkey, in *Industrial Materials Science and Engineering*, edited by L. E. Murr (Marcel Dekker, New York, 1984), p. 441.
2. J. D. Holder and G. W. Clark, in *Advanced Fibers and Composites for Elevated Temperatures*, edited by I. Ahmad and B. R. Noton (American Institute of Mining, Metallurgical, and Petroleum Engineers, Inc., New York, 1980), p. 225.
3. A. S. Yue, in *Quantitative Relation Between Properties and Microstructure*, edited by D. G. Brandon and A. Rosen (Israel University Press, Jerusalem, 1969), p. 209.
4. W. J. Minford, F. L. Kennard, R. C. Bradt, and V. S. Stubican, in *Ceramic Microstructures '76: With Emphasis on Energy-Related Applications*, edited by R. M. Fulrath and J. A. Pask (Westview Press, Boulder, Colorado, 1977), p. 456.
5. V. S. Stubican, R. C. Bradt, F. L. Kennard, W. J. Minford, and C. C. Sorrell, in *Tailoring Multiphase and Composite Ceramics*, edited by R. E. Tressler, G. L. Messing, C. G. Pantano, and R. E. Newnham (Plenum Press, New York, 1986), p. 103.
6. J. D. Hong, K. E. Spear, and V. S. Stubican, *Mat. Res. Bull.*, **14**, 775 (1979).
7. A. F. Jankowski and T. Tsakalakos, in *Layered Structures and Epitaxy, MRS Symp. Proc., Vol. 56*, edited by J. M. Gibson, G. C. Osbourn, and R. M. Tromp (Materials Research Society, Pittsburgh, Pennsylvania, 1986), p. 407.
8. D. Baral, J. B. Ketterson, and J. E. Hilliard, *J. Appl. Phys.*, **57** (4) 1076 (1985).
9. D. Wolf and J. F. Lutsko, *Phys. Rev. Lett.*, **60** (12) 1170 (1988).
10. R. C. Cammarata, in *Multilayers: Synthesis, Properties, and Non-Electronic Applications*, edited by T. W. Barbee, Jr., F. Spaepen, and L. Greer (Materials Research Society, Pittsburgh, Pennsylvania, 1989), p. 315.
11. R. C. Cammarata, *Scripta Metallurgica*, **20**, 479 (1986).
12. J. D. Currey, *Journal of Materials Education*, **9** (1,2) 120 (1987).
13. M. Sarikaya, K. E. Gunnison, M. Yasrebi, and I. A. Aksay, to appear in *Materials Synthesis Utilizing Biological Processes, MRS Symp. Proc., Vol. 174*, edited by P. Rieke, P. Calvert, and M. Auper (Materials Research Society, Pittsburgh, Pennsylvania, 1990), p. 109.
14. J. Cook and J. E. Gordon, *Proc. Roy. Soc.*, **A282**, 508 (1964).

15. L. S. Sigl, P. A. Mataga, B. J. Dalgleish, R. M. McMecking, and A. G. Evans, *Acta Metall.*, 36, (4) 945 (1988).
16. A. G. Evans and D. V. Marshall, *Acta Metall.*, 37 (10) 2567 (1989).
17. V. D. Kristic and M. Komac, *Phil. Mag.*, A51 (2) 191 (1985).
18. G. Kreimer, *Strength of Hard Alloys* (Consultants Bureau, New York, 1968), p. 6.
19. H. F. Fischmeister, in *Science of Hard Materials*, edited by R. Viswanadham, D. Rowcliff, and J. Gurland (Plenum Press, New York, 1983), p. 1.
20. A. J. Pyzik, I. A. Aksay, and M. Sarikaya, in *Ceramic Microstructures '86: Role of Interfaces*, edited by J. A. Pask and A. G. Evans (Plenum Press, New York, 1987), p. 45.
21. D. C. Halverson, A. J. Pyzik, and I. A. Aksay, *Cer. Eng. Sci. Proc.*, 6, 736 (1985).
22. D. C. Halverson, A. J. Pyzik, I. A. Aksay, and W. E. Snowden, *J. Am. Ceram. Soc.*, 72 (5) 775 (1989).
23. A. J. Pyzik and I. A. Aksay, in preparation.
24. M. Yasrebi, D. L. Milius, G. H. Kim, and I. A. Aksay, University of Washington, unpublished result (1990).

APPENDIX IV

Alginate as a Ceramic Processing Aid

by

N. B. Pellerin, G. L. Graff, D. R. Treadwell, J. T. Staley, and I. A. Aksay

submitted to
Journal of Industrial Microbiology
1991

ALGINATE AS A CERAMIC PROCESSING AID

by

Nancy B. Pellerin,[†] G. L. Graff,[‡] David R. Treadwell,[‡]

James T. Staley,^{†} and Ilhan A. Aksay[‡]*

Department of Microbiology,[†]

and

Department of Materials Science and Engineering;[‡]

and Advanced Materials Technology Center,

Washington Technology Center,

University of Washington,

Seattle, WA 98195

***Corresponding author.**

ABSTRACT

Alginic acid obtained from *Macrocystis pyrifera* (kelp) has been used in a novel way to produce stable suspensions of α - Al_2O_3 ceramic particles for use in processing high (> 40%) packing density compacts. Native alginate was effective in producing low viscosity, stable suspensions up to only 20 vol% solids since the high viscosity of the polymer solution interfered with the preparation of suspensions with solids concentrations above this limit. The hydrolysis products of alginic acid, polymannuronic acid- and polyguluronic acid-rich fractions, were effective in producing stable suspensions up to 30 and 40 vol%, respectively. In addition, the polyguluronic acid-rich fraction proved a more effective suspension stabilizer than the polymannuronic acid fraction. The higher charge density resulting from the tertiary structure of polyguluronic acid appears to be responsible for its more effective role as a dispersant.

INTRODUCTION

Recent progress in the field of ceramics has focused on the development of highly dense, homogeneous materials for new applications such as ceramic engine components and superconductive composites (18). For these applications, nonclay materials such as alumina (Al_2O_3) are synthesized in very small (submicron) sizes. Submicron particle systems yield finer grained products after sintering, provided that they can first be compacted to a high density state with uniform pore size distribution. However, a long-standing problem is that these submicron-sized particles are highly attracted to each other due to van der Waals forces, causing aggregations which effectively increase the particle size and leave undesired voids in the finished product (1). The prime requirement for a high green density in the compact is

that particles either first be completely dispersed in the solvent system and exhibit no agglomeration, or be weakly agglomerated to allow restructuring to a dense packing state (2).

One method to overcome agglomeration and achieve dispersion is to use a polyelectrolyte to coat the particles, which creates a net repulsive force between the particles due to electrosteric interactions (4,3). The synthetic polymer, poly(methacrylic acid) (PMAA) has been commonly used to disperse alumina in aqueous suspensions. This polymer causes a decrease in the interparticle attraction as reflected by a decrease in the viscosity of the suspension and, thus, an increase in the packing density of the powder compact (4,3). However, PMAA and its monomer, acrylic acid, are toxic and corrosive (14).

In this paper, we report the use of a naturally occurring, nontoxic polymer that can produce well-dispersed colloidal suspensions of submicron-sized alumina particles. We have demonstrated that alginate obtained from the marine alga *Macrocystis pyrifera* (kelp) has dispersing capabilities comparable to PMAA. Furthermore, it is neither toxic nor corrosive and thus the use of this biopolymer provides an attractive option for manufacturing ceramics with ecologically balanced procedures.

Alginate is a block copolymer of the isomers D-mannuronic (M) and L-guluronic (G) acids. The biosynthesis is thought to involve the initial formation of polymannuronic acid, followed by the epimerization of D-mannurosyl residues to L-gulurosyl residues (8). The two uronides are distributed along the chain in blocks of three types, polymannuronic acid (poly M), polyguluronic acid (poly G), and polymannuronic-guluronic acid (poly MG) (7,10,9,12). A similar polymer is produced extracellularly by some bacteria, including *Azotobacter vinelandii* (16) and various *Pseudomonas* species (13). *P. aeruginosa* strains noted for alginate production

have been obtained from patients suffering from respiratory infections accompanying cystic fibrosis (5). In the case of clinical isolates, it is thought that the production of polymer by the bacterium confers protection from antibiotics.

MATERIALS AND METHODS

Materials and Chemicals

The ceramic powder used in this study was a high purity (99.99%) α -Al₂O₃ with an average particle size of 0.4 μ m as determined by x-ray sedigraph (AKP-30 Sumitomo Chemical America, Inc., New York, N.Y.).

The polymer used was a low viscosity kelp alginate (75,000 - 100,000 MW) (Sigma Chemical Company, St. Louis, Mo.). Low molecular weight fractions were prepared by hydrolysis in 0.1 N HCl under reflux for 4 h. The solution was centrifuged, after which the pellet was dissolved using NaOH. The guluronic acid fraction was obtained by lowering the pH to 2.4 and collecting the precipitate; the mannuronic acid fraction was precipitated by further lowering the pH to 1.3. (J. M. Beale, personal communication.)

Reagent grade HCl and NaOH were used for pH adjustments. Distilled water was used throughout. Mannuronic acid lactone was obtained from Sigma Chemical Company (Sigma Chemical Company, St. Louis, Mo.).

Sedimentation Experiments

Sedimentation columns were prepared with 2 vol% α -Al₂O₃ in aqueous solutions of polymer. The suspensions were sonicated for 5 min, mixed on a magnetic stirrer for 30 min, and the pH adjusted to the experimental value before bringing the final volume to 10 ml. The

suspension was decanted into a conical bottom, graduated polystyrene tube (Falcon 2095, Becton Dickinson, Cockeysville, Md.) and left undisturbed for several weeks. Final powder compact volumes were measured to ± 0.1 ml. The wet sediment density was calculated as $[\text{theoretical volume/final volume}] \times 100$.

Viscosity Measurements

Suspensions for viscosity measurements were prepared with 30 - 40 vol% $\alpha\text{-Al}_2\text{O}_3$ in 0.5% (dry weight basis (dwb)) aqueous solution of polymer (pH 5 or 8) and mixed as above. Measurements were obtained by the method of Cesarano and Aksay (3) using a digital viscometer (Model RVT-D, Brookfield Engineering Laboratories, Inc., Stoughton, Mass.). Viscosities of polymer solutions were measured on a Rheometrics Fluid Spectrometer (Model 8400, Rheometrics Inc., Piscataway, N.J.).

Determination of Degree of Polymerization of Alginate Oligomers

Samples of the poly M and poly G fractions and unhydrolyzed alginic acid were each mixed with 1 ml of D_2O and dissolved by adding a few drops of 5% NaOD in D_2O . The pD of the solutions was adjusted to slightly acidic with 1% DCl in D_2O . Na_2EDTA was added to complex any Ca^{2+} present. The ^1H NMR spectra of the samples were recorded on a Varian VXR 300 spectrometer at 300 MHz and analyzed by the method of Grasdalen (7,6). The chemical shifts are reported in ppm downfield of internal 3-trimethylsilyl-1-propanesulfonic acid-2,2,3,3- d_4 sodium salt. The ratios of mannuronate to guluronate were determined from the integrals of the anomeric protons: M at 4.64 δ and G at 5.02 δ . The degrees of polymerization of the poly M and poly G fractions were estimated by the ratio of the sum of the

integrals of these two peaks to that of the reducing-end protons at 5.20 δ (see Table 1). The linewidths of the unhydrolyzed alginic acid were too great to yield useful information.

RESULTS AND DISCUSSION

Effect of pH on the Particle Packing Density

Several factors must be considered when working with polyelectrolytes in aqueous solutions. First, the dissociation behavior of the polymer is typically affected by the solution pH. The dissociation of a weak acid group on the polyelectrolyte depends on the overall degree of polymer dissociation, since dissociation of a proton from an already ionized polyacid is hampered by the negative potential of such a polyacid (11). Thus the pK_a varies for every acid site and increases as each successive site dissociates. Second, the surface charge of the alumina particles varies from highly positive at low pH to negative at high pH with the zero point of charge (zpc) occurring near pH 8.7 (4). These factors result in suspensions that are extremely pH sensitive.

In order to determine the optimum pH range for the alginate/alumina system, we prepared a series of sedimentation tests under different pH conditions (Fig. 1). At low pH (2.8), the suspension was flocculated, with a compact of less than 10% theoretical density. It is known that aqueous suspensions of $\alpha\text{-Al}_2\text{O}_3$ are electrostatically stable at this pH due to the high surface charge on the particles (1). The observed flocculation implies that when the polymer contains low numbers of dissociated COO^- sites (as at pH 2.8), the positive charges on the particle surface are neutralized by the negative sites on the adsorbed polymer, thus eliminating the coulombic repulsions between particles.

The increase in compact densities with increased pH reflects an increasing degree of dissociation of the polymer. Interestingly, maximum sediment densities were obtained near pH 8 where the polymer is fully dissociated and the surface of the alumina particles is slightly below the zpc. This condition provides the maximum electrosteric contribution from the polymer while providing a driving force for high affinity adsorption of the negatively charged polymer on the positive charge sites of the particle.

Effect of Polymer Concentration

To determine the optimum concentration of polymer required to disperse the alumina powder, a series of sedimentation tests was performed at a fixed pH of 8.5. Dilute (2 vol%) suspensions were prepared with various concentrations of polymer on a dry weight basis (dwb) of the powder. Figure 2 shows the wet sediment densities obtained in these suspensions after several weeks of settling. In the absence of polymer, the suspension is unstable, with particles spontaneously agglomerating and settling into poorly packed, ramified structures with packing densities of approximately 10% of the theoretical value. Addition of 0.1% (dwb) polymer had no observable effect, but at slightly higher polymer concentrations, the sediment densities increased dramatically. At a polymer concentration of 0.5% (dwb), the compacts reached a maximum density of greater than 40% theoretical density. This indicates that the added polyelectrolyte is acting to stabilize the particles in suspension by creating a barrier against spontaneous flocculation of the individual particles. This facilitates particle packing upon consolidation in the sediment, resulting in the higher densities observed.

Cesarano et al. (4) reported wet sediment densities of approximately 50% theoretical density for the poly(methacrylic acid)-Na (PMAA) stabilized alumina suspensions. The lower

packing densities (40%) observed with the alginate could be due to several effects. First, the higher molecular weight of the alginate (100,000) compared to the PMAA (15,000) would tend to create a thicker adsorbed polymer layer on each individual alumina particle (11). The increased volume occupied by the adsorbed polymer would increase the interparticle separation distance and could easily account for a 10% decrease in final sediment density. A second explanation might be the difference in charge density between the two polyelectrolytes. Fully dissociated PMAA has a charged COO^- site for each ethyl group along the polymer backbone. By comparison, the alginate contains a single carboxylic acid for each hexose unit. These differences in structure result in approximately twice (1.84 times) the number of charged sites for PMAA compared to alginate, given identical molecular weight polymer segments. This lower charge density along the polyelectrolyte backbone may result in alginate suspensions that are mildly agglomerated, with lower particle packing densities.

Figure 2 further shows a distinct maximum in sediment density at a polymer concentration of 0.5% (dwb), with a decrease in packing density at higher concentrations. This indicates that full surface coverage of the alumina particles by the alginate occurs at approximately 0.5% (dwb). The decrease in packing densities above the saturation adsorption limit is most likely due to excess polymer in solution causing depletion flocculation of the particles (3). As discussed in the following section, it is also possible that the excess alginate in solution is forming a soft gel which prevents close packing of the particles during sedimentation.

Viscosities of Highly Concentrated Suspensions

To better understand the role of the alginate in controlling particle-particle interactions, we measured the viscosities of concentrated alumina suspensions prepared with the polymer.

The viscosity of the suspension provides information on the effectiveness of the polymer in stabilizing the suspension.

In our experiments, we measured the viscosity of the suspension as the shear rate was decreased from 93 s^{-1} to 0.47 s^{-1} , held at 0.47 s^{-1} for 5 min, and then increased. Figure 3 shows the thixotropic loop obtained for a 30 vol% suspension of particles in alginate solution. After 10 min at a low rate of mixing, the viscosity nearly doubled, but as the rate of mixing was increased, the viscosity again decreased.

There are two possible explanations for the increase in viscosity at a low rate of mixing: (i) the polymer may be forming a gel structure which is disturbed by more vigorous mixing or (ii) the suspension may be unstable, i.e., the particles may be flocculating (agglomerating) to form a network structure in the suspension due to insufficient stabilization. Based on the following evidence, the first of these two phenomena appears to be the cause of the high viscosities.

First, when we prepared a 40 vol% suspension of particles in alginate (Fig. 4), the suspension showed different characteristics from the 30 vol% suspension. Here, the viscosity displayed less hysteresis, but at all rates the viscosity was 10-fold higher than the 30 vol% suspension. The suspension acted like a soft gel, leading us to suspect that the polymer was contributing to the high viscosity.

Second, when we compared the viscosities of solutions of alginate in water without the particles, we found that the viscosity of the polymer solution alone in the 30 vol% suspension to be 160 mPa·s and in the 40 vol% suspension to be 341 mPa·s. These two observations provide strong evidence that the polymer forms a gel in the solution.

Low Molecular Weight Fractions as Dispersants

We next investigated whether lower molecular weight fractions would be effective as dispersants and would avoid the problem of gel formation encountered with the native polymer. Kelp alginate (75,000 - 100,000 MW) was hydrolyzed in 0.1 N HCl for 4 h, after which two fractions were collected by fractional precipitation. Fraction G was collected by precipitation at pH 2.4. The degree of polymerization and uronide composition were determined by NMR (Table 1). This fraction contained an oligomer with an average degree of polymerization greater than 24 (≥ 4800 MW) and a ratio of guluronic to mannuronic acid of 6 to 1. The viscosities of solutions of the oligomer in water were reduced approximately one hundred-fold as compared to the native polymer (Table 2).

Fraction M, with an average degree of polymerization of about 18 and molecular weight ~ 3600 (Table 1), was precipitated at pH 1.3. It contained more than 10 mannuronate residues to 1 guluronate residue. Viscosity measurements were not performed, but the values would be expected to be similar to or less than the G fraction since the gel-forming capacity of the polymer is directly related to the guluronic acid content (15).

We also included the mannuronic acid monomer in this study to determine the effectiveness of a single uronic acid sugar as a dispersant. This was obtained by treating commercially available mannuronic lactone with base (final pH 8.3).

The packing densities obtained with these fractions show clearly that there are differences in their ability to stabilize suspensions (Fig. 5). The G fraction was effective over a wider concentration range than the native alginate, and slightly less oligomer was needed to produce an effect equal to the native polymer. The M fraction was effective only at higher concentrations

(0.4 to 0.5% dwb) of oligomer to particle. The monomer had only a slight effect at very high concentrations (1% dwb) and could not be considered a useful suspension stabilizer.

The viscosities of concentrated suspensions prepared with 0.5% (dwb) of the oligomers again show a difference between the fractions (Table 3). The M fraction stabilized suspensions at 30 vol% solids loading, while the G fraction was capable of stabilizing suspensions with 40 vol% solids. A fluid ($< 1 \text{ Pa}\cdot\text{s}$) 50 vol% suspension could not be prepared at pH 8 with the M fraction because of particle agglomeration, yet the G fraction yielded a weakly flocculated, low viscosity suspension at this solids loading.

The reason for these differences may lie in the molecular conformation of the two oligomers. In order for the bulky carboxyl groups to be in the energetically favored equatorial position, the two isomers adopt different chain forms when in solution (15). The resultant glycosidic bonds at positions 1 and 4 are equatorial in β -D-mannuronate but axial in α -L-guluronate. This would lead to a flat, ribbonlike conformation in polymannuronic acid sequences, whereas polyguluronic acid would adopt a buckled conformation. The buckled arrangement brings the oxygens on either side of the glycosidic bond in close proximity in the case of poly G, leading to a localized increase in charge density (17). This is likely the reason why polyguluronic acid acts as a more effective polyelectrolyte for the stabilization of ceramic particles than polymannuronic acid.

CONCLUSIONS

We have demonstrated that the uronic acid-containing polysaccharide (alginate) is a useful dispersant in preparing concentrated, aqueous suspensions of ceramic powders. This represents

an easily isolated, inexpensive, and nontoxic polymeric additive for potential commercial applications where ecologically balanced processing may be of concern.

In addition, we have shown that oligomeric fractions of the native alginates are equally effective, or superior, as dispersants in colloidal alumina suspensions. Therefore, the undesirable gelling characteristics of the high molecular weight alginates can be eliminated while maintaining the necessary suspension stabilizing properties.

ACKNOWLEDGMENTS

This work was supported by a grant from the United States Air Force Office of Scientific Research (AFOSR) and monitored under Grant No. AFOSR-88-0135. We thank John M. Beale and Blain Mamiya for helpful discussions.

LITERATURE CITED

1. Aksay, I. A. 1984. Microstructure Control through Colloidal Consolidation, pp. 94-104. *In* J. A. Mengels and G. L. Messing (ed.), *Advances in Ceramics 9, Forming of Ceramics*. American Ceramic Society, Columbus, Ohio.
2. Aksay, I. A. 1988. Principles of Ceramic Shape-Forming with Powder Systems, pp. 663-674. *In* G. L. Messing, E. R. Fuller, Jr., and H. Hausner (ed.), *Ceramic Powder Science II, Ceramic Transactions, Vol. 1*. American Ceramic Society, Columbus, Ohio.

3. Cesarano, J., III, and I. A. Aksay. 1988. Processing of Highly Concentrated Alumina Suspensions Stabilized with Polyelectrolytes. J. Am. Ceram. Soc. 71[12]:1062-1067.
4. Cesarano, J., III, I. A. Aksay, and A. Bleier. 1988. Stability of Aqueous Al₂O₃ Suspensions with Poly(methacrylic acid) Polyelectrolyte. J. Am. Ceram. Soc. 71[4]:250-255.
5. Govan, J. R. W. 1976. Antibiotic Therapy and Cystic Fibrosis: Increased Resistance of Mucoid *Pseudomonas aeruginosa* to Carbenicillin. J. Antimicrobial Chem. 2:215-217.
6. Grasdalen, H. 1983. High Field ¹H-NMR Spectroscopy of Alginate: Sequential Structure and Lineage Conformations. Carbohy. Res. 118:255-260.
7. Grasdalen, H., B. Larsen, and O. Smidsrød. 1979. A P.M.R. Study of the Composition and Sequence of Uronate Residues in Alginates. Carbohy. Res. 68:23-31.
8. Haug, A., and B. Larsen. 1971. Biosynthesis of Alginate. Part II. Polymannuronic Acid C-5-epimerase from *Azotobacter vinelandii* (Lipman). Carbohy. Res. 17:297-308.
9. Haug, A., B. Larsen, and O. Smidsrød. 1974. Uronic Acid Sequence in Alginate from Different Sources. Carbohy. Res. 32:217-225.

10. Haug, A., B. Larsen, and O. Smidsrød. 1966. A Study of the Constitution of Alginic Acid by Partial Acid Hydrolysis. *Acta Chem. Scand.* 20:183-190.
11. Hesselink, F. Th. 1983. Adsorption of Polyelectrolytes from Dilute Solution, pp. 377-412. In G. D. Parfitt and C. H. Rochester (ed.), *Adsorption from Solution at the Solid/Liquid Interface*. Academic Press, New York.
12. Larsen, B., O. Smidsrød, T. Painter, and A. Haug. 1970. Calculation of the Nearest-Neighbour Frequencies in Fragments of Alginate from the Yields of Free Monomers after Partial Hydrolysis. *Acta Chem. Scand.* 24:726-728.
13. Linker, A., and R. S. Jones. 1966. A New Polysaccharide Resembling Alginic Acid Isolated from Pseudomonads. *J. Biol. Chem.* 241:3845-3851.
14. The Merck Index, 11th edition. 1989. Merck and Co., Rahway, N.J.
15. Penman, A., and G. R. Sanderson. 1972. A Method for the Determination of Uronic Acid Sequence in Alginates. *Carbohy. Res.* 25:273-282.
16. Pindar, D. F., and C. Bucke. 1975. The Biosynthesis of Alginic Acid by *Azotobacter vinelandii*. *Biochem. J.* 152:617-622.

17. Rees, D. A. 1972. Shapely Polysaccharides. *Biochem. J.* 126:257-273.
18. Ulrich, D. R. 1990. Chemical Processing of Ceramics. *Chem. Eng. News.* 68[1]:28-40.

FIGURE LEGENDS

- Figure 1.** Wet sediment densities of 2 vol% suspensions of alumina in alginate (0.5% dwb alumina) prepared at various pH.
- Figure 2.** Wet sediment densities of 2 vol% suspensions of alumina prepared with various concentrations of alginate (dwb alumina). The pH of the suspensions was adjusted to 8.5 - 8.6.
- Figure 3.** Viscosity curve obtained from a 30 vol% suspension of alumina in 0.5% dwb alginate. Open squares represent values obtained during increasing shear rate. Solid squares represent values obtained during decreasing shear rate.
- Figure 4.** Viscosity curve obtained from a 40 vol% suspension of alumina in 0.5% dwb alginate. Open squares represent values obtained during increasing shear rate. Solid squares represent values obtained during decreasing shear rate. The arrow represents an off-graph value of 10,500 mPa·s at the shear rate of 0.5 s^{-1} .
- Figure 5.** Wet sediment densities of 2 vol% suspensions of alumina prepared with native alginate, polyguluronic acid, polymannuronic acid, or mannuronic acid monomer. The pH of the suspensions was adjusted to 8.3 - 8.6.

TABLE 1. NMR Data for Determination of Uronide Residue Composition and Degree of Polymerization of Hydrolyzed Alginate Fractions.*

Sample	Polymer Wt (mg)	Na₂EDTA Wt (mg)	Final pD	%G	D.P.
Poly M	10.2	2.2	5.0	10	18
Poly G	9.0	2.0	5.3	83	> 24

*Transients collected: 128.

TABLE 2. Viscosities of Native Alginate and Polyguluronic Acid in Water.*

Sample	Viscosity (mPa·s)	
	30 vol%	40 vol%
Poly G	0.9	4.9
Native alginate	160	341

*Solutions were prepared to yield the same final concentrations as were in the 30 and 40 vol% suspensions, but the particles were omitted.

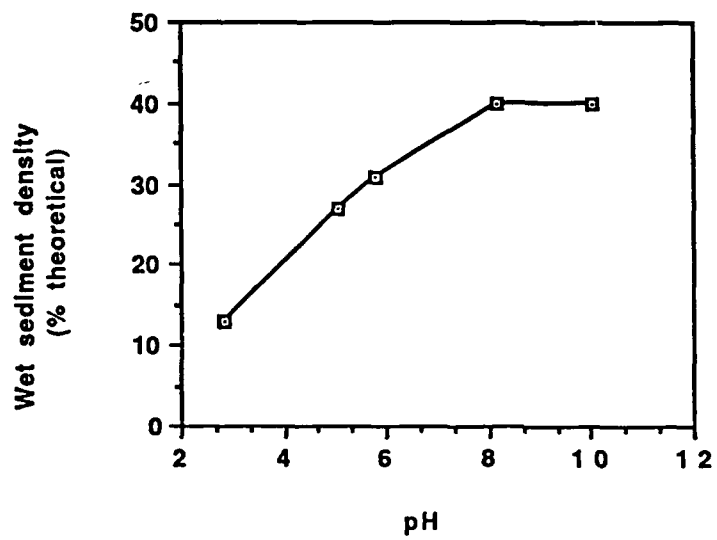
TABLE 3. Viscosities of Concentrated Suspensions of Alumina in Polymannuronic or Polygluronic Acid Fractions at a Shear Rate of 9.3 s^{-1} (mPa·s)

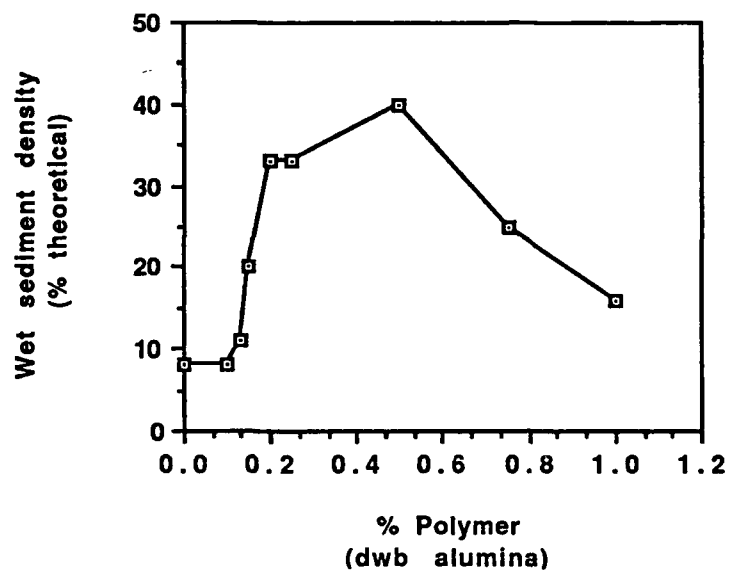
Fraction	pH	30 vol%	40 vol%	50 vol%
Poly G	8	40	230	470-625 Slightly flocculated
Poly G	5	< 20	35	110 Slightly flocculated
Poly M	8	95	465	Too viscous to be prepared

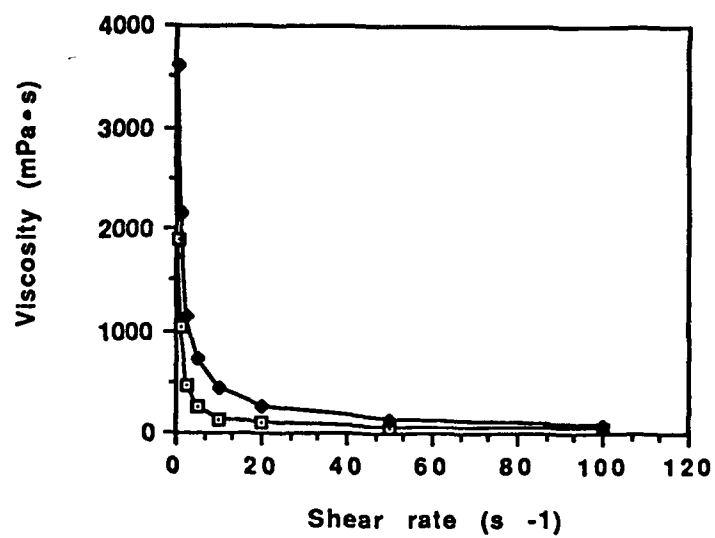
TABLE 3. Viscosities of Concentrated Suspensions of Alumina in Polymannuronic or Polygluronic Acid Fractions at a Shear Rate of 9.3 s^{-1} (mPa·s)

Fraction	pH	30 vol%	40 vol%	50 vol%
Poly G	8	40	230	470-625 Slightly flocculated
Poly G	5	< 20	35	110 Slightly flocculated
Poly M	8	95	465	Too viscous to be prepared

Fig 1







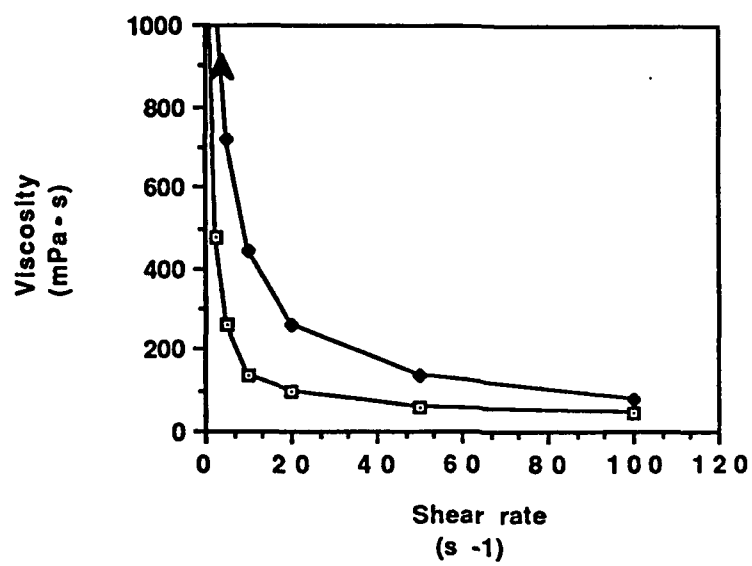
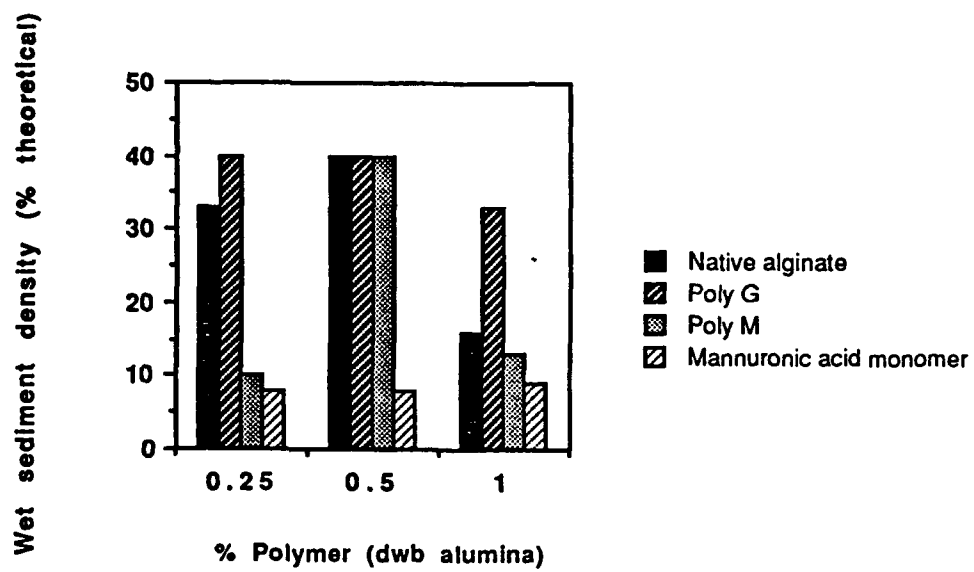


Fig. 5



APPENDIX V

Geometrical Arrangement of Magnetosomes in Magnetotactic Bacteria

by

W.-H. Shih, M. Sarikaya, W. Y. Shih, and I. A. Aksay

Materials Synthesis Based on Biological Processes

Materials Research Society Proceedings, Vol. 218

edited by M. Alper, P. C. Rieke, R. Frankel, P. A. Calvert, and D. A. Tirrell
(Materials Research Society, Pittsburgh, Pennsylvania, 1991) pp. 109-114

GEOMETRICAL ARRANGEMENT OF MAGNETOSOMES IN MAGNETOTACTIC BACTERIA

W.-H. SHIH, M. SARIKAYA, W. Y. SHIH, and I. A. AKSAY

Department of Materials Science and Engineering, and
Advanced Materials Technology Center, Washington Technology Center,
University of Washington, Seattle, WA 98195

Introduction

In 1975, Blakemore¹ discovered the freshwater magnetotactic bacterium *Aquaspirillum magnetotacticum* which navigates along the magnetic-field direction. Electron microscopic work showed that the magnetotactic bacteria contain magnetosomes which are intracytoplasmic membrane-bound particles of magnetite, Fe_3O_4 . The magnetosomes are within the single-domain size range ($\sim 500 \text{ \AA}$) of Fe_3O_4 . The magnetosomes within cells are often arranged in one or more chains with the chain axis more or less parallel to the axis of motility of the cell. A detailed study of the magnetic properties of magnetotactic bacteria can be found in the paper by Moskowitz.²

In this paper, we address the question of the arrangement of magnetosomes, with the intention of shedding light on the mechanism and sequence of the formation of magnetosomes. In a single chain of magnetosomes (Figure 1), all the magnetic moments are parallel to each other along the chain direction. The chain of magnetosomes thus has a permanent magnetic dipole moment equal to the moment of a magnetosome times the number of particles in the chain. The light scattering and birefringence experiments by Rosenblatt et al.³ confirmed that this was the case, and the resultant average magnetic dipole moment per cell was consistent with estimates based on the number of particles per cell from electron micrographs.

However, there have been many observations that multiple chains exist and the magnetic dipole moment configuration in this case is less clear. The goal of this study was to determine the possible magnetic moment configuration of multiple chains of magnetosomes. We adopted the chain of spheres model of Jacobs and Bean⁴ and calculated the magnetic energies of various magnetic moment configurations for each arrangement of magnetosomes. The lowest energy configuration was obtained for each arrangement. It was found that for the square-lattice arrangement of magnetosomes, the two chains would have opposite magnetic moments in order to stabilize this arrangement. However, for the close-packed arrangement of magnetosomes, the corresponding stable configuration would be that the magnetic moments of the two chains have the same orientation. For the purpose of navigating along a magnetic field, the bacteria would prefer the close-packed arrangement to maximize the net magnetic moment. This is indeed the case. Transmission electron microscopy (TEM) micrographs showed mostly close-packed arrangements for double chains (Figure 2). Furthermore, by comparing the energy gain of adding a particle at the end to adding one on the side of a chain, we found that it is always energetically favored to add a particle at the end of a chain. Therefore, from the energy minimization point of view, multiple chains are formed by combining existing single chains rather than by adding new particles one by one on the side of a single chain.

Chain of Spheres Model

The chain of spheres model of Jacobs and Bean⁴ can be used to describe the arrangement of magnetosomes. The interaction between two magnetic dipoles is

$$E = \frac{\mu_1 \mu_2}{r_{ij}^3} [\cos(\theta_i - \theta_j) - 3 \cos \theta_i \cos \theta_j] \quad (1)$$

where θ_i is the angle between the magnetic moment of particle i and the line connecting the centers of the two particles, and μ is the magnetic moment of a particle. For a chain of N particles, there are many possible magnetic moment configurations. The simplest configuration is parallel rotation, in which all the particles have moments pointing in the same direction with an angle θ with respect to the chain axis. In this case, the magnetic energy for a chain of N particles is

$$E_N = \frac{\mu^2}{a^3} (1 - 3\cos^2\theta) \sum_{j=1}^N \frac{N-j}{j^3}, \quad (2)$$

where a is the diameter of a sphere. Since all magnetic energy has a unit of μ^2/a^3 , we will omit that notation for convenience from here on in this paper. At the limit of $N \rightarrow \infty$ and $\theta = 0^\circ$, we obtained the energy per particle $E_0 = -2.404$. This energy E_0 is used as a criterion for determining whether a particular configuration of magnetic moment in multiple chains is stable or not. If the energy per particle of a particular configuration is larger than E_0 , then this configuration is considered not stable and the multiple chains will eventually separate.

Double Chains

The simplest multiple chain is a double chain. Two possible particle arrangements are considered: square-lattice and close-packed. An arrangement is defined as the pattern of the centers of all the particles. For simplicity, we considered the situation $N \rightarrow \infty$ first and then addressed the effect of finite N later.

For each arrangement, we minimize the interaction energy with respect to the angle θ and find the lowest energy configuration for each arrangement. We considered the parallel rotation configuration first. In the square-lattice arrangement, the magnetic moments in the two chains are anti-parallel, and the magnetic energy per particle due to dipole interaction is

$$E_{ps} = (1 - 3\cos^2\theta) \sum_{j=1}^{\infty} \frac{1}{j^3} + \frac{1}{2} (-1 + 3\sin^2\theta) + \sum_{j=1}^{\infty} \left\{ -1 + \frac{3}{1+j^2} (\sin^2\theta + j^2 \cos^2\theta) \right\} \frac{1}{(1+j^2)^{3/2}}. \quad (3)$$

Minimizing equation (3) with respect to θ , we obtained $\theta = 0^\circ$ and the energy $E_{ps} = -2.477$. Although the anti-parallel configuration is a stable configuration ($E_{ps} < E_0$), there is no net magnetic moment. The expression for a parallel configuration is similar to equation (3) except the signs change starting at the second term on the right-hand side. The parallel configuration has a net magnetic moment, but the energy, $E = -2.331$, is higher than E_0 meaning there is a repulsion between the two chains and the configuration is not stable. Therefore, the square-lattice arrangement can be stable but has no net magnetic moment.

In contrast, in the close-packed arrangement, the anti-parallel configuration has a magnetic energy per particle

$$E_{pc} = (1 - 3\cos^2\theta) \sum_{j=1}^{\infty} \frac{1}{j^3} + \sum_{j=0}^{\infty} \left\{ -1 + \frac{3}{1+j+j^2} \left(\frac{3}{4} \sin^2\theta + \left(\frac{1}{2} + j \right)^2 \cos^2\theta \right) \right\} \frac{1}{(1+j+j^2)^{3/2}}. \quad (4)$$

The minimum energy occurs at $\theta = 0^\circ$ and $E_{pc} = -2.226$. For the parallel configuration, the second term on the right-hand side of equation (4) changes sign, and $E_{pc} = -2.582$. Therefore, the parallel configuration is stable and at the same time has a finite net magnetic moment. The close-packed arrangement would be expected in TEM micrographs of double chains.

The other important magnetic dipole moment configuration is fanning, in which the magnetic moments of successive spheres in the chain fan out by rotating in alternate directions in alternate spheres. For a chain of spheres in the fanning configuration, the magnetic energy per particle is

$$E_f = (\cos 2\theta - 3\cos^2\theta)L_\infty + (1 - 3\cos^2\theta)M_\infty, \quad (5)$$

where

$$L_\infty = \sum_{j=1}^{\infty} \frac{1}{(2j-1)^3}, \quad M_\infty = \sum_{j=1}^{\infty} \frac{1}{(2j)^3}.$$

The lowest energy state for a single chain in the fanning configuration is $\theta = 0^\circ$ and $E_f = E_0$.

For double chains, in the square-lattice arrangement and anti-parallel fanning configuration, the resultant energy per particle is

$$\begin{aligned} E_{fs} = E_f + \frac{1}{2}(-1 + 3\sin^2\theta) + \sum_{j=1}^{\infty} \left\{ -1 + \frac{3}{1+4j^2}(\sin^2\theta + 4j^2\cos^2\theta) \right\} \frac{1}{(1+4j^2)^{3/2}} \\ + \sum_{j=1}^{\infty} \left\{ -\cos 2\theta - \frac{3}{1+(2j-1)^2}(\sin^2\theta - (2j-1)^2\cos^2\theta) \right\} \frac{1}{(1+(2j-1)^2)^{3/2}}. \end{aligned} \quad (6)$$

The lowest energy occurs at $\theta = 0^\circ$ and $E_{fs} = -2.477 = E_{ps}$. In the close-packed arrangement, we consider the parallel configuration only. The magnetic energy per particle in this case is

$$\begin{aligned} E_{fc} = E_f + \frac{1}{2} \sum_{j=0}^{\infty} \left\{ 1 - \frac{3}{1+j+j^2} \left(\frac{3}{4}\sin^2\theta + (1/2+j)^2\cos^2\theta \right) \right\} \frac{1}{(1+j+j^2)^{3/2}} \\ + \frac{1}{2} \sum_{j=0}^{\infty} \left\{ \cos 2\theta + \frac{3}{1+j+j^2} \left(\frac{3}{4}\sin^2\theta - (1/2+j)^2\cos^2\theta \right) \right\} \frac{1}{(1+j+j^2)^{3/2}}. \end{aligned} \quad (7)$$

The lowest energy occurs at $\theta = 0^\circ$, and $E_{fc} = -2.582 = E_{pc}$.

Although the fanning configuration does not produce any advantage in terms of energy and the results are the same as that of the parallel rotation configuration, there is a significant difference in the excitations of the energy minimum. The difference in excitations can most easily be seen by comparing the energy for a single chain. For a single chain in the parallel rotation configuration, equation (2) gives $E_p = -2.404 + 3.606\theta^2$ for small θ . Whereas in the fanning configuration, equation (5) gives $E_f = -2.404 + 1.503\theta^2$ for small θ . Therefore, if there is any excitation to a single chain, it will be in the fanning configuration rather than the parallel rotation configuration. Similar result can be obtained for double chains as well.

Formation of Double Chains

The question of where to add a new particle to an existing chain was also considered. This question was studied in the close-packed arrangement only since the square-lattice



Figure 1. TEM image of an *Aquaspirillum magnetotacticum*, displaying a single chain containing a row of particles.



Figure 2. Double-chain formation of magnetosomes in a bacterium



Figure 3. Smaller magnetosomes can be discerned towards the ends of a chain in this image of a bacterium.

arrangement is energetically unfavorable. The potential energy at the end of a chain of N particles is

$$\Delta_e = (1 - 3\cos^2\theta) \left(\sum_{j=1}^{N-1} \frac{1}{j^3} \right). \quad (8)$$

On the other hand, the potential energy on the side of a chain Δ_s depends on where the particle is located on the side. If N is even, and the particle sits at the middle on the side,

$$\Delta_s = \sum_{j=0}^{N/2} \left\{ 2 - \frac{6}{(1+j+j^2)} \left(\frac{3}{4} \sin^2\theta + (1/2 + j)^2 \cos^2\theta \right) \right\} \frac{1}{(1+j+j^2)^{3/2}}. \quad (9)$$

The minimum occurs at $\theta = 0^\circ$ for both equations (8) and (9). When $N \rightarrow \infty$, $\Delta_e = -2.38$ and $\Delta_s = -0.356$, and $\Delta_e < \Delta_s$. In fact, for all N values, $\Delta_e < \Delta_s$. Therefore, from the energy minimization point of view, a new particle is always added to the end of a chain rather than on the side. This result indicates that double chains are formed by combining two existing single chains rather than by adding new particles to the side of a chain. If two chains of magnetosomes have the same number of particles N , there exists a critical N_c such that for $N > N_c$, the two chains will combine, and for $N < N_c$, the two chains will separate. In the close-packed arrangement, using equation (4) and letting the limit of summation be finite, we found $N_c = 5$.

Transmission Electron Microscopy Observations

Analysis of the geometric arrangement of magnetosomes in *Aquaspirillum magnetotacticum* was done by TEM observations of samples that were prepared either by embedding and ultramicrotoming or by separately suspending on carbon films. In Figure 1, a row of magnetosomes, seen in a bacterium, are fairly uniform and form a single straight chain. We found that the particles along a chain are not in a single zone axis orientation but that there is a relative change of crystal orientation in each of the particles in the chain.

So far, no consistent rocking of the crystallographic axis with respect to the chain axis has been found. Double chains were also frequently observed and Figure 2 exhibits an example. It can be noted that the particles in the two chains are in a close-packed arrangement, although, in this particular projection, the lines joining the particle centers appear to have an alternation of 50° and 70° angles between them.

Most of the samples observed were from bacteria which were incubated 4 to 5 days, which corresponds to the upper portion of the growth curves for *Aquaspirillum magnetotacticum*.⁵ Not in all cases were the particles in a given chain the same size; particle size varied, especially towards the ends of a chain (Figure 3). As shown in Figure 3, the particles towards the ends gradually decrease in size. This indicates that "new" particles form at the ends of chains.

Other evidence that new particles may be added at the ends of an existing chain is shown in the study of the effect of ferric iron Fe^{+3} concentration on the magnetosomes' production.⁵ It was found that for Fe^{+3} concentration of less than 20 μM , very few magnetosomes were found in bacteria. At $\sim 20 \mu\text{M}$ Fe^{+3} concentration, 10 to 25 magnetosomes were found in bacteria. At higher Fe^{+3} concentrations, $\sim 200 \mu\text{M}$, multiple chains and chains with a large number of magnetosomes were observed in bacteria. This result supports the idea that a new magnetosome is added at the end of an existing chain.

Summary and Discussion

It was found that for the square-lattice arrangement of double chains of magnetosomes, the two chains have opposite magnetic moments in order to stabilize this arrangement. However, for the close-packed arrangement of magnetosomes, the stable state is such that the two chains have magnetic moments in the same orientation. For the purpose of navigating along a magnetic field, the bacteria prefer the close-packed arrangement to maximize the net magnetic moment. TEM micrographs show mostly close-packed arrangements for double chains. Furthermore, we considered the question of how the double chains are formed. By comparing the potential energies of a particle sitting at the end and on the side of a chain, we found that a new particle is always energetically favored to be added at the end of a chain. This indicates that double chains are formed by combining two existing chains rather than adding new particles on the side of a chain. For two chains of an equal number of particles N , there exists a critical number N_c such that for $N > N_c$, two chains will combine. Whereas if $N < N_c$, two chains will repel each other. Numerically, we found $N_c = 5$ in the case of a close-packed arrangement.

The present paper has considered only the energetics of various configurations. In certain arrangements of magnetosomes so far, but the question of possible thermal fluctuations should be addressed as well. The thermal energy available at room temperature is $kT \sim 4 \times 10^{-14}$ ergs. Whereas the energy scale of magnetic energy is μ^2/a^3 which is $\sim 0.3 \times 10^{-10}$ ergs for $\mu = 6 \times 10^{-14}$ emu and $a = 500$ Å. Therefore the thermal energy is on the order of 1/1000 of the magnetic energy and can be neglected. Even if the separation between magnetosomes were taken into account, the thermal energy is still small compared to the magnetic energy and can be neglected.

Acknowledgment

This work was supported by the Air Force Office of Scientific Research (AFOSR) under Grant No. AFOSR-89-0496. We thank Nancy Pellerin and Karen Reidel for the assistance in growing the bacteria.

References

1. R. P. Blakemore, *Science*, **190**, 377 (1975).
2. B. M. Moskowitz, R. B. Frankel, P. J. Flanders, R. P. Blakemore, and B. B. Schwartz, *J. Mag. Mag. Mat.*, **73**, 273 (1988).
3. C. Rosenblatt, R. B. Frankel, and R. P. Blakemore, *Biophys. J.*, **47**, 323 (1985); C. Rosenblatt, F. F. T. de Araujo, and R. B. Frankel, *J. Appl. Phys.*, **53**, 2727 (1982).
4. I. S. Jacobs and C. P. Bean, *Phys. Rev.*, **15**, 1060 (1955).
5. K. Reidel, N. Pellerin, and M. Sarikaya, unpublished research (1990).

APPENDIX VI

Morphology, Crystallography, and Defect Structures in Biocomposites

by

M. Sarikaya, J. Liu, and I. A. Aksay

submitted to

**Proceedings of a Workshop on
Design and Processing of Materials by Biomimicking**

edited by M. Sarikaya and I. A. Aksay

1991

HIERARCHICAL TWIN STRUCTURES AND MULTIPLE TILINGS IN THE NACRE OF ABALONE SHELL

Mehmet Sarikaya, Jun Liu, and Ilhan A. Aksay

Department of Materials Science and Engineering
Advanced Materials Technology Center, Washinton Technology Center,
University of Washington, Seattle, WA 98195 USA

The superior physical properties of biocomposites over those of synthetic materials have been attributed to their unique structural organization of the component phases. Through *biomimetic* approaches, it may be possible to manufacture new composites, such as cermets and cerpolys, with microarchitectures similar to biocomposites in order to achieve properties that will satisfy the demands for technological advancements not yet possible by current processing techniques. One of the keys to the success of any *biomimetic* approach is the understanding of the structures of biocomposites and the interrelationships between hard and soft tissues, at all levels of spatial resolution. The current work has been undertaken to study the detailed structure of the nacre of red abalone shell since this biocomposite has been shown to have excellent mechanical properties and, yet, has a relatively simple microarchitecture.

The nacre has the form of a "brick and mortar" microarchitecture with 0.5- μ m-thick aragonite platelets and a 20-nm-thick organic matrix between them. An analysis performed by transmission electron microscopy imaging and diffraction has revealed that, in the face-on configuration, the structure can be described by twinning on three different length scales: (i) first generation, incoherent twinning between platelets; (ii) second generation, coherent twinning between domains within platelets; and (iii) the third generation, nanoscale twins within domains. Both 60° and 90°-twin boundaries were observed at different length scales, a phenomenon which has never been encountered in natural mineral aragonite. The structures of biological soft tissues, such as tendon, are known to be hierarchical. To our knowledge, this is the first time that an inorganic component of a biological material has been shown to have a hierarchical structure. In this case, the hierarchical twin structure covers a length scale in six orders of magnitude, from the nanometer to millimeter scale.

Further studies indicate that aragonite platelets could be regarded as space filling tiles at each layer. Since each tile, i.e., a platelet, is twin related with the neighboring one on the same layer, this suggests that the underlying organic matrix must have a superstructure that perfectly fits all variants of twins in both 60° and 90°-symmetry platelets. This allows, as observed, platelets to have 3-, 4-, 5-, and 6-sided edges, hence, multiple tilings. A model for a lattice structure of the organic matrix is forwarded that satisfies all the experimentally observed crystallographic and space filling requirements for longitudinal and transverse directions.

Possible implications of these results on the macrostructure of the nacre in three different species of mollusks will be discussed in reference to *Pinctada margaritifera* and *Nautilus pompilius*, as well as *Haliotis rufescens*. Finally, these results show that by studying the hard tissues it may be possible to discern the structure of the organic matrix in these and other biological composites.

APPENDIX VII

Acidic Biopolymers as Dispersants for Ceramic Processing

by

N. B. Pellerin, J. T. Staley, T. Ren, G. L. Graff, D. R. Treadwell, and I. A. Aksay

Materials Synthesis Based on Biological Processes

Materials Research Society Symposium Proceedings, Vol. 218

edited by M. Alper, P. D. Calvert, P. C. Rieke, D. A. Tirrell, and R. Frankel

(Materials Research Society, Pittsburgh, Pennsylvania, 1991) pp. 123-28

ACIDIC BIOPOLYMERS AS DISPERSANTS FOR CERAMIC PROCESSING

N. PELLERIN,* J. T. STALEY,* T. REN,* G. L. GRAFF,
D. R. TREADWELL, and I. A. AKSAY

Department of Microbiology,* and Department of Materials Science and Engineering; and
Advanced Materials Technology Center, Washington Technology Center,
University of Washington, Seattle, WA 98195

Some acidic biopolymers serve as dispersants for colloidal processing of ceramics. One biopolymer we tested was alginate, a heteropolysaccharide containing two carboxylic sugar acids, D-mannuronic and D-guluronic. Kelp alginate was a suitable dispersant, provided that its viscosity was reduced by partial acid hydrolysis. Low molecular weight polymers rich in guluronic acid proved to be better dispersants than those rich in mannuronic acid, perhaps due to their greater charge density caused by their buckled molecular configuration. In situ processing of ceramic materials was tested by growing the alginate-producing bacterium, Azotobacter vinelandii, in the presence of alumina particles. Growth occurred at 15 vol% alumina in medium. Alumina particles which were exposed to such treatment showed a high packing density comparable to that with purified polymer. We also tested polypeptide polymers of the dicarboxylic amino acids, glutamate and aspartate, which also served as excellent dispersants for small alumina particles.

INTRODUCTION

Colloidal processing of submicron-size ceramic powders is impeded by interparticle attractions from van der Waals forces which cause aggregations that effectively increase the particle size and leave undesired voids in the finished product.¹ To achieve high density in a green compact it is desirable to disperse particles in a liquid medium to prevent the formation of strong agglomerates.²⁻⁴

Polyelectrolytes have been used in aqueous solvents to overcome agglomeration and achieve dispersion by coating the particles. In such a system, the pH is adjusted so that the polyelectrolyte and particles have opposite charges.² Further, the cake densities and viscosities of such systems are dependent not only on the solids loading of the suspension but also upon the concentration of polymer relative to the solids. Too little polymer results in incomplete coating of the particles and an agglomerated suspension. Excess polymer in the system causes depletion flocculation and loss of stability.³

We have investigated the use of several naturally occurring polyelectrolytes as dispersants for high purity, submicron-size Al_2O_3 powders. Naturally occurring polymers are nontoxic and biodegradable and, therefore, do not present the problems of handling and disposal that may be encountered with some of their synthetic counterparts. Since it has been known for many

years that the activity of microorganisms is responsible for the beneficial effects of aging of clays for ceramic processing.^{5,6,7,8} we directed our attention to polymers formed by bacteria and algae.

One polymer we investigated was dextran, formed by the bacterial genera *Leuconostoc* and *Streptococci*. While dextran was not effective as a dispersant, its derivative, dextran sulfate was.⁹ This indicated that a charged group was needed to interact with the surface charge of the particle in order to stabilize the dispersion. Unfortunately, however, the added sulfate ion is not removed by the sintering of dextran sulfate. Therefore, we sought polymers containing acidic groups such as carboxylic acids that are volatilized during processing. Alginate, an acidic polysaccharide, was next selected for examination as a dispersant for alumina. Alginate is a heteropolymer composed of mannuronic and guluronic acids and is obtained from the marine alga, *Macrocystis pyrifera* (kelp). It is also produced by the bacterium *Azotobacter vinelandii*.

A second group of organic polymers was also investigated. In particular, polypeptides containing a second acidic group in addition to the carboxyl involved in the peptide bond were studied. These include poly-glutamic acid which is produced naturally by the bacterium, *Bacillus licheniformis*, and poly-aspartic acid.

MATERIALS AND METHODS

The ceramic used in this study was a high purity (99.99%) Al_2O_3 , with an average particle size of 0.4 μm as determined by x-ray sedigraph (AKP-30, Sumitomo Chemical America, Inc., New York, N.Y.).

Low viscosity kelp alginate (75,000-100,000 molecular weight) was obtained from Sigma Chemical Company (St. Louis, Mo.). Low molecular weight fractions were prepared by hydrolysis in 0.1 N HCl under reflux for 4 h. The solution was centrifuged, after which the pellet was dissolved using NaOH. A guluronic acid-rich fraction (poly G) was obtained by lowering the pH to 2.4 and collecting the precipitate; a mannuronic acid-rich fraction (poly M) was precipitated by further lowering the pH to 1.3.¹⁰ Reagent grade HCl and NaOH were used for pH adjustments. Distilled water was used throughout. Other chemicals were obtained from Sigma Chemical Company.

Sedimentation columns were prepared with 2 vol% alumina particles in aqueous solutions of polymer. The suspensions were sonicated for 5 min, mixed on a magnetic stirrer for 30 min, and the pH adjusted to the experimental value before bringing the final volume to 10 ml. The suspension was decanted into a conical bottom, graduated tube and left undisturbed for several weeks. Final cake volumes were measured to ± 0.1 ml. The wet density was calculated as [final volume/theoretical volume] $\times 100$.

Suspensions for viscosity measurements were prepared with 30-40 vol% alumina powder in an aqueous solution of polymer and mixed as above. Measurements were obtained by the method of Cesarano and Aksay³ using a Digital Viscometer, Model RVTD, (Brookfield Engineering Laboratories, Inc., Stoughton, Mass.). The viscosities of the polymer solutions were

measured using parallel plates on a Rheometrics Fluid Spectrometer, Model 8400 (Rheometrics Inc., Piscataway, N.J.).

The poly M and poly G fractions were analyzed by the method of Grasdalen^{11,12} using ¹H NMR spectra obtained on a Varian VXR 300 spectrometer at 300 MHz.

Azotobacter vinelandii NCIB 8789 (National Collection of Industrial Bacteria, Aberdeen, Scotland) was maintained on Larsen's broth¹³ medium in cyst stage culture. Cells were counted by standard plate counting techniques.

Alginate was assayed by the *meta*-hydroxydiphenyl-sulfuric acid method.¹⁴ Because sucrose interferes with the assay, it was replaced by mannitol in the Larsen's medium.¹³ The polymer was harvested from culture supernatants by alcohol precipitation¹⁵ after which it was dissolved in distilled water and dialyzed overnight.

The amount of polymer adsorbed to the particles was measured by preparing a 5 vol% alumina suspension containing a known amount of polymer. After ultrasonication for 2 min, the pH of the suspension was adjusted to around 8. The suspension was centrifuged to pellet the particles and the polymer remaining in solution was assayed.

RESULTS AND DISCUSSION

Algal Alginate as a Dispersant

Aqueous suspensions of alumina in polyacids are sensitive to changes in pH. The surface charge of the alumina particles varies from highly positive at low pH to negative at high pH with the zero point of charge (zpc) being around pH 8.7.² Further, the degree of ionization of the polymer is pH dependent. In order to determine the optimum pH range for the alginate/alumina system, we prepared 2 vol% suspensions at various pHs and measured the density of the resulting cakes. Maximum sediment densities were obtained near pH 8-9 where the polymer is fully dissociated and the surface of the alumina has a slight positive charge.

Wet sediment densities of 2 vol% alumina suspensions showed a dependence on polymer concentration relative to powder concentration (Table I). Too much or too little polymer resulted in flocculated suspensions with low-density cakes. The maximum packing density was obtained at a polymer concentration of 0.5% dry weight basis (dwb) alumina. This indicates full surface coverage of the particles at this concentration. Above the saturation adsorption level there was a decrease in cake density, most likely due to excess polymer resulting in gel formation which prevents close packing in the wet cake.

The viscosity of a highly concentrated suspension (30 vol% alumina) showed thixotropic behavior. There are two possible explanations for the increase in viscosity at a low rate of mixing: (i) the polymer may be forming a gel structure which is disturbed by more vigorous mixing or (ii) the suspension may be unstable. A 40 vol% suspension displayed less hysteresis, but the viscosities were approximately 10-fold higher than the 30 vol% suspension. An equivalent solution of polymer alone, without the particles, had a viscosity of 431 mPa·s, strongly suggesting that the polymer itself was forming a gel.

Table I. Wet sediment densities of 2 vol% suspensions of alumina in kelp alginate [MW 75,000-100,000; degree of polymerization (\overline{DP}) 380-515].

Concentration of polymer (dwb alumina)	Wet sediment density (% theoretical)
0	8 Flocculated
0.1	9 Flocculated
0.125	11 Flocculated
0.15	20 Slightly flocculated
0.20	33 Dispersed
0.25	33 Dispersed
0.50	40 Dispersed
0.75	25 Flocculated
1.0	16 Flocculated

In order to reduce the viscosity of the native polymer, we partially hydrolyzed it, yielding two fractions: one mannuronic acid-rich (poly M, molecular weight, $\sim 2,400$); the other guluronic acid-rich (poly G, molecular weight, $> 5,000$). The poly G fraction proved to be 100-fold less viscous than the native alginate. Sedimentation tests of 2 vol% suspensions and viscosities of high solids loaded suspensions revealed that the poly G fraction was superior to either the native alginate or the poly M fraction as a dispersant (Table II).

Table II. Viscosities of concentrated suspensions of alumina in poly G, poly M, or native alginate fractions at a shear rate of 9.2 s^{-1} .

Fraction	30 vol%	40 vol%	50 vol%
Poly G	$< 20 \text{ mPa}\cdot\text{s}$	$35 \text{ mPa}\cdot\text{s}$	$110 \text{ mPa}\cdot\text{s}$ Slightly flocculated
Poly M	95	465	Too viscous to be prepared
Alginate	*140-445	*2460-3720	Too viscous to be prepared

*Unstable

The reason for these differences probably lies in the conformation of the oligomers in solution. NMR studies¹¹ reveal that the two adopt different chain forms when in solution such that the bulky carboxyl group is in the equatorial position. This would lead to a flat, ribbonlike conformation in polymannuronic acid sequences. In contrast, polyguluronic acid would adopt a buckled conformation, giving an arrangement whereby the oxygen atoms on adjoining residues are in close proximity, leading to a localized increase in charge density.¹⁶ The high charge density is likely the reason why polyguluronic acid is a more effective dispersant than polymannuronic acid.

Bacterial Alginate as a Dispersant

We have also investigated whether bacterial alginate can be produced in an *in situ* process in which the alumina particles are incubated with *Azotobacter vinelandii* while polymer is being synthesized. It might be of commercial interest to know if such an *in situ* process is feasible. We have found that *Azotobacter vinelandii* are able to grow in 5, 10, and 15 vol% suspensions of alumina in Larsen's medium. Over a four-day period the bacteria produced sufficient polymer to effectively treat the particles. Cake densities were enhanced 49% and 58% over that of the untreated controls in the 5 and 10 vol% suspensions. Further, the viscosities of these suspensions were reduced 4-fold (from 480 to 120 mPa-s) at a shear rate of 9.3 s^{-1} and 100-fold (from 6000 to 100 mPa-s) at a shear rate of 9.3 s^{-1} respectively, over that of the controls. We suspect that the poorer packing density and higher viscosity of the 5 vol% suspension was due to excess polymer in the suspension.

Adsorption studies, in which we mixed the particles with a polymer solution and determined the amount of polymer remaining in solution after adsorption, have shown that 1 g of particles adsorbs 3.23 mg of bacterial alginate at pH 8.

In order to simplify the system, we investigated the possibility of producing the polymer in a nongrowing bacterial population. For this purpose cells were first grown on Larsen's medium and then resuspended in nitrogen and sulfur-limited salt solutions. By limiting these nutrients but still providing a carbon source for the production of the polymer, we hoped to maximize polymer production per cell. Three solutions were used: solution 1, which contained a carbon source only; solution 2, which contained a carbon source and phosphate buffer; and solution 3, which contained a carbon source, phosphate buffer, and sodium acetate (additional carbon source). Pre-grown *Azotobacter vinelandii* cells were inoculated in the solutions to a cell density of 2.8×10^5 . Growth did not occur in solutions 1 and 2; polymer production was only 5.9 $\mu\text{g/ml}$ in solution 1, but 30.5 $\mu\text{g/ml}$ or 100 $\mu\text{g}/1000$ cells was achieved in solution 2. In solution 3, growth occurred to a final density of 5.0×10^6 , and polymer production per 1000 cells was the same as in solution 2.

Thus, it is possible to limit the number of cells in the system, while increasing the level of production of polymer per cell. Our calculations show that in solution 2 and with an alumina particle diameter of $0.4 \mu\text{m}$, 3×10^7 cells of *A. vinelandii* are sufficient to coat 1 g of particles or a single cell can coat 232,000 alumina particles.

We also determined whether the bacterial cells could be removed from the *in situ* system after the particles became coated. After cultivation for 6 d in an alumina suspension, the culture was centrifuged, yielding a pellet of the ceramic particles overlain by a pellet of bacterial cells. The cells were scraped off and the particle pellet was resuspended in distilled water. After washing in this manner five times, the bacterial numbers were reduced from 5.6×10^7 per gram particles to 85 cells per gram particles, indicating that the bacterial cells do not strongly adhere to the particles. In contrast to the cells, over 99% of the polymer remained bound to the particles when coated particles were subjected to the same washing regime.

These results indicate that *Azotobacter vinelandii* can be used as a source of polymer which acts as an effective dispersant for small-size alumina particles. Furthermore, we have demon-

strated that the bacterium may be used in an *in situ* process whereby the bacterial culture produces alginate while incubating in an alumina suspension, obviating the need to extract the polymer from the culture before mixing it with the particles.

Acidic Polypeptides as Dispersants

Sedimentation tests using 2 vol% suspensions of alumina in various concentrations of polyamino acids indicate that they also are effective as dispersants for small size powders. The polymers thus far tested are poly-D-glutamic acid, poly-L-glutamic acid, poly-(α , β)-DL-aspartic acid, and poly-L-aspartic acid. We have attained wet cake densities of over 50% of the theoretical density volume in simple sedimentation columns using only gravity to compact the cakes. No differences were noted in the cake densities obtained with D and L isomers of the same polyamine.

ACKNOWLEDGEMENT

This work was supported by the Air Force Office of Scientific Research under Grant No. AFOSR-88-0135.

REFERENCES

1. I. A. Aksay, in *Advances in Ceramics, Vol. 9, Forming of Ceramics* edited by J. A. Mengels and G. L. Messing (American Ceramic Society, Columbus, Ohio, 1984), p. 94.
2. J. Cesarano III, I. A. Aksay, and A. Bleier, *J. Am. Ceram. Soc.*, **71**, 250 (1988).
3. J. Cesarano III and I. A. Aksay, *J. Am. Ceram. Soc.*, **71**, 1062 (1988).
4. T. K. Yin, I. A. Aksay, and B. E. Eichinger, in *Ceramic Powder Science II, Ceram. Trans.*, Vol. 1, edited by G. L. Messing, E. R. Fuller, Jr., and H. Hausner (American Ceramic Society, Westerville, Ohio, 1988), p. 654.
5. D. P. Glick, *J. Am. Ceram. Soc.*, **19**, 169 (1936).
6. D. R. Baker and D. P. Glick, *J. Am. Ceram. Soc.*, **19**, 209 (1936).
7. D. P. Glick, *J. Am. Ceram. Soc.*, **19**, 240 (1936).
8. H. Spurrier, *J. Am. Ceram. Soc.*, **4**, 113 (1921).
9. G. L. Graff, unpublished.
10. J. M. Beale, personal communication.
11. H. Grasdalen, *Carbohydr. Res.*, **118**, 255 (1983).
12. H. Grasdalen, B. Larsen, and O. Smidsrod, *Carbohydr. Res.*, **68**, 23 (1979).
13. G. Skjak-Braek, H. Grasdalen, and B. Larsen, *Carbohydr. Res.*, **154**, 239 (1986).
14. J. Montreuil, *Carbohydrate Analysis - A Practical Approach*, (IRL Press, Limited, Oxford, England, 1986), p. 175.
15. T. R. Jarman, L. Deavin, S. Slocombe, and P. C. Righelato, *J. Gen. Microbiol.*, **107**, 59 (1978).
16. D. A. Rees, *Biochem. J.*, **126**, 257 (1972).

APPENDIX VIII

Multiple Tilings with Hierarchical Twin Structures in the Nacre of Red Abalone

by

M. Sarikaya, J. Liu, and I. A. Aksay

to be submitted to
Physical Review B
1991

Note: This paper will be an extension of the *Science* paper that follows and will discuss the crystallography in much more details.

Abstract:

The structure of the hard tissue in the nacre of red abalone, *Haliotis rufescens*, was studied by transmission electron microscopy imaging and diffraction. We found that the nacre structure is based upon hierarchical twinning: (i) first generation twins among platelets having incoherent boundaries, (ii) second generation twins between domains having coherent boundaries within a given platelet, and (iii) nanometer-scale third generation twins within domains. Since the platelets grow as separate crystals in the early stage, this long-range crystallographic relationship between the inorganic crystals indicates that the nucleation and growth process of crystals is mediated by the organic matrix and that the organic template structure is also long-range ordered. We further propose a superlattice structure based on the possible twin variants and suggest that the organic matrix structure, or the arrangement of nucleation sites, should be compatible to the superlattice. Multiple tiling based upon this superlattice allows us to construct all the crystallographic and morphological platelet configurations observed in nacre. Possible implication of these results on the microstructure of nacre in relation to the final shapes of shells of molluscs are discussed.

APPENDIX IX

Multiple Tilings with Hierarchical Twins: A TEM Study of the Nacre Structure of Red Abalone Shell

by

J. Liu, M. Sarikaya and I. A. Aksay

to be submitted to
Science
1991

**MULTIPLE TILINGS WITH
HIERARCHICAL TWINS:
A TEM STUDY OF THE NACRE STRUCTURE
OF RED ABALONE SHELL**

Jun Liu, Mehmet Sarikaya, and Ilhan A. Aksay

Department of Materials Science and Engineering,
Washington Technology Center,
University of Washington, Seattle, WA 98195

The art of tiling, which is defined as covering a plane with a family of closed sets without gaps or overlaps, has been used for a long time for decoration purposes such as pattern design in textiles and quilts, in mosaics and paintings, and in building constructions (1). Tiling is also utilized by biological systems (2), but it is seldom realized that by studying the pattern design in those systems we can derive information about the growth mechanisms. In this paper, we will discuss a unique tiling system we discovered in nacre of red abalone, and its relationship to the crystalline structures both in hard and soft tissues. From this study we wish to extract information about the organisms that controls the growth of the crystals.

Nacre is a laminated composite material found in mollusc shells (3). The highly ordered structures and the unique properties, e.g., high fracture toughness and strength (4-7) makes the understanding of the growth process and the interrelationships between the microstructure and the properties valuable to biological sciences, materials science and engineering, and electronic industry. Previous studies suggested that the formation of the inorganic crystals were regulated by the organic matrix through epitaxial growth (8-13). But to date the structures of neither the inorganic phase nor the organic phases have been fully understood. In nacre, the inorganic phase, which is CaCO_3 in aragonite form, and the organic phase, are arranged in a "brick-and-mortar" microarchitecture. The aragonite platelets are about 5 μm in length and 0.25 to 0.5 μm in thickness, and the organic phase is about 200 \AA thick (3-12). Early diffraction studies (14) illustrated that the platelets on a given layer are aligned in the c direction of the orthorhombic unit cell of the aragonite lattice. It was further suggested that the platelets were arranged in a "mosaic pattern" without definite crystallographic relationships between them in

the a-b plane. Similarly, it was suggested that only local ordering existed in the organic matrix, which was responsible for the mosaic polycrystalline pattern in the aragonite crystals.

In the previous diffraction studies (14), the samples were first broken into small pieces and then subjected to drastic sample preparation procedures. These sample preparation procedures not only cause structural changes, but also make it difficult to study long range ordering. In addition, in most studies it was not possible to investigate the structures on a fine scale. In this research, transmission electron microscopy imaging and diffraction techniques were used to study the the structures of the inorganic phase on a length scale ranging from nanometer to millimeter. The sample preparation method and the microscopy technique we used allow the structures to be preserved. Contrary to earlier suggestions that the aragonite crystals were randomly aligned in the a-b plane, we found that the aragonite crystals are highly ordered over several decade of length scales through hierachical twinning (multiple tiling). From this observation we conclude that the organic template should also be aligned over a long distance in stead of having a mosaic patterns. Further we propose that the organic matrix should have a template structure which is compatible to a superlattice generated by manipulating the possible twin variants. Multiple tiling based upon this superlattice allows us to explain all the crystallographic and morphological platelet configurations observed in nacre. We hope that futher study along this line will shed more light on the how the organisms modifies the overall shape of the shells.

In this paper the nacre section of a shell from a mature red abalone, *Haliotis rufescens*, was studied. We chose red abalone (collected in Baja California) because they are abundant

in the eastern Pacific Ocean region and are available in sizes sufficiently large for standard mechanical property evaluation (3-7). Thin sections from the shell were prepared for TEM study by low temperature (liquid nitrogen) ion milling technique. The microscopy on carbon-coated samples was performed with a Philips EM430T TEM/STEM operating at 300 kV. To further reduce sample damage during observation, TEM samples were kept on a liquid nitrogen double-tilt sample holder maintaining a sample temperature of about 110 K.

We first studied both the geometrical arrangement of and the crystallographic relationship among the aragonite platelets. In the face-on view, each layer of the nacre is composed of closely packed platelets (Fig. 1a and 1b). The platelets have either three, four, five, or six edges. The geometrical organization of platelets often exhibit sixfold symmetry as shown in Fig. 1a and 1b, where six platelets have an arrangement with an approximately 60° angle between each pair (60° twin boundaries). The crystallographic orientations between the platelets on the a - b plane are not random, as suggested (14), but are mostly related to one another by twinning, as shown by the diffraction patterns in Fig. 1c and 1d. The [001] single crystalline pattern in Fig. 1c is from the interior of a platelet; the pattern in Fig. 1d are recorded from the boundary between two platelets incorporates two superimposed patterns. Analysis of the two patterns reveals that they are correlated to each other by a twin relationship with the twin plane being {110} parallel to the [001] direction of the crystal, i.e., either (110) or ($\bar{1}\bar{1}$ 0). The images in Fig. 1a and 1b were recorded by slightly tilting the sample (a few degrees) to bring each of the three alternate platelets into a strongly diffracting condition so that they exhibit a dark diffraction contrast. The platelets *A*, *C*, and *E*, therefore, are all in the same orientation and the remaining three, *B*, *D*, and *F*, are in a twin orientation with the first set. Although

the diffraction patterns are slightly misaligned about the c -direction, the twin relationships between them are preserved. In fact, the SAD pattern recorded from all of the platelet boundaries shown in Fig. 1 reveals the same twin reflections, indicating that each platelet is related to the one next to it by a $\{110\}$ twin relation. In this paper, we refer to the twinning between aragonite platelets as *incoherent first generation twinning*.

Further studies revealed that many platelets are not single crystals but are comprised of several domains, and that the domains are related to each other by twinning as well. Fig. 2a shows a four-domained platelet with 90° domains. The diffraction pattern in Fig. 2b, recorded from the interior of one of the domains, indicates that the platelet is again perpendicular to the $[001]$ electron beam direction. The diffraction pattern in Fig. 2c recorded from a domain boundary exhibits twin splitting of (110) reflections. A close examination of the crystal structure of aragonite shows that the 90° twin boundaries can be accommodated by including two atomically flat (110) twin planes (reflection twins) and two zig-zag boundaries (180° -rotation twins). This kind of twinning is called *second generation coherent twins*, and there is no misalignment in the c -direction among the domains within a platelet.

In an ideal hexagonally shaped platelet having six twin-related domains, the angle between each pair of domains must be 60° , with the six domains completing 360° for the whole platelet. This is not possible in aragonite since the outer edges of the platelets are parallel to $\{110\}$ planes and the angle between each pair of (110) planes is 63.5° . This, therefore, must be accommodated by lattice deformation during the formation of twin-related domains in a aragonite platelet, which can be accomplished by either slipping (dislocation formation) or by

twinning (15), with the latter preferred in ionic crystals (15). Imaging of the microstructure at higher magnifications shows that each domain in a given platelet actually contains two sets of nanometer scale twins, each forming $\{110\}$ planes. Figure 4 shows the two variants of ultrafine twins forming angles of about 63.5° or 127° , which is similar to growth twins in geological minerals (16,17). The accommodation of the 3.5° -strain is possible through the formation of these nanometer scale defects on the $\{110\}$ planes, which allows the lattice to be deformed towards the periphery of the platelet. In fact, in most cases, the outer periphery of the platelets has a convex shape, the apex being in the middle of the edge, and the region of the edge where the two domains meet is inwardly curved. We call these ultrafine twins the *third generation nanometer-scale twins* as they take place at the lowest dimensional scale.

In summary, we found that there are three scales of twinning in the face-on configuration of the nacre section of red abalone shell: (i) first generation twins among platelets having incoherent boundaries, (ii) second generation twins between domains having coherent boundaries within a given platelet, and (iii) nanometer-scale third generation twins within a domain. It should be noted that the twin and domain boundaries can be either 60° or 90° , although we only showed examples of 60° twin boundaries and 90° domain boundaries. Therefore, these twin structures encompass a six-orders of magnitude size scale covering a range from nanometer to submillimeter and reveal a hierarchical structure for hard tissue in a biological material. Although six-fold twin structures also occur in geological aragonite, the hierarchical arrangement of twins in nacre is unique in the sense that each platelet is completely separate from one another during the early stage of growth. Even after the crystalization is completed, all the platelets are still separate from one another by an organic membrane. On the other hand, in

geological aragonite (16-18) the mimetic twin domains always grow one after another. The fact that the separate platelets grow simultaneously and yet they retain certain crystallographic relationship between them suggest that the growth process is mediated by the organic template below the crystals, and that the organic matrix also has a long-range ordering. In the following section we discuss how these hierarchical twins originate and the implication it has for the structure of the organic template on which the aragonite crystals are grown.

The interaction between the organic species and the crystals include both electrostatic and stereochemical forces(8-14, 19). Therefore, nucleation and growth of crystals will be influenced by both the nearest and high order interactions. Aaragonite crystal structure belongs to the space group Pmcn (No. 62) with lattice parameters $a = 4.94 \text{ \AA}$, $b = 7.94 \text{ \AA}$, $c = 5.72 \text{ \AA}$. The calcium atoms would give the crystal a pseudo-hexagonal symmetry in [001] projection, but the CO_3 groups reduce the symmetry to orthorhombic. The nucleation and growth involves both the calcium ions and the CO_3 groups, but for simplicity, only the arrangement of the calcium ions will be illustrated in this paper. We examine the aragonite lattice in the [001] projection with the Ca ions highlighted. To understand the origin of the hierachical twins, we superimpose the lattices on all three possible twins with a 63.5° rotation with respect to each other and generate a new superlattice structure, which we call the superstructure (Fig. 4a). If the nucleation and growth of aragonite platelets take place on the underlying organic matrix, the geometrical configuration of the active sites for the binding of the Ca^{2+} ions on the organic matrix must accommodate this superlattice, and thus, all the twins in the nacre. Since twinning takes place at all length scales, the orgainc template structure should also be aligned over all length scales. The most like solution for this problem is that the organic matrix, or the

arrangement of the active nucleation sites, have a single crystalline lattice structure over a wide area which is compatible to the superlattice. A local crystalline organization of the organic matrix, with no relationship between the neighboring areas, and, hence, without a long-range order, would result in the formation of aragonite crystals without any definite crystallographic relationship among the platelets. For example, a pseudo-hexagonal arrangement, which is indicated by the circles in Fig. 4a, would satisfy the requirement for the organic matrix. The crystalline pseudo-hexagonal lattice is a possible solution since many two-dimensional membranes tend to form hexagonal lattices during self-assembly (20).

The superlattice shown in Fig. 5a allows the generation of the overall hierarchical twin structures by tracing along the possible twin boundaries. One construction is illustrated in Fig. 4b which contains all the shapes, geometry, and crystallography-related features discussed in this paper, such as five-edged platelets with 90° domains, sixfold symmetry of plates, and six- and three-edged domains. The fact that one can generate all the possible configurations this way again illustrates that we need a compatible organic matrix over a wide range of length scale to accommodate all the twin relationships, rather than the lattice of a single domain or a single platelet.

The construction of the aragonite platelets used in this paper is called multiple tiling in mathematics (1). In nacre, nature used this technique to form a highly ordered structure which is compatible both with the soft tissue and the crystalline structural constraints of the hard tissue. This unique ordering, originated from the atomic or molecular structures of both the organic and inorganic tissues, extends to all length scales to form different shapes of shells.

The issue of shapes, as well as the microstructural formation we discussed in this paper, is of essential importance in materials science and other fields. Many gastropods, cephalopods and bivalves have aragonite crystallites as the fundamental building blocks in nacre, but have grossly differing overall shell shapes. For example, in red abalone, the shell is quite flat; in nautilus, the shell is round and forms a very elegant chambered structure in which even the separation chamber walls are made of nacre. The study of the origin the development of the tiling pattern in such nacre structures will provide us with not only the information about the mechanisms of crystal growth, but also clues to how the animal control the shape of its shell. Further studies are required on various species of these organisms, both on the crystallography of the mineral component and on the structural and compositional analyses of the organic matrices in order, to understand their structures and the unifying, underlying principles for the organization and formation of the various shapes of the nacre structure. These principles would serve as guide lines for design and processing of synthetic materials via biomimicking for advanced properties.(21)

References

1. For review, see B. Grunbaumin "Tilings and Patterns", (W. H. Freeman and Company, New York, 1987); M. C. Escher, "Art and Science", edited by H. S. M. Coxeter, M. Emmer, and M. L. Teaber (North Holland, Amsterdam, 1988).
2. E. Kellenberger, "Assembly in Biological Systems", in "Polymerization in Biological Systems", Ciba-Foundation Symposium 7 (Elsevier, Amsterdam, 1972); V. A. Greulich, "Plant Function and Structure" (Macmillan Co., New York, 1973).
3. R. T. Abbott, "Sea Shell of the World", (New York, 1962); J. E. Morton, "Molluscs", (Hutchinson of London, 1979); "Studies in the Structure, Physiology and Ecology of Molluscs", edited by V. Fretter (Academic Press, New York, 1968); C. Gregoire, "Structure of the Molluscan Shell", Chemical Zoology, Vol. 45-102 (1972); S. M. Wise, "Microarchitecture and Mode of Formation of Nacre (Mother of Pearl) in Pelecypods, Gastropods, and Cephalopods", Ecloae Geol. Helv., 63 (3), 775-795 (1970).
4. J. D. Currey, "Biological Composites", J. Mater. Edu., [9] 118-296 (1987).
5. A. P. Jackson, J. F. V. Vincent, and R. M. Tunner, "The Mechanical Design of Nacre", Proc. Roy. Soc. London, B234, 415-440 (1988).
6. M. Sarikaya, K. E. Gunnison, M. Yasrebi, and I. A. Aksay, "Mechanical Property-Microstructural Relationships in Abalone Shell", in *Materials Synthesis Using Biological Processes*, P. C. Rieke, P. D. Calvert, and M. Alper (eds.) pp 109-116 (Materials Research Society, Pittsburgh, 1990).

7. Proceedings of a workshop on *Design and Processing of Materials by Biomimicking*, April 2-4, 1991, Seattle, M. Sarikaya and I. A. Aksay (eds.), to be published, 1991.
8. E. M. Greenfeld, D. C. Wilson, and M. A. Crenshaw, "Ionotropic Nucleation of Calcium Carbonate by Molluscan Matrix," *Amer. Zool.*, **24**: 925-932 (1984).
9. N. Watanabe, "Crystal Growth of Calcium Carbonate in the Vertebrates," *Prog. Crystal Growth Charac.* **4**, 99-147 (1981); or ii. N. Watanabe, "Studies on Shell Formation," *Ultrastructure Research*, **12**, 351-370 (1965).
10. G. Bevelander and H. Nakahara, "An Electron Microscope Study of the Formation of the Nacreous Layer in the Shell of Certain Bivalve Molluscs," *Calc. Tiss. Res.*, **3**, 84-92 (1969).
11. "Biomineralization," K. Simkiss and K. M. Wilbur (Academic Press, New York, 1989); "On Biomineralization," H. A. Lowenstam and S. Weiner (Oxford University Press, New York, 1989).
12. K. M. Wilbur, "Shell Formation and Regeneration," in: "Physiology of Mollusks," K. M. Wilbur and C. M. Yonge (eds.) 243-282 (Academic Press, New York, 1964).
13. S. Weiner and W. Traub, "Macromolecules in Mollusc Shells and Their Functions in Biomineralization," *Phil. Trans. R. Soc. Lond.*, **B304**, 425-434 (1984); ii. S. Weiner, "Organization of Extracellularly Mineralized Tissues: A Comparative Study of Biological Crystal Growth," *CRC Critical Reviews in Biochemistry*, **20** [4] 365-380 (1986); L. Addadi and S. Weiner, "Interaction between acidic proteins and Crystals: Stereochemical Requirement in Biomineralization," *Proc. Natl. Acad. Sci.*, **82**, 4110-4114 (1985).
14. S. Weiner and W. Traub, "X-ray Study of the Insoluble Organic Matrix of Mollusk Shells", *FEB. Letters*, **111**, 311 (1980); S. Weiner, Y. Talmon, and W. Traub, "Electron Diffraction

- of Mollusc Shell Organic Matrix and their Relationships to the Mineral Phases", *Int. J. Biological Macromolecules*, 5, 326 (1983);
15. "Theory of Dislocations," J. P. Hirth, and J. Lothe (McGraw-Hill, New York 1968).
 16. W. L. Bragg, "The Structures of Aragonite", *Proc. Royal Soc. London, Ser. A*, 17 (1924).
 17. H.-R. Wenk, D. J. Barber and R. J. Reeder, "Microstructures in Carbonate", in "Reviews in Mineralogy", Vol. 11, edited by R. J. Reeder, (BookCrafters, Inc., Chelsea, Michigan, 1983); A. D. Negro and L. Ungaretti, "Refinement of the Crystal Structure of Aragonite", *The American Mineralogist*, Vol. 56, 769-772 (1971);
 18. M. Senechal, "The Genesis of Growth Twins", *Sov. Phys. Crystallogr*, 25 (5), 520-524, (1980).
 19. I. Weissbuch, L. Addadi, M. Lahar, and L. Leiserowitz, "Molecular Recognition at Crystal Interfaces", *Science*, 253, 637-695 (1991).
 20. N. Unwin and R. Henderson, "The Structure of Proteins in Biological Membranes", *Science*, 78-94.
 21. S. Mann et al., "Biom mineralization: New Routes to Crystal Engineering," in *Materials Synthesis Using Biological Processes*, P. C. Rieke, P. D. Calvert, and M. Alper (eds.) (Materials Research Society, Pittsburgh, 1990). Nature paper
 22. Mathematical frame on multiple tilings -- a math book reference.
 23. This work is supported by the Air Force Office of Scientific Research under a Grant No. AFOSR-89-0496. **Figure Captions**

Figure 1 a-b. Face on view of nacre. Fig. 1a and 1b were recorded by slightly tilging the specimen along the c-direction. The nacreous layer consists of close packing of 3, 4, 5, 6-edged platelets, and the platelets often exhibit sixfold symmetry.

Figure 1 c-d. Diffraction revealed the platelets are related to one another on {110} planes. Fig 1c is a single crystalline diffraction pattern from one platelets. Figure 1d is the diffraction pattern from boundaries between platelets, showing twin relationships.

Figure 2a. Domain structures within platelets.

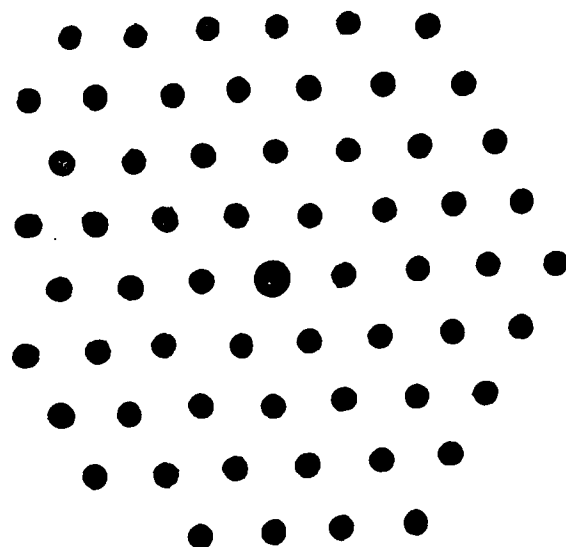
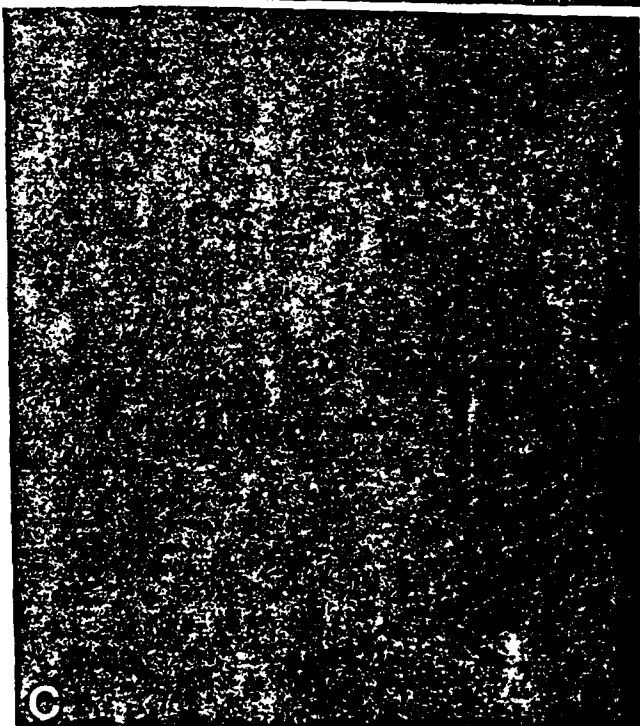
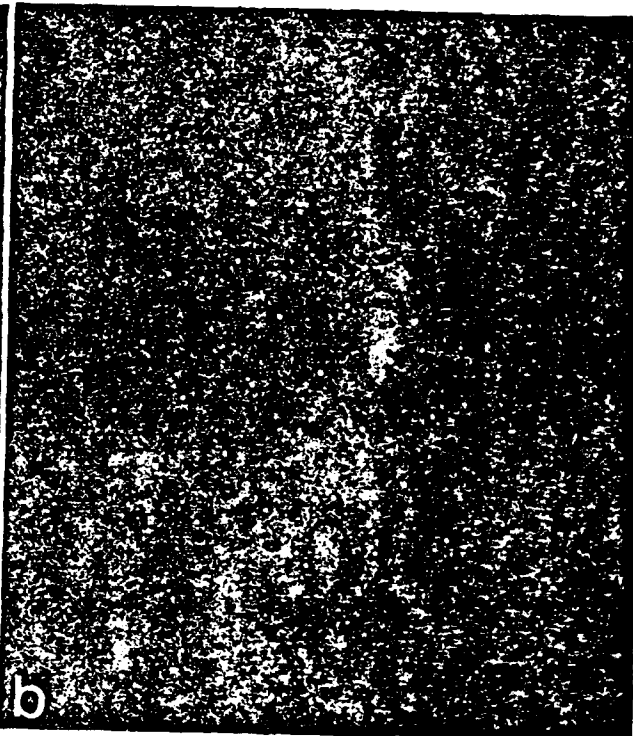
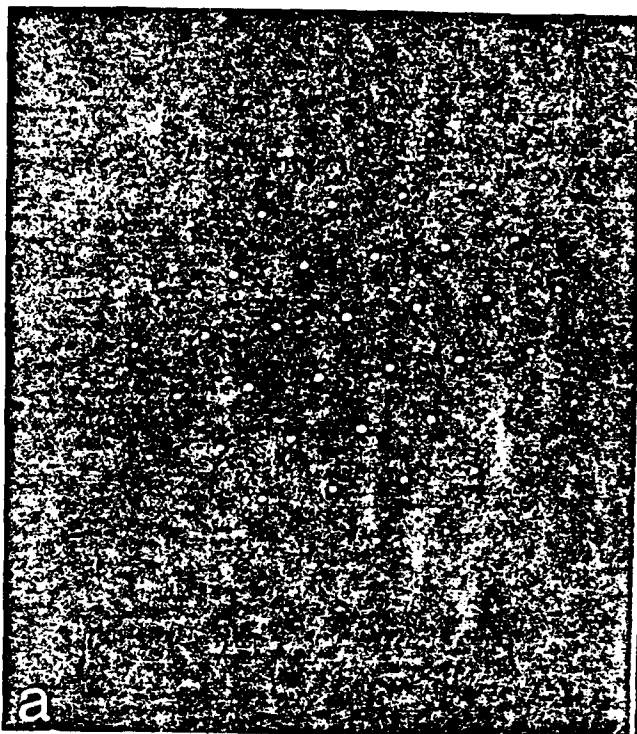
Figure 2b. Single crystalline diffraction pattern from one domain.

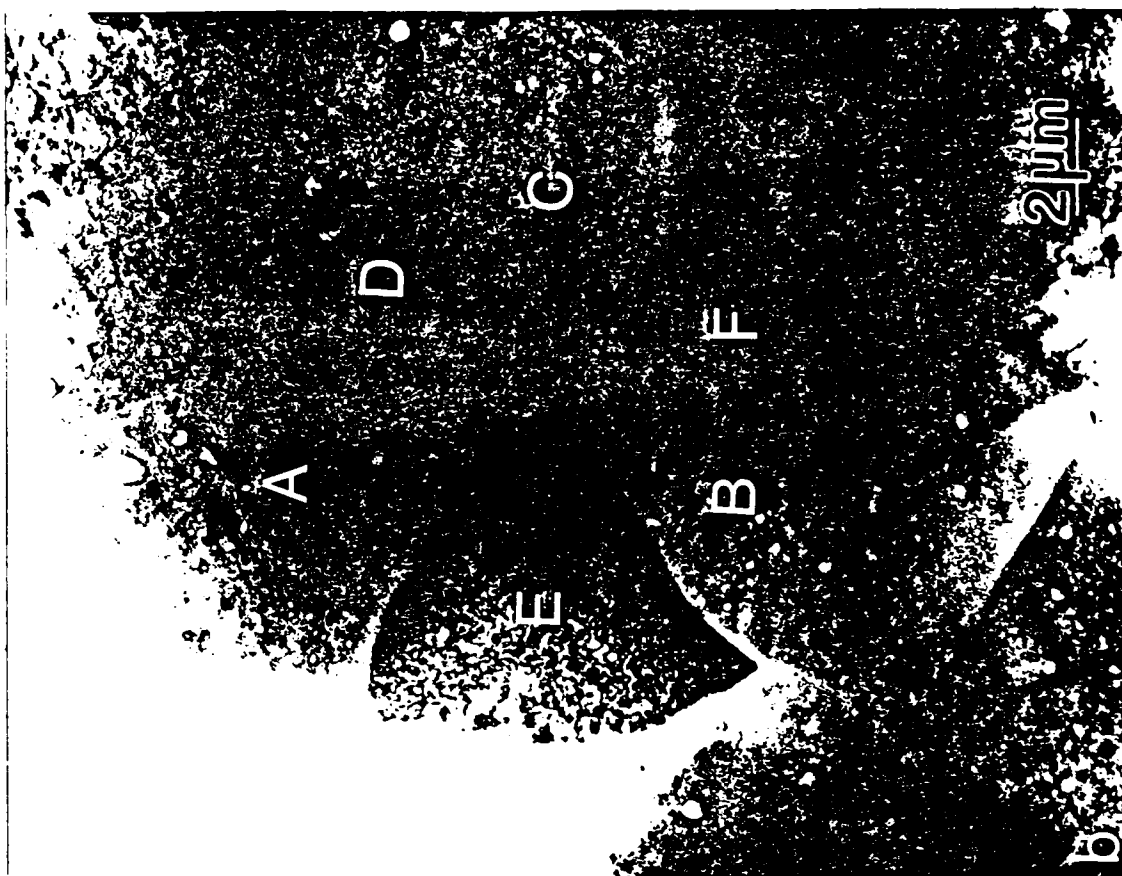
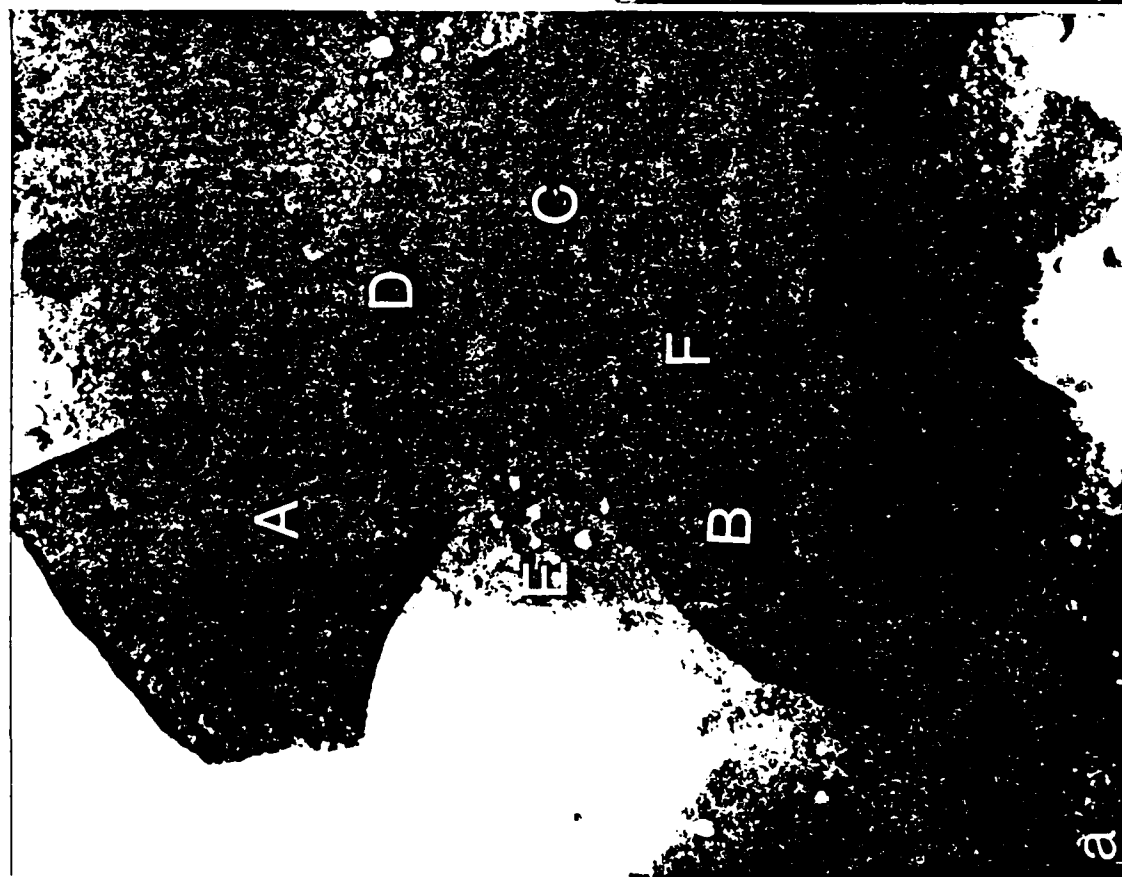
Figure 2c. Twin diffraction pattern from domain boundaries.

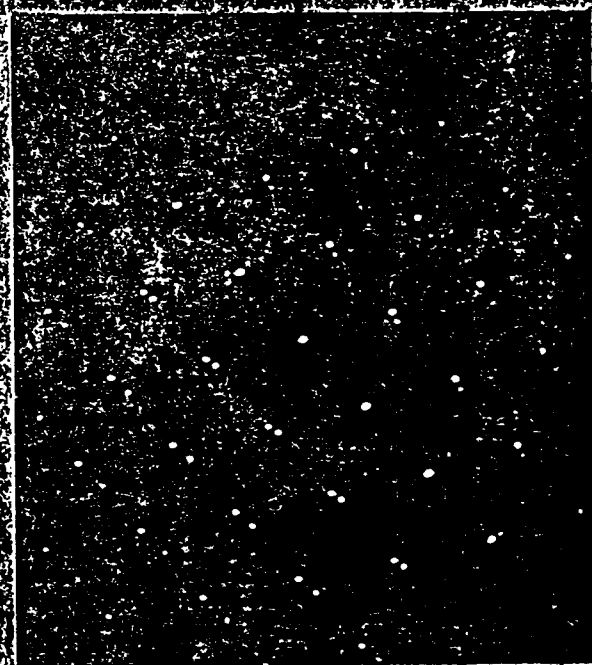
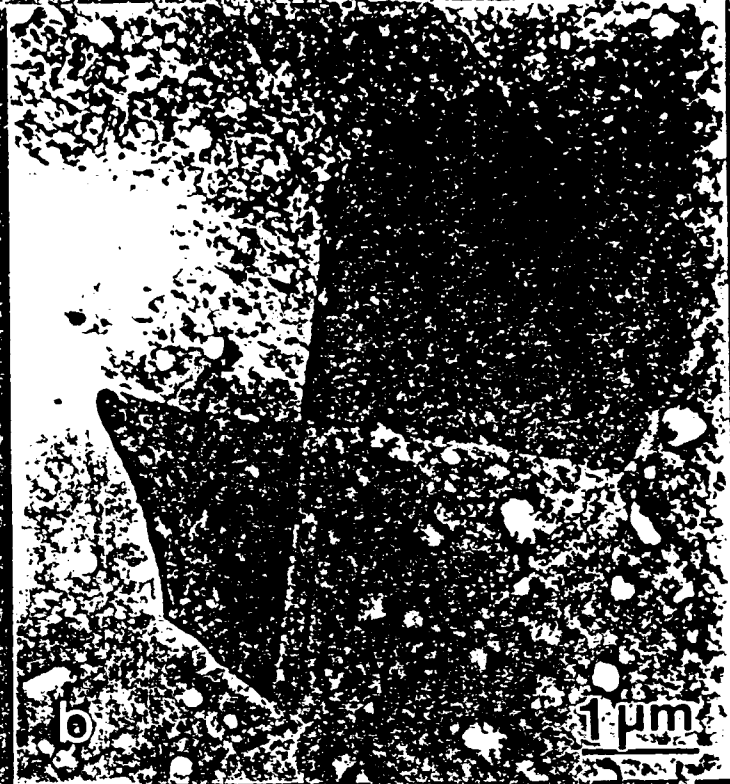
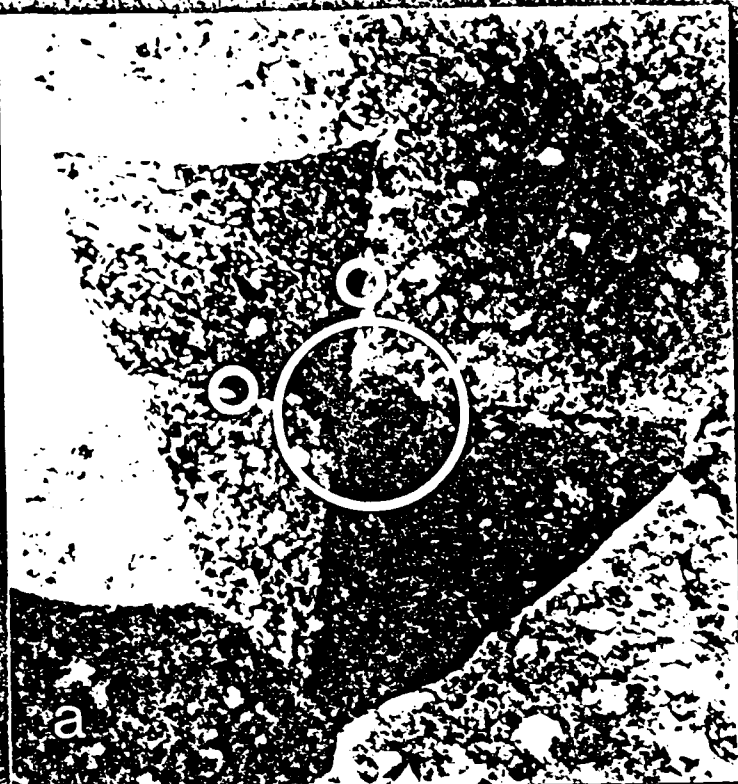
Figure 3. Nanotwins within domains.

Figure 4a. Superlattice generated by superimposing possible twin crystal lattice structures. The circles are a imaginary lattice structure for the organic matrix.

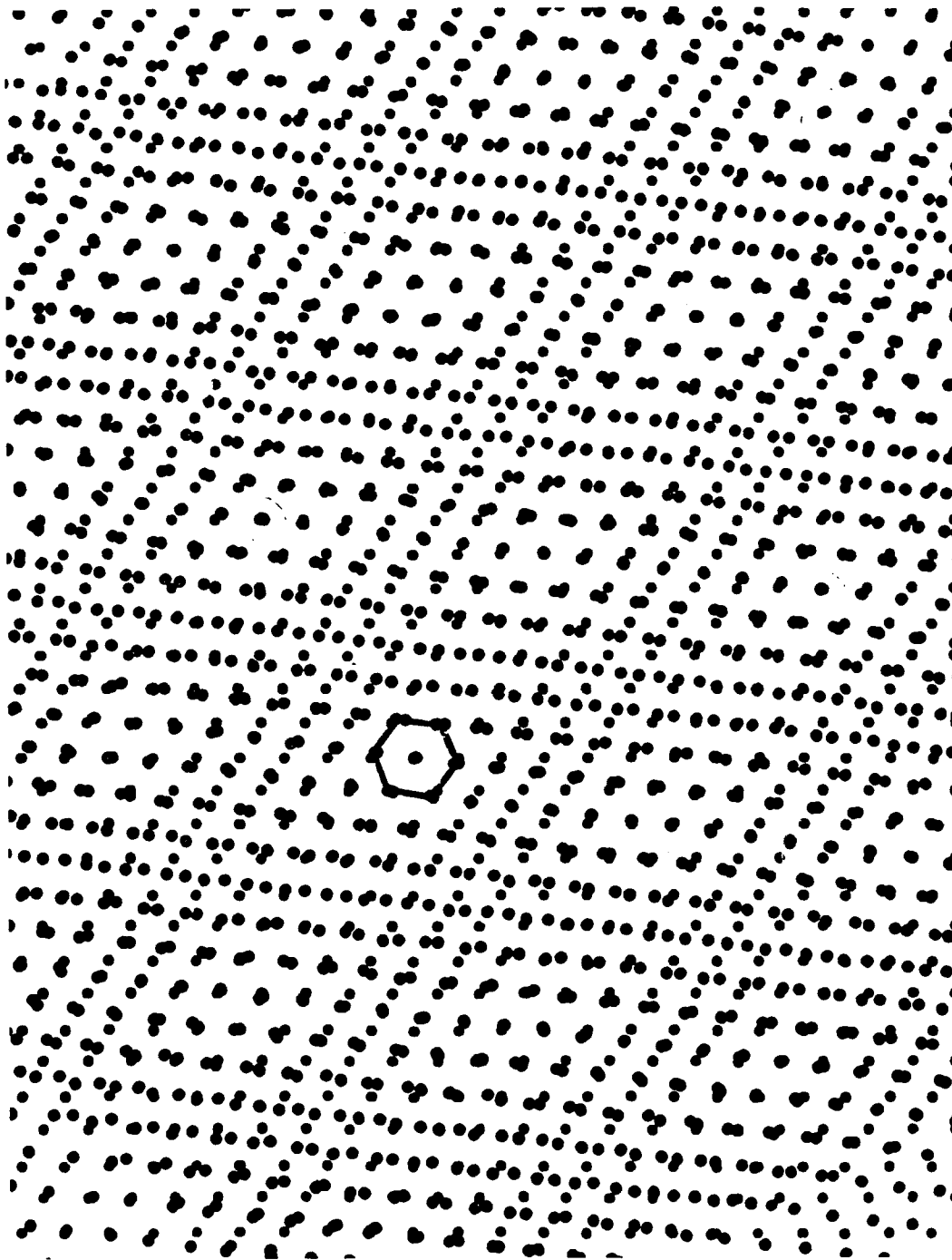
Figure 4b. All the tiling patterns can be constructed on the superlattice by tracing along possible twin boundaries.

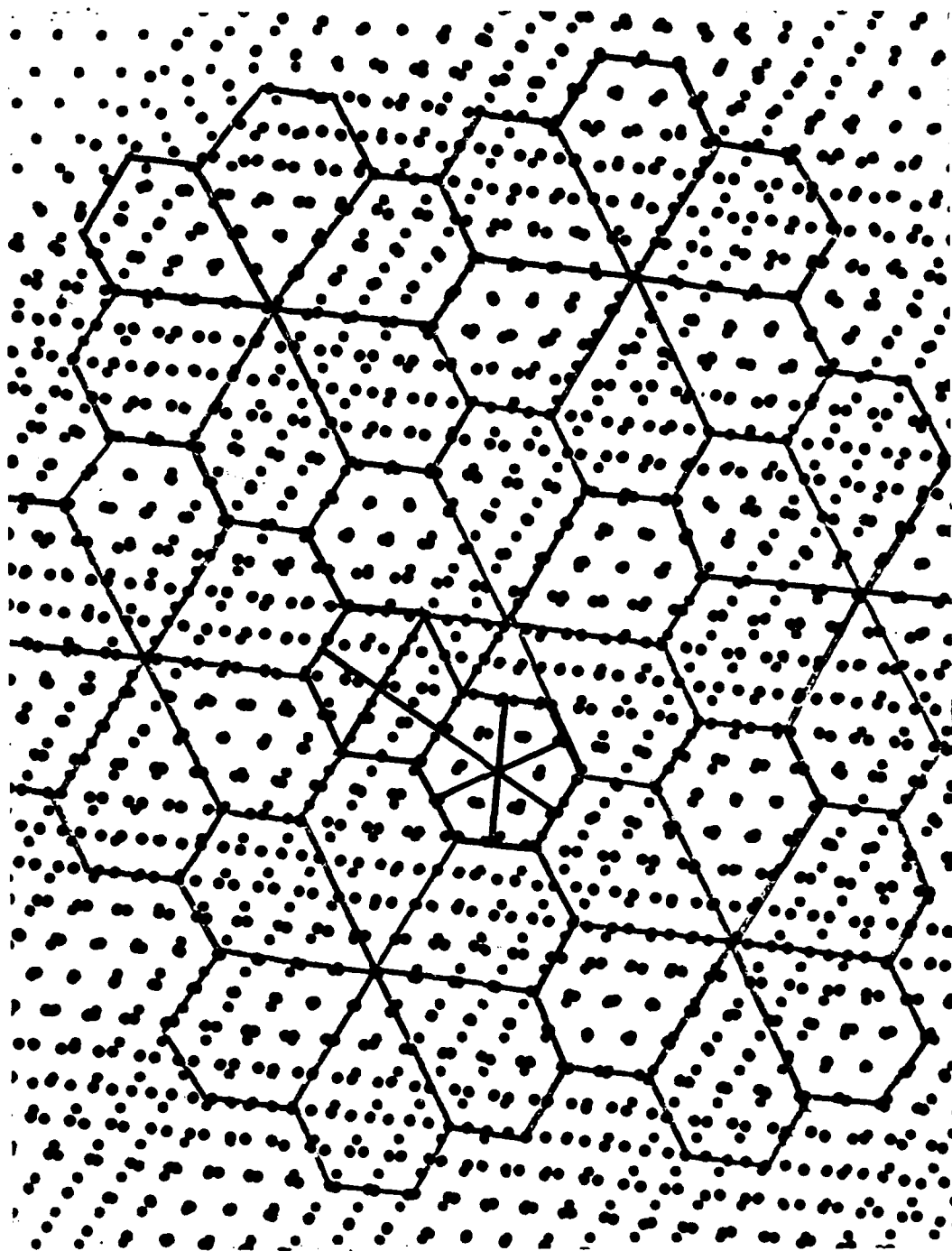














APPENDIX X

The Nacre of Abalone Shell: A Natural Multifunctional Nanolaminated Ceramic-Polymer Composite Material

by

M. Sarikaya and I. A. Aksay

to be submitted to
Structure, Cellular Synthesis, and Assembly of Biopolymers
edited by S. T. Case
(Springer-Verlag, New York, 1992)

Table of Contents

1	Introduction: Nanocomposite Materials and Biological Composites.....
2	Mechanical Properties of Nacre
2.1	Toughness and Strength in Nacre
2.2	Toughening Mechanisms
2.3	Strengthening Mechanisms
3	Design Guidelines for the Processing of Biomimetic Laminated Composites.....
4	Structure of the Abalone Shell: Prismatic and Nacreous Layers.....
4.1	Structure of the Shell at the Macro Level
4.2	Structure of the Nacre at the Nanometer Level.....
4.2.1	Morphology of Inorganic Phase: Aragonite
4.2.2	Crystallography of Aragonite Platelets
5	Structure of the Organic Matrix and Its Relationship
6	Summary, Future Directions, and Concluding Remarks.....
7	Acknowledgements
8	References

APPENDIX XI

Bioinspired Processing of Composite Materials

by

I. A. Aksay and M. Sarikaya

Proceedings of The Centennial International Symposium on Ceramics
(Japanese Ceramic Society, Tokyo Japan, 1991)

BIOINSPIRED PROCESSING OF COMPOSITE MATERIALS

Ilhan A. Aksay and Mehmet Sarikaya

Department of Materials Science and Engineering, and
Advanced Materials Technology Center, Washington Technology Center,
University of Washington, Seattle, Washington, USA 98195

*Biologically produced composites possess hierarchical architectures with synergistic variations from atomic to macroscopic dimensions. Consequently, these biocomposites display unique properties that are affected by processes operating at all levels of the length scale. As a source of inspiration for new design concepts, we examine the structure of nacre (abalone shell) and show that a similar architectural design for laminated ceramic/metal and ceramic/polymer composites, produced by totally artificial methods (biomimetics), results in improvements in the mechanical properties of the laminates compared to the same phase-composition materials of isotropic morphology. We also examine the formation of nanometer-sized particles in a microorganism (*Aquaspirillum magnetotacticum*) and illustrate process mechanisms somewhat similar to those used by this microorganism (bioduplication) that can be utilized to synthesize multiphase and nanosized particles in phospholipid vesicles.*

I. Introduction

When materials are manufactured with an emphasis on tailoring their properties through microstructural control, the extent of this control is generally at a specific length scale. For instance, the mechanical properties of most metallic materials are controlled through the manipulation of dislocation dynamics at the nanometer length scale, whereas the mechanical properties of ceramic materials are controlled through the propagation of cracks that are initiated from defects of micrometer length scales.

In contrast, many biologically produced materials are very complex in structural design at a spectrum of length scales varying from atomic to macroscopic dimensions and possess unique hierarchical architectures [1-6]. Cellulose-based aggregates in wood [7], collagen-based aggregates in skin, cartilage, and bone [1-3,5,6,8], and chitin-based aggregates in seashells [1,4,6,9-13] are excellent examples of nature's way of designing composites for multifunctional applications by efficient and ecologically balanced methodologies. These hierarchically structured materials display unique properties that are affected by processes operating at all levels of the length scale spectrum [1-13].

It is interesting to note that when we attempt to engineer composites with functions similar to those found in biological materials, the architectural design of the manmade materials

also starts to display similar hierarchical features and multifunctionality. For instance, the architecture of fiber-reinforced automobile tires, which are designed to perform a multitude of functions, is very similar to the hierarchical design observed in intestinal tissue or elephant trunk. However, it is quite unlikely that the engineers who came up with these innovative designs had any knowledge of their similarity to biological analogs.

Our contention is that if we were to utilize biological systems as a source of *inspiration* for new design and processing concepts, then more manmade materials might display these unique architectural features and thus multifunctional performance characteristics [14]. We envision two approaches to achieve this goal of *bioinspired* processing: (i) *biomimetics* and (ii) *bioduplication*. The biomimetic approach aims at designing hierarchical structures by synthesis and processing methodologies that are largely artificial with respect to the biological processing mechanisms. However, these artificially engineered composites will exhibit structural features similar to those found in biological composites. For instance the example of automobile tire mentioned above falls into this category. Conversely, the bioduplication approach aims at producing hierarchical structures by mechanisms very similar to those observed in biological synthesis and processing methodologies.

In support of this bioinspired processing concept, in this paper we provide examples from both the biomimetic and the bioduplication approaches on the synthesis and processing of ceramics and ceramic-based composites. For the biomimetic approach, we first summarize our recent studies on the structure and properties of abalone shell and illustrate that similar structures and thus properties can be modeled in laminated ceramic/metal (cermet) and ceramic/polymer (cerpoly) composites by using totally artificial process methodologies. With respect to our Japanese hosts of this symposium, we acknowledge them as the originator of this concept of artificially produced laminated ceramic/metal composites since Samurai sword appears to be the first manmade laminated ceramic/metal composite that displays striking similarities to the structure of abalone shell.

In the category of bioduplication, we use the bacterium *Aquaspirillum magnetotacticum* as an example of a microorganism that produces nanometer-sized superparamagnetic magnetite particles. We then illustrate that mechanisms somewhat similar to those used by this microorganism can be utilized to synthesize ceramic particles of different structures and compositions in phospholipid vesicles.

II. Design in Biologically Produced Ceramic/Polymer Composites

Most biologically produced composites are built upon a fibrous framework of either collagen, chitin, or cellulose and always reveal a hierarchical structure that originates at the molecular level [1-3,7,8,12,13]. In all cases, the structures are formed by groupings of discrete units in the form of fibrils, which themselves are composed of smaller subfibrils and microfibrils. These highly interacting fibrous units are organized to form a variety of oriented

hierarchical composite systems that are designed to meet a spectrum of functional requirements. For instance, a classical hierarchical system that connects muscle and bone is tendon, which in use is subjected almost exclusively to uniaxial tensile stresses along its length. The hierarchical structure of tendon displays six discrete levels of organization [2,3,8]: (i) at the molecular level, a triple helical arrangement of polypeptide chains forms the basic tropocollagen molecule at a length scale of 1.5 nm; (ii) tropocollagen molecules aggregate to form microfibrils at a length scale of 3.5 nm; (iii) microfibrils are packed into a lattice structure forming subfibrils at a length scale of 10-20 nm; (iv) the subfibrils are joined to form fibrils at a length scale of 50-500 nm; (v) these fibrils serve as the basic building blocks to form fascicles at a length scale of 50-500 μm ; and (vi) two or three fascicles together form the structure referred to as tendon. This multilevel organization then imparts both nonlinear reversible mechanical properties and toughness to the tendon. If the tendon is subjected to excessive stresses, individual elements at different levels of the hierarchical structure fail independently [2,3,6]. These elements absorb energy and protect the tendon as a whole from catastrophic failure.

In collagen, the tropocollagen molecules are arranged with a stagger that results in a 64 nm band structure and a 30-40 nm gap between the molecules [1,12]. This gap is believed to be associated with the nucleation of the hydroxyapatite mineral as the inorganic phase leading to the formation of bone [1,5,12]. Similar to the role that collagen plays in the formation of bone, a chitin-based fibrous framework acts as the template for the formation of the orthorhombic form of calcium carbonate (aragonite) crystals in nacre, or mother of pearl [4,9-13]. Here, the structure is composed of layers of aragonite platelets held together by a matrix of acidic proteins organized around the network of chitin fibrils (Fig. 1) [1,4,6,9-13].

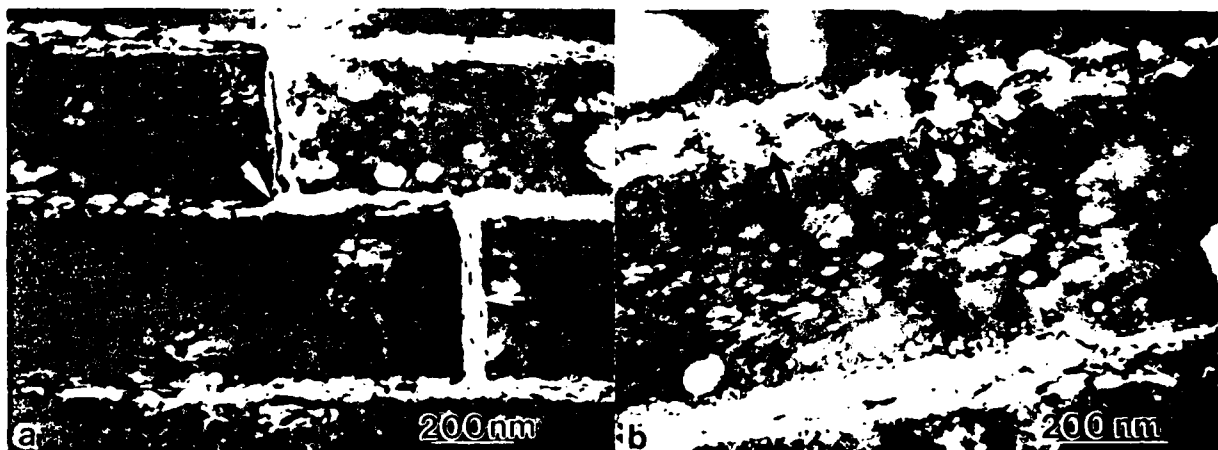


Figure 1(a) and (b). Conventional transmission electron microscopy (TEM) images of cross section of abalone shell revealing the nacre structure. Dark layers are the ceramic phase and the light color interfacial regions contain a fibrous network of organic tissue as highlighted with arrows [9].

In Figs. 1 and 2, the aragonite layers are shown to be highly regular, about 0.25-0.5 μm thick [9-11]. These layers are glued together by ultrathin, 10 nm, tough, proteinaceous composite nanoscale layers that are specifically functionalized to bond to the inorganic layers [1,12]. This rigid, predominantly inorganic ($\sim 95\%$ by volume) hierarchical composite is toughened by the organic nanoscale layer, as is evident from the fact that the fracture path is both relatively wide and tortuous with inorganic platelets held by organic ligaments. There is also a significant irreversible deformation of the overall composite due to the sliding of platelets over the organic layers as shown in Fig. 2(a-b) [11].

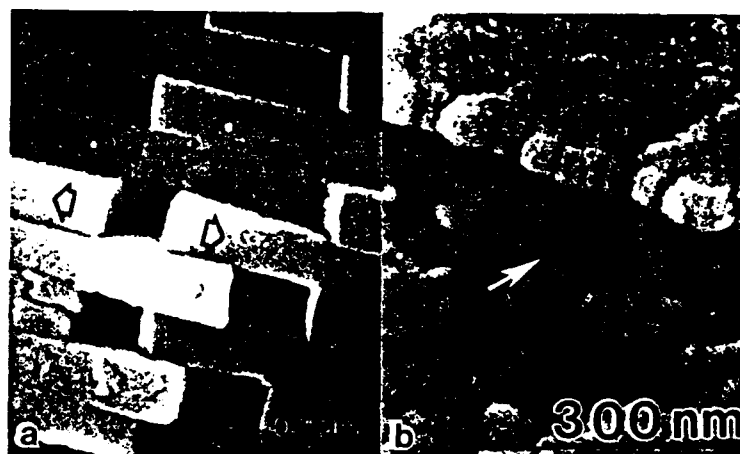


Figure 2. (a) Sliding of aragonite platelets during crack propagation in nacre and (b) ligament formation by the organic matrix between the platelets [11].

The resultant layered composite, incorporating hard inorganic layers (aragonite platelets) surrounded by a nanometer-thick organic matrix, is an excellent nanoscale layered design for a perfect impact resistant material, as evidenced from both the toughness and strength increases in nacre compared to single crystalline aragonite (Fig. 3). In the case of nacre, both the fracture toughness and fracture strength increase significantly. Unusual toughening mechanisms, in particular irreversible deformation, may be responsible for the increase in toughness in what is practically a ceramic material. Studies [11] on crack propagation behavior indicate that two mechanisms play a key role in enhancing the toughness: (i) energy dissipation during sliding of the aragonite layers, resulting in an overall plastic deformation of the composite (Fig. 2(a)); and (ii) energy dissipation during stretching of the chitin filaments (Fig. 2(b)). In both cases, the presence of an ionic bond between aragonite and the organic layer is believed to be essential for optimization of the properties. To date, however, there is no clear explanation that can account for the strength increases in these biological ceramic/polymer composites. The increase in strength cannot be explained based solely on the effect of the size of the layers and the rule of mixtures. The best explanation that we can presently put forward is that the tensile stress applied to the nacre is transferred to compressive stresses during loading. As evident from the

inward bulging of the edges of the indentation [10], this stored energy during loading results in dilation during load release; the failure of the composite appears to take place during unloading. Although not fully understood, this failure mode effectively increases the overall strength of the composite many orders of magnitude.

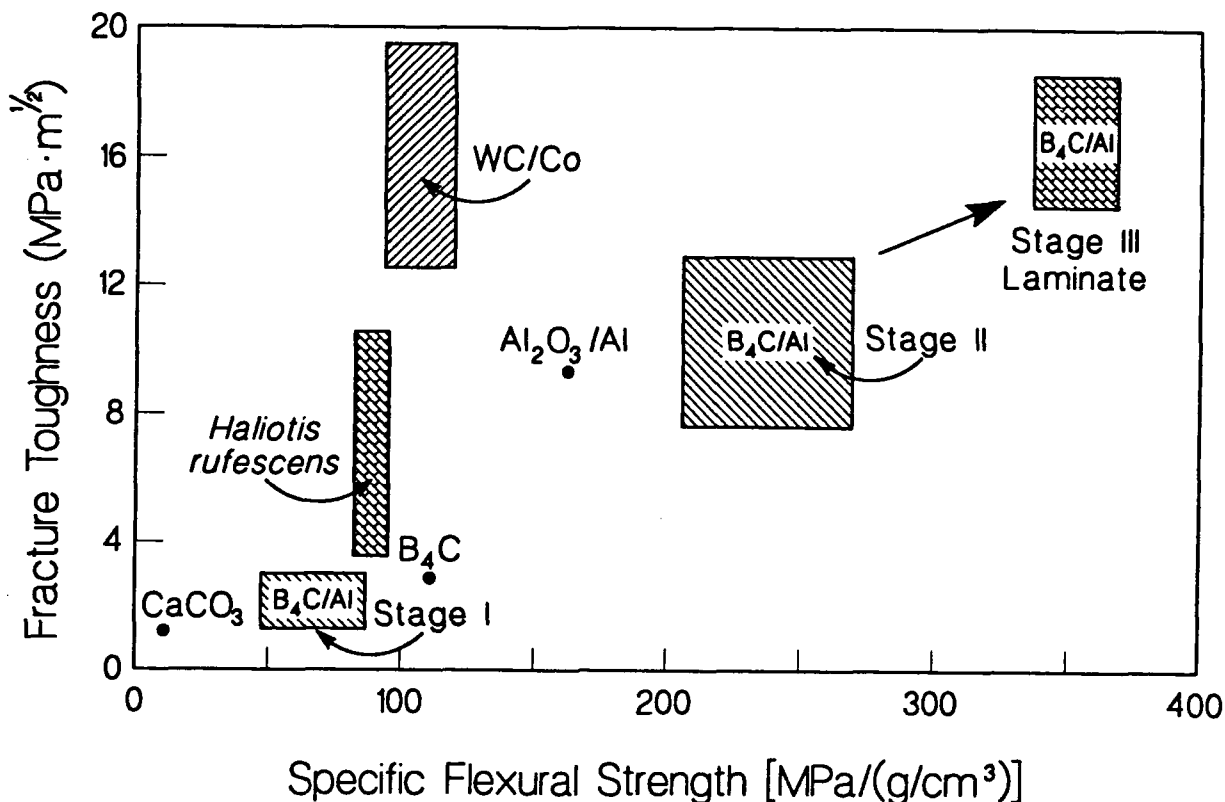


Figure 3. Mechanical properties of the nacre of red abalone (*Haliotis rufescens*) compared to ceramics and ceramic-based composites. In *Stage I*, the processing of boron carbide/aluminum was done by hot pressing of mixed powders. In *Stage II*, an infiltration technique was used to process an isotropic and bicontinuous composite. In *Stage III*, the lamination techniques described in this paper were used.

III. Synthesis and Processing of Hierarchical Structures

The example of nacre as a hierarchically structured biological ceramic/polymer composite illustrated in Section II indicates the design principles that synthetic hierarchical structures will require in order to achieve superior properties. Synthetic examples given in this section illustrate two key points: (i) by mimicking the architecture of biological composites through artificial methods, it is possible to improve upon the properties of composites even though we may not quite understand how biological composites are produced; and (ii) by realizing that the first approach will ultimately be insufficient, longer range research on bioduplication will aid in advancing the progress in biomimetics by integrating biological methodologies with synthetic ones. We also recognize that the concept of biomimetics is not a totally new concept since

many conventional composites are already produced with hierarchical structures that are similar to those found in biological counterparts.

(A) *Biomimetic Approach:*

Laminated Ceramic/Metal and Ceramic/Polymer Composites: Based on the design criteria derived from nacre [11], we have been working on the processing of cermet and cerpoly laminated composites through tape casting and liquid infiltration techniques, specifically with boron carbide/aluminum [15,16] and boron carbide/polymer [17] composites, respectively. In both cases, significant increases in both the fracture toughness and fracture strength have been observed (Fig. 3). Toughening mechanisms similar to those that operate in biological composites also operate in these synthetic laminates (Fig. 4). However, the improvements in the properties of synthetic laminates are still far inferior to the properties of laminated biological composite structures. The conjecture is that a major reason for our failure to achieve the values of the biological composites is because our current processing strategies do not permit processing of laminates on the micro- and nanometer scales.

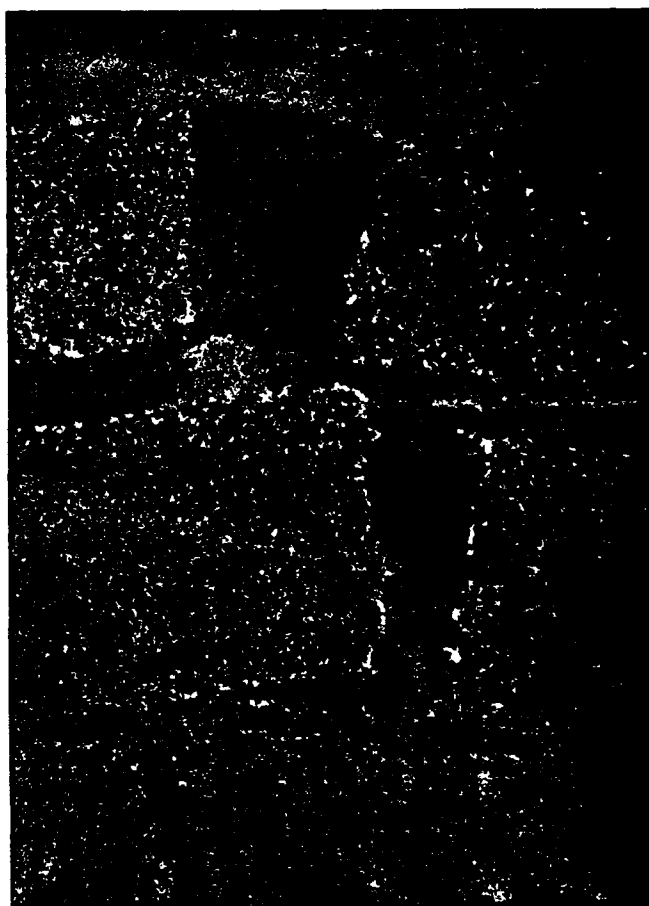


Figure 4. Fracture pattern of a laminated boron carbide/polypropylene composite illustrating polymer bridging within and between the ceramic layers ($\sim 90 \mu\text{m}$) [17].

These laminated composites can be formed by one of three basic methods: (i) partially sintered ceramic tapes are sandwiched with metal or polymer sheets and then heated to induce infiltration of the metal or the polymer; (ii) nonsintered ceramic tapes are stacked, partially sintered, and then infiltrated with metal or polymer; and (iii) nonsintered ceramic tapes of different porosity are laminated (stacked and pressed), partially sintered, and then infiltrated. In all cases, the resulting structure is a ceramic/metal or ceramic/polymer laminated composite with metal or polymer at intra- and interlayers (Fig. 4).

Mechanical property testing of laminated boron carbide/aluminum cermets in four-point bending showed increases in fracture strength and toughness over the same aluminum-content materials with an isotropic morphology (Fig. 3). When the aluminum content of laminated samples was altered by changing the ratio between the aluminum-rich and boron carbide-rich layers in the microstructure, a ratio of 6 to 1 of high-boron-carbide-content tape to low-boron-carbide tape (and hence the aluminum-rich region in the post-infiltration microstructure) with a 33.5 vol% aluminum content resulted in the highest fracture strength (945 MPa).

After the proper ratio of high boron carbide content to low boron carbide content (or aluminum-rich) laminae was determined to be 6 to 1, simultaneous changes in the size of both laminae were made while maintaining the ratio. The effect of changing the thickness of the laminae on both fracture strength and fracture toughness was in agreement with the Hall-Petch relation. The coarsening of the microstructure by increasing the tape thicknesses degraded the mechanical properties, with values approaching those for isotropic samples. Finer 6 to 1 ratio graded laminate structures have not been processed at this time due to the difficulty in casting and handling tapes thinner than 15 μm .

In the case of boron carbide/polypropylene laminates, the work of fracture of the laminates similar to the ones shown in Fig. 4 showed a 30- to 40-fold increase over monolithic and porous preforms. But no strength increase was observed.

Samurai Sword: A Laminated Nanocomposite: The practice of controlling the microstructure of materials at the nanoscale to achieve desired properties has a long history, especially in metallurgy [18]. Understanding the microstructures in successful ancient materials is essential both for developing "microarchitectural design" concepts for modern multifunctional composites as well as generating new alloy microstructures. For instance, it has been known for many centuries that laminated steels make stiff, strong, and tough swords by alternating thin layers of a stiff metal alloy with thin layers of a tough alloy. These remarkable composite structures are still being studied today [19,20]. An excellent example of this is Damascus steel, which was developed in the Middle East during the late iron age, more than 2000 years ago. The steel was used mostly for armor applications requiring high toughness as well as high strength and hardness. The metallurgy that produced Damascus steel is based on a simple thermomechanical cycle which forms a composite microstructure containing soft and hard phases. Originally "cast" high carbon steel (>1.0-2.0 wt% C) is homogenized at 1200°C,

which produces coarse austenite (γ) grains. The steel is then cooled slowly through the γ -carbide (Fe_3C) region during which pre-eutectoid carbides form at prior austenite grain boundaries. The coarse microstructure is "broken down" during forging at temperatures of 750°-900°C, and carbides spheroidize to form strings of particles in refined austenite grains. Quenching into warm water (40°-80°C) from about 750°C transforms the fine austenite grains into fine needles of brittle but strong martensite, which is a supersaturated ferrite. The material is then annealed at 200°-300°C to produce tempered fine carbides (200-500Å) to form what is now still strong, but relatively tough, martensite needles. The resulting microstructure is then tough martensite containing ultrafine precipitates with hard strings of carbides decorating prior austenite grain boundaries.

Many variations of iron-based microstructures have since been developed by modifying the thermomechanical treatments and, most notably, by "composite lamination," which incorporates both pure iron (soft and tough) and high and medium carbon steels (hard and strong). An excellent example of this is Samurai sword, which is truly "nanolaminated" and is an ideal material for its purpose because of its unique combination of toughness, hardness, and rigidity [21,22]. These three properties in one material, however, are contradictory: that is, toughness implies a soft material that bends easily; hardness is associated with brittle material; and rigidity requires high strength at low strain. Apparently, Japanese smiths many centuries ago developed these composites based on techniques similar to the earlier techniques of Damascus steel-making and by knowing how thermomechanical treatments and compositional adjustments can change the steel's properties.

The final body of the Samurai sword blade is a hierarchical structure consisting of a soft inner core (ferrite) with a hard outer core (low-carbon martensite). The steel is produced first in the form of a laminated iron and steel blank with dimensions 1.5 cm thick by 5 cm wide and 15-20 cm long. The blank is inserted into pine ash (carbon source) and heated white hot (about 600°-800°C) and then doubled onto itself by hammering until it takes its original width. This process is repeated fifteen to twenty times. Four similar blanks are then welded together, and the same thermomechanical treatment is repeated five times. Eventually, the resulting blank, presumably, forms a laminate with the thickness of each lamellae equal to a few nanometers [21,22]. The surface of the blade (the laminated blank) is then scraped and ground to shape. The final blade is covered with a mixture of clay and fine sand and dried. The blade is then heated to about 900°C and quenched in a room temperature bath of oil or water by inserting the tip first and then the sharp edge horizontally. The final blade has a curved shape with the sharp edge having mostly a hard and strong martensitic structure and the back edge consisting of the relatively soft ferritic microstructure, providing ultra-rigidity to the overall material.

It should be noted here that the microstructures of lath martensitic steels and nacre are very similar. It is the martensite lath, which has dimensions similar to the aragonite platelets in nacre (both about 0-25 μm thick), that provides strength. The thin film retained austenite (50-

500 Å thick) [23] that covers the martensite platelets (laths) is similar to the organic layer (~ 200 Å) covering the aragonite platelets in the nacre. Furthermore, in both cases, the interfaces are very strong between the hard and soft phases. In nacre, adjacent aragonite platelets have their [001] axis perpendicular to the platelet/organic matrix interface, with plates rotating slightly (1-5°) with respect to this axis. In martensite, similarly, the adjacent laths have a common <110> axis, perpendicular to the α'/γ interface, with laths rotating slightly (1-6°) with respect to this axis. In both cases, the matrices (organic phase in the nacre and austenite in lath martensitic structures) have the same orientation throughout. However, the difference between the two structures is that the lath martensite contains packets (three 70° variants of martensite grains, with their attendant austenite grains, randomly distributed throughout the sample) [23]. In the nacre, the local arrangement of the layered structure is repeated throughout the sample. Therefore, lath martensite is a true three-dimensional structure, with local laminated domains, resulting in isotropic mechanical properties. Nacre, on the other hand, is a true two-dimensional microstructure possessing unprecedented high anisotropic properties.

(B) Bioduplication Approach:

Vesicle-Mediated Multicomponent Processing: Intravesicular precipitation of inorganic, crystalline particles is a very common method of producing nanosized particles in biological systems [24,25]. For example, nanometer-sized magnetite particles are fabricated in intracellular vesicles by certain types of bacteria with precise control over particle morphology and orientation (Fig. 5) [24,25]. Various investigators have already demonstrated that single component particles can be precipitated within synthetic vesicles as a model system for the study of biomineralization [26]. Below, we illustrate the extension of these methods to the processing of multicomponent particles [27].

Particle precipitation within vesicles has several fundamental differences from bulk precipitation methods due to the unique properties of the lipid bilayer. In addition to forming a reaction cell, which limits the particle size, the bilayer serves as a semipermeable membrane to ion diffusion. Generally, phospholipid vesicles are nearly impermeable to cations, with typical permeability coefficients between 10^{-12} to 10^{-14} cm/s. Diffusion rates of anions, on the other hand, are usually quite low (10^{-10} cm/s for Cl^-). This characteristic imposes a kinetic restraint on precipitation due to the diffusion restrictions across the bilayer and produces a system in which cations are essentially "trapped" within the phospholipid cage until precipitation can occur. This could potentially enhance chemical homogeneity within the system and facilitate the aqueous precipitation of water-soluble phases (such as $\text{Ba}(\text{OH})_2$).

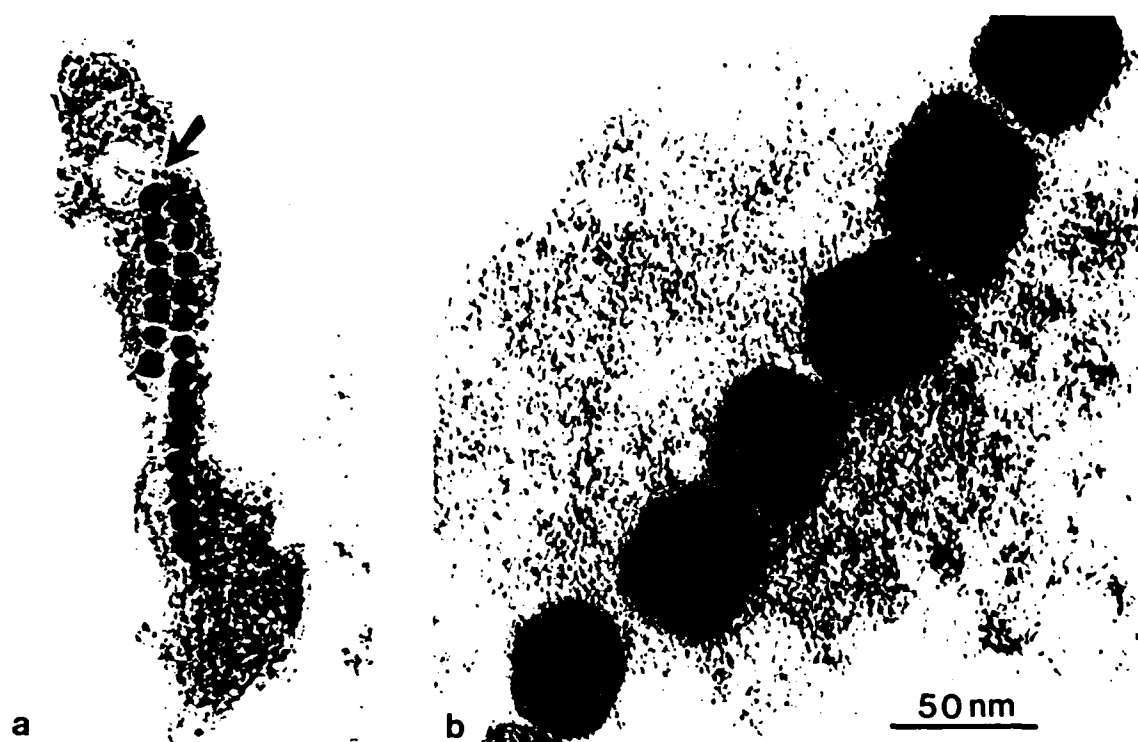


Figure 5. String of single crystalline magnetite particles in magnetic bacteria, *Aquaspirillum magnetotacticum*. Both are TEM images.

Figure 6 shows a transmission electron microscopy (TEM) image of the vesicle-formed particles using Y, Ba, Cu, and Ag nitrate precursors. The lipid membrane was not stained in these experiments and, therefore, is not visible. The particles are roughly spherical, crystalline, and well-dispersed. A mean particle diameter of 34.8 nm with a standard deviation of 13.2 nm was determined from TEM micrographs of 470 different particles. It is important to compare the particle sizes with the starting sizes of the original vesicles. Theoretically, the particle sizes should be smaller than the vesicles from which they were formed. Light-scattering experiments showed the vesicle size in deionized water to be approximately 59 nm. Since the presence of ions in solution can have pronounced effects on the morphology and phase transitions of vesicles, we also measured sizes in the presence of the nitrate salts. The vesicle size increased to 99 nm under the high ion concentrations. In both cases, the results confirm that the particle size is smaller than the corresponding vesicle size.

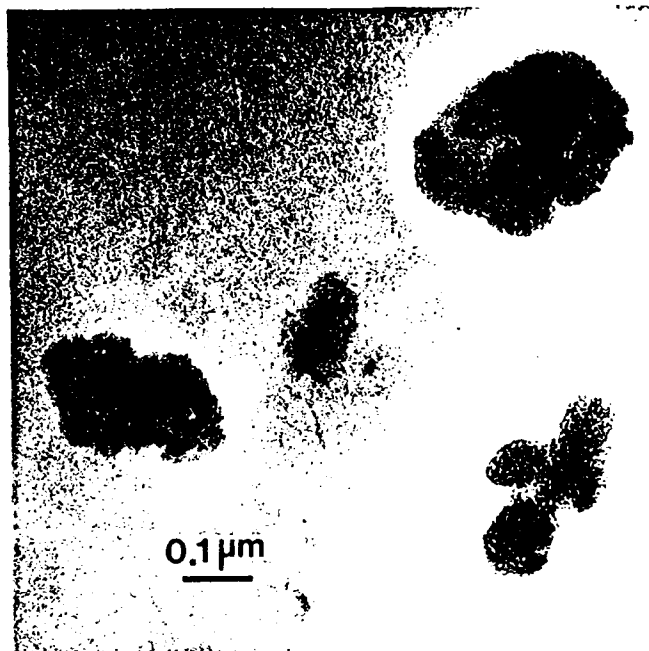


Figure 6. TEM micrograph of multicomponent particle formed within vesicle [27].

Although the vesicle-mediated particle formation system exhibits some exciting advantages over more conventional methods of powder production, there are also some distinct problems with the system. By far the most serious is that the ratio between elements in the formed particles is not consistent with the beginning solution ratios. Most pronounced is the barium to silver ratio. Although the starting solution contained eight times more barium than silver, the final particles were always rich in silver. In order to provide solutions to this problem, future research has to be directed toward understanding the association of ionic species in solution with the phospholipid bilayer by approaches discussed elsewhere [28-30].

IV. Conclusions

We have illustrated that by processing materials with architectural designs similar to those of biological composites (*biomimetics*), it is possible to improve upon their properties. The nacre of abalone shell which is a nanoscale-laminated composite of ~ 95 vol% aragonite and a chitin-based organic tissue possesses significantly higher values both in strength and toughness than its ceramic constituent phase. The microscale-laminated composites of boron carbide/aluminum discussed in this paper similarly displayed increases both in strength and toughness. Microscale-laminated boron carbide/polypropylene composites showed only a toughness increase. Since in both cases, the improvements are not yet as impressive as observed in the biological composites, we predict that nanoscale lamination may be necessary to achieve further improvements.

We have also demonstrated that phospholipid vesicles can be used as reaction vessels for the synthesis of ultrafine, well-dispersed, multicomponent ceramic particles by a processing approach which is similar to the methods used in biological systems (*bioduplication*). Here, the chemical inhomogeneity of the system can be restricted to the individual vesicle size, which is approximately 40 nm. We also found that precise control over chemical stoichiometry in multicomponent systems may be difficult to achieve due to differences in ion permeabilities, trapping efficiencies, and interactions between various cations and the vesicle membrane. This bioduplication approach to processing nanosized particles is truly multifunctional since the system simultaneously acts as: (i) a reaction cell for particle precipitation, (ii) an ion selective membrane that affects precipitation kinetics, and (iii) a barrier to prevent spontaneous agglomeration of the ultrafine particles.

Acknowledgments

The research described in this paper was sponsored by the U.S. Air Force Office of Scientific Research under Grant Nos. AFOSR-91-0040 and AFOSR-91-0281, by the U.S. Department of Energy through a subcontract by Battelle, Pacific Northwest Laboratory under Contract No. 0722348-A-F1, and by the IBM Corporation. The assistance of M. S. Wallace and D. M. Dabbs in the preparation of the manuscript is appreciated.

References

1. S. A. Wainwright, W. D. Biggs, J. D. Currey, and J. M. Gosline, *Mechanical Design in Organisms*, Princeton University Press, Princeton, New Jersey, 1976.
2. J. Kastelic, I. Palley, and E. Baer, "A Structural Mechanical Model for Tendon Crimping," *J. Biomech.*, **13** [10] 887-93 (1980).
3. J. J. Cassidy, A. Hiltner, and E. Baer, "Mechanical Properties of Biological Polymers," *Annual Rev. Materials Sci.*, **15**, 455-82 (1985).
4. A. P. Jackson, J. Vincent, R. M. Turner, "The Mechanical Design of Nacre," *Proc. Royal. Soc., B*, **234** [1277] 415-40 (1988).
5. J. Currey, *The Mechanical Adaptations of Bones*, Princeton University Press, Princeton, New Jersey, 1984.
6. J. Vincent, *Structural Biomaterials*, revised edition, Princeton University Press, Princeton, New Jersey, 1990.
7. *The Chemistry of Solid Wood, Advances in Chemistry Series, No. 207*, ed. R. M. Powell, American Chemical Society, Washington, D.C., 1984.

8. E. Baer, A. Hiltner, and H. D. Keith, "Hierarchical Structure in Polymeric Materials," *Science*, **235**, 1015-22 (1987).
9. J. Liu, M. Sarikaya, and I. A. Aksay, "Hierarchical Twins and Multiple Tiling in Nacre," unpublished work, University of Washington, Seattle, Washington.
10. K. E. Gunnison, "Structure-Mechanical Property Relationships in a Biological Ceramic Polymer Composite: Nacre," M.S. Thesis, University of Washington, Seattle, Washington, 1991.
11. M. Sarikaya, K. E. Gunnison, M. Yasrebi, and I. A. Aksay, "Mechanical Property-Microstructural Relationships in Abalone Shell," in *Materials Synthesis Utilizing Biological Processes, MRS Symp. Proc., Vol. 174*, eds. P. C. Rieke, P. D. Calvert, and M. Alper, Materials Research Society, Pittsburgh, Pennsylvania, 1990, pp. 109-16.
12. H. A. Lowenstam and S. Weiner, *On Biomineralization*, Oxford University Press, Oxford, 1989.
13. K. Simkiss and K. M. Wilbur, *Biomineralization: Cell Biology and Mineral Deposition*, Academic Press, San Diego, California, 1990.
14. I. Amato, "Heeding the Call of the Wild," *Science*, **253** [5023] 966-68 (1991).
15. A. J. Pyzik and I. A. Aksay, "Microdesigning of B₄C-Al Cermets," in *Processing of Ceramic and Metal Matrix Composites*, ed. H. Mostaghaci, Pergamon Press, New York, 1989, pp. 169-80.
16. M. Yasrebi, G. H. Kim, K. E. Gunnison, D. L. Milius, M. Sarikaya, and I. A. Aksay, "Biomimetic Processing of Ceramics and Ceramic-Metal Composites," in *Better Ceramics Through Chemistry IV, MRS Symp. Proc., Vol. 180*, eds. B. J. J. Zelinski, C. J. Brinker, D. E. Clark, and D. R. Ulrich, Materials Research Society, Pittsburgh, Pennsylvania, 1990, pp. 625-35.
17. S. S. Khanuja, "Processing and Structure-Property Relationships of Boron Carbide/Polymer Composites," M.S. Thesis, University of Washington, Seattle, Washington, 1991.
18. C. S. Smith, *A History of Metallography*, University of Chicago Press, Chicago, 1965.
19. J. Wadsworth and O. D. Sherby, "On the Bulat - Damascus Steels Revisited," *Progress in Materials Science*, **25** [1] 35-68 (1980).
20. J. Wadsworth, D. W. Kum, and O. D. Sherby, "Welded Damascus Steels and A New Breed of Laminated Composites," *Metal Progress*, **129** [7] 61-7 (1986).

21. E. C. Bain, "Nippon-to, An Introduction to Old Swords of Japan," *J. Iron and Steel Inst.*, **200** [2] 265-82 (1962).
22. L. Kapp, H. Kapp, and Y. Yoshihara, *The Craft of the Japanese Sword*, Kodansha Intl. Ltd., Tokyo, 1987.
23. M. Sarikaya, H. Togushige, and G. Thomas, "Lath Martensite and Bainite in Low Alloy Steels," in *Proc. Intl. Conf. Martensitic Transformations*, Japan Institute of Metals, 1986, pp. 613-18.
24. R. P. D. Blakemore, D. Maratea, and R. S. Wolfe, "Isolation and Pure Culture of a Freshwater Magnetic *Spirillum* in Chemically Defined Medium," *J. Bacteriol.*, **140** [2] 720-29 (1979).
25. S. Mann, R. B. Frankel, and P. P. Blakemore, "Structure, Morphology, and Crystal Growth of Bacterial Magnetite," *Nature*, **310** [5976] 405-07 (1985).
26. J. H. Fendler, *Membrane Mimetic Chemistry*, John Wiley, New York, 1982.
27. H. Liu, G. L. Graff, M. Hyde, M. Sarikaya, and I. A. Aksay, "Synthesis of Ultrafine, Multicomponent Particles Using Phospholipid Vesicles," in *Materials Synthesis Based on Biological Processes, MRS Symp. Proc.*, Vol. 218, eds. M. Alper, P. D. Calvert, P. C. Rieke, D. A. Tirrell, R. Frankel, Materials Research Society, Pittsburgh, Pennsylvania, 1991, in press.
28. S. Mann, "Molecular Recognition in Biomineralization," *Nature*, **332** [6159] 119-24 (1988).
29. S. Mann, B. R. Heywood, S. Rajam, and J. D. Birchall, "Controlled Crystallization of CaCO_3 under Stearic Acid Monolayers," *Nature*, **334** [6184] 692-95 (1988).
30. I. Weissbuch, L. Addadi, M. Lahav, L. Leiserowitz, "Molecular Recognition at Crystal Interfaces," *Science*, **253** [5020] 637-45 (1991).

APPENDIX XII

Synthetic and Biological Nanocomposites

by

M. Sarikaya and I. A. Aksay

Proceedings of 5th International Conference on Ultrastructure Processing

edited by L. L. Hench and J. K. West

(Wiley, New York, 1991)

Synthetic and Biological Nanocomposites

Mehmet Sarikaya and Ilhan A. Aksay

Department of Materials Science and Engineering, and
Advanced Materials Technology Center, Washington Technology Center,
University of Washington, Seattle, Washington 98195 USA

submitted to

1991 Ultrastructure Conference

June 20, 1991

Abstract

The effects of structures on the mechanical properties of laminated composites, with lamination at the nanometer scale, are discussed by presenting two example systems, one inorganic and the other biological. The first example is from a metallic system that forms a lath martensitic structure due to a phase transformation in the Fe-C binary alloy. In this case, the heavily dislocated martensitic units are hard and strong (supersaturated with carbon) and are surrounded by ductile retained austenite thin films. The second example is nacre, a biological composite, consisting of relatively hard (CaCO_3) platelets surrounded by a soft proteinaceous matrix, resulting in a brick and mortar micro-architecture. In both cases, the hard component has a thickness in the range of 100-500 nm and the soft component of about 10-50 nm. The unique structural organization of the components gives the overall composite an excellent combination of mechanical properties in terms of hardness, strength, and toughness. In this paper, the structures of these materials are discussed in detail and some guidelines are presented for the future synthesis of nanolaminated composites.

1.0 An Introduction to Nanocomposite Materials

Properties of materials are structure-sensitive and, hence, control of the structure on a continuous length scale from the nanometer to the micrometer to the macrometer range is essential. For instance, metallic and ceramic composites and monoliths with layered microstructures and homogeneous matrices containing nanometer scale second phases offer

significant advantages in controlling the physical properties of materials.¹ Examples include layered compound semiconductors in which both the chemistry and atomic structure of the interfaces are controlled for improved electronic properties;² high-temperature ceramic superconductors, such as $\text{YBa}_2\text{Cu}_3\text{O}_{7-x}$,³ which have ultrathin ($\sim 1.5\text{-}2.5$ nm) transformation twin boundaries with low oxygen ordering in which the twin boundaries act as flux pinning sites resulting in an increase in critical current densities in high applied magnetic fields;⁴ and low-carbon/low-alloy steels that are strong but tough due to a hard lath martensitic structure and ductile thin film retained austenite.^{5,6} In the case of biological composites,⁷ the control of the structure begins at the nanometer dimension and scales up in secondary, tertiary, quaternary structures, resulting in a final structure that is often hierarchical. Hierarchical biological composites include all polymeric composites such as exoskeletons (cuticles) of insects, ceramic-polymer composites in skeletons of vertebrates and in seashells, and ultrafine paramagnetic⁸ and semiconducting⁹ particles found in bacteria and algae. Furthermore, in biological materials the resulting structure is multifunctional, conducting heat and electrical pulses and providing mechanical responses.

In this paper, we provide detailed analyses on the structures and properties of two novel nanocomposites: (i) high-strength/high-toughness lath martensitic steels, and (ii) nacre of abalone shell. Our goal here is to illustrate that the nanoscale integration of metallic, ceramic, and polymeric phases in a composite can result in a unique combination of enhanced properties. We hope that these two examples will provide pathways for the processing of more novel synthetic structures.

2.0 Examples of Nanocomposite Systems

Techniques such as those used in the formation of laminated composite structures at the nanoscale have been developed through phase transformations, especially in metal alloy systems, by carefully selecting the correct alloy composition and controlling the heat treatment (cooling). An excellent example is the high-strength/high-toughness lath martensitic steels developed during the 1970s and early 1980s.¹⁰ These structures are nanocomposites in scale and have soft (austenite) and hard (martensite) phases with a uniform distribution of fine (nanometer scale) carbide precipitates, closely controlled to give the best combination of mechanical properties involving strength and toughness in the final material. This successful composite system having structural variations at the nanometer scale will be discussed in more detail in Section 2.1 and will be closely related to the biological composites in Section 2.3. In Section 2.2, an ancient technique used to make a metal/ceramic composite will be presented.

2.1 Lath Martensitic Microstructures in Steels

Low-carbon ($< 0.3 \text{ wt\%}$)/low-alloy ($< 5.0 \text{ wt\%}$) steels are used in a variety of applications from armor to heavy machinery. These steels are heat treated by a simple procedure that, with modification, gives a myriad of microstructures, resulting in a wide variation in properties (Fig. 1). Low-alloy/low-carbon steels are probably the best examples among all synthetic materials systems in terms of developing composite microstructures on a wide dimensional scale (from nanometer to micrometer) with a high degree of control over the mechanical properties.

Quenching the alloy (about 100°C/s) from a homogenization temperature (usually above 1000°C) to room temperature results in a microstructure composed of a metastable mixture of martensitic laths (0.2-0.5 μm x 2-5 μm x 5-20 μm) with a continuous thin film of (5-50 nm thick) retained austenite decorating the lath boundaries⁵ (Fig. 2). The Fe-C equilibrium diagram displays a eutectoid transformation at 723°C and 0.8 wt% C composition. Above 723°C austenite (γ -iron, fcc) is the stable phase. Below 723°C ferrite (α -iron, bcc) is the stable phase and has a maximum solubility of C at about 0.02 wt%. A low or a medium C steel (0.05-0.4 wt%) quenched from the austenite phase field undergoes a shear transformation resulting in a metastable martensitic phase which has supersaturated C in the lattice that orders along the c-direction, and hence, the crystal structure becomes bct, where the tetragonality changes with C in solution. What is unusual is that the microstructure contains a thin film retained austenite continuously surrounding the martensite phase which is in the form of dislocated laths (Fig. 2(a-b)). Since the bct lattice of Fe is highly strained due to the supersaturation of C, the elastic modulus and the strength of martensite are very high (50 GPa and 5 GPa, respectively).⁵ Correspondingly, martensite is brittle. On the other hand, austenite is tough (in the case of austenitic steels, K_{Ic} is about 150 $\text{MPa}\cdot\text{m}^{1/2}$) but not as strong as martensite because of the easy slip in the fcc lattice resulting in plastic deformation. Therefore, the final microstructure in a low-carbon lath martensitic steel is basically a nanocomposite with component martensitic and austenitic phases that provide the strength and toughness of the material, respectively. Furthermore, in these structures the properties of component phases can further be modified by a low-temperature tempering. For example, tempering the quenched structure at 200°C for 2 h produces Widmanstätten Fe_3C (cementite) – plate-shaped with a thickness of 10-20 nm –

which results in a substantial increase in fracture toughness without a significant loss in strength of the composite structure.

Layered structures can be readily obtained in many other metallic and ceramic systems with two or more components whose phase diagrams display eutectic or eutectoid transformations. Metallic (such as Cu-Nb),¹¹ ceramic (B₄C-SiC),¹² and intermetallic systems (Al-Ti-Nb)¹³ can form *in situ* composites. Depending on the cooling rate from the high-temperature single-phase homogenization region, a certain degree of control over the thickness of the lamellae is assured, but not usually at the nanometer level. Some of the structural features in the Fe-C system discussed above include: (i) a martensitic transformation, resulting in a metastable microstructure which contains the high-temperature parent phase, austenite, indicating that kinetics dictates the final microstructure; (ii) lamination at the nanometer level; and (iii) the thorough distribution of lath martensitic packets (or colonies), resulting in a true three-dimensional composite. The effect of adding alloys, such as Cr, Mn, Ni, and Si, is to change the kinetics, such as the martensite start temperature, which affects the C-diffusion rates and the stability of the retained austenite,¹⁰ as well as to change some of the intrinsic properties of the component phases.

The unusual presence of a high-temperature austenite phase in the form of thin films is attributed to several stabilization mechanisms:¹⁰ (i) compositional stabilization due to the high C content in austenite films (up to 1.0 wt%), (ii) mechanical stabilization due to a high degree of deformation of the austenite lattice between the martensite laths, and (iii) chemical stabilization from the locking of the α'/γ interfaces due to C saturation at the coherency dislocations forming Cottrell atmospheres. Even at high cooling rates (10^4 °C/s), C atoms leaving the α'

lattice ahead of the interface move into the γ lattice and/or accumulate at the interface, stabilizing the austenite.

Each martensite lath in a given region obeys a specific crystallographic orientation relationship with the retained austenite, either a Kurdjumov-Sachs or Nishiyama-Wassermann relationship, that results in a $\{111\}_{\gamma}$ (parallel to $\{110\}_{\alpha'}$) habit.^{10a} In each packet, martensite laths (all having the same $[110]$ direction) belong to the same variant, which is a 70° rotation with respect to the neighboring packet. Therefore, in a given austenite grain, there are three variants of martensite, resulting in an overall structure which is a true three-dimensional composite with local lamination of component phases at the nanometer scale. As a result of this process, a unique lath martensitic microstructure develops which displays a room temperature fracture toughness, K_{Ic} , of about $100 \text{ MPa}\cdot\text{m}^{1/2}$ and a tensile yield strength, σ_Y , of about 1.4 GPa .¹⁰

2.2 *Samurai Sword: An Ideal Nanocomposite Alloy*

The practice of controlling the structure of materials at the nanometer scale to achieve desired properties has a long history, especially in metallurgy. Understanding the microstructures in ancient materials can be useful both for developing “micro-architectural design” concepts for modern multifunctional composites as well as generating new alloy microstructures. An excellent example of this is Damascus steel, which was developed in the Middle East during the late iron age, more than 2000 years ago. The steel was used mostly for armor applications, which required high toughness as well as high strength and hardness. The metallurgy that

produced Damascus steel is based on a simple thermomechanical cycle that forms a composite structure containing soft and hard phases.¹⁴ Originally "cast" high-carbon steel (wt% C > 1-2%) is homogenized at 1200°C, which produces coarse austenite (γ) grains. The steel is then cooled slowly through the γ -carbide (Fe_3C) region during which pre-eutectoid carbides form at prior austenite grain boundaries. The coarse microstructure is "broken down" during forging at temperatures of 750°-900°C, and carbides spherodize to form strings of particles in refined austenite grains. Quenching into warm water (40°-80°C) from about 750°C transforms the fine austenite grains into fine needles of brittle but strong martensite, which as discussed previously is a supersaturated ferrite. The material is then annealed at 200°-300°C to produce tempered carbides (20-50 Å) in what is now still strong but relatively tough martensite needles. The resulting microstructure is then tough martensite containing ultrafine precipitates with hard strings of carbides located at prior austenite grain boundaries.

Many variations of these iron-based structures have since been developed by modifying the thermomechanical treatments, most notably by "composite lamination," which incorporates both pure iron (soft and tough) and high and medium carbon steels (hard and strong).¹⁵ An excellent example of this is the Samurai sword, which is truly "nanolaminated" and is an ideal material for its purpose because of its unique combination of toughness, hardness, and rigidity.¹⁶ These three properties in one material, however, are contradictory; that is, toughness implies a soft material that bends easily, hardness is associated with brittle material, and rigidity requires high strength. However, Japanese smiths, many centuries ago, developed these composites based on techniques similar to the earlier techniques of Damascus steel-making by

understanding how thermomechanical treatments and compositional adjustments can change the steel's properties (Fig. 3).

The final body of a sword blade is a hierarchical structure consisting of a soft inner core (ferrite) with a hard outer core (low-carbon martensite). The steel is produced first in the form of a thick, laminated iron and steel blank with dimensions 1/2" thick by 2" wide and 6 to 8" long.¹⁷ The blank is inserted into a pine ash (carbon source) and heated white hot (about 600° to 800°C) and then doubled onto itself and hammered until it again has its original dimensions (Fig. 3). This process is repeated fifteen to twenty times. Four similar blanks are then welded together, and the same thermomechanical treatment is repeated five times. The resulting blank forms a laminate with the thickness of each lamellae equal to $2^{25}/4 \times 5 \times 2^{25}$ or a few nanometers. At this time, the surface of the blade (the laminated blank) is scraped and ground to shape. The final blade is covered with mixture of clay and fine sand, and then dried. The blade is then heated to austenitizing temperature (about 900°C) and quenched to room temperature in a bath of oil or water by inserting the tip first and then the sharp edge horizontally. The final blade has a curved shape with the sharp edge having mostly a hard and strong martensitic structure and the back edge consisting of the relatively soft ferritic microstructure. Both are nanolaminates, which provide the ultrarigidity to the overall material. Although no quantitative measurements have been made to date, the composite has been known to have an excellent combination of impact resistance, strength, and toughness in practice.¹⁸

2.3 Nacre of the Red Abalone Shell: A Natural Ceramic-Polymer Laminated Material

It is coincidental that the lath martensitic structures discussed in Section 2.1 are similar in design on a local scale to the structure of nacre, which forms the basis of many shells such as those from gastropods, cephalopods, and mollusks.¹⁹ Both the lath martensitic structures and the biologically occurring nacre structure are similar in that they (i) are laminated on a fine scale, (ii) have a hard and strong phase (martensite in steel and aragonite in nacre) that is thicker than the soft and tough phase (austenite in steel and an organic proteinaceous matrix in nacre), (iii) have a hard phase 100-500 nm thick and a soft phase 10-20 nm thick, and (iv) have soft phases in both cases of about 2-4% by volume. It is not coincidental, however, that both structures provide a good combination of strength and toughness with adequate hardness in the overall composite. For the purposes of micro-architectural design, the structure of nacre is described in detail below.

The method used by organisms in processing materials is in many ways more controlled than synthetic methods. In the formation of biological materials, therefore, organisms can efficiently produce complex and hierarchical microstructures with unique properties at spatial levels ranging from the molecular (10^{-10} m) to the macroscopic (10^{-3} m), and with greater control. The dynamism of these systems allows the collection and transport of the raw constituents; the nucleation, configuration, and growth of new structures (self-assembly); and the repair and replacement of old or damaged components.

Nacre, a ceramic-polymer nanocomposite of red abalone shell (*Haliotis rufescens*), for example, displays a unique structure-property correlation.²⁰ A longitudinal cross-section of the

red abalone shell displays two types of structures: the outer prismatic layer and the inner nacreous layer. Two forms of CaCO_3 , calcite (rhombohedral, $R\bar{3}c$) and aragonite (Pmnc), constitute the inorganic component of the organic-inorganic composite in the prismatic and the nacreous layers, respectively.

The mechanical properties of nacre, i.e., σ_f (fracture strength) and K_{Ic} (fracture toughness), have been evaluated in the transverse direction (perpendicular to the shell plane) and exhibit values of 180 MPa and about $10 \text{ MPa}\cdot\text{m}^{1/2}$, respectively (Fig. 4). In addition to a substantial increase in strength, there is an increase in the fracture toughness of at least 40 times in nacre compared to the fracture toughness of monolithic CaCO_3 ($K_{Ic} < 0.25 \text{ MPa}\cdot\text{m}^{1/2}$) based on a straight notch three-point bend test. In terms of specific strength, nacre is comparable to many monolithic ceramics; in terms of toughness, nacre is a better material. It is surpassed by only the most successful ceramic-metal composites (cermets): WC-Co (density 14.5 g/cc),²¹ Al_2O_3 -Al (density 2.8 g/cc),²² and B_4C -Al (density 2.65 g/cc),²³ all of which have the form of a three-dimensional network and, hence, have isotropic properties.

The study of crack propagation behavior in nacre reveals a high degree of tortuosity not seen in traditional brittle (such as Al_2O_3) and tough (ZrO_2) ceramics, indicating that certain toughening mechanisms, such as crack blunting, branching, and "layer pullout," operate in the shell. A closer examination of the microstructure reveals that cracks mostly advance through the organic layer and with difficulty as this process is accompanied by sliding of the CaCO_3 layers (when there is a shear component of the resolved stress) and by the bridging of the organic ligaments (when there is a normal stress component), as shown in Fig. 5(a-b). It is these last two mechanisms that contribute most to the toughening of nacre. These processes

absorb considerable energy that would otherwise be used in the propagation of cracks through the material, resulting in controlled crack propagation and hence a damage tolerant composite.

The superior mechanical properties of the nacre section of abalone shell (which is 96-98% CaCO_3 and about 2-4% organic matter) over those of synthetic ceramics and their composites come from the unique "brick and mortar" micro-architecture. Figure 6 shows the alternating layers of the hexagonally shaped 100-500 nm-thick aragonite crystals (platelets) that form the hard component and the thin (10-20 nm) organic substance (a nanolaminate of chitin, proteins, and macromolecules) that provides the "ductile" component of the microstructure. It appears, therefore, that the organic matrix not only acts as the lifeline of the shell but also is an indispensable structural component of the resultant ceramic-polymer composite. The conclusion that can be drawn from these observations is that in the composite (i) the biopolymer component has to be soft and sticky, and (ii) the inorganic component has to be hard, and (iii) interfaces between the soft and the hard components must be strong. These guidelines may serve as a design basis for enhancing impact and wear resistance in future nanolaminated engineering materials, such as cerpolys (ceramic-polymers) and cermets (ceramic-metals), incorporating soft and hard components.

3.0 Summary

From the above, it is clear that structures of lath martensitic steels and nacre are very similar. In steels, it is the martensite lath, which has dimensions similar to CaCO_3 in nacre (both about 200-500 nm thick), that provides strength. The thin film retained austenite (5-50

nm thick) that covers the martensite platelets (laths) is similar to the organic layer (10-20 nm) covering the aragonite platelets in the nacre. Furthermore, in both cases, the interfaces are very strong between the hard and soft phases. In terms of crystallographic relationships in nacre, adjacent CaCO_3 platelets have their [001] axis perpendicular to the platelet/organic matrix interface, with plates rotating slightly ($1-5^\circ$) with respect to this axis. In martensite, similarly, the adjacent laths have a common $\langle 110 \rangle$ axis, perpendicular to the α'/γ interface, with laths rotating slightly ($1-6^\circ$) with respect to this axis. In both cases, the matrices (organic phase in the nacre and austenite in lath martensitic structures) have the same orientation throughout. However, the difference between the two structures is that the lath martensite contains packets (three 70° -variants of martensite crystals) within each pre-austenite grain that are randomly distributed throughout the sample. In nacre, the local arrangement of the layered structure is repeated throughout the thickness of the sample. Therefore, lath martensite is a true three-dimensional microstructure with local laminated domains that produce its isotropic mechanical properties. Nacre, on the other hand, is a true two-dimensional microstructure possessing high anisotropic properties.

Unfortunately, other than expensive techniques such as molecular beam epitaxy, presently we do not have commercially viable techniques to produce nanolaminated structures as good as the two novel examples discussed in this paper. We hope that future research will provide more practical processing schemes to accomplish the goal of achieving cermet and cerpoly composites.

4.0 Acknowledgments

The work was supported by the Air Force Office of Scientific Research (AFOSR) and was monitored under Grant Nos. AFOSR-88-0135, AFOSR-89-0496, AFOSR-91-004, and AFOSR-NC-003.

5.0 References

1. R. P. Anders et al., Research Opportunities on Cluster and Cluster-assembled Materials--A Department of Energy, Council on Materials Science Panel Report, *J. Mater. Res.*, **4** (3) 707 (1989).
2. T. P. Pearsall, Silicon-Germanium Alloys and Heterostructures: Optical and Electronic Properties, *CRC Critical Reviews in Solid State and Materials Science*, **15** (6) 551 (1989).
3. M. Sarikaya, R. Kikuchi, and I. A. Aksay, Structure and Formation of Twins in Orthorhombic $\text{YBa}_2\text{Cu}_3\text{O}_{7-x}$, *Physica C*, **152**, 161 (1989).
4. U. Welp, W. K. Kwok, G. W. Crabtree, and K. G. Vandervorst, Magnetization Hysteresis and Flux Pinning in Twinned and Untwinned $\text{YBa}_2\text{Cu}_3\text{O}_{7-x}$, Single Crystals, *Appl. Phys. Lett.*, **57** (1) 84 (1990).

5. (a) J. McMahon, Ph.D. Thesis, University of California, Berkeley (1973).
(b) R. Raghavan, Ph.D. Thesis, University of California, Berkeley (1976).
(c) R. V. Narasinha Rao, Ph.D. Thesis, University of California, Berkeley (1978).
(d) M. Sarikaya, Ph.D. Thesis, University of California, Berkeley (1982).
6. M. Sarikaya, H. Togushige, and G. Thomas, Lath Martensite and Bainite in Low Alloy Steels, in *Proc. Intl. Conf. Martensitic Transformations*, Japan Institute of Metals, 1986, p. 613.
7. (a) H. A. Lowenstam, Minerals Formed by Organisms, *Science*, **211**, 1126 (1981);
(b) J. A. Currey, Biological Composites, *J. Mater. Edu.*, **9** (1/2) 118 (1987).
8. R. P. Blakemore, Magnetotactic Bacteria, *Science*, **190**, 377 (1975).
9. C. T. Dameron, Biosynthesis of Cadmium Sulphite Quantum Semiconductor Crystallites, *Nature*, **338**, 596 (1989).
10. (a) M. Sarikaya and G. Thomas, Lath Martensites in Low Carbon Steels, *J. de Physique*, Colloque (4) supplement au no. 12, Tome 43, 1982 Decembre, p. C4-563-568;
(b) M. Sarikaya, G. Thomas, J. W. Steeds, S. J. Barnard, and G. D. W. Smith, Solute Element Partitioning and Austenite Stabilization in Steels, in *Proc. Intl. Conf. Solid-Solid*

Phase Transformations, H. I. Aaronson and C. M. Wayman, Eds., American Society of Metals, 1982, p. 1421.

11. J. Berk, J. P. Harbison, and J. L. Bell, Anomalous Increase in Strength of In-Situ Formed Cu-Nb Multifilamentary Composites, *J. Appl. Phys.*, **49** (12) 6031 (1979).
12. W. J. Minford, F. L. Kennards, R. C. Bradt, and V. S. Stubican, Directionally Solidified Ceramic Eutectics: Microstructures, Crystallography, and Mechanical Properties, in *Ceramic Microstructures '76*, R. M. Fulrath and J. A. Pask, Eds., Westview Press, Boulder, Colorado, 1977, p. 456.
13. E. Ense and H. Margolin, *Trans. Metall. Soc. AIME*, **221**, 151 (1960).
14. J. Wadsworth and O. D. Sherby, "On the Bulat. Damascus Steel Revisited," in *Progress in Mater. Sci.*, Vol. 25, 1980, p. 15.
15. C. S. Smith, *A History of Metallography*, University of Chicago Press, Chicago, 1965.
16. E. C. Bain, Nippon-tô, An Introduction to Old Swords of Japan, *J. Iron and Steel Inst.* London, **200**, 265 (1962).

17. L. Kapp, H. Kapp, Y. Yoshihara, *The Craft of the Japanese Sword*, Kodansha Intl. Ltd., Tokyo, 1987.
18. B. S. Lyman, Metallurgical and Other Features of Japanese Swords, *J. of the Franklin Institute*, 13 (January 1896).
19. J. Currey, Biological Composites, *J. Materials Edu.*, 9 (1-2) 118 (1987).
20. M. Sarikaya, K. E. Gunnison, M. Yasrebi, and I. A. Aksay, Mechanical Property-Microstructural Relationships in Abalone Shell, in *Materials Synthesis Utilizing Biological Processes, MRS Symp. Proc., Vol. 174*, P. C. Rieke, P. D. Calvert, and M. Alper, Eds., Materials Research Society, Pittsburgh, Pennsylvania, 1990, p. 109.
21. H. E. Exner and J. Garland, A Review of Parameters Influencing Some Mechanical Properties of WC-Co Alloys, *Powder Metallurgy*, 13, 13 (1970).
22. M. S. Newkirk, A. W. Urquhart, H. R. Zwicker, and E. Bretal, Formation of LanxideTM Ceramic Composite Material, *J. Mater. Res.*, 1 (1) 81 (1986).
23. D. C. Halverson, A. J. Pyzik, I. A. Aksay, and W. E. Snowden, Processing of B₄C-Al Composites, *J. Am. Ceram. Soc.*, 72 (5) 775 (1989).

Table I. Natural and Synthetic Nanocomposite Materials

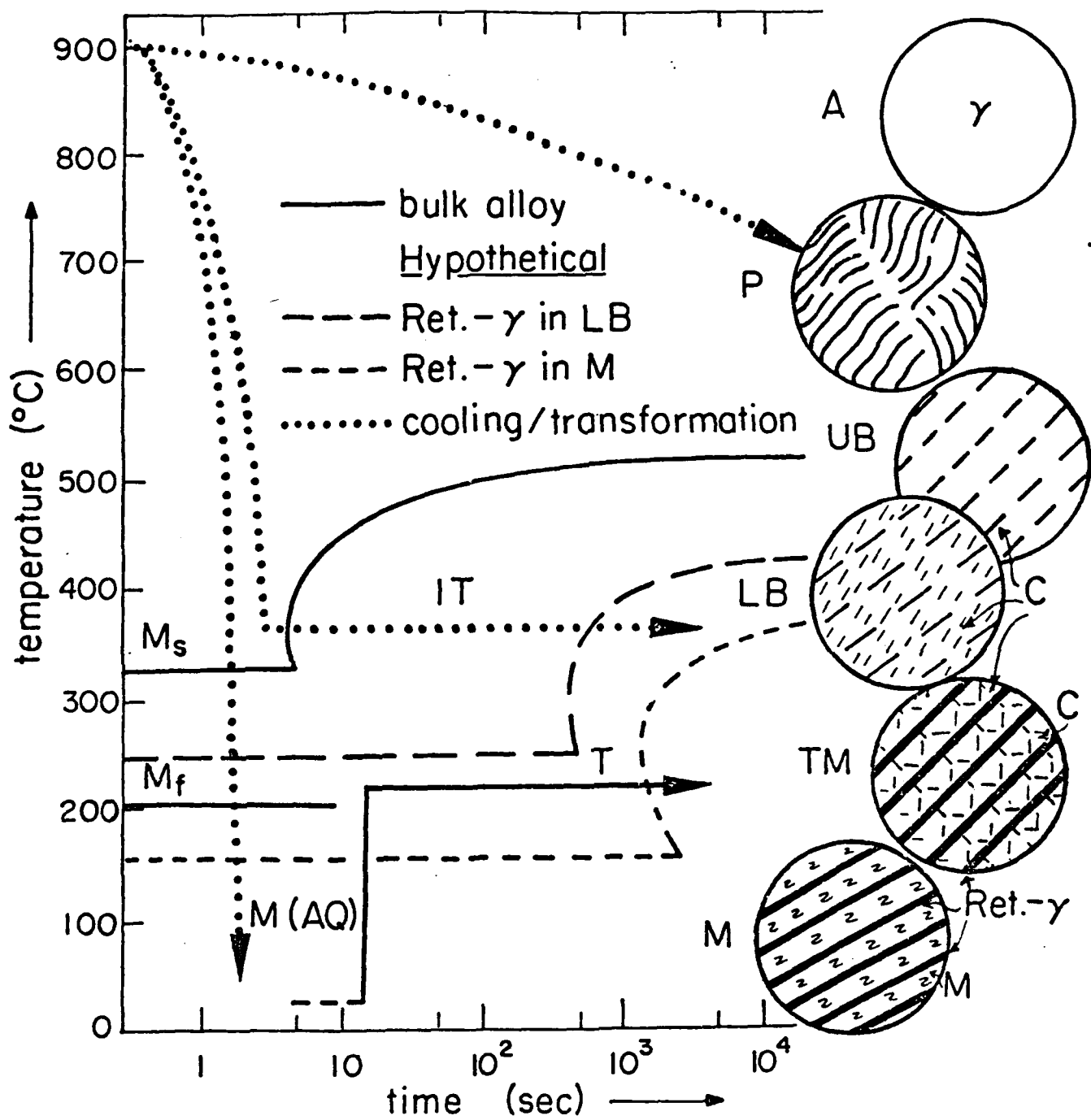
Natural	Dimension of the		Dimension of the	
	Second Phase	Synthetic	Second Phase	
clays (2-D)	~ 1 nm	semiconductor heterostructures (2-D)	1 nm layers	
opal (2-D)	~ 1 nm	high-temperature superconductors (2-D)	1 nm layers	
seashells (2-D)	1-100 nm	lath martensite (3-D)	5 - 50 nm layers	
		samurai sword (2-D)	1 - 3 nm layers	
			(calculated)	
		Ti-C multilayers (2-D)	2 - 10 nm	

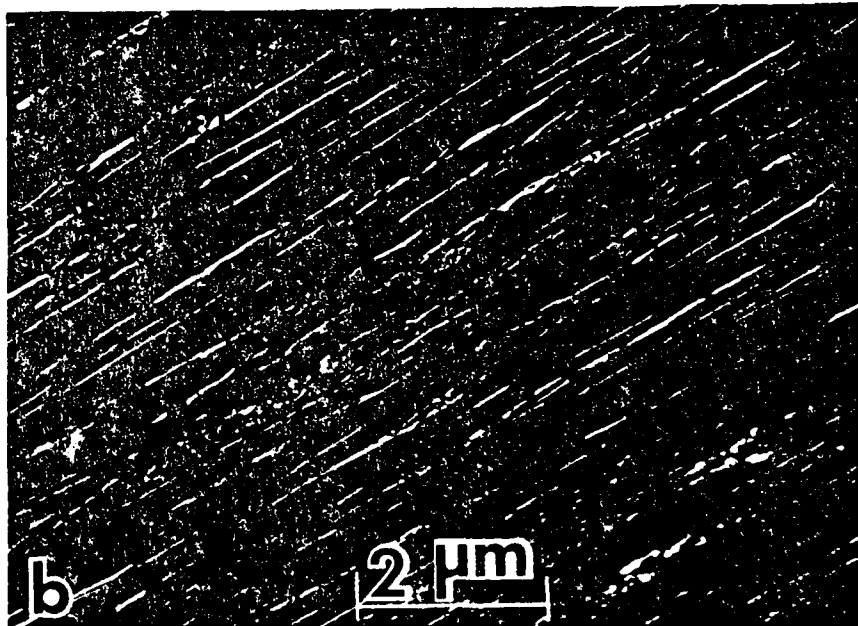
Figure Captions

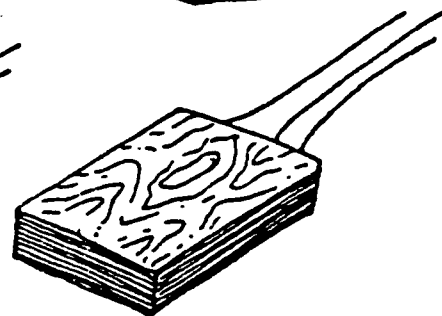
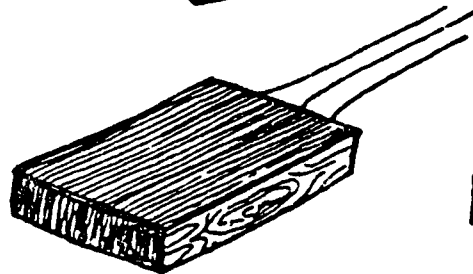
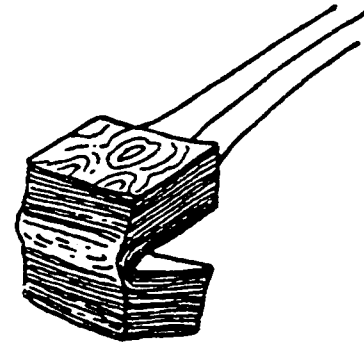
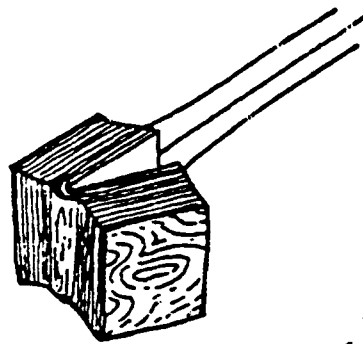
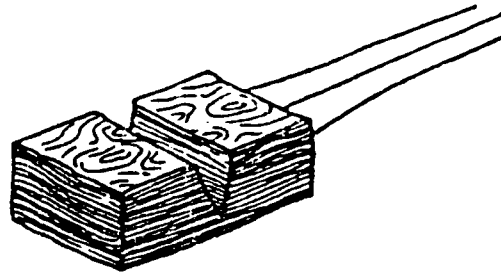
- Figure 1.** TTT diagrams for bulk steel and hypothetical steels having the compositions of retained austenite (Ret- γ) phases in lower bainite (LB) and martensite (M), respectively. Microstructures produced by different cooling routes from austenite phase field are also schematically indicated (A: austenite; C: carbide; IT: isothermal transformation; T: tempering; P: pearlite; TM: tempered martensite; and UB: upper bainite.);
- Figure 2.** (a) Bright field and (b) dark field images, the latter recorded by using the retained austenite reflection, reveal dislocated martensite laths, with a common $\langle 110 \rangle_M$ direction, and thin film retained austenite, with $\langle 111 \rangle_A$ parallel to $\langle 110 \rangle_M$ in each packet.
- Figure 3.** The making of samurai swords: two Jihada. Masame grain is produced when the unhammered face of the forged block of steel is used to form the surface of the blade. Itame is made by using the hammered face, creating a laminated appearance resembling nacre or a wood surface.
- Figure 4.** Mechanical properties of the nacre section of the red abalone shell (96% CaCO_3 , 4% organic) as compared to common high-technology ceramics and cermets. Note the increase of properties in nacre compared to monolithic CaCO_3 .

Figure 5. (a) and (b) are secondary electron images in SEM revealing crack propagation characteristics in the nacre structure; and sliding of CaCO_3 platelets and ligament formation in the organic matrix, respectively.

Figure 6. TEM BF image in cross-section revealing the "brick and mortar" micro-architecture of CaCO_3 platelets, C, and organic matrix, O, in the nacre section of red abalone shell.

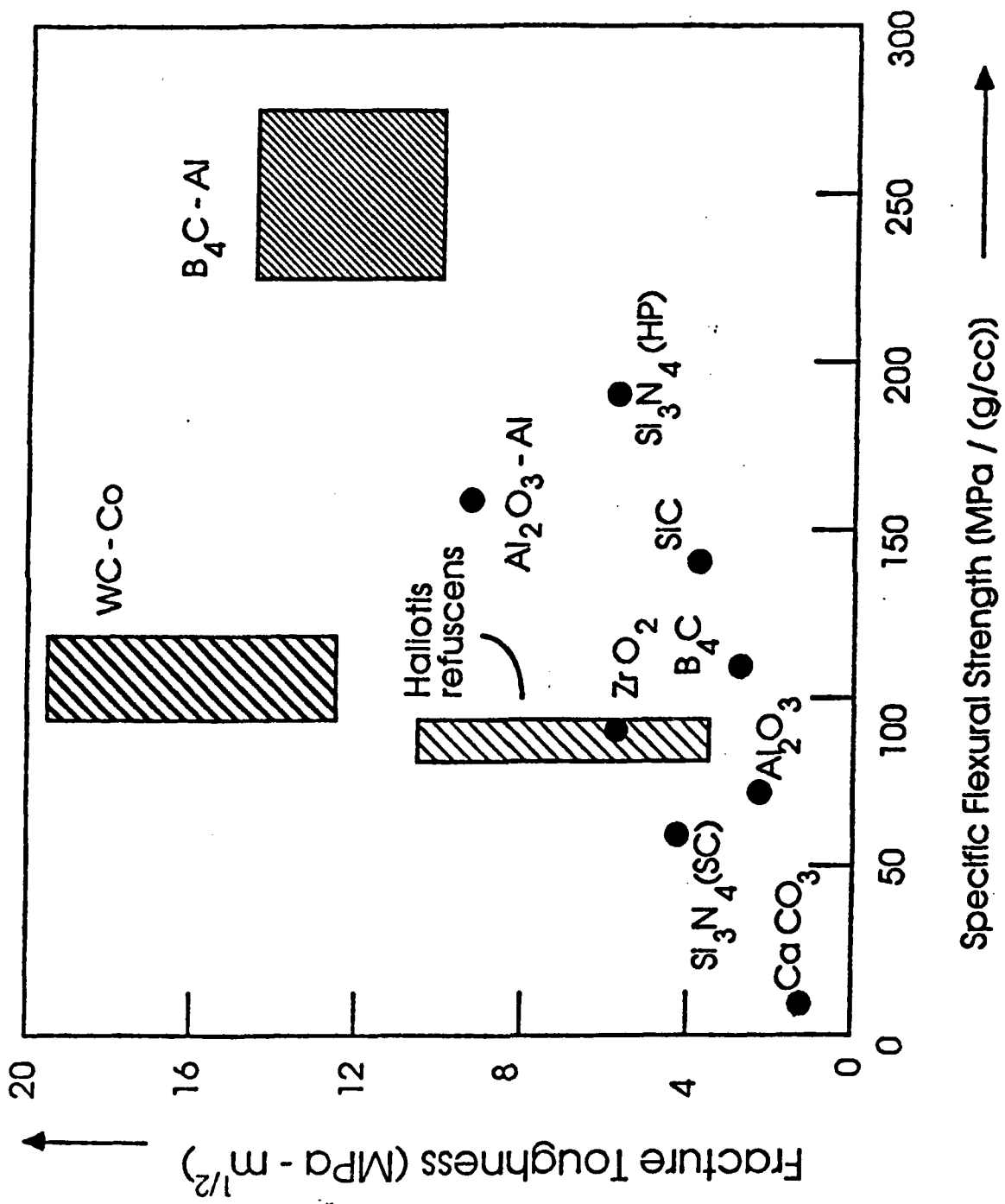


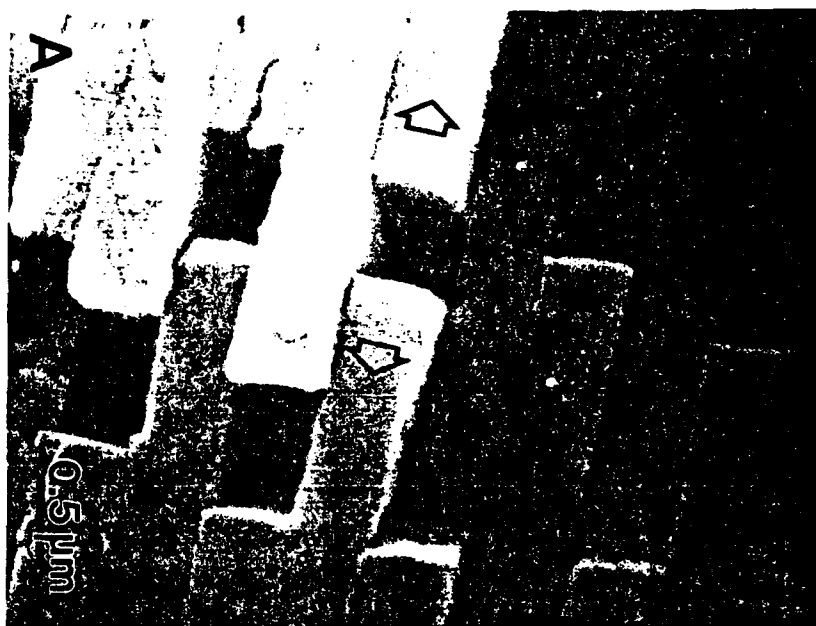


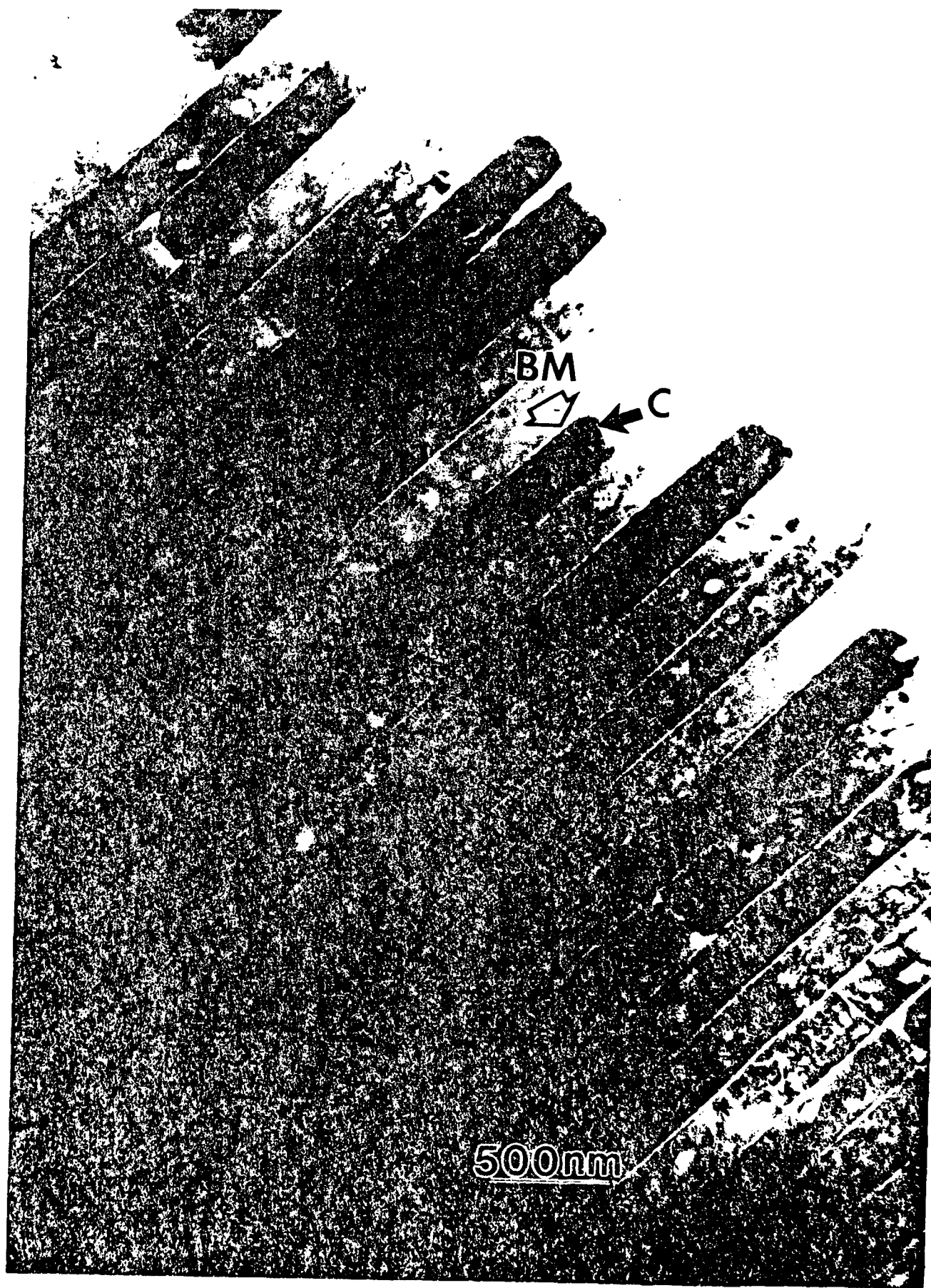


Masame

Itame







APPENDIX XIII

Microstructure-Property Relationships in Biocomposites

by

I. A. Aksay and M. Sarikaya

Biostructures as Composite Materials

Proceedings of ARO Workshop

edited by E. Baer and I. Ahmed

(U. S. Army Research Office, Research Triangle Park, NC, 1990) pp. 171-74

MICROSTRUCTURE-PROPERTY RELATIONSHIPS IN BIOCOMPOSITES

Ilhan A. Aksay and Mehmet Sarikaya

*Department of Materials Science and Engineering, and
Advanced Materials Technology Program,
The Washington Technology Center,
University of Washington, Seattle, WA 98195*

Progress is being made in materials processing in improving microstructural control down to the nanometer scale, as materials at this scale exhibit unprecedented properties (such as mechanical, electrical, superconductive, and optical).¹⁻⁴ The processing of these synthetic materials is based on the additive principle, in which component phases with varying properties are fused together in an ordered manner to form a multiphase system. Conventionally, these structures can be achieved by phase transformations (precipitation-hardened alloys) or by mechanical mixtures at the microscale level (metal and ceramic matrix composites).⁵ More advanced processing involves ion beam techniques (such as molecular beam epitaxy and liquid and vapor deposition)^{3,4} in which the microstructure is controlled at the nanometer level. In order to meet the demands of modern technology for better properties, more complex systems have to be developed through more intricate and energy-efficient processing strategies.

The approach taken by living organisms in processing composites is in many ways more controlled than the synthetic methods. In the formation of biological composites, living organisms can design and produce, efficiently, complex microstructures having unique properties at all spatial levels (down to the nanometer scale), and in more controlled ways at the molecular dimension.⁶⁻⁸ It is desirable, therefore, to produce man-made materials by using processing approaches similar to those used by the living organisms, i.e., by biomimicking. This present research has been initiated to study some of the principles inherent in the processing methods used by organisms in producing composites and their physical properties as related to microstructures. In this short note, we summarize the results of a recent study on the microstructures of the red abalone shell (*Haliotis rufescens*) in relation to its mechanical properties.

A longitudinal cross-section of the abalone shell displays two types of microstructures: an outer prismatic layer and an inner nacreous layer. Two forms of CaCO_3 , calcite (rhombohedral, $R\bar{3}c$) and aragonite (orthorhombic, $Pmnc$) constitute the inorganic component of the organic-inorganic composite in the prismatic and the nacreous layers, respectively. The structure and the properties of the nacreous layer are described here, as this is the part which displays a good combination of mechanical properties.⁹

Mechanical properties, i.e., σ_f (fracture strength) and K_{IC} (fracture toughness), have been evaluated in the transverse direction (perpendicular) to the shell plane. They exhibit values of 180 MPa and about $7.0 \text{ MPa}\cdot\text{m}^{1/2}$, respectively. The study of the crack propagation behavior reveals a high degree of tortuosity, not seen in the more traditional brittle (such as Al_2O_3) and

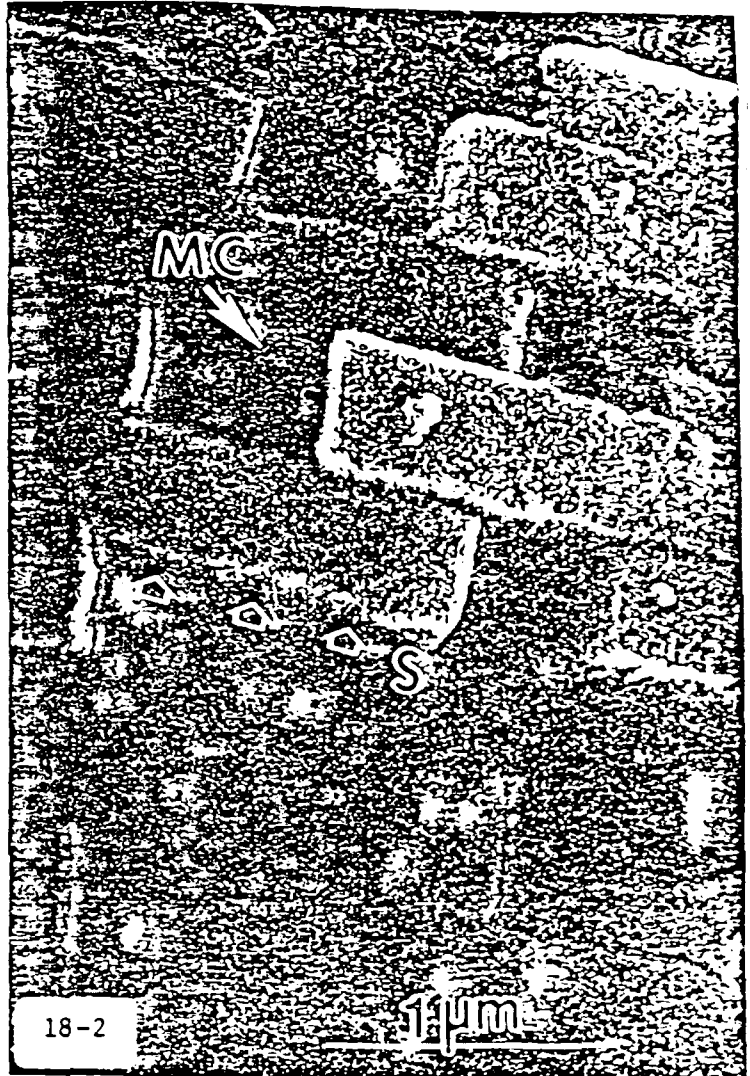
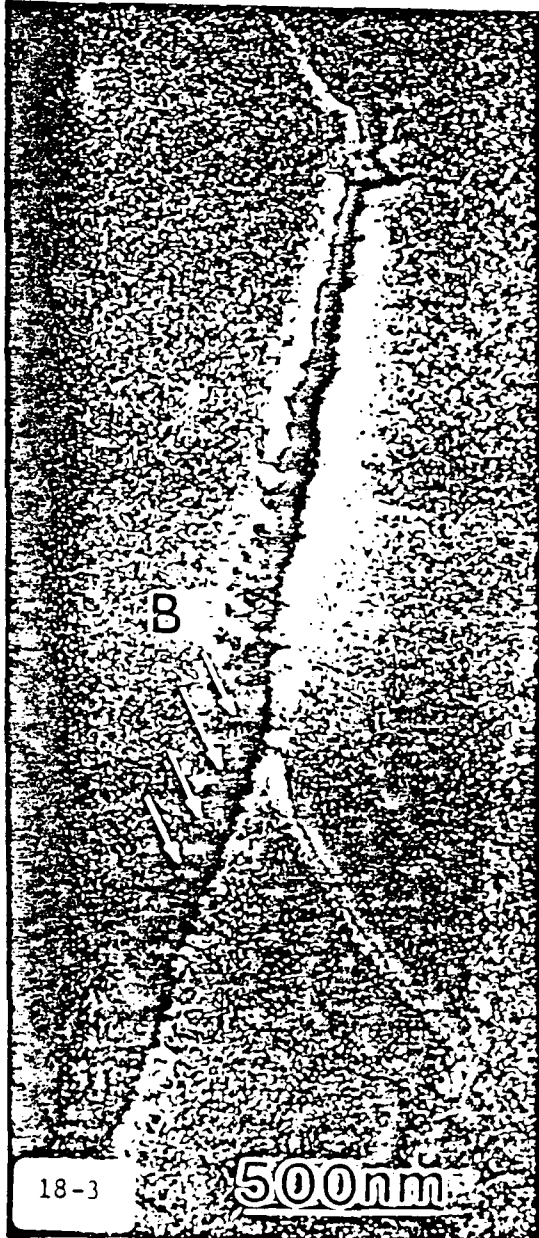
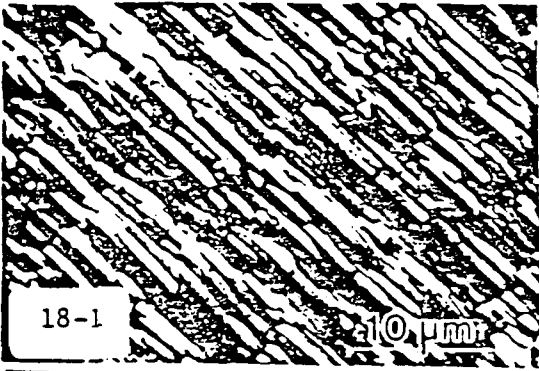
high toughness (ZrO_2) ceramics,¹⁰ indicating certain toughening mechanisms, such as crack blunting, branching, and "layer pull-out" operating in the shell (Figure 1). A closer examination of the microstructure reveals that cracks mostly advance through the organic layer and with difficulty, as this process is accompanied by sliding of the CaCO_3 layers (when there is a shear component of the resolved stress) and by the bridging of the organic ligaments (when there is a normal stress component), as shown in Figures 2 and 3, respectively. It is these last two mechanisms which mostly contribute to the toughening of the shell.

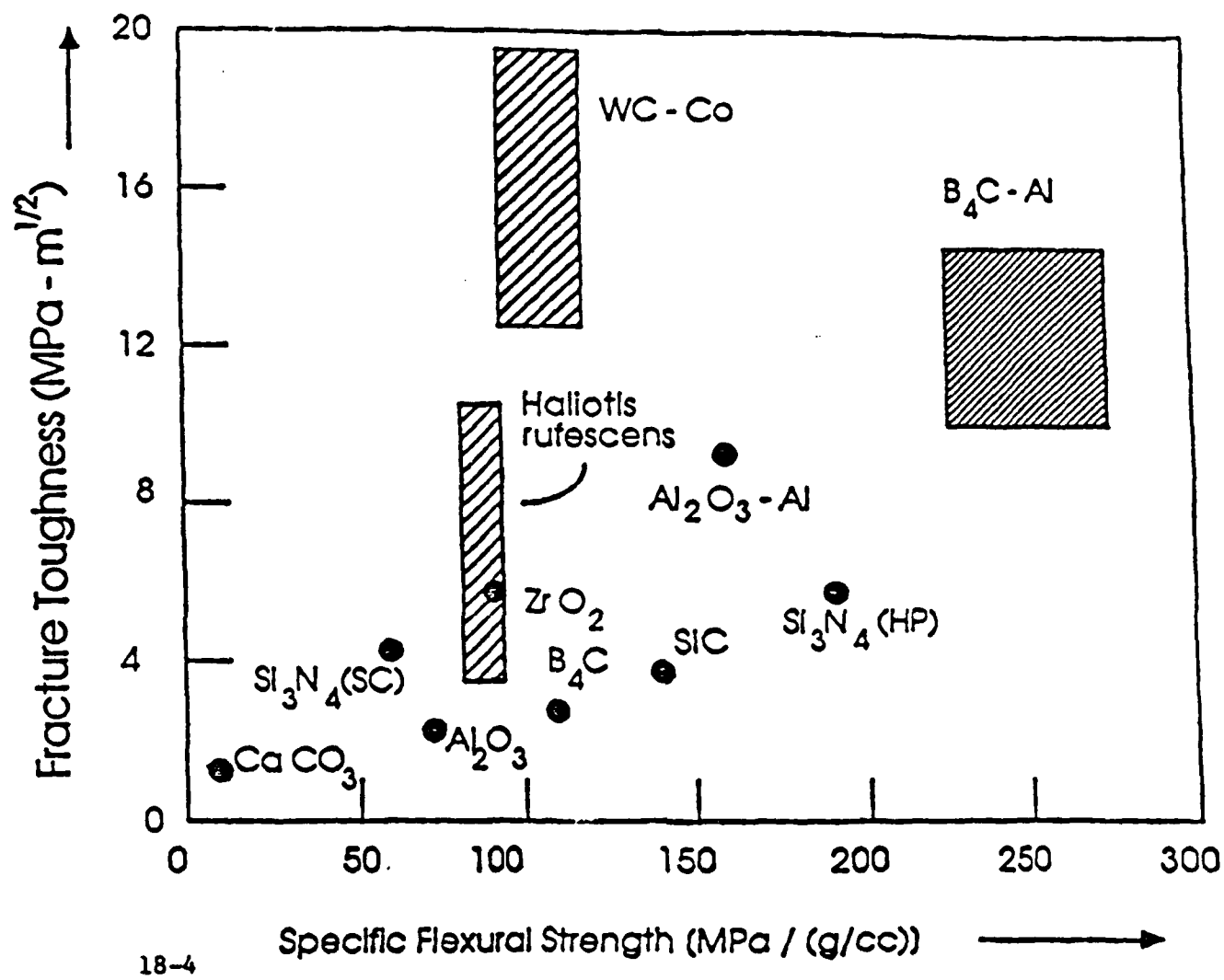
The superior mechanical properties of abalone shell compared to those of the more traditional ceramics and their composites (plotted in Figure 4) comes from its unique "brick and mortar" microstructure. A TEM micrograph (Figure 5) recorded in the transverse direction shows the alternating layers of hexagonal-shaped 0.2-0.5 μm thick aragonite crystals which form the hard component, and the thin (20-50 nm) organic substance in between (lipids and proteins), providing the ductile component of the composite.

Preliminary results on the mechanical properties of B_4C -Al (35%) laminated cermets designed on the basis of the above observations, indicate a 30% increase in the fracture toughness of the composite. This increase in the cermet toughness is attributed to the same toughening mechanisms observed in abalone shell. Further improvement in both strength and toughness is expected with the decrease in the thickness of the composite layers (down to submicrometer levels); in the present case, the smallest thickness of the layers in the cermet laminate is about 10 μm , far too thick to benefit the effects of the lamination. Consequently, the present research is directed to the processing of cermets with submicrometer-layer thicknesses to achieve this goal in conjunction with the studies of the quantitative effects of the organic layer in sea shells.

This research was supported by the Air Force Office of Scientific Research under Grants Nos. AFOSR-87-0114 and AFOSR-89-0496.

1. F. Spaen, "The Art and Science of Microstructural Control," *Science*, 235 1010 (1987).
2. R. C. Cammarata, "The Supermodulus Effect in Composition Modulated Thin Films," *Scripta Met.*, 20 883 (1980).
3. M. S. Dresselhaus, "Intercalation of Layered Materials," *Materials Research Society Bulletin*, 12 (3) 24 (1987).
4. *Metallic Superlattices: Artificially Strong Materials*, edited by T. Sinjo and T. Takada (Elsevier, Amsterdam, 1987).
5. A. Kelly and R. L. Nicholson, *Strengthening Methods in Crystals*, (Wiley, New York, 1971).
6. H. A. Lowenstam, "Minerals Formed by Organisms," *Science*, 211 1126 (1981).
7. S. Mann, "Mineralization in Biological Systems," *Structure and Bonding*, 54 124 (1983).
8. S. Weiner, "Organization of Extracellularly Mineralized Tissues: A Comparative Study of Biological Crystal Growth," *CRC Critical Reviews in Biochemistry*, 20 [4] 365 (1986).
9. J. D. Currey, "Biological Composites," *J. Materials Educ.*, 9 (1-2) 118 (1987).
10. *Deformation of Ceramic Materials II*, edited by R. C. Tressler and R. C. Bradt (Plenum, New York, 1984).





APPENDIX XIV

Toughening Mechanisms in Abalone Shell

by

K. E. Gunnison, M. Sarikaya, and I. A. Aksay

Proceedings of the XIIth International Congress for Electron Microscopy
(San Francisco Press, San Francisco, 1990) pp. 196-97

TOUGHENING MECHANISMS IN ABALONE SHELL

Katie E. Gunnison, Mehmet Sarikaya, and Ilhan A. Aksay

Department of Materials Science and Engineering; and
Advanced Materials Technology Center, Washington Technology Centers,
University of Washington, Seattle, WA, USA 98195

Abalone shell (*Haliotis Rufescens*) is a naturally occurring ceramic/polymer composite material. The system displays a unique laminated structure of calcium carbonate (aragonite) crystals in a matrix of biological macromolecules. The CaCO_3 crystals and the organic matrix are arranged in a miniature "brick and mortar" structure referred to as nacre.¹ Figure 1 is a TEM bright field micrograph illustrating the high degree of order observed in this microstructure.

Although the nacre region of the shell is more than 95% CaCO_3 by volume, the natural matrix material and the arrangement of the microstructure lead to a substantial increase in the observed mechanical properties.² Mechanical tests performed on the nacre region show a fifty-fold increase over that of pure bulk CaCO_3 (Fig. 2), which also compares with other ceramic and cermet systems.

Vickers microhardness testing was performed on samples polished for optical microscopy. Crack propagation features were observed by standard SEM techniques and analyzed in an attempt to identify the possible toughening mechanisms that are operating in the nacre structure. The cracks generally travel by a tortuous path, often displaying microcracks and crack branching. However, these mechanisms alone are not sufficient to account for the observed mechanical properties. Further analysis determined that when the resolved applied stress is parallel to the plane of the layers, the crystals often *slide* past one another without actual failure of the interface (Fig. 3). When the resolved applied stress is normal to the plate layers, the organic matrix extends to form *ligaments* which inhibit further opening of the crack (Fig. 4). These mechanisms suggest that strong interfaces between the matrix and the crystals, ligament formation, and plasticity of the matrix are instrumental in the toughening processes of this unique microstructure.

These observations can serve as a basis for design criteria of laminated ceramic/metal and ceramic/polymer composites for improving the anisotropic mechanical properties, such as impact resistance, of materials for structural applications.³

1. J. D. Curry, *Biological Composites* (Elsevier, Amsterdam, 1983).
2. M. Sarikaya, K. E. Gunnison, and I. A. Aksay, *Materials Synthesis Utilizing Biological Processes, MRS Symp. Proc.*, edited by P. C. Rieke, P. D. Calvert, and M. Alper (Materials Research Society, Pittsburgh, PA, 1990).
3. This work was supported by the Air Force Office of Scientific Research (AFOSR) under Grant No. AFOSR-89-0496.

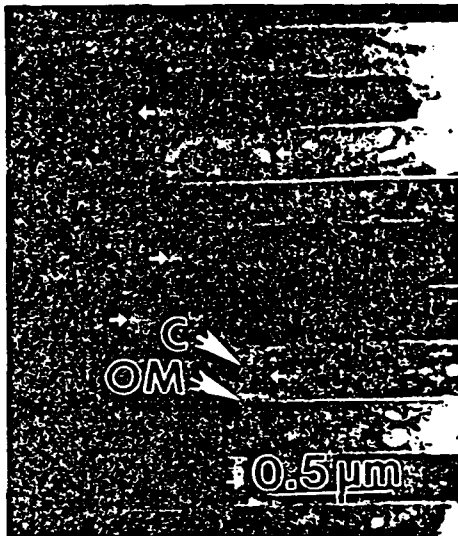


Fig. 1. TEM BF image showing the "brick and mortar" microstructure of the nacre in abalone shell.

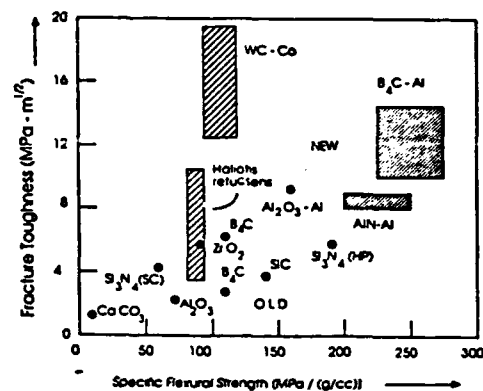


Fig. 2. Mechanical properties of abalone shell compared to cermet and ceramic systems.

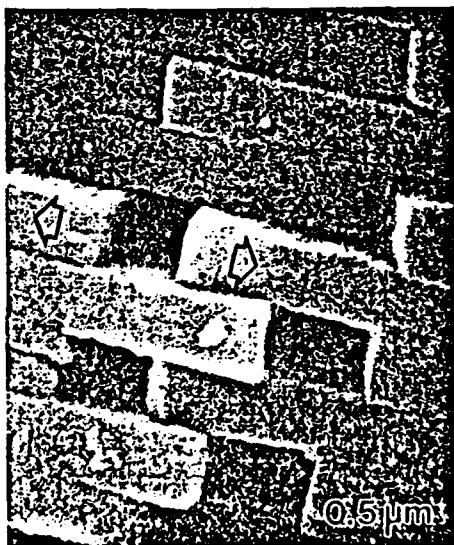


Fig. 3. SEM micrograph clearly records the sliding in the direction of the arrows.

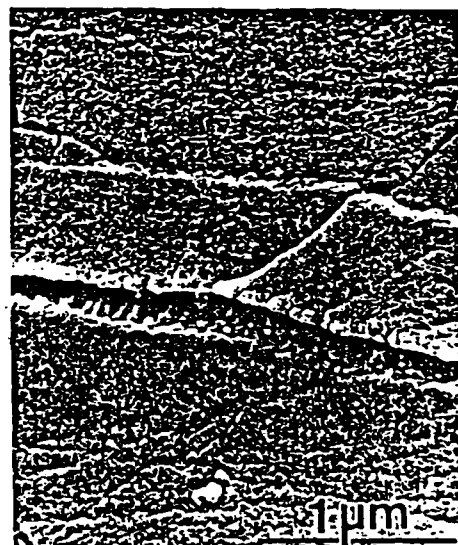


Fig. 4. SEM micrograph showing the organic ligament formation between the CaCO₃ layers when the resolved stress is in the transverse direction (arrows).

APPENDIX XV

Seashells as a Natural Model to Study Ceramic-Polymer Composites

by

M. Sarikaya, K. E. Gunnison, and I. A. Aksay

Proceedings of the 47th Annual Meeting EMSA

edited by G. W. Bailey

(San Francisco Press, San Francisco, 1989) pp. 558-59

SEASHELLS AS A NATURAL MODEL TO STUDY CERAMIC-POLYMER COMPOSITES

Mehmet Sarikaya, Katie L. Gunnison, and Ilhan A. Aksay

Department of Materials Science and Engineering, and the Washington Technology Center, University of Washington, Seattle, WA 98195

Interests in ceramic/polymer composites are increasing mainly because of their superior physical properties for structural and electronic applications. Naturally produced composites, such as seashells, are ideal to study the formation, microstructure, and physical properties of these composites as these materials have far superior properties with well-defined microstructures than man-made ones which require complex fabrication techniques. In this paper, a summary of a recent study on the microstructure of abalone shell (*Haliotis refuscens*) will be described in conjunction with its mechanical properties.

A longitudinal cross-section of abalone shell displays two types of microstructures: outer *prismatic* layer and inner *nacreous* layer.¹ Two forms of CaCO_3 , calcite (rhombohedral, $R\bar{3}c$) and aragonite (orthorhombic, $Pm\bar{c}n$) constitute the inorganic component of the organic/ceramic composite in the prismatic and nacreous layers, respectively. The structure and properties of the nacreous will be described here as this is the part which provides a good combination of mechanical properties for the seashell.²

Mechanical properties of the nacreous layer have been evaluated in the direction perpendicular to the shell plane. The fracture strength, σ_f (four point bending) is 180 MPa and fracture toughness, K_{IC} (three-point bending) is in the range 5.5 to 11.0 $\text{MPa}\cdot\text{m}^{1/2}$. Vickers indentation in the transverse direction indicates that cracks do not radially extend from the corners of the indenter, as would be expected from a brittle ceramic, but from regions close to the edge in various directions and follow tortuous paths (Figure 2). This is attributed to the toughening mechanisms that are operating, including microcracks, and crack branching and blunting. The major contribution to toughening comes from deformation, seen as sliding of layers on each other (Figure 3). Finally, the "pull-out" mechanism also operates as dramatically illustrated in Figure 4.

The superior combination of anisotropic mechanical properties of the abalone shell over the ceramic monoliths and composites comes from its unique microstructure in the form of "brick and mortar." In the transverse direction of this microstructure, the shell consists of alternating layers of the ceramic (0.2-0.5 μm) crystals of aragonite in the shape of hexagonal "bricks" forming on each layer and providing the hard component of the composite. The thin (10 to 30 nm) organic substance (lipids and proteins), between the layers, provides the ductile component of the composite.³

1. S. W. Wise, *Eclogae. geol. Helv.*, 63/3, 775-797 (1970).
2. J. D. Currey, *Biological Composites*, *J. Mater. Educ.*, 120-196 (1983).
3. M. Sarikaya and I. A. Aksay, unpublished research, University of Washington.
4. This work was supported by AFOSR under grant No. AFOSR-88-135

Figure 1. SE image (SEM) of cracks emanating from the edges of an indentation.



Figure 3. SE image (SEM) of the surface of a fractured sample displaying the "pull-out" mechanism.

Figure 2. SE image (SEM) illustrating the sliding of ceramic layers over the organic interlayer.

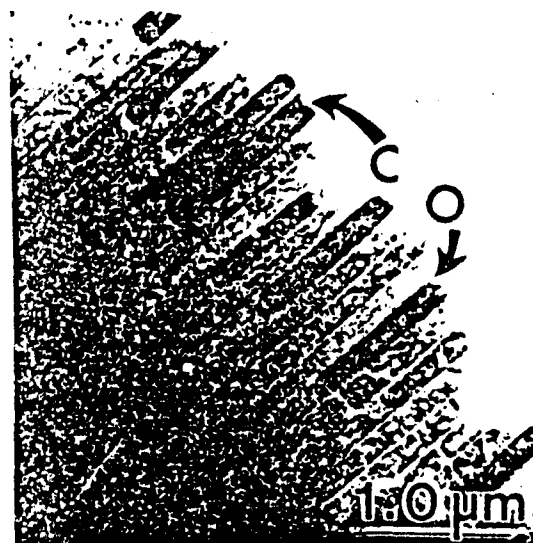
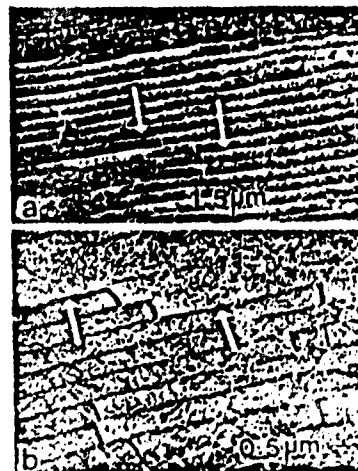


Figure 4. Bright field image (TEM) of cross-section of the shell revealing the ceramic (C) and organic (O) layers.

APPENDIX XVI

Hierarchical Twin Structures in Nacre of Red Abalone Shell

by

J. Liu, M. Sarikaya, and I. A. Aksay

Proceedings of 49th Annual Meeting EMSA

edited by G. W. Bailey

(San Francisco Press, San Francisco, CA, 1991) pp. 946-47

HIERARCHICAL TWIN STRUCTURES IN THE NACRE OF RED ABALONE SHELL

Jun Liu, Mehmet Sarikaya, and Ilhan A. Aksay

Department of Materials Science and Engineering, University of Washington, Seattle, WA 98195

The nacre structure of red abalone (*Haliotis rufescens*) shell has a higher strength^{1,2} and fracture toughness² at room temperature compared to some monolithic ceramics. The unusual mechanical properties may be attributed to the unique microarchitecture that can be described as a laminated composite of about 95% CaCO₃ and 5% organic matter (a combination of proteins, chitin, and other macromolecules). It is desirable to form synthetic materials having a microarchitecture similar to the nacre through a *biomimetic* approach to obtain improved mechanical properties. In order to achieve this goal, it is necessary to have a better understanding of the microstructure of the nacre at different length scales. The purpose of this work was to examine the structure of nacre in more detail. It has been found that the structure is actually composed of twins which are hierarchical from the nanometer to sub-millimeter scale.

In the edge-on configuration, the nacre is composed of aragonite platelets (thickness 0.25 to 0.5 μm) with their flat faces in [001] direction. The platelets are arranged in a "brick and mortar" microarchitecture with an organic matrix (~ 20 nm) forming the glue between the platelets (Fig. 1). In the face-on configuration, the structure can be described by twinning on three different length scales: first generation, incoherent twinning between platelets; second generation, coherent twinning between domains within platelets; and the third generation, nanoscale twins within domains. Both 60° or 90° twin boundaries have been observed at different length scales. Figure 2 illustrates the six-fold symmetry twin boundaries between platelets where A, C, and E platelets are twin related to platelets B, D, and F, respectively, but they are tilted slightly about the *c*-direction. Fig. 3 illustrates the 90° boundaries within a platelet, in which the four domains are related to each other by twinning, and platelets I and II which are also twin related.

Six-fold symmetry twinning within a platelet is usually observed in natural aragonite since it has an orthorhombic structure (Pmcn) with lattice parameters $a = 4.94 \text{ \AA}$, $b = 7.94 \text{ \AA}$, and $c = 5.72 \text{ \AA}$, but, 90° twin boundaries are less common in nature. It should be noted that the 90° boundary can be accounted for by forming four twin-related domains. However, to form hexagonal platelets, there should be only a 60° angle between each pair of domains, with six domains completing 360° for the whole platelet. This is not possible since the outer edges of the platelets are parallel to {110} twin planes. The angle between {110} planes is 63° and this leaves 3° unaccounted for, and, therefore, causes each domain to be highly strained. Careful analysis of each domain indicates that there are two sets of growth twins forming on {110} planes as illustrated in Fig. 4. The presence of these fine scale defects indicates that the 3°-strain is accommodated by the formation of these twins. As observed, some of the strain can also be released by a slight misalignment among the domains along the *c*-direction.

In summary, there are three scales of twins: (i) first generation twins between platelets, (ii) secondary twins between the domains in a given platelet, and (iii) nanoscale twins within domains. It is well known that the structure of biological soft tissues, such as tendon, have highly ordered hierarchical structure. To our knowledge, this is the first time it has been shown that the inorganic component of a biological structure also has a hierarchical structure. In this case, the hierarchical twin structure covers four orders of magnitude size scale ranging from nanometer to sub-millimeter, again revealing highly ordered microarchitecture in the nacre of red abalone.³

1. J. D. Currey, in *The Mechanical Properties of Biological Materials*, edited by J. F. V. Vincent and J. D. Currey, (Cambridge Univ. Press, London, 1980) pp. 75-98.
2. M. Sarikaya et al., Mater. Res. Soc. Proceedings, Vol. 174 (1990) pp. 109-116.
3. This work is supported by the Air Force Office of Scientific Research under the Grant Nos. AFOSR-87-0114 and AFOSR-89-0496.



Fig. 1 Brick-and-mortar micro-architecture of the nacre of the abalone shell.

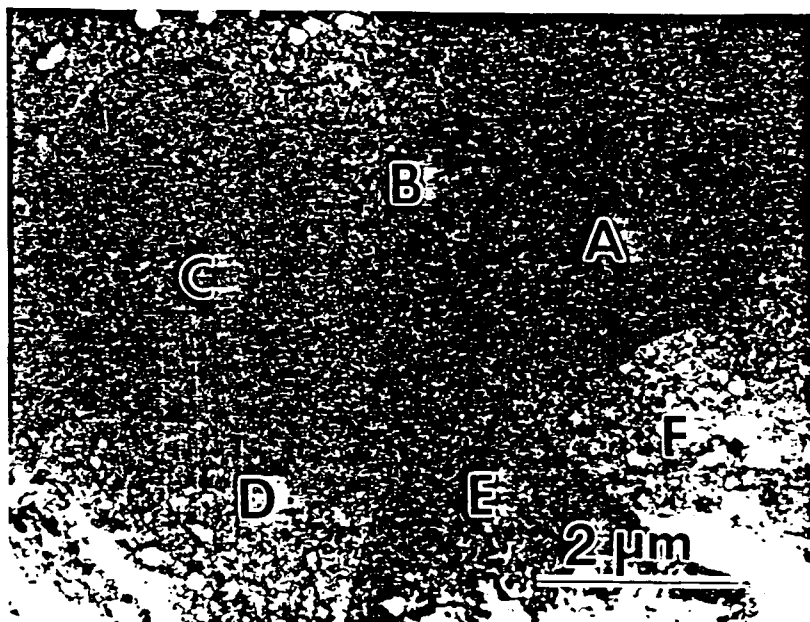


Fig. 2 First generation twins in a six-fold configuration.

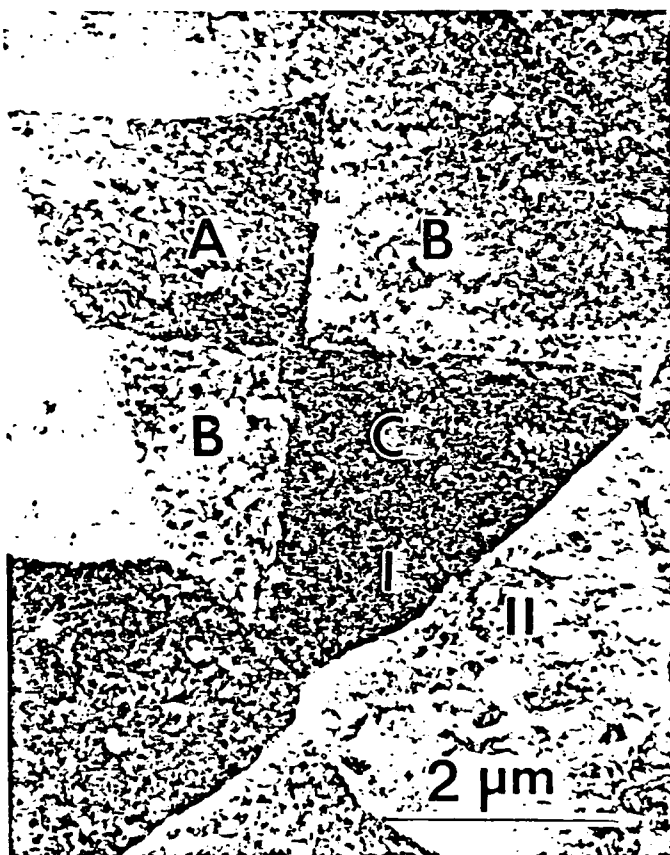


Fig. 3 Second generation twins in a four-fold configuration, and first generation twins between the platelets I and II.



Fig. 4 Third generation twins on a fine scale on (110) and (110) planes in a domain.

APPENDIX XVII

Centrifugation and Filtration Methods for Preparation of Magnetotactic Bacteria for Ultramicrotome Sectioning

by

N. B. Pellerin, K. Reidel, J. N. Lee, K. E. Gunnison, and M. Sarikaya

A Report

The magnetosomes and whole cells are being studied by transmission electron microscopy to elucidate the mechanism of particle formation in bacteria and to understand the structure of magnetosome membrane. The following sections describe the procedures for the preparation of thin sections necessary for TEM studies.

Part A. Centrifugation Method for Preparation of Magnetotactic Spirillum for Ultra-Microtome Sectioning

Initially the cells were received and centrifuged at 1000 g for 20 minutes in order to pellet the cells into a known volume at the bottom of the test tube. Plastic test tubes may be used for easier removal of the final pellet. Some cell damage was believed to have taken place and a lower g value for longer centrifugation time might be more appropriate.

The cell growth medium was pipetted off and the initial fixative of 2% Paraformaldehyde and 2% Glutaraldehyde in 0.1 M NaCacodylate at pH 7.4 was added. The pellet can be broken up with the turbulent motion caused by the pipet in order to reduce the density and size of the pellet. This initial fixative is used to preserve the cell proteins. The cell-fixative mixture was left in a refrigerator at 4°C for 24 hours to allow complete fixation to occur throughout the pellet particles. The fixative must diffuse through the cell membranes and the time for fixation is directly related to the size of the pellet and the density of the cells.

The pellets were washed with 0.1 M NaCacodylate, pH 7.4, to remove the initial fix. The washing process involved pipetting the wash on and mixing the samples with the action of the pipette. The washing procedure was continued for about 30 minutes with several fresh addition of the wash being applied.

A second fixative of 1% Osmium Tetroxide in 0.1 M NaCacodylate, pH 7.4, was added for 20 minutes. This fixative is used to fix the lipids of the cell membranes.

The samples were then again washed for three 10-minute washes with 0.1 M NaCacodylate, pH 7.4. A final washing with distilled water was then done.

The samples were then embedded in a 2% agar mixture which had to be dissolved in distilled water at 45°C. The inability of the agar to completely dissolve in the water was bypassed through filtration of the agar prior to embedding of the samples. The agar was added

The transition fluid of propylene oxide was then applied for two 5-minute washes. This was then followed by gradual medcaste resin infiltration starting with a 1:3 mixture of resin to propylene oxide for 2-3 hours. This was then replaced by a 1:1 solution which was allowed to set for 24 hours and then a 3:1 solution which also set for 24 hours. The final embedding was then completed with two changes of 100% resin.

The samples were then pressed between layers of aluminum and allowed to polymerize prior to sectioning. Sectioning was performed with an ultramicrotome and sectioned samples were suspended on a carbon film attached to a copper TEM grid. Samples were then stored in a desiccator for future use.

Part B. Filtration Method for Preparation of Magnetotactic Spirillum for Ultra-Microtome Sectioning

The general procedure for sample preparation is the same as that used for the samples which had been centrifuged into pellets. However, the filtration method leads to less cell damage through removal of the centrifugation process. The filtration method also proved to be simpler to perform in that the cells were all contained within syringe filters and were thus much easier to handle.

Initially the cells were removed from their growth test tubes with a syringe and directly applied to the filters. Two separate filter types were used including a 0.22 μm nylon filter and a 1.0 μm Nuclepore filter. Two initial fix concentrations were also used including a solution of 1% Glut and 2.5% Para in 0.1 M Cacodylate with .01 M MgCl_2 , and a solution of 2% Glut in 0.1 M NaCacodylate with .01 M MgCl_2 . The magnesium chloride was added in an attempt to preserve the cell membranes better. The samples were allowed to fix at 4°C for 24 hours.

After fixation the samples were then washed with 0.2 M NaCacodylate, pH 7.4, for two 5-minute washes. This was then followed by 0.1 M NaCacodylate, pH 7.4, for four 5-minute washes. These washes were completed by addition of the washing medium to the filter through the use of syringes. The washing solutions were also filtered prior to addition in order to insure the removal of any impurities which might have been present. These impurities could lead to difficulties in sectioning on the ultramicrotome.

The samples were then fixed with a solution of 1% osmium tetroxide in 0.15 M NaCacodylate, pH 7.4, for 30 minutes. The samples were then subjected to one 5-minute washing with 0.2 M NaCacodylate and four 5-minute washes with 0.1 M NaCacodylate. The samples were then washed with distilled water for two 2-minute washes.

The dehydration steps were then completed with 5-minute washes in 15, 35, and 50% ethanol. The filter holders were then opened and the filters removed. The Nuclepore filters can be screwed open to remove the filters while the nylon filters had to be broken open. The filters were then cut in half and marked as to the side which supported the cells. The filters were then placed within small sample jars for the continuation of the process.

The dehydration process was then continued with three 10-minute washes with 70%, one 5-minute wash with 95%, and three 10-minute washes with 100% ethanol.

to the pellets while still warm because it solidifies on cooling. The cells were gently mixed with the agar and then the material was allowed to solidify.

The agar was then cut into 2-3 mm squares in order to insure complete diffusion of the additives to follow. These small samples were then placed within laboratory sample jars for the remainder of the process. During subsequent mixing, care had to be taken to insure that the samples did not wash out of the jars with the addition of solutions.

Dehydration steps were then taken to remove all the water from the cells. The dehydration steps must be done slowly in order to maintain the cell structures present and not induce collapse of the cell membranes. Initially 15% ethanol was washed over the samples for 5 minutes. This was then followed with 35% and 50% ethanol each for 5 minutes. The 70% solution was applied in three 10-minute washes in order to reduce the shock to the cells as the final water was withdrawn. The 95% solution was then applied for 5 minutes and followed by 100% ethanol for three 10-minute washes.

A transition solution of propylene oxide was then applied to the samples for two 5-minute washes. The solution serves as an interface between the ethanol and the final resin.

The final resin infiltration was then completed through a gradual addition of medcaste resin to the propylene oxide solution. Initially a 3:1 solution of propylene to resin was applied to the samples and allowed to set for 1 hour. This was then replaced with a 1:1 solution and allowed to set for 24 hours. A 1:3 solution was then applied and again the samples were allowed to set for 24 hours. This extended time was required in order to insure that the resin had fully diffused into the cells. Finally, a 100% resin solution was added and changed twice in order to achieve full removal of the propylene oxide. The samples were pressed between layers of aluminum and weighted to insure distribution of the cells within the resin.

The final samples were then allowed to polymerize in a 50-55°C oven for 36-48 hours. The samples were then ready for sectioning to mounts for use with the ultra-microtome.

Samples prepared by this method are presented in Figure 10.

APPENDIX XVIII

*The Correlation Between the Microstructure and Mechanical Properties of Nacre
Structure in Pinctada Shell*

by

*S. Sawyer, M. Sarikaya, and I. A. Aksay

*Student Senior Thesis Project
July 1991

Abstract

Nacre is a microstructure found in many sea shells. It is a two phase structure with one phase being calcium carbonate crystallites, and the other phase being an organic fibrous protein. The two phases form a brick and mortar type structure. The calcium carbonate comprises 95% of the entire structure. This structure shows incredible mechanical properties when its constituent components are considered. The correlation between the microstructure and the mechanical properties was investigated. The nacre structure was tested for strength and toughness. The average strength was found to be 220 MPa and the average toughness was found to be 10 MPa-m^{1/2}. These values are comparable to high performance ceramics like tungsten carbide and boron carbide. Photomicrographs were taken with a (Scanning Electron Microscope) SEM to investigate how the structure fractured. It seems that the crystallites or plates in the structure pull away from each other. This means that the cracks have to change paths and go around the plates thus hindering crack propagation. It was also observed that the organic matrix and the crystallites have a very strong bond also contributing to the superior mechanical properties.

Introduction

As the demand for stronger and tougher materials increases, the need to study biological composites also increases. Biological composites are such things as seashells and bones. The composites are made of complex and even hierarchical microstructures which are produced at room temperature and in adverse conditions such as at the bottom of the ocean. The main constituent of seashells and bone is calcium carbonate which is a very weak material. When the composites are tested for their mechanical properties, though, they have shown to demonstrate superior values. This leads to our investigation of the relationship between the superior mechanical properties and the microstructure of the nacre structure in the pinctada shell. The nacre structure was studied because it has the best properties of all shell structures including the prismatic, foliated, crossed-lamellar, complex crossed-lamellar, and homogeneous structures.

The nacre structure is made of two distinct phases. One phase comprises at least 95% of the structure while the other comprises 5% of the other structure. The phase comprising the majority of the structure is calcium carbonate. The other phase comprising the 5% is an organic binder. The structure has the appearance of bricks and mortar; the bricks being calcium carbonate crystallites and the mortar being the organic matrix. The crystallites have the aragonite or orthorhombic form of CaCO_3 . They are platelets with a hexagonal shape. The platelets are up to $1.0\text{ }\mu\text{m}$ in thickness and $10\text{ }\mu\text{m}$ across. The size of the platelets varies greatly. The crystallites are surrounded by the organic matrix. The organic matrix is similar to a polymer matrix in that it contains a high degree of cross-linkage. This cross-linkage effects the mechanical properties. The organic resembles the keratin-myosin-epidermin-fibrin group of fibrous protein. (Taylor and Layman, 1972)

A schematic of the nacre structure (Figure 1) and a photomicrograph (Figure 2) taken with a SEM showing the structure are shown below.

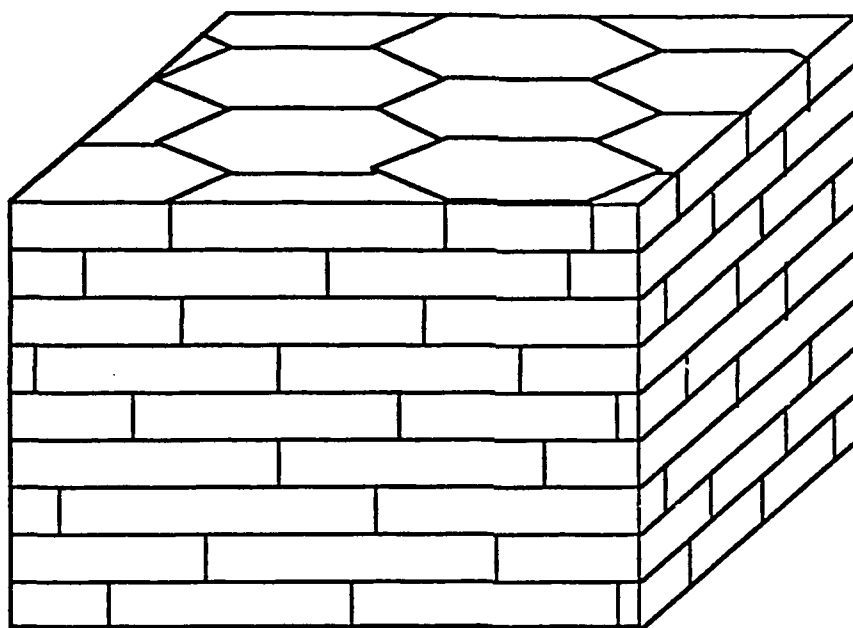


Figure 1: Brick and Mortar structure of Nacre

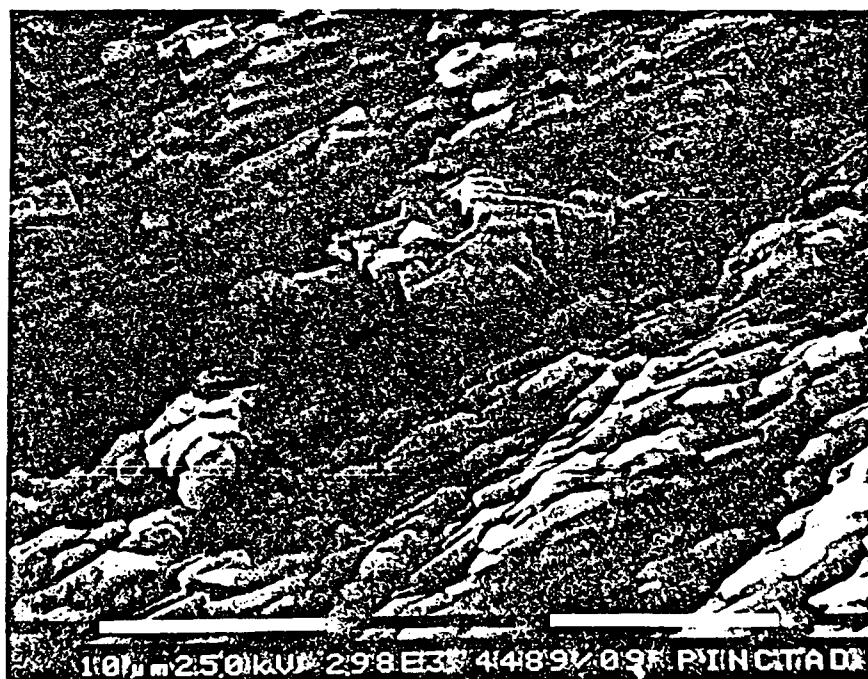


Figure 2: SEM micrograph of the nacre structure

The mechanical property/ microstructure relationship in the nacre structure was studied so as to find the secret behind the superior strength and toughness of the structure. This could lead to possible biomimicking. This means the structure of the biological composite would be mimicked using different constituent components. These components would themselves have better mechanical properties and using them to produce a similar composite would increase their properties even more. The composite materials could be used for impact resistance on military equipment and even on satellites in orbit.

Sample Preparation

The majority of the study was the production of the test specimens. The pinctada shells used were the biggest ones that could be found. They were purchased from jewelers. Even though they were the biggest ones found, they were small compared to similar shells like abalone. The small size of the shells made it difficult to find large enough areas that were flat. A flat area was needed because the samples being made were rectangular with a square cross section.

In order to obtain the desired sample shape, a large amount of machining was needed. The shell itself was initially cut with a diamond blade table saw. A flat area was cut out of the shell. This flat area was further cut into large rectangular pieces with a slow speed saw again using a diamond blade. These rectangular pieces were then mounted onto a piece of glass which was then mounted onto a large piece of steel. They were mounted using crystal bond. This caused further problems because the crystal bond must be heated to melt it. This in turn heats the sample which damages the organic matrix. This could possibly decrease the strength of the organic. The glass used was microscope slides. The reason for this was to prevent damage to the steel when the samples were cut. The glass is cheap and easily replaced.

The reason for mounting the samples on the steel plate leads to the next step in the process. The samples needed to be ground to make the two sides parallel and flat. This was done with a Do-All grinding and cutting machine. The Do-All machine held down the samples by means of the steel plate being magnetically bound to a moving table. Each side of the rectangular piece needed to be ground to a flat surface. This involved grinding one side then heating up the steel plate, glass and sample again so it could be removed. The sample was then turned over and remounted. The second side was then ground to a flat surface.

After the rectangular piece was ground flat on both sides, the thickness of the piece was measured. Using this measurement, the rectangular piece was cut into long pieces with a square cross section. The cutting was also done on the Do-All machine using a diamond blade. After the samples were cut, they were removed from the glass and the excess crystal bond was eliminated using acetone. The acetone was used sparingly so as not to damage the organic binder. This method caused some problems in removal. Some of the samples were broken while being removed.

Half of the samples made were going to be used for fracture toughness tests. These samples needed a notch cut in them for the test. After the samples were removed using acetone, they had to be remounted again so the notch could be cut. The notch was made using the Do-All machine with a diamond blade. The notch was cut to a depth equal to half the height of the sample. It was cut perpendicular to the platelet arrangement on face formed on the inside of the shell.

The samples ranged in size due to the large amount of curvature in the pinctada shell. The shells were different sizes; therefore, it was not possible to make the samples all the same size. The samples were 2.5 cm to 3.8 cm in length. The height and width were from 0.9 mm to 2.6 mm. There was a concern about the layers of crystallites having a curvature within the samples themselves. After the samples were made though, this did not seem to be a problem.

Test Methods

Two major tests were done to study the mechanical properties. They were the four point bend test and the three point bend test. Both tests were done using a instron machine in the compression mode. The four point bend test was used to find the fracture strength, while the three point bend test was used to find the fracture toughness. A

schematic of the two test methods can be found below in Figure 3 and 4.

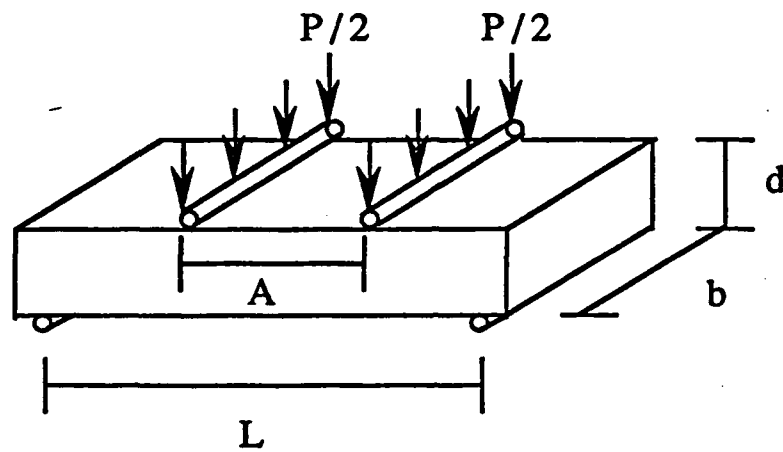


Figure 3: Fracture Strength Test

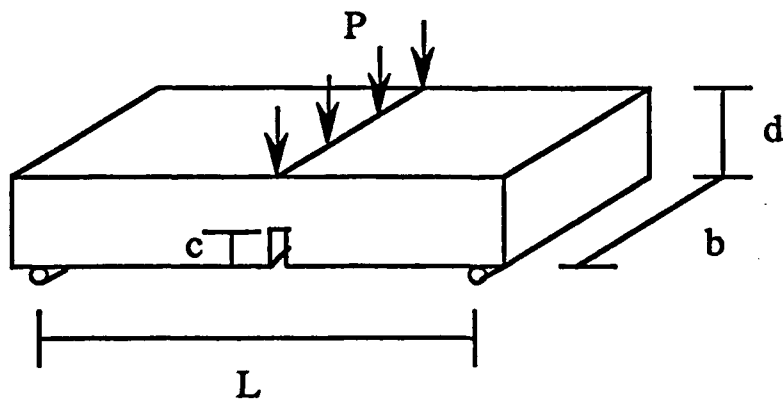


Figure 4: Fracture Toughness Test

For the four point bend test, the top span was 2.54 cm in length and the bottom span was 1.27 cm in length. The cross head speed used was 0.05 mm/min. For the three point bend test, the gage length was 2.70 cm in length. The cross head speed used was also 0.05 mm/min. The data points were taken at a rate of 10 points/sec.

A SEM was used to take photomicrographs of the fracture surface. It was also used to find the sizes of the platelets as well as their shape. The SEM was used to investigate the color difference in the nacre structure of the shells. The inner most nacre structure has a white color while the layer next to it has a dark, almost black structure. It was found that the microstructure of the two layers were not different so they were not separated during sample preparation.

Results and Discussion

The instron recorded the load exerted on the samples over time for both the fracture strength and fracture toughness tests. The load at fracture was used to calculate the values for fracture strength and fracture toughness.

The equation used to find the fracture strength of the samples was as follows:

$$\sigma_f = (3P(L-A)) / (2bd^2)$$

σ_f = fracture strength (MPa) P = Load (N)

A = lower span length (m) L = top span length (m)

d = depth (m) b = breadth (m)

The upper and lower spans were 2.54 cm and 1.27 cm respectively. Ten samples were tested. The value calculated for the fracture strength was 220 MPa with standard deviation of 67 MPa.

The equation which gives the fracture toughness of the samples is as follows:

$$K_{Ic} = (3PLc^{1/2}) / (2bd^2) * \{ 1.90 + 0.0075(L/d) + (-3.39 + 0.0800(L/d))(c/d) + (15.40 - 0.2175(L/d))(c/d)^2 + (-26.24 + 0.2815(L/d))(c/d)^3 + (26.28 - 0.1450(L/d))(c/d)^4 \}$$

K_{Ic} = fracture toughness (MPa-m^{1/2})

P = load (N)

L = gage length (m)

c = crack length (m)

b = breadth (m)

d = depth (m)

The gage length used was 2.7 cm. Seven samples were tested. The fracture toughness was calculated to be 10 MPa-m^{1/2} with a standard deviation of 6 MPa-m^{1/2}.

These values calculated for fracture strength and fracture toughness have a wide spread. This is due to natural defects in the crystallites and the natural curvature of the layers. It is also due to cracks which formed in the samples during preparation. Since a large amount of machining was necessary to make the desired samples, microcracks could have easily formed during the process. Some samples started to crack before the test was started. This was due to the fact that the load had to be placed just on top of the sample. Since it had to be done manually, some of the samples were loaded before the computer started to take data.

These values were compared to strength and toughness values for other high performance materials. A plot of fracture toughness vs. specific fracture strength was made and is shown below in Figure 5.

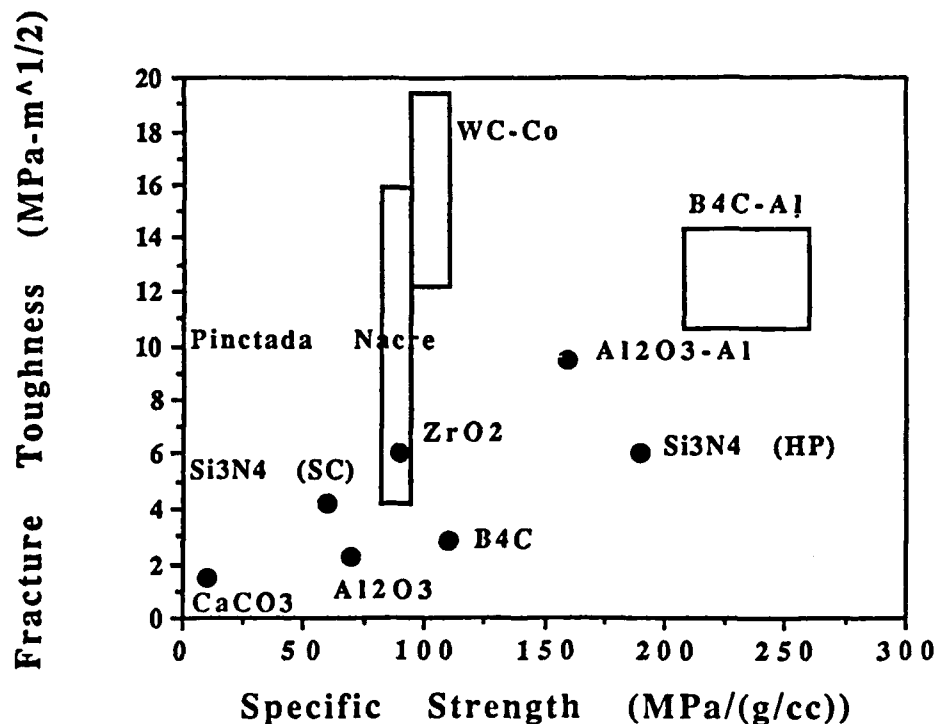


Figure 5: Toughness vs. Specific Strength

From the plot it can be seen that the nacre structure which is made up of at least 95% calcium carbonate had much higher values for strength and toughness. When compared to other higher performance composites like tungsten carbide with cobalt matrix and boron carbide with an aluminum matrix; it can be seen that the nacre structure can also be considered a high performance material. The nacre has a higher specific strength and toughness than alumina and silicon nitride (SC), and a higher toughness than boron carbide, silicon carbide, silicon nitride (HP), alumina with an aluminum matrix, and zirconia.

These superior mechanical properties lead to a discussion on the toughening mechanisms. It could be seen from the photomicrograph taken with the SEM that when the samples fractured, the plates pulled away from each other (Figure 6). This indicates that the cracks propagated around the plates instead of through them. This prevents catastrophic fracture due to the great loss of energy when the cracks have to change path several times throughout the structure.



Figure 6: Micrograph of the fracture surface of nacre demonstrating plate pull-out

When the samples were tested in three and four point bending, an observation was made. It seemed that even after the material had broken and lost its ability to withstand a load, it still appeared intact. This demonstrates the strong bond between the crystallites and the organic matrix. Since there is a strong bond, the organic matrix will stretch and dissipate some of the energy needed for crack propagation.

There have been other toughening mechanisms observed in the nacre structure of abalone shells (Sarikaya et al.). Since the both the abalone and pinctada nacre structures both show pull-out and have similar values for strength and toughness, it is probable that the pinctada nacre also has these other toughening mechanisms. The mechanisms include crack blunting and bridging, microcrack formation, crack bridging, and sliding of crystallites. The crack blunting and branching as well as the microcrack formation lead to a crack propagation behavior called tortuosity. This is not evident in other high toughness ceramics. These mechanisms also dissipate the energy of crack propagation thus preventing the crack from traveling through the material. The crack bridging occurs when the organic binder stretches between the layers. This again demonstrates the strong bond between the organic matrix and the calcium carbonate crystallites. The last toughening mechanism involves the layers of crystallites sliding over each other. This is similar to dislocation slip in metals. (Sarikaya et al)

Conclusions

The average fracture strength of the nacre structure was found to be 220 MPa and the average fracture toughness was found to be 10 MPa-m^{1/2}. From the research done and the values calculated for strength and toughness, it can be seen that the nacre structure has great mechanical properties and can be considered a high performance material. Its mechanical properties are comparable to other high performance laminates and better than many other tough ceramic materials.

It seems that the structure formed by the calcium carbonate crystallites and the organic fibrous protein matrix is a major factor in the great mechanical properties. The toughening mechanisms which are involved with this structure give it the high toughness values. I have found that plate pull-out and a strong bond between the matrix and the crystallites contribute to the properties of the nacre structure. Other toughening mechanisms found in similar materials include plate pull-out, crack bridging and blunting, microcrack formation, crack bridging, and plate sliding (Sarikaya et al).

It seems that the correlation between the microstructure and mechanical properties is due to the highly complex microstructure. The structure makes the cracks change paths several times; therefore dissipating vital energy for crack propagation. In addition, the strong bond between the matrix and the crystallites also contributes to the mechanical properties. The strong bond gives the composite some elasticity thus preventing catastrophic failure. It also seems vital that a majority of the structure must be a phase of high hardness and that the other phase is the connecting phase which has high plasticity. The combination of these two phases contributes to the strength and toughness of the materials.

If this structure can be mimicked using a phase with higher hardness and a phase with higher plasticity, a new material with far better

properties than any other can be developed. The material could be used for impact resistance on military and space equipment.

Appendix

Raw data for each sample

Sample	Test Type	Height (m)	Width (m)	Crack (m)	Load (N)	Strength(Pa)	Toughness (Pa-m ^{1/2})
1	Toughness	2.55E-03	1.90E-03	1.50E-03	1.329	N/A	3.0226E+06
2	Toughness	1.90E-03	2.60E-03	1.00E-03	6.867	N/A	1.3180E+07
3	Toughness	2.55E-03	1.90E-03	1.40E-03	8.829	N/A	1.6609E+07
4	Toughness	2.50E-03	2.00E-03	1.25E-03	0.000	N/A	broke before test
5	Toughness	2.00E-03	1.90E-03	1.00E-03	0.105	N/A	2.2343E+05
6	Toughness	2.55E-03	1.65E-03	1.50E-03	5.886	N/A	1.5415E+07
7	Strength	1.95E-03	1.90E-03	N/A	65.230	1.7200E+08	N/A
8	Strength	2.00E-03	2.35E-03	1.00E-03	5.886	N/A	1.0127E+07
9	Toughness	1.95E-03	1.35E-03	N/A	7.850	2.9131E+07	N/A
10	Strength	2.00E-03	1.60E-03	1.00E-03	5.145	N/A	1.3001E+07
11	Strength	1.90E-03	1.40E-03	N/A	51.940	1.9578E+08	N/A
12	Strength	1.50E-03	1.35E-03	N/A	35.310	2.2145E+08	N/A
13	Strength	1.25E-03	1.95E-03	N/A	38.270	2.3928E+08	N/A
14	Strength	1.35E-03	1.70E-03	N/A	28.470	1.7505E+08	N/A
15	Strength	1.90E-03	1.15E-03	N/A	41.200	1.8905E+08	N/A
16	Toughness	1.50E-03	1.75E-03	7.50E-04	0.000	N/A	broke before test
17	Strength	1.35E-03	1.45E-03	N/A	35.430	2.5541E+08	N/A
18	Strength	1.20E-03	1.20E-03	N/A	34.110	3.7604E+08	N/A
19	Strength	1.50E-03	9.00E-04	N/A	16.550	1.5569E+08	N/A

Bibliography

- William F. Brown, Jr. & John E. Srawley, Plain Strain Crack Toughness Testing of High Strength Metallic Materials
- J. D. Currey, "Biological Composites", Journal of Materials Education, Version II, 1987, pp 122-191
- J. D. Currey & J. D. Taylor, "The Mechanical Behavior of Some Molluscan Hard Tissues", Journal of Zoology, London, 1974, 173, pp 395-406
- J. D. Currey, "Further Studies on the Mechanical Properties of Mollusc Shell Material", Journal of Zoology, London, 1976, 180, pp 445-453
- R. W. Davidge, Mechanical Behavior of Ceramics, Cambridge Press, Cambridge, 1979
- M. Sarikaya, K. E. Gunnison, M. Yasrebi, I. A. Aksay, Mechanical Property-Microstructural Relationships in Abalone Shell, summary of a paper submitted to Journal of Materials Research
- J. D. Taylor & Martin Layman, "The Mechanical Properties of Bivalve (Mollusca) Shell Structures", Palaeontology, Vol 15, Part 1, 1972, pp73-87
- Test Specimens and Strain Measuring Instruments, Laboratory Devices Co., Auburn, CA

APPENDIX XIX

Self-Healing in Abalone Shells

by

*H. Denham, K. E. Gunnison, and I. A. Aksay

***Student Senior Thesis Project**
June 1991

INTRODUCTION

I began this experiment in the self-healing of abalone shells because I had an interest in exploring the relationship between natural composites and man's efforts to duplicate them (biomimicking). The goal of this experiment was focused on the mechanism of repair in abalone shells. This goal has many aspects and due to its size I was unable to fully define the mechanism within the time frame of this project. The aspects that are most interesting are the sensing mechanisms. The animal must know it needs to heal, begin the healing, and then at some point decide that it has healed sufficiently and stop the process. The structure that the abalone heals with may be the nacre that predominates its shell or may be a quick patch job with no concern for the structure, just that the hole is filled.

The overall scope of my work was the drilling of small holes in the shells of live abalone, and examining the healing process. To accomplish this several arrangements were made. First the acquisition of abalone and arranging for their care was coordinated with the Seattle Aquarium. With this initial organization, the experiment continued with the animals being drilled and allowed to heal.

The experimental design was to drill several small holes (roughly 2 mm diameter) in the abalone, and allow them to heal. Once healed the animals were to be sacrificed and the healed regions examined. The examination was to include optical transmission microscopy, scanning electron microscopy, and possibly transmission electron microscopy. Due to the length of the healing process, the analysis of the healed regions has not been completed.

PROCEDURE

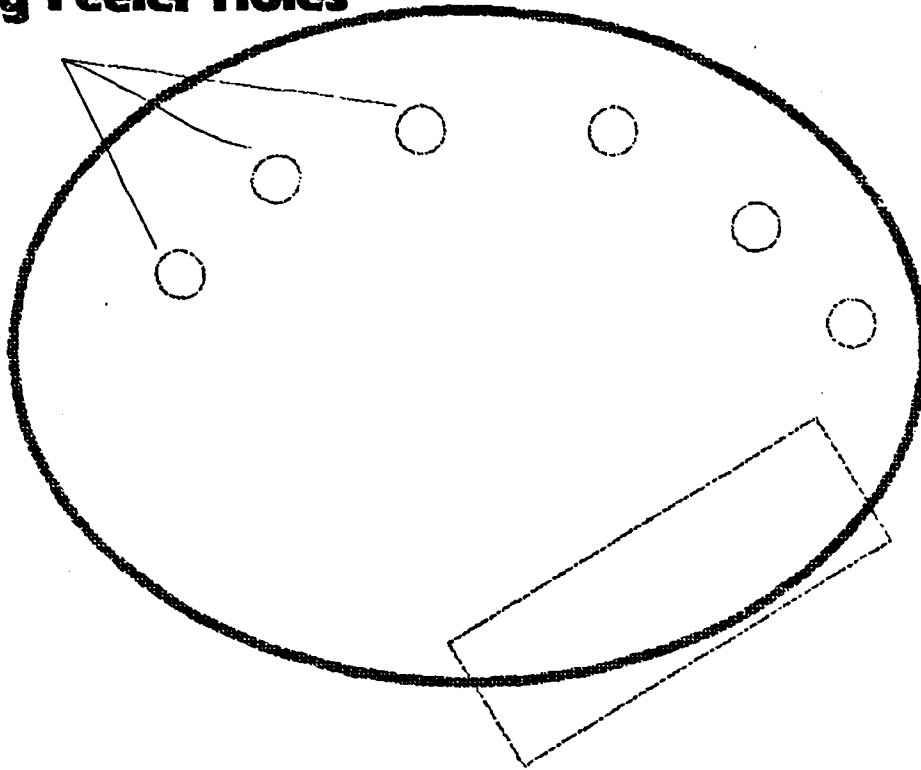
I began this experiment by arranging for the Seattle Aquarium to provide twelve abalone. The Aquarium also agreed to care for the animals providing both tank space and regular feeding. Two of the abalone were chosen for a survival test to see if the drilling would prove fatal. Two holes, roughly 2 mm in diameter, were drilled in each shell, being sure to penetrate through the entire shell but not to damage the animal. The holes were drilled with a dental drill. These two were then returned to the tank. After a period of two months, with the two drilled animals alive and well, the rest of the animals were shuttled to the dentist and drilled. Each animal received two or three 2 mm holes depending on the size of the animal, with the smaller ones receiving only two holes. The holes were drilled along the leading edge of the shell, the growth region (figure 1). The animals were then returned to the aquarium and allowed to heal. The healing progress was monitored by occasional optical examination with a stereoscope at low magnifications.

The healing was allowed to progress for five months while the experimental design was changed. The original plan had been to sacrifice the animals in order to perform analysis on the healed region. Instead of this it was decided that the healed region could be removed from the animal without killing the abalone by core drilling. Subsequent healing of the larger drilled area might also provide further insights into the healing mechanism. Core drill bits (diamond impregnated) with an inside diameter of 3/8" were obtained to execute this plan.

With adequate signs of healing, five of the animals were subjected to the core drilling. Each animal had one healed region removed with the core drill, removing all healed regions was thought to be too traumatic for the abalone's survival. These samples were then prepared for analysis.

The principal method of analysis chosen was scanning electron microscopy. The samples were prepared for this in different ways. One sample was examined "as is," one sample was ground down close to the healed region, and one sample was cut across the healed region and polished for examination. The remaining samples were held for a decision based on the results seen in the other samples.

Existing Feeler Holes



**Leading Edge
and Drilling Zone**

Figure 1: Abalone Shell

RESULTS

The abalone were able to heal the holes that were drilled in them to different degrees and in different ways. The larger of the animals were the slowest to show healing and some have yet to heal. This may be due to the size of the hole compared to the size of the shell or due to the less active growth seen in the older animals. The smaller sized animals were the fastest to heal with the drilled holes covered within the first month. The medium sized animals healed within the five month period.

The way that the animals healed has given some insight into the healing mechanism. The hole was not healed through the full thickness of the shell. The healing began at a partial depth and continued inward toward the animal. It appears that due to the radius of the hole, the animal can't get the shell building materials up to the surface of the hole (figure 2). Whether or not this is a mechanical limit will be better understood if the abalone are able to heal the core drill holes. This would mean that the mantle of the abalone must be involved with the growth, as it is the only "live" portion of the animal in intimate contact with this part of the shell.

The healing continues inward toward the animal as is evidenced by a prominent bump on the inner shell below the drill site. This suggests that the animal wants a certain thickness of shell between itself and the ocean, and thus continues the growth in the only direction available. How far this growth might continue inward is not known but may be determined by further study.

The examination of the healed regions with the scanning electron microscope (SEM) has only begun and the results so far are inconclusive. The first micrograph (figure 3) is of the surface of the healed region looking straight down the drilled hole. There was quite a bit of charging due to the difficulties in sputter coating holes. What this micrograph shows is a different surface than seen elsewhere on the shell. What appear to be plate like structures are too large to be nacre.

Some of the more interesting micrographs were found along the wall of the drilled region (figures 4 and 5). Here were found regions where the alignment of nacre plates was disordered and in places nearly perpendicular. This may be an artifact of the drilling or a hurried attempt to fill the hole with little regard for the structure.

The micrographs of the cross section of the healed region proved inconclusive with nothing to compare them with. More cross sections need to be prepared to verify the findings.

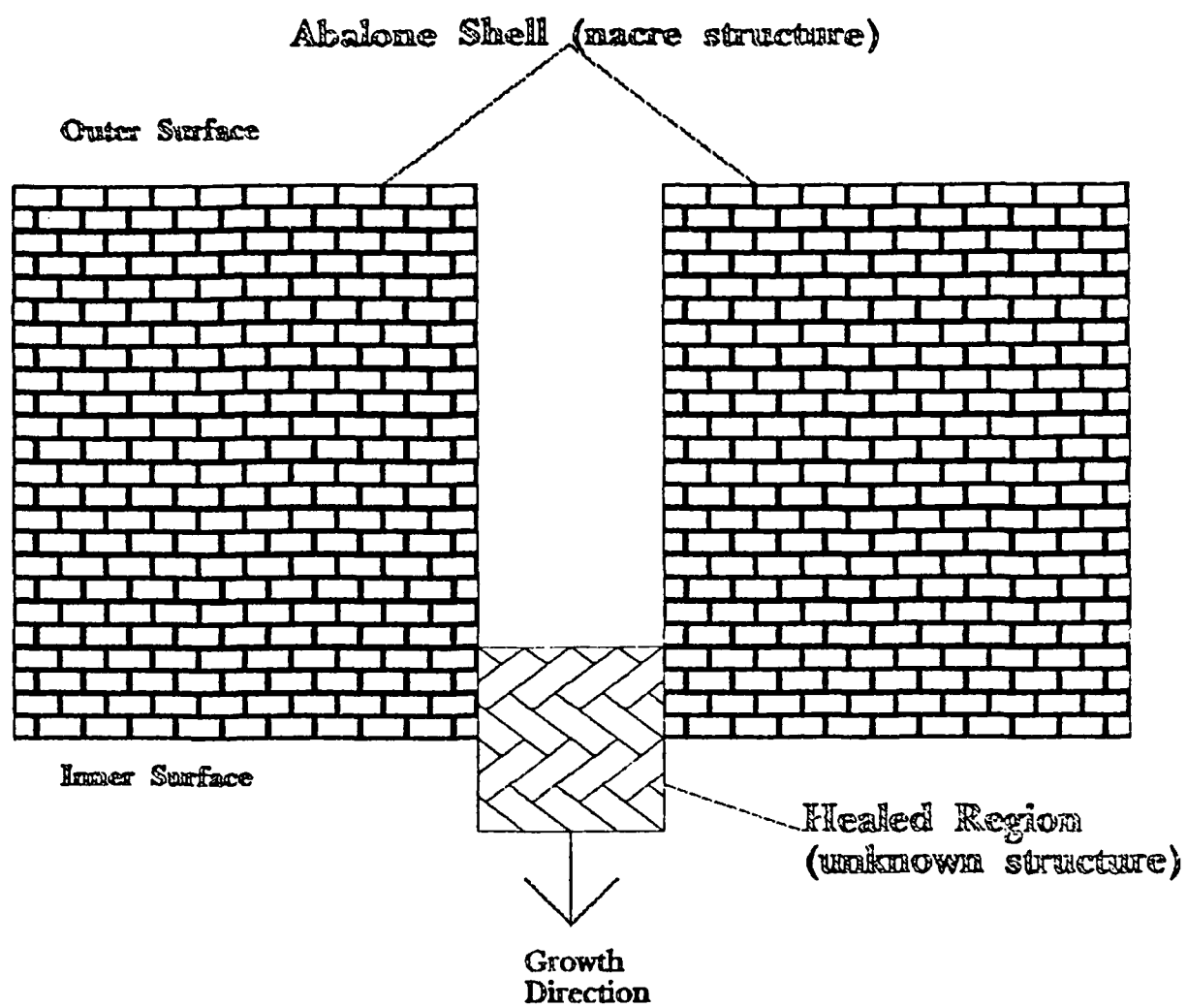


Figure 2: Cross Section of Healed Region



Figure 3: SEM of Surface of Healed Region



Figure 4: SEM Wall of Drilled Hole

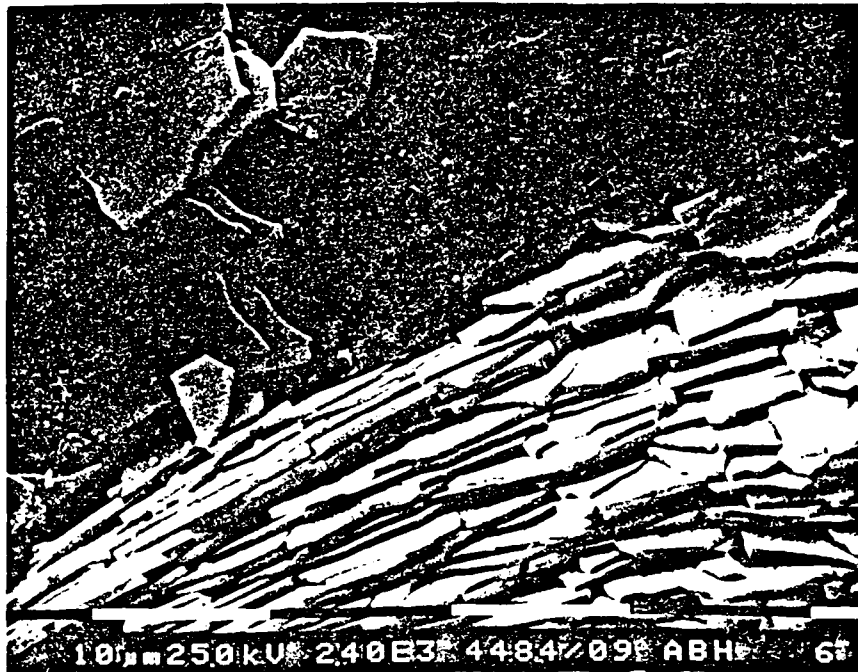


Figure 5: SEM Wall of Drilled Hole

CONCLUSIONS

This experiment in the self-healing of abalone shells has raised some interesting issues and shed some light on others. When considering biomimicking a better understanding of the mechanisms of repair would be helpful. There are many aspects of the repair process that were examined in part. The abalone is able to sense a drilled hole in its shell and take action to repair the hole. The holes drilled were completely through the shell, whether the animal could sense a shallower hole is not known, but would provide more insight into the sensing mechanism.

The abalone is unable to heal clear to the top of a 2 mm hole, perhaps due to mechanical limitations. Whether these limitations are mechanical could be determined by examining different sized holes and the depth of the hole healed. This may easily be done with the abalone that currently are in the process of healing the core drillings. The total thickness of the healed region is also of interest, as the abalone heal inward far enough to leave a prominent bump on the inner surface of the shell, below the drill site. Whether this thickness desired is for structural purposes or because the animal wants a specific minimum thickness is unknown. This would be another good area for research, as the sensing mechanism must somehow know when to stop healing, and why.

The structure of the healed region is what I had hoped to determine with this project, but as with most research, many new questions are raised along the way. I was unable to conclusively define the structure of the healed region, due to the constraint of the time. I have seen micrographs suggesting a disordered nacre structure as well as an unrecognized structure, further data is needed to verify either finding. The healing process is slow and I may not have examined the finished healing. This means that the shell may still heal through the thickness, but this is very doubtful as the growth must occur near the mantle. Further examination of the samples I obtained as well as the animals still healing may provide the necessary information to specify the structure.

The healing process provides many aspects that could prove very useful in the field of biomimicking. Further study in this fascinating field is necessary to make conclusions on the self-healing of abalone shells.

APPENDIX XX

Processing of Ceramic Particles with Azotobacter vinelandii

by

T. Ren, N. B. Pellerin, J. T. Staley, G. L. Graff, and I. A. Aksay

Paper to be Submitted

1991

Abstract

Alginate from the bacterium, *Azotobacter vinelandii*, was an effective dispersant for small ceramic particles (400 nm diameter alumina). Furthermore *A. vinelandii* grew and produced alginate in the presence of up to 15 vol% alumina particles indicating that an *in situ* process might be developed to use this bacterium to coat ceramic particles with its alginate dispersant. In *in situ* processing experiments, the sedimentation heights of alumina suspensions were significantly reduced and the viscosities of 5 and 10 vol% suspensions were reduced four- and 60-fold over controls, respectively. The bacteria could be readily removed from the ceramic particles by washing. However, the dispersant bound firmly to the particles and could not be removed by repeated washing in distilled water. 3.22 mg of the polyuronic acid bound to one gram of alumina particles. By calculation, the polymer produced by a single *A. vinelandii* cell under *in situ* non-growth conditions coated approximately 2.5×10^5 alumina particles.

Introduction

Since prehistoric times clay beds were prepared by potters by amending them with organic materials such as urine, manure-water, and tannin. This practice of "aging" resulted in making the clay materials more plastic and therefore more readily workable for pottery production.

Early in the 20th century several scientists performed experiments which implicated microorganisms in clay aging. In 1902 Stover noted that clays which were sterilized did not exhibit the plastic qualities of properly aged clays containing bacteria (21). Furthermore, if the sterilized clay was inoculated with previously aged clay, it acquired the workability properties of normally aged clays within two to four weeks. Spurrier (1921) demonstrated the growth of filamentous algae in aging clay and hypothesized that the products of their growth contributed to the increase in plasticity (20).

Glick (7, 8) and Baker and Glick (3) noted that fine clays were aged in commercial cellars for several weeks to a year. New cellars were prepared by inoculating fresh clay material with small amounts of well aged clays. Several bacteria were isolated from the seasoned clays and identified as species of *Bacillus* and *Pseudomonas* as well as other genera.

One is naturally led to inquire how microorganisms are able to increase the plasticity of clays. Since the current state of art technology in ceramic processing employs synthetic polymers as dispersants, we hypothesized that microbial exopolymers, such as polysaccharides or polypeptides, may be responsible.

Ceramic particles such as alumina are highly charged. As the size of the particles becomes smaller, the charges become increasingly important in ceramic processing (2). Unamended small ceramic particles agglomerate into hierarchical structures that are loosely packed and contain irregular void spaces. Synthetic polymers from petrochemicals such as polymethacrylic acid (PMAA) and polyacrylic acid (PAA) are currently used as dispersants to coat alumina particles in advanced ceramic processing thereby permitting their close packing (5,6). However, commercial PMAA may contain formaldehyde and PAA may contain residual amounts of acrylic acid, both of which are toxic. Furthermore, they are produced from precursors that are toxic and/or carcinogenic. In contrast, naturally occurring polymers are non-toxic and do not pose problems of disposal since they are readily degraded by natural processes.

Earlier studies from this laboratory showed that the bacterial glycan, dextran. Though dextran was ineffective as a dispersant, when it was modified chemically to produce dextran sulfate, it became a satisfactory dispersant (Graff *et al.*, in preparation). Like the acrylic polymers, dextran sulfate has an acidic side-group which is thought to be the important feature for alumina dispersion. However, because of the sulfate groups, dextran sulfate is not completely removed by sintering.

Therefore we set out to determine whether naturally occurring acidic polymers could be used as dispersants. The first naturally occurring acidic polymer we studied is alginate, an alpha 1-4-linked linear copolymer of β -D-mannuronic and β -L-guluronic acid (10,11,12, 14) synthesized by several species of marine algae (4). Polymers of a molecular weight of about 5,000 were found to be satisfactory dispersants for alumina processing (Pellerin *et al*, submitted). The purpose of this study was to determine whether bacterial alginate from *Azotobacter vinelandii* (9, 17) would also serve as an effective a dispersant of ceramic particles and, if so, whether an *in situ* process could be developed to produce bacterial alginate in the presence of ceramic particles.

Materials and Methods

Bacterial cultivation. *Azotobacter vinelandii* NCIB 8789 (National Collection of Industrial Bacteria, Aberdeen, Scotland) was maintained on Larsen's broth medium in first stage culture. Cyst stage cultures (stock culture) were subcultured every 2 months to fresh broth, grown at 30 °C for 2 days and stored at 4 °C. Working cultures were subcultured from the stock culture when needed. Normal Larsen's medium contains: sucrose, 20 g; K_2HPO_4 , 1.0 g; $MgSO_4 \cdot 7H_2O$, 1.0 g; $FeSO_4 \cdot 7H_2O$, 50 mg; $Na_2MoO_4 \cdot 2H_2O$, 5 mg; $CaCl_2$, 50 mg; NH_4 acetate, 2.3 g; distilled water, 1 liter; pH 6.5. For plate cultures, 1.8% agar was added to the broth.

Bacterial counts and cyst observations. Bacterial cells were counted by standard plate count techniques on solid Larsen's medium. Cyst formation of *A. vinelandii* was observed directly using a phase microscope.

Determination of polysaccharide in culture suspensions. Bacteria were removed from the culture by centrifugation at 22,000 xg for 40 min. Polysaccharide in the supernatant was determined by the *meta* - hydroxydiphenylsulphuric acid assay (16). Mannitol (20 g per liter) was used in place of sucrose as a carbon source in the growth medium due to its minimal interference with the colorimetric analysis when this assay was used. Low viscosity kelp alginate (Sigma) was used as the standard for this assay. Spectral work was conducted with a Gilford Response II spectrophotometer (Gilford Instrument Laboratories, Oberlin, OH) or a Spectronic 20 spectrophotometer (Bausch & Lomb, Rochester, NY).

Polysaccharide harvest. *A. vinelandii* NCIB 8789 was shaken in the Larsen's broth at 30°C for 5 days. Bacterial cells were removed by centrifugation at 22,000 xg for 40 min. Three volumes of 2-isopropanol were then added to the supernatant for precipitation (13). The precipitate was washed with 2-isopropanol 2-4 times, and then dissolved in distilled water before dialysing against dH_2O overnight. After alcohol precipitation the polysaccharide was lyophilized.

Ceramic particles. The ceramic particle used in this study was high purity (99.99%) Al_2O_3 , with an average particle size (diameter) of 400 nm (AKP-30, Sumitomo Chemical America, Inc., New York, N.Y.).

pH adjustment of particle suspensions. Because the pH of the particle suspension is affected by the degree of mixing (1), suspensions for sedimentation tests, rheological measurements and broth cultures were mixed more than 0.5 h (in most situations, overnight) on a magnetic stirrer. The pH was adjusted to the experimental value initially, and then readjusted after mixing.

Sedimentation tests. Sedimentation columns were prepared with 2 vol% (in *in situ* test, this is 5 to 10 vol%) AKP-30 in aqueous solutions of polymer. The suspensions were sonicated for 5 min and mixed on a magnetic stirrer for 0.5 h. The pH of the suspension was adjusted to the experimental value before bringing the

final volume to 10 ml. The suspension was decanted into a conical bottom, graduated polystyrene tube (Falcon 2095, Becton Dickinson) and left undisturbed at room temperature for some time (in most situations, three-four weeks). Final sedimentation heights were measured to ± 0.1 ml.

Viscosity measurements. Viscosity measurements were obtained using a Rheometrics Fluid Spectrometer, Model 8400 (Rheometrics Inc., Piscataway, N.J.). Suspensions (about 15 ml) for viscosity measurements were prepared as above.

Washing of the bacterial polysaccharide from the AKP-30. 200 ml Larsen's broth with mannitol as a carbon source was inoculated with a 1 ml suspension of *A. vinelandii* cells and shaken at 30°C for 5 days. The culture was centrifuged at 22,000 $\times g$ for 40 minutes to remove the bacterial cells. Five volume percent alumina (5.94 g AKP-30) was added to 28.5 ml of the supernatant and then ultrasonicated for 2 min for complete mixing. The suspension was adjusted to pH 8, and the concentration of polyuronic acid remaining in the supernatant was determined by the *meta*-hydroxydiphenyl - sulphuric acid assay. Then the pellet was washed three times. After each washing, the polymer concentration of the supernatant was assayed. The amount of the polymer bound to the particles was calculated by difference.

Removal of bacterial cells from *in situ* system. The bacterium was cultured with 5 vol% ceramic particles at 30°C for 5 days on a shaker, and then centrifuged for 40 min. at 22,000 $\times g$. This resulted in three layers: the ceramic particles at the bottom, a very thin layer of bacterial cells in the middle, and the spent broth at the top as supernatant. The supernatant was decanted and the top of the pellet column removed with a sterile pipette. The newly exposed surface was then washed 8-10 times with sterile water to remove loosely associated bacteria before the pellet was resuspended in sterile water to volume. Bacterial numbers were determined in this suspension by plate counts.

Nutrient limitation tests. *A. vinelandii* was cultivated in normal Larsen's broth for about 24 h, and the cells were harvested by centrifugation. The cell pellet was washed twice and then resuspended with sterile saline. A sample was removed for bacterial enumeration and 1 ml of this suspension was inoculated into 99 ml of modified nutrient-deficient Larsen's broth. Three modified Larsen's media were used: 1: mannitol, 20 g; dH₂O, 1 liter. 2: mannitol, 20 g; K₂HPO₄, 65 mg; MgSO₄·7H₂O, 40 mg; FeCl₂·4H₂O, 1.7 mg; dH₂O, 1 liter; 3: mannitol, 20 g; K₂HPO₄, 65 mg; KH₂PO₄, 32 mg; MgSO₄, 40 mg; FeCl₂, 1.7 mg (13); Na acetate, 1.5 g (15); dH₂O, 1 liter. After incubation for 96 h, the bacterial numbers and polyuronic acid concentration were determined.

Results

Production of alginate by *A. vinelandii*. The production of alginate during growth was determined by sampling batch cultures periodically and analyzing for viable cell counts and alginate production. Bacterial cell numbers peaked after 20 to 40 hours and cyst production (18) began toward the end of logarithmic growth (between 40-60 h). Polyuronic acid secretion corresponded closely with the onset of cyst formation, i.e., in the late logarithmic to early stationary phase of growth. The pH varied somewhat during growth of the culture (pH 6.3 to 7.5), but its relationship to growth and alginate production were not studied here. The yield of alginate, harvested by precipitation from culture supernatants with 2-isopropanol, ranged from 0.8 -1.2 g dry weight/liter broth.

Bacterial alginate as a dispersant. The alginate obtained from *A. vinelandii* cultures was tested for its ability to act as a dispersant for alumina by the preparation of 2 vol% suspensions of alumina particles. The resulting sedimentation heights show clearly that bacterial alginate is an effective dispersant and acts in a manner similar to kelp alginate (Figure 1). The optimum concentration for sedimentation occurred using 0.5 % polysaccharide (dry weight basis, of polymer to particles) for both alginates.

***In situ* production of alginate.** The foregoing results indicate that bacterial alginate can be used as a dispersant for ceramic particles. The question arises as to the most expedient method that could be used to deliver the alginate to the particles. The simplest and most direct means of doing this would be by the development of an *in situ* process in which the bacterium is grown with the particles while it produces the alginate. Therefore we initiated work to determine whether the bacterium could be grown in the presence of the particles and at the same time produce alginate. This was tested in 5, 10, and 15 vol% alumina suspensions inoculated with approximately 3.0×10^3 bacterial cells per ml Larsen's medium and incubated at 30°C for 4 days.

Organisms grew at all concentrations of alumina although bacterial yields were reduced somewhat at higher alumina concentrations (Figure 2). The bacterial numbers in the cultures increased to 5.1×10^7 , 7.5×10^6 , and 8.2×10^5 /ml of suspension from the inoculum concentration of 3.0×10^3 /ml for the 5, 10, and 15 vol%, respectively. A control culture without alumina increased to 3.1×10^8 /ml during the 4 day incubation period. As the concentration of the particles increased each 5 vol%, the bacterial cell yield was reduced about 10-fold. This reduced yield may be due to reduced oxygen concentrations or to pH effects of the alumina or a combination of both. Polymer was detected in the supernatant of each culture. Because of its adsorption to the particles, the amounts detected were not quantitated.

We next evaluated whether the particles became coated with polymer during growth of the bacterium. The 5 and 10 vol% suspensions which had been incubated

with *A. vinelandii*, and their sterile controls were adjusted to the same pH before testing. Sedimentation test results show that the sedimentation height in a 5 vol% suspension was 51% of the sterile control, and for the 10 vol% suspension, 42% of the control (Figure 3) indicating that polymer was being produced and coating the particles.

Viscosity is another method of assessing the effectiveness of a dispersant. Well dispersed systems are characterized by low viscosity because the particle-particle attractions have been overcome (2,6). The viscosities of the inoculated 5 and 10 vol% suspensions were reduced four-fold (from 0.48 to 0.12 poise at 10 rpm) and 60-fold (from 6.0 to 0.1 poise at 10 rpm) over the controls.

One of the potential problems encountered in the *in situ* processing of ceramic materials is the possible deleterious effect of the cells on the quality of the final ceramic product. Ideally cells should either be grown separately from the particles using a filter system or removed after they have been grown in the presence of the particles. Since we grew cells in direct contact with the particles, we were interested in determining whether cells could be readily removed without removing the polymer. To study this, successive washings were undertaken to determine whether bacterial cells could be removed from the particles (Table 1). After cultivation for 6 days at 30°C, bacterial cell numbers in the *in situ* system were 5.6×10^7 per ml of particle suspension (mixture of bacterial cells, particles, and nutrient solution) before washing. Cell counts in the pellet gradually decreased after each successive washing with sterile water. After the fifth washing, there were only 85 cells per ml of the pellet resuspension. Therefore, the bacterial cells do not bind strongly to the particles and are readily removed by successive washings.

Separate experiments using particles and cell-free culture supernatant containing alginate were conducted to assess the amount of polymer adsorbed to the particles and the degree of adsorption (Table 2). In contrast to the bacterial cells, washing had little effect on the removal of polymer bound to alumina. Thus, when the alumina (5.94 g) was added to the supernatant containing the polymer (927 µg/ml), and removed subsequently by centrifugation, it had adsorbed 588 µg/ml of the alginate. By calculation it was determined that a total 2.97 mg of bacterial polyuronic acid was adsorbed by a gram of AKP-30 particles. After the first washing of the adsorbed particles, only 5 µg/ml was detected in the supernatant and none could be detected after further washing. Therefore, more than 99% of the polymer that was initially bound remained adsorbed to the particles even after three successive washes.

Use of non-growing cells for *in situ* processing. One logical route to consider for *in situ* ceramic processing is the use of pre-grown bacterial suspensions that are capable of alginate production under non-growing conditions. This would allow polymer production under conditions of greater control over pH, carbon source concentration, mineral base medium composition, and cell

concentrations, all of which would be expected to have some influence on an *in situ* process. Furthermore, a condition might be found in which polymer production could be accomplished by a minimum bacterial biomass, since bacterial cells would be undesirable in the final product.

For this purpose, washed suspensions of *A. vinelandii* were inoculated into the four different nutrient-limited media to a final cell concentration of 2.8×10^5 /ml (Table 3). Growth did not occur in either modified medium 1 which contained only mannitol or medium 2 which contained mannitol and buffer. In modified medium 1, the yield of the polyuronic acid was very low (only 5.8 μ g/ml), but in modified medium 2 the polyuronic acid production was 30.5 μ g/ml, or 100 ng/1000 cells. This yield compared favorably with the yield in modified medium 3 comprising mannitol, a higher buffer concentration, and sodium acetate. In contrast, under normal growth conditions in Larsen's medium, the bacterium produced only 2.7 ng alginate/1000 cells. In all media tested, the bacteria lost motility and developed to the cyst stage.

Discussion

Clay aging resembles other empirical processes developed by humans, such as the alcoholic and lactic fermentations, and bread leavening, that have unwittingly involved microorganisms. However, the actual mechanism(s) that underlies this microbial aging process is still only poorly understood. The results of this study suggest that the production of natural acidic bacterial exopolymers may by the underlying explanation for this phenomenon.

Comparable dispersion was noted between the kelp and bacterial alginates suggesting their similar physicochemical properties. The exopolyuronic acid from *Azotobacter vinelandii* is not only structurally similar to the alginate from marine algae [both alginates contain blocks of M, blocks of G and blocks of MG, as well as the same ratio of poly G to poly M as the alginate from marine algae (19)]. The primary difference between the alginate from *A. vinelandii* and algae is that Oacetyl groups are associated with some of the mannuronic acid residues of the former. However, the ester-linked acetate groups do not contribute to the charge (one of the main factors influencing dispersion) on the polymer(22,23).

It is of interest to note that the range of polysaccharide concentration for best sedimentation is about 0.5% (Figure 1) which is close to the concentration (0.32%) at which the polymer was fully adsorbed to the particles (Table 3). Too little or too much polysaccharide resulted in poorer sedimentation. This result also agrees with the results using other polymers (5,6). If insufficient polymer is present, dense packing cannot occur. If excess polymer is present, the polymer interacts with itself to cause gelling, leaving void spaces in the cake. Thus, the poorer packing density found at the lower concentration of alumina, i.e., 5 vol% versus 10 vol% in the *in situ* growth experiment, is likely due to excess alginate production. It was also observed

that the adsorption of polymer can be influenced somewhat by other experimental conditions including ultrasonication time and the pH of the sample suspension (data not included here).

The high affinity of the polymer for the particles was demonstrated by the the experiments in which the coated particles were subjected to several successive washings in distilled water (Table 2). Over 99% of the polysaccharide remained adsorbed to the particles even after three washings.

From the results of these experiments it is possible to calculate the number of ceramic particles that can be coated by the polyuronic acid produced by a single *A. vinelandii* cell (assuming growth on modified medium 2 and an alumina particle size with a radius $r = 200$ nm). From the polysaccharide adsorption data (Table 2), we know that about 2.97 mg polyuronic acid are required to coat one gram of particles and this amount of polymer is produced by about 2.97×10^7 cells of *A. vinelandii* (Table 3). Thus, in theory, the polyuronic acid produced by a single bacterial cell on medium 2 can coat about 2.5×10^5 AKP-30 particles.

The results of this study indicate that *Azotobacter vinelandii* can be used in an *in situ* process to produce alginate in the presence of alumina particles. Furthermore, whereas bacterial cells do not adhere strongly to the particles and can be easily removed by washing, the alginate they produce is strongly bound to the particles and cannot be removed by repeated washings. Moreover, only a small number of non-growing cells is required to coat a large number of particles. While it was not the intent of this study to design a specific procedure for a commercial *in situ* process for coating advanced ceramic materials, the results of this study should be useful for anyone who wishes to develop such a process using the alginate-producing bacterium, *Azotobacter vinelandii*.







In addition, the results of this study suggest that commercial pottery manufacture with raw clays could benefit from a fuller understanding of the microbiology of the aging process. Perhaps the use of appropriate bacterial inocula, carbon sources, and other nutrients could improve polymer production and dramatically hasten the seasoning process and make it more reproducible and efficient in a manner similar to that which is used to commercially control the alcoholic and lactic fermentations.

References

1. **Aksay, I.A., F.F. Lange, and B.I. Davis.** 1983. Uniformity of $\text{Al}_2\text{O}_3\text{-ZrO}_2$ composites by colloidal filtration. *J. Am. Ceram. Soc.*, 66 [10]: C-190-192.
2. **Aksay, I.A.** 1984. Microstructure control through colloidal consolidation, p.94-104. in J.A.Mengels and G.L. Messing (ed.), *Advances in Ceramics*, vol. 9, Forming of Ceramics. Am. Ceram. Soc., Columbus, Ohio.
3. **Baker, D.R., and D.P. Glick.** 1936. Sterilization effects on properties of clays, *J. Amer. Ceram. Soc.*, 19: 209-212.
4. **Booth, E.** 1975. Seaweeds in industry, p. 219-268. *In* J. P. Riley and G. Skirrow (ed.), *Chemical Oceanography*. Academic Press, London.
5. **Cesarano III, J., and I.A. Aksay.** 1988a. Stability of aqueous Al_2O_3 suspensions with poly(methacrylic acid) polyelectrolytes, *J. Am. Ceram. Soc.*, 71 [4]: 250-55 .
6. **Cesarano III, J., and I.A. Aksay.** 1988b. Processing of highly concentrated alumina suspensions stabilized with polyelectrolytes, *J. Am. Ceram. Soc.*, 71 [12]: 1062-67.
7. **Glick, D. P.,** 1936. The microbiology of aging clays. *J. Amer. Ceram. Soc.*, 19: 169-175.
8. **Glick, D. P.,** 1936. The effects of various treatments upon the aging of a ceramic body. *J. Amer. Ceram. Soc.*, 19: 240-242.
9. **Gorin, P. A. J., and J. F. T. Spencer.** 1966. Exocellular alginate acid from *Azotobacter vinelandii*. *Can. J. Chem.* 44: 993-998.
10. **Grasdalen, H., B. Larsen and O. Smidsrød.** 1979. A P.M.R. study of the composition and sequence of uronate residues in alginates. *Carbohy. Res.* 68: 23-31.

11. **Haug, A., B. Larsen and O. Smidsrød.** 1966. A study of the constitution of alginic acid by partial acid hydrolysis. *Acta Chem. Scand.* **20**: 183-190.
12. **Haug, A., B. Larsen and O. Smidsrød.** 1974. Uronic acid sequence in alginate from different sources. *Carbohy. Res.* **32**: 217-225.
13. **Jarman, T.R., L. Deavin, S. Slocombe, and P.C. Righelato.** 1978. Investigation of the effect of environmental conditions on the rate of exopolysaccharide synthesis in *Azotobacter vinelandii*. *J. Gen. Microbiol.* **107**: 59-64.
14. **Larsen, B., O. Smidsrød, T. Painter and A. Haug.** 1970. Calculation of the nearest-neighbour frequencies in fragments of alginate from the yields of free monomers after partial hydrolysis. *Acta Chem. Scand.* **24**: 726-728.
15. **Larsen, B. and A. Haug.** 1971. Biosynthesis of alginate: part I, composition and structure of alginate produced by *Azotobacter vinelandii*. *Carbohy. Res.* **17**: 287-96.
16. **Montreuil, J.** 1986. *Meta*-hydroxydiphenyl-sulphuric assay, in M. F. Chaplin and J. F. Kennedy (ed.), *Carbohydrate Analysis - A Practical Approach*, p.175. IRL Press, Limited, Oxford, England.
17. **Pindar, D.F. and C. Buche.** 1975. The biosynthesis of alginic acid by *Azotobacter vinelandii*. *Biochem. J.* **152**: 617- 622.
18. **Sadoff, H.L.** 1975. Encystment and germination in *Azotobacter vinelandii*. *Bacteriol. Reviews.* **39** [4]: 516-539.
19. **Skjåæk-Bræk, G., B. Larsen, and H. Grasdalen.** 1985. The role of *O*-acetyl groups in the biosynthesis of alginate by *Azotobacter vinelandii*. *Carbohy. Res.*, **145**: 169-174.
20. **Spurrier, H.** 1921. The " why " of ageing clay, *J. Amer. Ceram. Soc.*, **4**: 113-118.
21. **Stover, E.C.,** 1902. Bacterial growth as a factor in aging clay mixtures. *Trans. Amer. Ceram. Soc.*, **4**: 183;

Figure Legends

- Figure 1 Sedimentation (in cake height volume, ± 0.1 ml) of 2vol% suspensions of AKP-30 alumina (theoretical packing volume is 0.2 ml) with kelp and bacterial alginate at various concentrations of the polymer. Kelp alginate () sedimentation columns were prepared at pH 8.5-8.6; bacterial alginate () columns at pH 7.9-8.0.
- Figure 2 Growth of *Azotobacter vinelandii* at various solids loadings of alumina inoculated with 3.4×10^3 cells/ml.
- Figure 3 Results of *in situ* processing of alumina particles by growing cultures of *Azotobacter vinelandii*. Before sedimentation columns were prepared, the pH was adjusted to the same value as the sterile control. Sterile controls contained culture medium and particles; inoculated columns contained cells, culture medium and particles and the alginate produced by the bacteria.  : Sterile control, pH = 7.68;  : Inoculated (final cell concentration = 3.2×10^7), pH=7.60;  : Sterile control, pH=8.29; and  : Inoculated (final cell concentration = 8.1×10^6), pH=8.4.

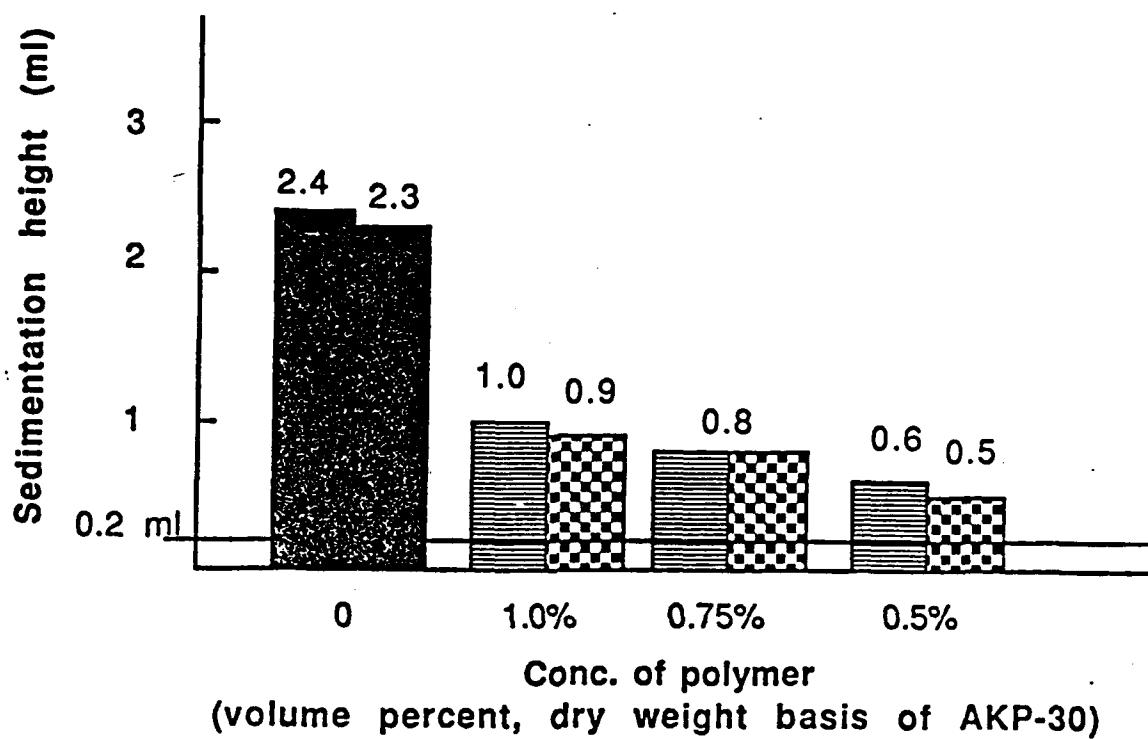


Figure 1

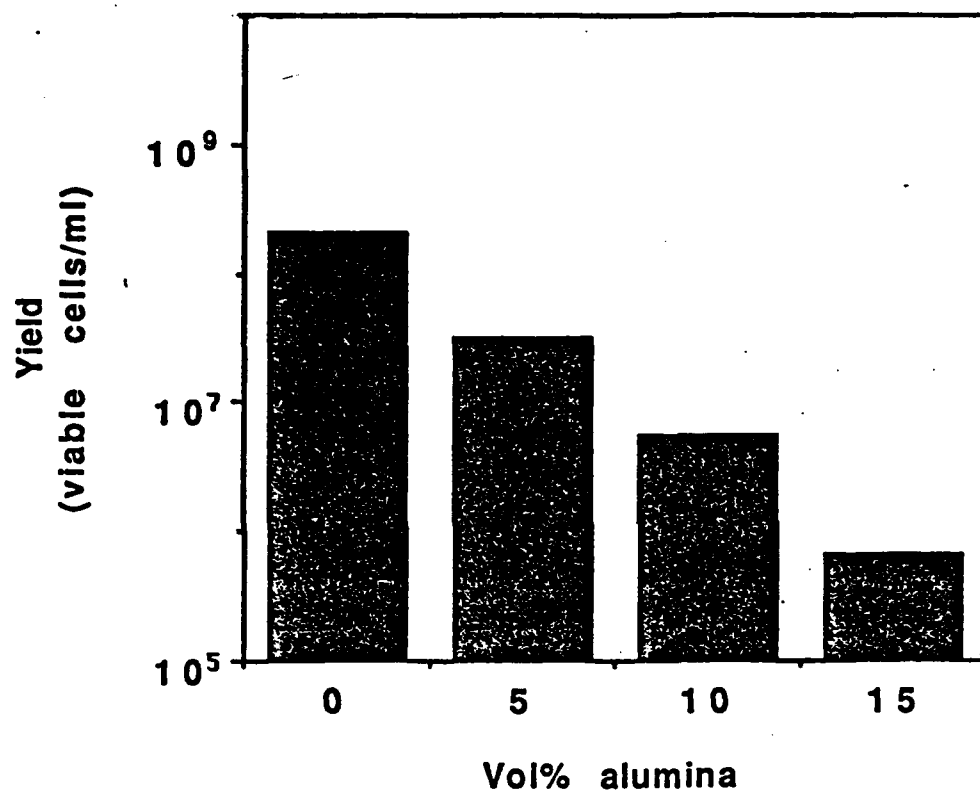


Figure 2

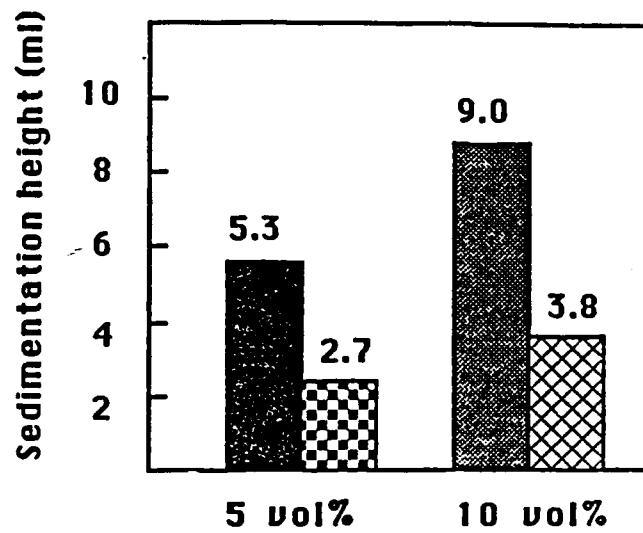


Figure 3

Table 1: Removal of *A. vinelandii* cells from alumina particles by washing

Treatments	Viable cells/ml suspended pellet
Before washing:	5.6×10^7
After washing:	
First	3.2×10^5
Second	1.3×10^3
Third	8.2×10^2
Fourth	4.8×10^2
Fifth	8.5×10

APPENDIX XXI

Growth of Aquaspirillum magnetotacticum: Magnetite Making Bacteria

by

K. Reidel,* N. B. Pellerin, and M. Sarikaya

***Student Progress Report, 1990**

AQUASPIRILLUM MAGNETOTACTICUM EXPERIMENT II

SUMMARY

The objective of the work involved with *Aquaspirillum magnetotacticum* was to produce healthy bacteria and determine the relative number of cells containing magnetosomes which could then be related to a growth curve. Two types of media were inoculated and monitored, the standard 1319 and 1319-succinate only. The standard 1319 medium produced healthy bacteria with the highest count of 4.6×10^8 cells/ml (7th day after inoculation). Osmolality, partial pressure of O_2 and CO_2 , and pH were checked for the 1319-succinate only medium. TEM samples were prepared from both of the cultures to analyze bacteria with magnetosomes. However, better preparation techniques need to be developed for fixing, staining, concentrating, and rinsing the bacteria. Relative numbers of magnetosome containing bacteria of population could not be determined.

OBJECTIVE

The purpose of Experiment II was to produce healthy *Aquaspirillum magnetotacticum* so that a growth curve could be determined. The objective was to also relate magnetosome production to the growth curve in order to determine day of best magnetosome production relative to number of bacteria containing magnetosomes.

PROCEDURE

Two test medias were prepared following the basic 1319 recipe for Magnetic Spirillum media (ATCC Media Handbook). Media #1 (1319-succinate only), however, was prepared using double the amount of

succinic acid and no tartaric acid. Neither Media #1 or Media #2 (1319) were prepared with the agar (used for semi-solid media). Mixing of media was followed by purging with N₂ gas for 10 minutes then anaerobically filling 150 ml vials which were capped with sealed rubber stoppers. The vials were then autoclaved and cooled.

Two vials of each medium were inoculated with new culture. After several days (time to allow bacteria to adjust to new medium), 1 ml of inoculum was removed from each medium, examined under the microscope, and counted for number of bacteria per ml of media. Two test samples of each type of medium (one vial was for testing and the other for a backup) were inoculated with the appropriate amount of inoculum in order to start the samples with the same amount of bacteria, approximately 2.5×10^6 cells/ml.

Starting with day 1 (day of inoculation) and ending at day 8, a 1 to 2 ml daily sample from each type of inoculated medium (1319-succinate only & 1319) was removed from the same test vial. Each sample was examined daily for appearance, reaction to a magnet, and counted for the number of bacteria cells per ml. Examination of bacteria appearance and reaction to magnet was performed with the microscope after placing a small amount of medium on a slide. Mobility, condition, and size of the bacteria was recorded as well as noting changes in direction of movement as a magnet was moved neared the slide. Counting was achieved through the use of a counting chamber following the instructions in the "Manual of Methods for General Bacteriology".

Osmolality, partial pressure of O₂ and CO₂, and pH were checked periodically during the bacteria growth for the 1319-succinate only medium. A one ml sample of the inoculum was extracted with a syringe then sent to the lab to have the osmolality checked by freezing point depression. Partial pressures and pH were checked from the same sample.

A sample for each day of the 1319-succinate only media and samples of 1319 media from day 5 thru 8 were fixed with a glutaraldehyde

preparation. Gluteraldehyde fixing was accomplished by the following method:

- 1 ml culture placed in microfuge tube
- Add 10 ul - 50% gluteraldehyde solution
- Wait 15 minutes
- Add 50 ul - 50% glut. solution
- Let sit overnight then pipet off all but a few drops

This resulted in a total gluteraldehyde fixative dilution of 3%.

Transmission Electron Microscopy (TEM) samples were prepared from the fixed samples of bacteria solution. TEM was to be used in order to determine the ratio of magnetosome containing bacteria to total number of bacteria. Fixed samples of the cultures were prepared by first centrifuging for 15 minutes at 10K R.P.M.s at a temperature of approximately 4°C. A small amount of solution was then dropped onto carbon coated copper grids and allowed to settle from 5 to 10 minutes. Excess solution was carefully blotted off with filter paper. A rinse of 1% aqueous ammonium acetate was used in the same manner as the bacteria solution.

RESULTS

The growth curves for the 1319-succinate only and 1319 media samples are shown graphically in Figure 1. The data for these graphs can be found in table 1. The 1319 culture produced a much higher growth curve (reaching a count of 4.6×10^8 by the seventh day) than the 1319-succinate only media.

Osmolality for the 1319-succinate only media remained about 35 mOsm/kg. Partial pressure for this same media indicated that the percent O_2 increased slightly (5.3% to 7.0%) from the 2nd to the 4th day while the CO_2 dropped from 2.0% to 1.6% for the same time period. The pH of this media changed very slightly from 6.61 to 6.63.

The results of the TEM samples that were analyzed can be seen in the micrographs found in Figures 2 thru 5.

DISCUSSION

Keeping the main objective of this experiment in mind, producing many healthy *Aquaspirillum magnetotacticum* with maximum magnetosome inclusions, two media were chosen to culture the bacteria in. The standard 1319 media has been proven to grow healthy bacteria. The 1319-succinate only medium was chosen because of reported data on medium with succinate as the sole carbon source producing larger numbers of magnetotactic cells (Blakemore). It was also known from this same literature that tartrate as the only carbon source would produce greater numbers of bacteria, but with a smaller ratio being magnetotactic cells (1319 medium contains both tartrate and succinate). The growth curves from this experiment clearly show a greater number of bacteria produced with the 1319 medium. A high count of 4.6×10^8 cells/ml for 1319 was achieved as compared to a maximum count of 1.3×10^7 for the 1319-succinate only.

Just prior to inoculating the test media, samples of the two cultures were microscopically examined. The 1319-succinate only culture contained very healthy, mobile, and uniform sized bacteria. Most of the bacteria reacted to the movement of a magnet held close to the slide sample. The 1319 culture contained some unhealthy bacteria yet many were mobile and only a few reacted to the magnet. Because of the promising initial condition of the 1319-succinate only bacteria, emphasis was placed on this culture during the testing.

Throughout the experiment the condition of the bacteria continued to change. The 1319-succinate only remained healthy over-all in appearance, though the number of noticeable unhealthy bacteria did increase slightly. Mobility of the bacteria decreased from that initially observed. Reaction to the magnet also decreased and the uniform size of the bacteria became more varied. The 1319 bacteria size variation was constant during the experiment as well as the limited reaction to the magnet. The healthy appearance of these bacteria decreased during the first three days then appeared to increase along with the mobility for the

rest of the test. The change in health and mobility of the 1319 bacteria correlated well with their respective growth curve.

Osmolality, pH and partial pressure of O_2 and CO_2 were monitored for the 1319-succinate only on the days indicated in Table 1. *Aquaspirillum magnetotacticum* are dependent on the condition of their growth medium. To optimize growing conditions and to fix bacteria and maintain the structure of the membranes, the osmolality of the media must match that of the bacteria. Osmolality of the fixative solution (gluteraldehyde) is reported to be about 600-800 mOsm/kg, that of the growth medium at 300-500 mOsm/kg, and large cells have been measured (internal) at 1300 mOsm/kg (Dennis Kunkel). The large difference between the osmolality of the medium (35 mOsm/kg) and that of the fixative and probable internal cell would possibly cause distortions in the membranes of the bacteria even before fixation. Questions are raised on the effect of the seemingly low osmolality of the inoculated medium. The results indicate that further testing would be beneficial in determining optimum osmolality conditions. Suggested additional work would include increasing the nutrient concentrations (increasing osmolality and possible cell growth) or KH_2PO_4 concentration, or adding a non-metabolized compound such as agar to increase osmolality.

The pH of the culture remained basically the same (6.61 & 6.63) as was expected from previous work. Monitoring the pH was used as an indication of a change or reaction in chemical activity of the bacteria in response to the media. A medium may be suitable for the initiation of growth, but as the bacteria population increases, chemical changes can take place from the growth and metabolism of the organisms. Thus it was determined that the medium and bacteria pH were compatible through the 4th day of growth.

The partial pressure of O_2 and CO_2 was also checked on the 2nd and 4th day after inoculation. Monitoring the percent O_2 allows some understanding of the growth conditions of the bacteria. *Aquaspirillum magnetotacticum* are obligate anaerobes. If vials of culture are allowed free exchange with air, the bacteria will not grow to significant numbers. The highest counts can be obtained when the initial O_2 concentration is 12

or 21%. However, if the bacteria start out with a O_2 concentration greater than 6%, magnetic cells would not be produced during growth. Also, if initial O_2 concentration is 1 to 3%, cells will grow with the shortest lag time (Blakemore). On the 2nd day of inoculation, O_2 was 5.3%. This correlated with the large number of bacteria that reacted with the magnet. By the 4th day the O_2 had increased to 7.0%. A sufficiently low enough amount to support continued growth of the obligate anaerobes. The growth curve dropped at this point, but continued on with an increase till the 7th day. Possibly the increasing O_2 concentration attributed to the decreasing number of bacteria reacting to the magnet. Further studies in this respect would be beneficial toward producing high counts of bacteria and magnetosome containing cells.

Autotrophic bacteria require between 1 to 5% of CO_2 in the media (Stanier). The percent CO_2 dropped from 2% (2nd day) to 1.6% (4th day). Sufficient amount of CO_2 was present to sustain growth up to the 4th day. Since the growth curve increased from the 4th to the 7th day, the concentration of CO_2 was not a limiting factor to cell production up to this time period.

TEM samples were not adequately prepared to give results of the relative number of magnetosome containing cells. Examining the four micrographs shows distorted bacteria with little structure definition and excess debris present. It was difficult to even find enough bacteria on the grids to analyze. Techniques need to be developed to fix the cells so that the structure is preserved, to properly rinse the grids to remove impurities, and to concentrate the bacteria to increase the number of cells for analyzing.

CONCLUSION

In conclusion, it has been determined that healthy bacteria can grow using the 1319 as well as the 1319-succinate only media. However, greater numbers of bacteria are grown in the 1319 media. The relative number of magnetosome containing bacteria could not be determined using the present techniques for fixing and preparing TEM grids. Work needs to be done on improving preservation of the cells. It is also

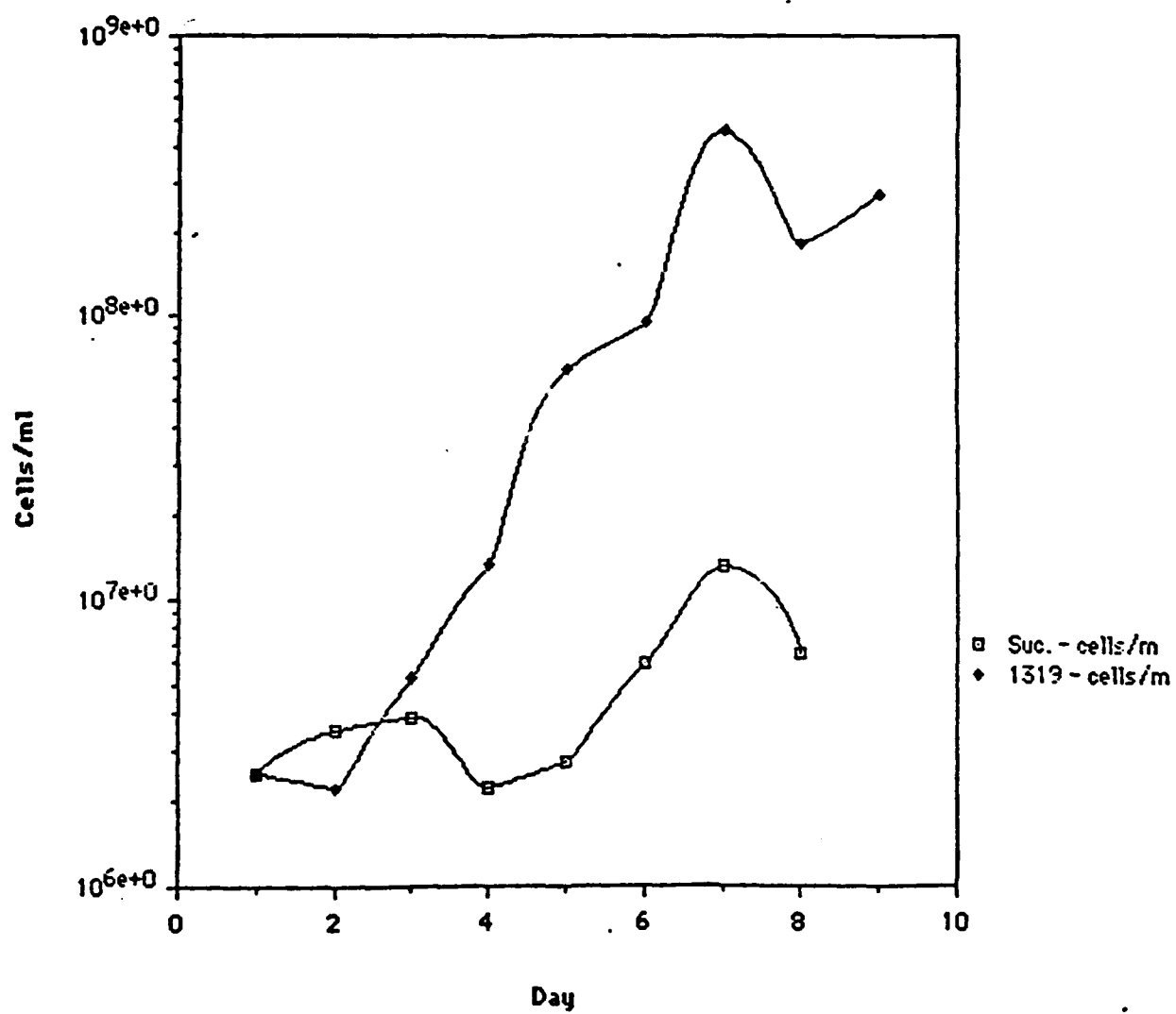


Figure 8. Growth curve for *Aquaspirillum magnetotacticum* in media 1319 and media 1319 with succinate.

suggested that further study be done on the osmolality condition of the media in relation to the bacteria.

REFERENCES:

1. Blakemore, R.P., D. Maratea, and R. S. Wolfe. 1979. *Isolation and Pure Culture of a Freshwater Magnetic Spirillum in Chemically Defined Medium* Journal of Bacteriology, Vol. 140, No. 5: 720-729.
2. Cote, R., Editor, 1984. ATCC Media Handbook, 1st Ed. American Type Culture Collection, Maryland.
3. Stanier, Roger Y., Michael Doudoroff, and Edward A. Adelberg. 1970. The Microbial World. Prentice-Hall, Inc., New Jersey.

TABLE 1

DATA COLLECTED FROM EXPERIMENT II

DAY	COUNT #1	COUNT #2	OSMOLALITY	PARTIAL PRESSURE		
	1319-Suc. only x 10 ⁶ cells/ml	1319 x 10 ⁶ cells/ml		1319- Suc. only % O ₂	% CO ₂	pH
1	2.5	2.5	35			
2	3.5	2.2	35	5.3	2.0	6.61
3	3.9	5.3	32			
4	2.2	13.2	35*	7.0	1.6	6.63
5	2.7	64.0				
6	5.9	94.0				
7	13.0	460.0				
8	6.4	180.0				
9		270.0				

* Osmolality also checked for buffer used in preparing 50% gluteraidehyde solution (188 mOsm/kg)

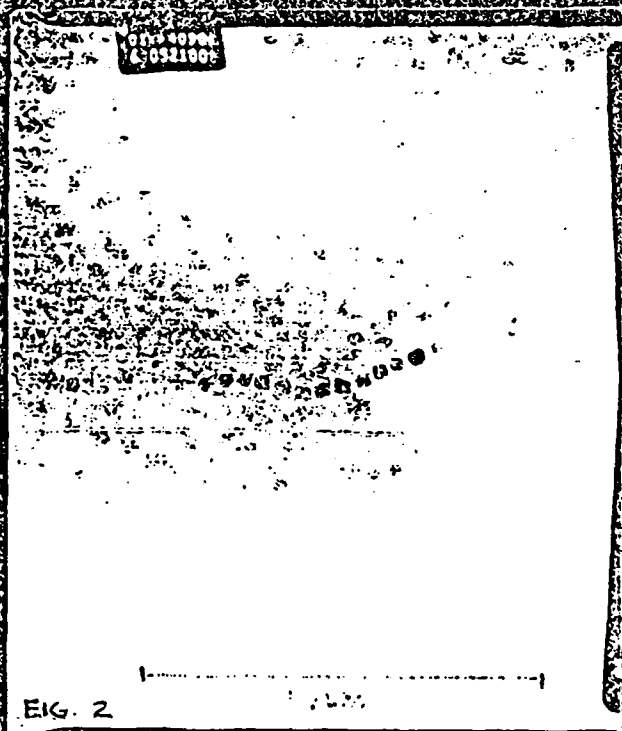


FIG. 2

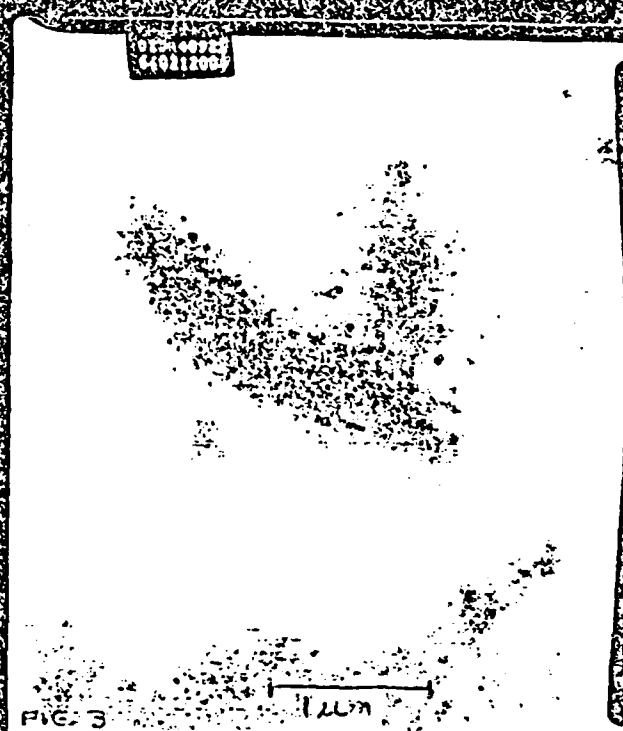


FIG. 3



FIG. 4

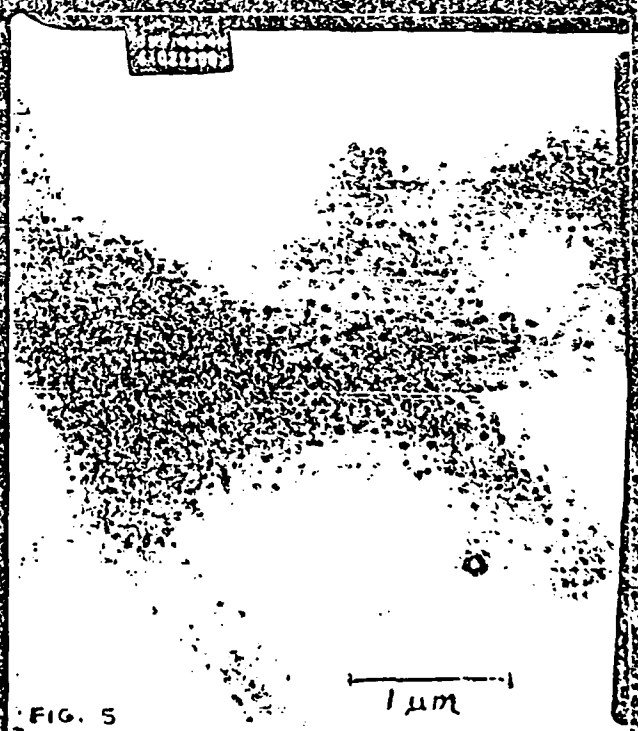


FIG. 5

AQUASPIRILLUM MAGNETOTACTICUM
EXPERIMENT III
MAGNETOSOMES

Department of Materials Science
Senior Project

AQUASPIRILLUM MAGNETOTACTICUM
EXPERIMENT III
MAGNETOSOMES

OBJECTIVE

The purpose of Experiment III was to grow healthy *Aquaspirillum magnetotacticum* bacteria in 1319 medium in which pyruvic acid had been added. Growth was monitored over an adequate period of time (6 days) to determine optimum growth period. Comparison of growth curves were made with previous experiments in order to determine most successful medium for preparing cultures in. Magnetosome production for the bacteria was to be examined in order to determine highest yield relative to day of growth curve.

PROCEDURE

Test medium was prepared with the following recipe:

Magnetic Spirillum Growth Medium 1319 with Pyruvate -

Double Dist. water	900.0 ml
Wolfe's Vitamins	10.0 ml
Wolfe's Minerals	5.0 ml
0.01 M Ferric Quinate	2.0 ml
0.1% Resazurin	0.45 ml
KH ₂ PO ₄	0.63 g
NaNO ₃	0.34 g
Ascorbic acid	35.0 mg
Tartaric acid	0.37 g
Succinic acid	0.37 g
Sodium acetate	0.05 g

Add components while stirring then adjust pH to 6.75 with NaOH.
Autoclave 15 minutes at 121 °c. Cool to approximately 50 °c and

add aseptically the following filter-sterilized solution:

Pyruvic acid	0.4 g
Distilled water	100.0 ml

Aseptically fill containers to the rim with sterile medium and screw cap tightly. Inoculate heavily (~ 2.0 ml - 140 ml bottles) leaving no headspace of air.

Tubes of culture were aseptically filled using a Laminar flow hood. Medium was placed in 20 (15ml) tubes and 4 (140ml) bottles, filled completely (to allow as little of air space as possible), then sealed with screw caps.

Inoculum for Experiment III was prepared from frozen concentrated bacteria. Frozen bacteria is held in -80°C freezer then thawed in 30°C H₂O. Thawed culture was added to one 15 ml tube (from which some of medium is removed) and topped off with fresh medium to remove head space. Inoculated tube was stored in 30°C incubator.

Transfer of inoculated culture into four 15ml tubes (approximately 1ml of culture per medium tube) was performed three days after initial inoculation of first 15ml tube. Again samples were topped off to prevent air space and stored in incubator. The remaining inoculated culture was frozen to preserve for future supply.

To preserve the culture, 0.9ml of culture was placed into sterile microfuge tubes to which 0.1 ml of DMSO (prevents damage to bacteria from crystal formation during freezing) was added. Samples were then placed in -20°C freezer for 0.5 to 1 hour then removed and placed in -80°C freezer for storage.

A second transfer was performed again four days after first transfer to ensure adjustment of bacteria to medium. The best of the inoculated cultures from the first four 15ml transfer tubes was chosen to use in transfer to four more uncultured tubes (one tube was discarded because of poor turbidity indicating inadequate growth). Procedure followed was as

previously described. Remaining culture (2 tubes not used in transfer and remaining culture from transfer tube) was again frozen for future use.

To begin experimental work on growth of bacteria, five days after second transfer, culture from best samples was transferred into two 140ml bottles (Test Sample #1 - experiment & Test Sample #2 - backup). Removal of 20mls of uninoculated medium from 140ml bottles was followed with the addition of 17mls of culture and topped off with sterile medium. A small amount of culture was saved from the transfer tubes in order to determine beginning culture count of experimental colonies (the 140ml bottles). Counting was achieved through the use of a counting chamber following the instructions in the "Manual of Methods for General Bacteriology" (Calculations in Appendix). Day 1 in the experimental results refers to the count at this beginning bacteria population.

A small amount of culture for each day of growth (Day 1-6) was removed from Test Sample #1 in order to count the cells/ml, examine condition of bacteria, and prepare TEM grids for examination of magnetosomes.

Transmission Electron Microscopy (TEM) samples were prepared from the fixed samples of bacteria culture. Fixing and concentrating samples was done as follows:

- Placed 1ml culture in microfuge tube
- Added 10 ul of 50% Gluteraldehyde and waited 15 minutes
- Added 50 ul of 50% Gluteraldehyde and let sit 2 hours
- Microfuged culture and fixative for 1 minute
- Pipeted off top 2/3 of liquid
- Added 1 ml buffer (pH 7.4) *
- Microfuged culture, fixative, and buffer mix for 1 minute
- Pipeted off top 2/3 of mix

*Buffer

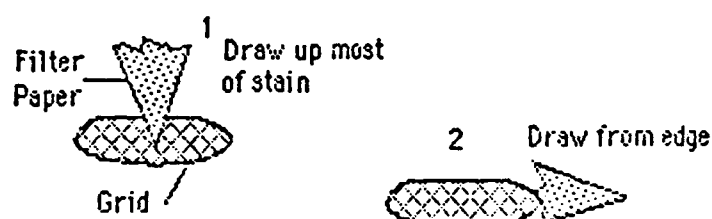
NaCl	.75 g	Na ₂ HPO ₄	.115 g or
KCl	.02 g	Na ₂ HPO ₄ - 7H ₂ O	.217 g
KH ₂ PO ₄	.02 g		

Added double distilled water to 150 ml.

The TEM samples were prepared using carbon-coated copper grids. Two grids were prepared for each day of growth (except day 1, one grid only) during the six day growth period. A small drop of concentrated culture was placed on the grids and allowed to sit for 20-30 minutes after which excess culture was removed with filter paper. Staining was done with 2% aqueous ammonium molybdate:

2% Aqueous Ammonium Molybdate -

- Small drop of stain was applied to grid
- Waited 30 - 60 seconds
- Withdrew stain with filter paper as illustrated
- Allowed grid to dry



Examining the daily TEM preparations under the light microscope, Day 3 samples were seen to contain excess crystallized material. Therefore, Day 4 grids were prepared with one unstained and the other stained. Day 6 samples were also prepared with and without stain, however, the unstained grid was also rinsed with syringe filtered distilled water instead of buffer.

For six consecutive days, daily samples of the bacteria culture of *Aquaspirillum magnetotacticum* were counted to monitor growth, examined for appearance, and fixed and prepared for TEM work.

RESULTS AND DISCUSSION

The graphical results for the growth curves of the Pre-Experiment, and Experiment II & III can be seen on the following page. The main comparison

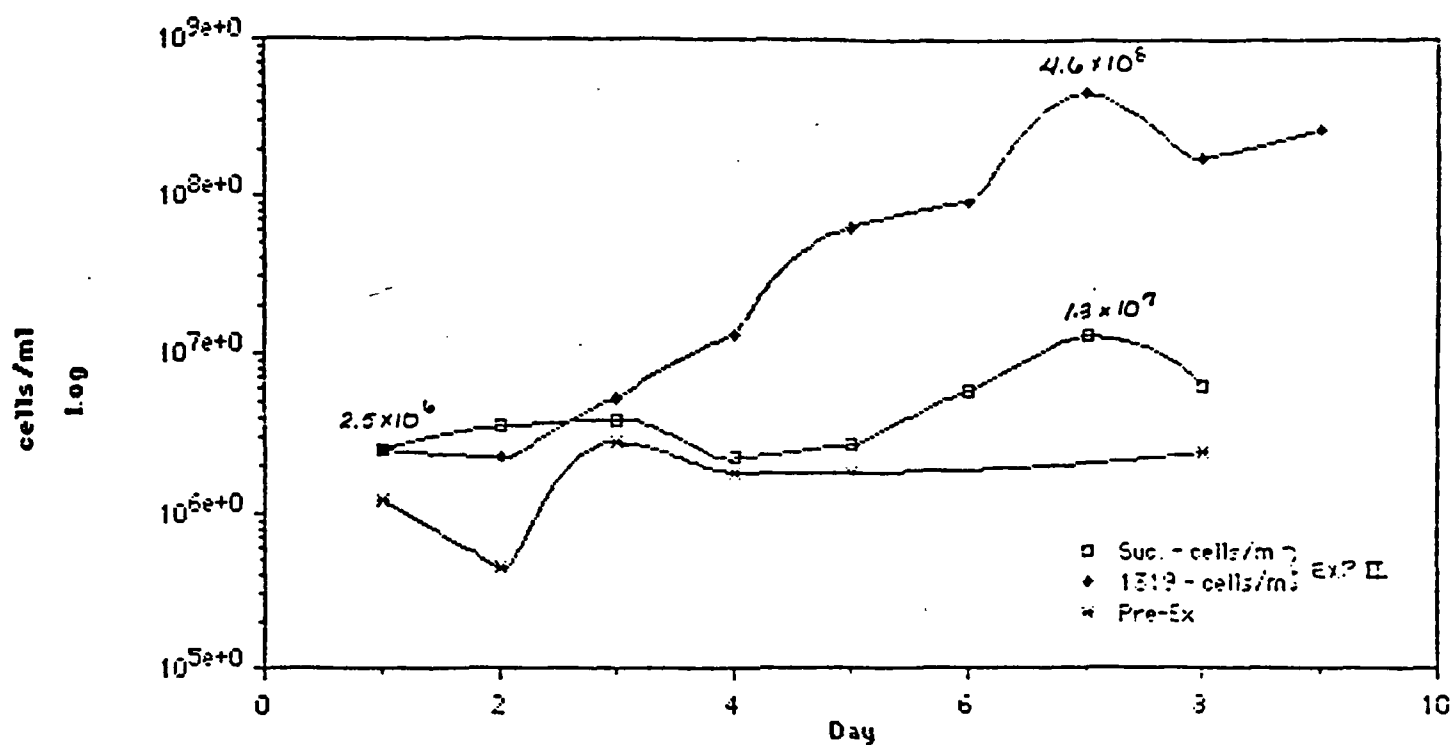


FIGURE 1 GROWTH CURVE EXPERIMENT II AND PRE-EX

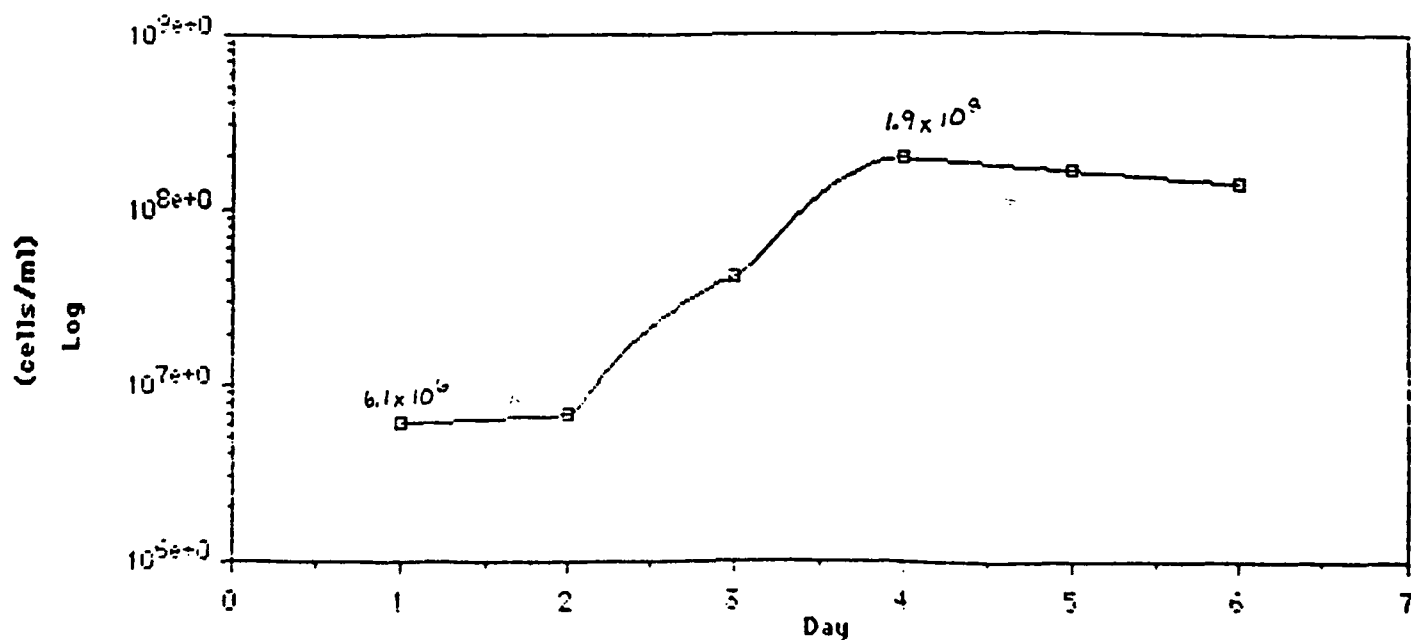


FIGURE 2: GROWTH CURVE EXPERIMENT III
1312 W/ PYRUVIC ACID

to be made is between that of the 1319 medium (refer to *Aquaspirillum Magnetotacticum* Experiment II) and 1319 with pyruvic acid (Exp. III). Both of these media produced healthy bacteria and exhibited good results in the growth curves. The change in count over the growth period for Exp. II (4.6×10^8) was slightly more than that of Exp. III (1.8×10^8). However, Exp. III reached maximum growth in four days as compared to 7 days for Exp. II. From previously published works on *Aquaspirillum magnetotacticum*, the bacteria generally show exponential growth. The differences in the time it took the bacteria to reach maximum growth for the two medias could be attributed to the fact that Exp. III culture was inoculated at an initially higher cell count, further into the exponential growth. The overall result of using the 1319 with pyruvic acid media showed similar maximum cell counts to that of published data.

Examining daily the culture (Exp. III) under the light microscope showed healthy and very mobile bacteria until Day 5 when mobility decreased through Day 6. This corresponded to the decline in cell count.

The real significance of using the 1319 with pyruvic acid medium in Exp. III can be seen in the TEM results. If a comparison of the micrographs from Exp. II is made with those of Exp. III it can be seen that the 1319 with pyruvic acid medium produced bacteria with more magnetosomes, longer chains of magnetosomes as well as some double chain magnetosomes. Experimental results indicate that this medium with the added pyruvate was beneficial to the production of magnetosomes.

One of the main objectives in completing Exp. III was to determine the number of magnetosomes relative to the day in growth curve. It was planned that the TEM work would produce micrographs from which the number of magnetosomes per bacteria could be determined. However, it was evident upon examining the bacteria with the TEM that it would not be possible to make the counts. Many of the bacteria were over-laying each other and thus were difficult to individually identify. The number of micrographs of the bacteria needed to give significant or credible counts were also not possible. Results from examining grids from Day 3, 5, & 6, showed an increase in magnetosomes relative to previous experimental work

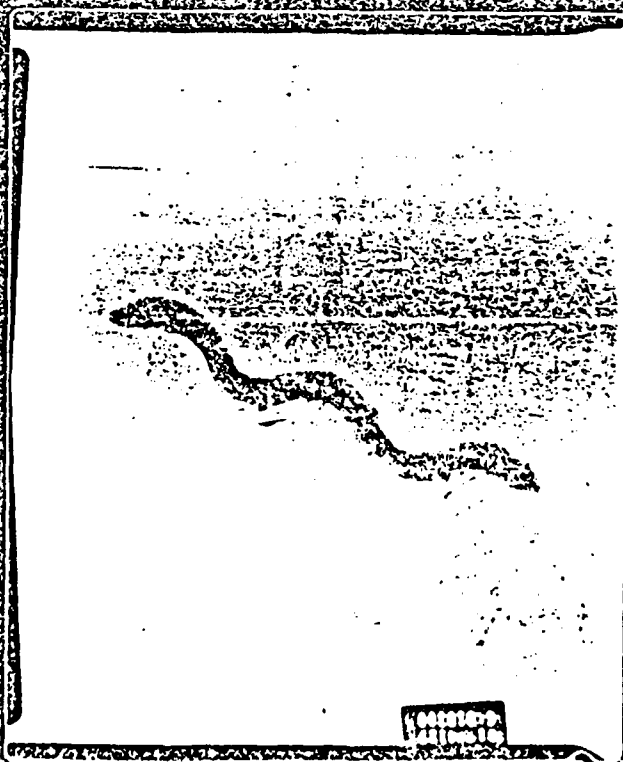
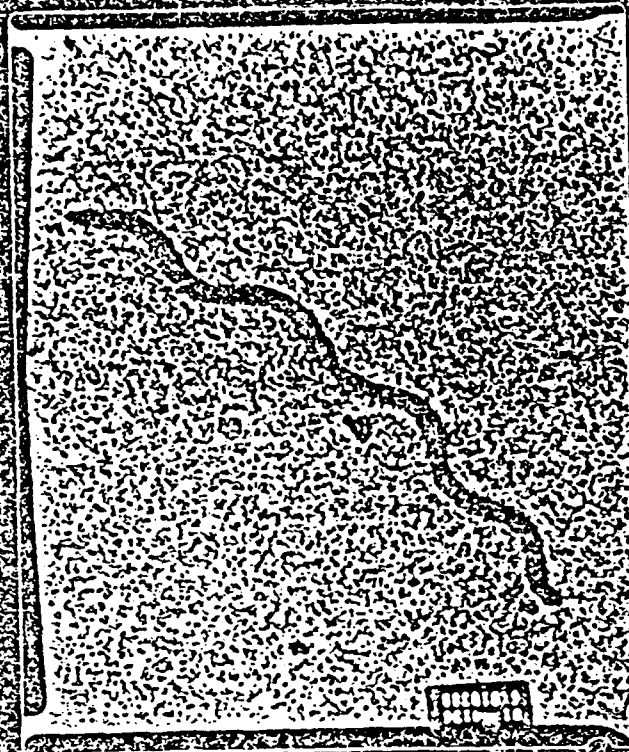
done so far during this project. Day 5 & 6 micrographs show more bacteria and magnetosomes than Day 3. From the limited data available (Day 1,2,& 4 were not viewed with the TEM) it is presumed that the days of best magnetosome production occurred during Day 5 & 6.

CONCLUSIONS

In conclusion, it has been determined that the 1319 with pyruvic acid medium produces healthy and mobile bacteria with counts that correlate with published data. The advantage of using this medium over the 1319 medium of Exp. II is that the magnetosome production appears to be increased as well as the lengths of some of the chains, with double chains also noted. Bacteria with the highest yield of magnetosomes appear during the 5th and 6th day of the growth curve (from the data analyzed).

REFERENCES:

1. Blakemore, R.P., D. Maratea, and R. S. Wolfe. 1979. *Isolation and Pure Culture of a Freshwater Magnetic Spirillum in Chemically Defined Medium* Journal of Bacteriology, Vol. 140, No. 5: 720-729.
2. Cote, R., Editor, 1984. ATCC Media Handbook, 1st Ed. American Type Culture Collection, Maryland.



APPENDIX XXII

Sample Preparation and Cutting for TEM

by

J. M. Lee*, N. B. Pellerin, K. E. Gunnison, and M. Sarikaya

***Student Senior Thesis Project**

May 10, 1991

SAMPLE PREPARATION AND CUTTING FOR TEM

**SENIOR PROJECT
(WINTER QUARTER 1991)**

SUPERVISOR : DR. SARIKAYA

**MYUNG JIN LEE
MAY 10TH 1991**

Previously, the bacteria samples were prepared in filter .
However, because of its sensitivity, the bacterias are observed as exploded condition under TEM. Therefore, new method of preparing bacteria for TEM was necessary.

PREPARATION OF *AQUASPIRILLUM MAGNETOTACTICUM* FOR THIN SECTIONING

1. One week old broth culture, forms look good, healthy, respond to magnet. added 2 - 1 ml aliquots of 25% gluteraldehyde directly to the culture, 15 minutes apart. Stored at 4C over weekend.
2. Prep looked pretty good under microscope (,10% of the cells look lysed). Spun 20 min, 3000 rpm in IEC tabletop centrifuge. Decanted.
Resuspended pellet in 2ml of 0.1 M cacocylate, plus 20 ul 1 M MgCl₂ and 0.3 ml of 25% gluteraldehyde. 4 C, 4 hr.
Rinsed twice by spinning 20 min., decanted and resuspended in 2 ml 0.1 M Na caco.
Stained by suspending in 1 ml 0.1 M Na caco with 1% osmium tetroxide, 4C. overnight.
3. Spun and rinsed 2 x in 0.1 M Na caco. Embedded in 2% noble agar, cut blocks and placed them in 1 ml 0.1 M caco., 1% osmium tetroxide for 10 min to stain agar.
Rinsed 3 x in 0.1 M Na caco.
Dehydration series in cold ethanol:

35%	10 min
50	10
70	overnight, 4C
4.

95	10, brought to room temperature
100	5
100	5

Embedding (all at room temp)

	100% propylene oxide	10 min
	3 prop: 1 Medcast resin	6 hr
	1 prop: 1 resin	24 hr
5.	1 prop: 3 resin	
6.	100 % resin, left uncapped	
7.	100 % resin with accelerator, 2 hr	
	Into oven	24 hr.

Two samples were treated in same course as shown above, then formed and placed in oven as different shapes.

Sample I : After the last 100% resin treatment, the sample and old resin were poured into an small aluminium container.

Sample II : After the last resin treatment, pour new resin into triangle shape form. Then removed a piece of sample from the chemical treatment and place it into the form.

Samples were placed in oven for 24 hours and then cutted into pieces with diamond glider. Best piece were chosen and glued on top of a capsule. Then the samples were cutted with glass knives.

Sample 2 shows fairly good cutting condition as long as the cutting work is held in no vibrated, quiet room. Sample I seems to get clean cut up to half part of surface, but get wavy shape on rest of part. Same results were obtained with a diamond knife.

The major factors that determine the quality of sections are the cutting edge of the knife, the knife angle, the cutting speed the

embedding material, the face of the specimen block, and the fluid in the collecting trough. Even the addition of electrolytes or nonelectrolytes to a buffer may affect the cutting properties of an embedding medium. There would be several sources of causes for sample 1 result. However, most possible two sources are old resin and agar in this case. The resin of sample 1 wasn't fresh. When old resin absorbed into the bacteria, it caused hard and brittle condition of sample and make the knife become dull more faster than normal condition. Also when agar placed in the resin, the resin should be filtrate into the agar evenly. However, the old resin doesn't absorbed evenly, and it caused different hardness of the sample.

ANALYSIS

The embedding material was main cause of the problem in this case. However, as mentioned previously, there are many factors that determine the quality of sections. The knife edge need to cut ultrathin sections must be adequately sharp and hard. Also, success in obtaining ultrathin sections of good quality depends partly on the speed of cutting. As a general rule, sectioning should be performed with a relatively slow speed. Each time the cutting edge of a knife moves through the embedded material, the resulting vibrations distort the elastic system of the microtome and specimen block. If the cutting speed is too high, the vibrations will overlap, resulting in variations in section thickness. Too high a cutting speed may also cause wrinkles and fine chatter parallel to the cutting edge in the sections, since when cut at high speeds, plastic tend to fracture as they are deflected by the cutting edge. A very slow cutting speed is also undesirable because changes in temperature and draft during a cycle will cause thermal drift. In our experiment, when we cut bacteria with medicast resin, 0.3-0.5 mm/sec is seemed recommendable.

Other main source of problem is section flotation. It is primary related to the shape of the meniscus of the flotation fluid. In general, a convex meniscus tends to over-wet the cutting edge, resulting in the wetting of the face of the specimen block. When this happens, the back of the knife facet also picks up some flotation fluid. Under these conditions, it is impossible to obtain

sections. On the other hand, a concave meniscus may not wet the knife facet to the very end, which results in the sections being stuck to the knife and their crumpling. Therefore, the optimal wetting of the knife is achieved when the meniscus is almost flat, provided the knife angle is neither acute nor obtuse to an appreciable degree.

In order to obtain electron micrographs of good quality, it is imperative that sections be kept free from every possible type of contamination. A section can pick up contamination from the moment it is cut until the time it is micrographed. The sources of contamination are varied. Two most common sources are follow;

Dirt - the possible sources of this kind of contamination include the knife edge, the floatation fluid, the grids, the grid container, the trough and atmosphere. It is obvious that to avoid or at least lessen this type of contamination, certain precautionary measures are necessary. Most of these source can be minimize by cleaning before using.

Oil Films - the sources of grease or oil film contamination are also varied but mostly from the floatation fluid, the knife face, the grid and its container, the trough, the fingers and the wax applicator. It is advisable to clean with acetone before use them.

With developed sample preparation, and precaution of above problems, the sample sections for TEM would have better result.

APPENDIX XXIII

*Structure-Mechanical Property Relationships in a
Biological Ceramic-Polymer Composite: Nacre*

by

K. E. Gunnison

M. S. Thesis
University of Washington
June 14, 1991

GRADUATE STUDENT THESES*

* Only the abstract pages and the list of contents are included. The complete copies of the theses can be obtained upon request to one of the principal investigators.

Structure-Mechanical Property Relationships in a Biological
Ceramic-Polymer Composite: Nacre

by

Katie Emaline Gunnison

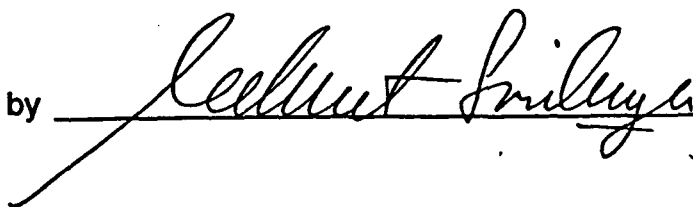
A thesis submitted in partial fulfillment
of the requirements for the degree of

Master of Science in Materials Science and Engineering

University of Washington

1991

Approved by



Program Authorized
to Offer Degree

Materials Science and Engineering

Date

June 14, 1991

University of Washington

Abstract

Structure-Mechanical Property Relationships in a Biological
Ceramic-Polymer Composite: Nacre

by Katie Emaline Gunnison

Chairperson of the Supervisory Committee: Professor Mehmet Sarikaya
Department of Materials
Science and Engineering

The objective of this work was to study nacre, a biological ceramic-polymer composite, to determine structure-property relationships. Nacre is a naturally occurring laminated composite found in mollusk shells. The structure contains calcium carbonate crystals in the form of aragonite and an organic matrix material. The mechanical properties of nacre are better than those of monolithic calcium carbonate which makes up 95-98% of the composite. The highly ordered micro-architecture incorporating thin films (100 Å thick) of organic matrix makes nacre both a tough and a strong composite. The engineering significance of the nacre structure has been noted by biologists and zoologists and, although some models have been proposed, the structure property relationships have not been fully understood. Therefore, this study was undertaken (i) to evaluate the mechanical properties with respect to the micro-architecture and (ii) to better understand the structure of the organic matrix and its morphological relationship with the inorganic component.

In this work 4-point bending strength and 3-point bend fracture toughness tests were performed and the results averaged 180 MPa and 7 MPa-m^{1/2}, respectively. Fractographic studies with SEM identified two significant toughening mechanisms; (i) ligament formation in the organic matrix and, (ii) sliding of the aragonite platelets upon each other. The unique 'brick and mortar' microstructure of the nacre allows for high energy absorption, damage tolerance, and the prevention of catastrophic failure.

The structure of the organic matrix was studied in ultramicrotomed sections with and without the aragonite platelets intact. We found that the organic matrix is indeed a multilayered laminated composite at the nanometer level, but thinner than previously thought. The morphology of the interface between the organic and the inorganic regions suggests the presence of an "interphase" region. This and the laminated structure of the organic matrix would explain the mechanical properties of the organic matrix and the overall stability of the composite.

In presenting this thesis in partial fulfillment of the requirements for a Master's degree at the University of Washington, I agree that the Library shall make its copies freely available for inspection. I further agree that extensive copying of this thesis is allowable only for scholarly purposes, consistent with "fair use" as prescribed in the U.S. Copyright Law. Any other reproduction for any purpose or by any means shall not be allowed without my written permission.

Signature Kate Munro

Date June 14, 1991

TABLE OF CONTENTS

	<i>Page</i>
1.0 Introduction	1
2.0 Background	3
2.1 Mollusk Shell Research	3
2.1.1 Shell Structures	4
2.1.2 Shell Mechanical Properties	8
2.1.2.1 Strength	8
2.1.2.2 Toughness	10
2.1.2.3 Modulus of Elasticity	11
2.1.2.4 Hardness	12
2.1.2.5 Organic Matrix Effects	12
2.1.3 Structure of the Organic Matrix	15
2.1.3.1 Crystal Growth Mechanism	15
2.1.3.2 Organic Matrix Composition and Crystallography	17
2.2 Electron Microscopy	23
2.2.1 Sample Preparation	24
2.2.2 Electron Microscopy Induced Damage	27
2.3 Remaining Problems	32
2.4 Research Objectives	33
3.0 Experimental Procedure	35
3.1 Mechanical Testing	35
3.2 Sample Preparation for Electron Microscopy	38
3.2.1 Ion Beam Milling	38
3.2.2 Microtoming	40
3.2.3 Organic Matrix Preservation	45
3.2.4 SEM Sample Preparation	49
3.3 Electron Microscopy	49
4.0 Results and Discussion	50
4.1 Mechanical Property-Structure Correlations	50
4.1.1 Mechanical Testing Results	50
4.1.2 Toughening Mechanisms	53
4.1.3 Strengthening Mechanisms	66
4.2 Transmission Electron Microscopy	68
4.2.1 Structure of the Organic Phase	68
4.2.2 Structure of the Inorganic Phase	71
5.0 Summary and Conclusions	80
6.0 Current Status and Future Directions	82
7.0 References	84

LIST OF FIGURES

<i>Number</i>		<i>Page</i>
1.	Diagram of Shell Structures	5
2.	Diagram of Proposed Organic Crystallography	21
3.	<i>Haliotis</i> and <i>Pinctada</i>	36
4.	Diagram of Mechanical Testing Orientation	37
5.	Diagram of Platelet Orientation in Microhardness Testing	39
6.	Diagram of Collodion Grid Preparation	42
7.	Diagram of Gelatin Capsule Preparation	43
8.	Diagram of Microtome Block Preparation	44
9.	TEM Image of Microtomed Thin Section	47
10.	Diagram of Staining Procedure	48
11.	SEM Image of Thick Organic Layer	51
12.	Graph of Mechanical Properties	52
13.	SEM Image of Fracture Surface of Nacre	55
14.	SEM Image of Microhardness Indentation Oblique to the Platelets	56
15.	SEM Image of Microhardness Indentation Parallel to the Platelets	57
16.	Diagram of Possible Indentation Load Dissipation	59
17.	SEM Image of Crack Tortuosity	61
18.	SEM Image of Platelet Sliding During Deformation	62
19.	SEM Image of Ligaments Parallel to the Platelets	63
20.	SEM Image of Ligaments Perpendicular to the Platelets	65
21.	TEM Image of Organic Matrix	69
22.	TEM Image of Over-Stained Organic Matrix	70
23.	TEM Image of Lead Citrate Stained Thin Section	72
24.	TEM Image of Microtomed Organic-Inorganic Interface	73
25.	TEM Image of Interphase Region	74
26.	TEM Image of Ion Beam Milled Thin Section	75
27.	Diagram of Proposed Interphase Region	77
28.	TEM Image of Gold Stained Section	78

ACKNOWLEDGMENTS

I would like to thank Dr. Mehmet Sarikaya for his invaluable assistance and enthusiasm during this research. I would also like to thank Dr. Ilhan Aksay for his guidance and support. I gratefully acknowledge G. H. Kim for his never ending patience and interest and Dr. Dennis Kunkel for patiently teaching me the skills of microtoming. I also gratefully acknowledge Dr. Jun Liu for his patience and guidance on the electron microscope and for hours of intriguing discussions.

I would like to thank AFOSR for supplying the financial support necessary for this work. Finally I would like to thank all of my friends and family for their support and understanding.

APPENDIX XXIV

Processing of Ceramic Suspensions with Biologically Produced Polymers

by

G. L. Graff

M. S. Thesis
University of Washington
June 14, 1991

**COLLOIDAL PROCESSING OF CERAMIC SUSPENSIONS WITH
BIOLOGICALLY PRODUCED POLYMERS**

by

Gordon L. Graff

**A thesis submitted in partial fulfillment
of the requirements for the degree of**

**Master of Science in
Materials Science and Engineering**

University of Washington

1991

Approved by _____
(Chairperson of Supervisory Committee)

Program Authorized
to Offer Degree: **Materials Science and Engineering**

Date: **March 22, 1991**

University of Washington

Abstract

Processing of Ceramic Suspensions with Biologically Produced Polymers

by Gordon L. Graff

Chairperson of the Supervisory Committee: Professor Ilhan A. Aksay

Department of Materials Science and Engineering

The primary objectives of this research were, first, to determine whether a biologically produced macromolecule could be found that would compare favorably to the best synthetic polymers as a suspension stabilizer. If such a molecule was located, our second goal was then to determine the stability mechanisms operative in the system. The specific molecules we tested were the polysaccharides dextran, dextran sulfate, alginate, polyguluronic acid, and polymannuronic acid.

Detailed studies on the solution and rheological behavior of dextran sulfate and polyguluronic acid have conclusively shown that these molecules function as polymeric stabilizers in aqueous α - Al_2O_3 suspensions. By optimization of the polyguluronic acid - Al_2O_3 system, we prepared low viscosity (110 mPa·s at a shear rate of 9.3 s^{-1}), stable suspensions with solids loadings of 50 vol%. This rivals values obtained using the best synthetic polyelectrolyte dispersants.

We have also determined that electrostatic stabilization resulting from highly charged electric double layers is the dominant stability mechanism operative in the systems tested. High affinity adsorption of the anionic polyelectrolytes creates a

sufficient repulsive surface charge on the individual particles to provide suspension stability. By measuring polymer adsorption isotherms, we also determined that the polysaccharides adsorbed in a flat conformation (polymer segments in trains) on the alumina surface thus limiting the possibility of steric interactions in the suspension.

In addition, we found that the existence of highly charged functional groups (SO_3^- , COO^-) on each monomer was required before effective suspension stability could be attained, and that the viscosity of the concentrated Al_2O_3 suspensions was extremely pH sensitive even when the polymer dissociation behavior changed only slightly with pH. Finally, the polymeric stabilizer, polyguluronic acid, had no adverse effects on the consolidation and densification behavior of the alumina compacts and monoliths.

These findings suggest that biologically produced molecules, in addition to synthetic polymers, should be considered an important source of potentially useful additives for powder processing.

TABLE OF CONTENTS

	Page
List of Figuresiii
1. Introduction	1
2. Utilization of Chemically Modified Biopolymers: Demonstration of Concept	6
2.1 Abstract	6
2.2 Introduction	6
2.3 Materials and Experimental Methods	8
2.3.1 Materials and Chemicals	8
2.3.2 Experimental Methods	10
2.4 Results and Discussion	11
2.4.1 Surface Charge of Al_2O_3	11
2.4.2 Dextran and Dextran Sulfate	14
2.4.3 Solution Behavior of Dextran Sulfate	21
2.4.4 Suspension Stability as a Function of pH	24
2.5 Conclusions	30
3. Utilization of a Biopolyelectrolyte (Alginate) in the Preparation of Highly Concentrated Suspensions of Al_2O_3 Powder	31
3.1 Abstract	31
3.2 Introduction	31
3.3 Background Information	33
3.4 Materials and Experimental Methods	34
3.4.1 Materials and Chemicals	34
3.4.2 Experimental Methods	36
3.5 Results and Discussion	37
3.5.1 Development of Surface Charge on $\alpha-Al_2O_3$	37
3.5.2 Suspension Behavior of Native (high MW) Alginates	38
3.5.3 Behavior of Hydrolyzed Alginate - Al_2O_3 Suspensions	43
3.5.4 Stability Mechanisms of Polyguluronic acid	49
3.5.5 Consolidation and Densification Behavior	59
3.6 Conclusions	62
4. Conclusions	64
References	67
Appendix. Consolidation Behavior of Nanometer-sized Ag_2O Particles Formed Within Phospholipid Vesicles	70

LIST OF FIGURES

	Page
Figure 1 Structure of dextran and dextran sulfate monomers	9
Figure 2 Schematic illustration of charged and uncharged surface site densities in relation to surface pH (pH_s^+) for Al_2O_3 surfaces	13
Figure 3 Sedimentation density for 2 vol% AKP-20 alumina suspensions versus amount of dextran (MW 9,400) and dextran sulfate- Na^+ (MW 5,000 and 500,000) at pH 8.2	15
Figure 4 Particle/agglomerate size distribution of AKP-20 alumina suspensions with added dextran (MW 9,400) and dextran sulfate- Na^+ (MW 5,000) at pH 7 . . .	17
Figure 5 Amount of dextran (MW 9,400) and dextran sulfate- Na^+ (MW 5,000) adsorbed on AKP-20 alumina as a function of initial amount of polymer added at pH 7	18
Figure 6 Fraction of acid groups dissociated versus pH for dextran sulfate- Na^+ (MW 5,000) and poly(methacrylic acid)- Na^+ (MW 15,000)	20
Figure 7 Amount of dextran sulfate- Na^+ (MW 5,000) adsorbed on AKP-20 alumina as a function of initial polymer added	22
Figure 8 Viscosity at 9.3 s^{-1} versus pH for 50 vol% AKP-20 alumina suspensions stabilized with dextran sulfate- Na^+ (MW 5,000) and poly(acrylic acid)- Na^+ (MW 6,000)	25
Figure 9 Relative number of dissociated sulfate sites and electrophoretic mobilities versus pH for 20 vol% AKP-20 alumina suspensions stabilized with dextran sulfate- Na^+ (MW 5,000)	26
Figure 10 Structure of sodium alginate	35
Figure 11 Sedimentation density for 2 vol% AKP-20 alumina suspensions versus amount alginate added (a) at pH 8, and suspension pH (b) at 0.5% (dwb) polymer	39
Figure 12 Viscosity versus shear rate for alumina suspensions with 0.5% (dwb) alginate at pH 8.3	42

Figure 13	Sedimentation density for 2 vol% AKP-20 alumina suspensions with added poly G, alginate, poly M, and mannuronic acid monomer	45
Figure 14	Viscosities at 9.3 s^{-1} of AKP-20 suspensions in polymannuronic or polyguluronic acid fractions (pH 8)	46
Figure 15	Conformation of the disaccharide of guluronic acid (top) showing increased local charge density when compared to the ribbon-like conformation of mannuronic acid dimer	48
Figure 16	Fraction of acid groups dissociated versus pH for the polyguluronic acid oligomer	50
Figure 17	Adsorption isotherms for polyguluronic acid on AKP-20 alumina	52
Figure 18	Viscosity at 9.3 s^{-1} versus pH for 50 vol% AKP-20 alumina suspensions stabilized with polyguluronic acid	55
Figure 19	Relative number of dissociated carboxylic acid sites and electrophoretic mobilities versus pH for AKP-20 alumina suspensions stabilized with polyguluronic acid	56
Figure 20	Consolidation and densification behavior of $\alpha\text{-Al}_2\text{O}_3$ prepared from aqueous suspensions with added polyguluronic acid	60
Figure 21	Microstructures of sintered $\alpha\text{-Al}_2\text{O}_3$ (1550°C for 1 hr.) prepared from aqueous suspensions containing added polyguluronic acid, (a) pH 5.2, (b) pH 7.7, (c) pH 10.0	61
Figure A-1	TEM micrographs of vesicle formed Ag_2O particles with (a,b), and without (c,d) vesicle membrane	74

APPENDIX XXV

*Copies of News Clippings on Biomimetic Research Conducted by the UW Group
Under the Sponsorship of AFOSR*



Cooling Continents With a Living Blanket

Materials Science

Ivan Amato reports from Boston at a meeting of the Materials Research Society

Mollusk teaches ceramics to scientists

Red abalone fashion calcium carbonate—the stuff of chalk—into complex arrangements that yield rugged shells up to 40 times more fracture resistant than the blackboard implement. Scientists at the University of Washington in Seattle aim to mimic the mollusks' material-making approach for designing synthetic ceramics that can take a beating.

A close look at an abalone shell reveals two layers, both made of calcium carbonate but organized into different microstructures with different properties. The rough outside layer derives from a mineral form known as calcite. But it is the aragonite form found in the inner, nacreous layer that makes the shell remarkably resistant to breakage.

An even closer look at this layer's architecture shows why. The nacreous layer has a laminated, brick-and-mortar structure, says Mehmet Sarikaya, who is conducting the work with Katie E. Gunnison and Ilhan A. Aksay. The micron-wide bricks are made of fine, high-quality calcium carbonate crystals. For mortar, the abalone secretes its own version of Superglue made of a concoction of organic compounds whose formula the researchers now seek to unravel.

By deliberately stressing abalone shells and then examining the resulting microcracks with electron microscopes, the scientists have observed at least five possible toughening mechanisms. The most important of these, suggesting ways of toughening synthetic materials, are the sliding of adjacent calcium carbonate layers and the formation of crack-bridging "ligaments" in the organic mortar layers, Sarikaya says.

With abalone shell as their model, Aksay and colleague Mehrdad Yasrebi have assembled a synthetic, multilayered structure using the tough ceramic material boron carbide for the bricks and aluminum as the mortar. Scientists term such ceramic-metal composites "cermets." Preliminary results indicate that this cermet is up to 40 percent more fracture resistant than conventional, less structured arrangements of the same materials, Sarikaya says.

Getting the creeps out of superconductors

Researchers still don't know just how a certain class of ceramic superconductors can carry electricity resistance-free at far less frigid temperatures than any previously discovered superconductors. Nonetheless, materials scientists continue to chip away at fabrication problems that threaten to keep these remarkable ceramics from becoming useful in some potentially far-reaching items—such as superconducting electrical power lines—featured on many a technological wish list.

R. Bruce van Dover and E. Michael Gyorgy of AT&T Bell Laboratories in Murray Hill, N.J., separately report bombarding thin films of an yttrium-barium-copper-oxide superconductor with neutrons and protons, respectively. The micro-flack generates imperfections in the ceramic, which researchers know are necessary to counter the so-called flux-creep problem. Without a good distribution of the imperfections, lines of magnetic energy tend to creep around in a superconductor's crystal lattice, impeding electrical current.

Bombarding nearly perfect single crystals of the oxide in this way enables them to carry up to 100 times more current than untreated crystals, van Dover and Gyorgy say. Leonardo Civalo of IBM's Thomas J. Watson Research Center in Yorktown Heights, N.Y., reports similar results using proton bombardment.

Other AT&T researchers, led by Sungho Jin, report another way of getting the defects into small grains of the same material. Using a sequence of heating and cooling steps to convert a precursor ceramic into the oxide, Jin's team obtains micron-sized grains that carry about 10 times more current than similar grains made by other methods.

Space Sciences

Venus volcanism: Another hint

Add another item to the list of evidence some scientists cite as indicating that cloud-engulfed Venus remains a volcanically active planet.

In 1983, Larry W. Esposito of the University of Colorado in Boulder reported that the ultraviolet spectrometer aboard the Pioneer Venus spacecraft had measured a steady drop in the amount of sulfur dioxide in the planet's cloud tops (SN: 10/1/83, p.213). He interpreted this as a possible sign that a large volcanic eruption had injected the sulfur compound into the atmosphere shortly before the Venus-orbiting craft reached its target five years earlier, and that the amount of the gas had gradually declined ever since. Now, Paul G. Steffes of the Georgia Institute of Technology in Atlanta reports that, in addition to the cloud-top measurements, "we have evidence for the first time that levels of sulfur dioxide have been dropping off in the atmosphere below the clouds."

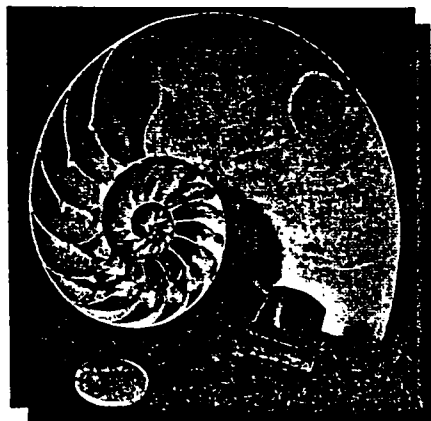
Venus' major cloud layer lies about 48 kilometers above the planet's surface, Steffes notes. The evidence for a declining amount of sulfur dioxide beneath it was detected by Steffes and Jon M. Jenkins of Georgia Tech, together with Michael J. Klein of Jet Propulsion Laboratory in Pasadena, Calif. The data consist of radio emissions from Venus with wavelengths of 1.3 centimeters, detected with the 43-meter radiotelescope of the National Radio Astronomy Observatory in Green Bank, W. Va., and the 70-meter NASA radiotelescope at Goldstone, Calif. The emissions pass through Venus' atmosphere on the way to Earth, so an increase in their intensity indicates a decrease in the amount of Venusian sulfur dioxide available to absorb them.

Jenkins and Steffes also report a decline in the amount of sulfuric acid vapor in the Venusian atmosphere, based on the weakening of 13-cm transmissions from the spacecraft. The Earthward radio beam reaches different depths in Venus' atmosphere as the spacecraft moves, so researchers can use it to calculate differences with altitude. The sulfuric acid and sulfur dioxide almost surely have a common source, Steffes says, even without evidence confirming that volcanoes continue erupting on Venus.

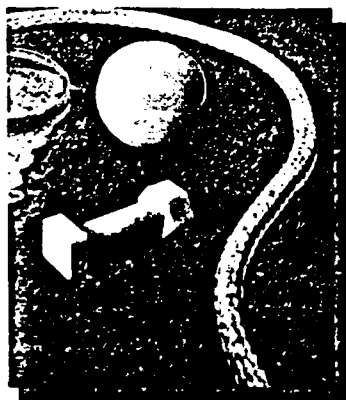
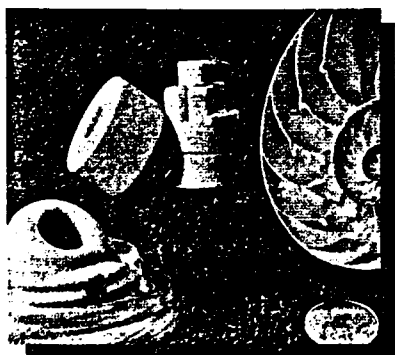
Other scientists have reported additional possible signs of volcanic activity there: radar measurements suggesting rough edges on some surface features, indicating they are too young geologically for erosion to have smoothed them; and radio emissions interpreted by some researchers (though others disagree) as evidence of lightning, similar to that observed over some eruptions on Earth. None of these findings provides sufficient evidence to prove the existence of volcanoes, however, and those of Steffes' group remain inconclusive as well.

Part of the problem is scientists' inability to link either the sulfur dioxide or the sulfuric acid measurements with a particular location on the planet's surface. Sulfur dioxide is widely distributed, and although the sulfuric acid does seem more abundant near the Venusian equator than over the polar regions (suggesting upward atmospheric circulation at the poles and "downwelling" at the equator), the data do not pin down longitudes with any more accuracy than about 40°.

NASA's Magellan spacecraft, due to reach Venus next summer with a more powerful transmitter and a much larger antenna than those of Pioneer Venus, should provide the most detailed radar views yet of that planet. Though even Magellan may not locate a surface source for the presently declining atmospheric sulfur dioxide supply, there is a small chance—if volcanoes are indeed still erupting—that it will detect topographic features that differ measurably from those appearing in past radar maps, perhaps indicating fresh lava flows. Magellan scientists hope the craft will last long enough to cover the planet twice, taking about eight months to complete each mapping and perhaps showing differences between them.



Chemical Processing of Ceramics



Donald R. Ulrich, Air Force Office of Scientific Research

Ceramics are older than history. But new types of ceramics with properties unlike any made previously are now being produced by the application of new chemical technology.

Traditional ceramics are inorganic, nonmetallic solids that are stable at high temperatures, usually up to 1000 °C. Advanced ceramics are being developed that are stable at temperatures to 1500 °C or higher. At the same time, development of ceramics intended for use at less than 1000 °C is driven by the need for materials with new and useful combinations of properties, such as mechanical and electrical performance. High-temperature ceramics like mullite and yttria-containing zirconia-alumina composites, ceramic-metal composites like boron carbide-aluminum, polymer-ceramic composites, and biomimetic ceramics are all examples of newly developed advanced ceramic materials.

Ceramics can be either crystalline or noncrystalline. Crystalline ones are made by consolidating powders into compacts using either dry-pressing techniques or liquid suspensions. Such powder compacts contain individual grains of the powder separated by pores so

that the powder typically fills only 25 to 60% of the volume of the compact. To make the final ceramic, this density is increased by applying heat or heat and pressure in a process called sintering. Depending on composition, the temperatures required to produce dense ceramics range from 1300 to greater than 2000 °C.

Many changes take place during the transformation from the porous compact to a strong, dense ceramic. The grain size increases, pore shapes change, and the pores become smaller or disappear completely. Sometimes solid-state reactions form new ceramic phases.

Noncrystalline ceramics, also known as amorphous ceramics or glass, are made by melting particles and homogenizing them at temperatures as high as 2000 °C. The melt is shaped and cooled or quenched to form a noncrystalline solid. Glass-ceramics, a family of crystalline ceramics, form as glasses and are later crystallized by heat treatment.

Conventional ceramic processing starts with powders that are produced synthetically without strict chemical control or from grinding up naturally occurring minerals. These starting materials are neither ultrapure nor ultrahomogeneous. Chemical processing of ceramics overcomes these problems. By controlling the composition of the ceramic at the molecular level or at a slightly larger level known as the ultrastructure, many properties of the final ceramic can be much improved.

Conventional processing tries to control ceramic properties by understanding the physical behavior of ceramic materials at the microstructural level. This microstructure is composed of grains or crystallites in the 100- to 10,000-nm range "cemented" together by an interface called the grain boundary.

Such an approach, however, has disadvantages. Ceramics formed by these methods still contain pores, and porosity—when it is above a critical size—lowers mechanical strength. Moreover, localized chemical and physical variations develop within regions of the ceramic smaller than the microstructure. Such regions, called ultrastructures, are 1 to 100 nm in size and include surfaces, interfaces, grain boundaries, and sometimes second phases.

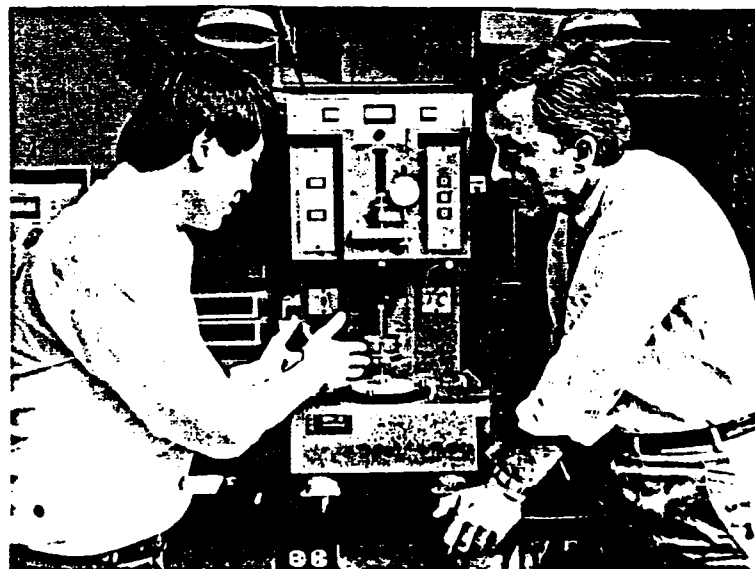
Impurities commonly segregate at grain boundaries. Sometimes glass phases form at the boundary. If the concentration of impurities is high enough, they can form a new grain boundary phase, giving rise to nanometer-scale heterogeneities. These heterogeneities represent defects at the ultrastructural level that can severely limit the use of ceramics in certain applications, such as in ceramic engine components and large-scale optical devices. Viscous deformation of a heterogeneous phase in silicate glass, for example, can cause the glass to break suddenly during use.

The potential for such defects in current advanced ceramics is a major constraint on their use. H. Kent

Bowen, Joel Clark, and their colleagues at the ceramics processing research laboratory of Massachusetts Institute of Technology find failure of advanced ceramic parts varies greatly depending on the product, but ranges from 30 to 75%. Modeling and analysis by Bowen and Elaine P. Rothman of 5-cm-diameter silicon carbide disks that are used as wear-resistant parts and seals show that only 40% of parts made from low-cost, low-quality starting powders (those that are coarse grained with a mean particle size of 5000 nm) pass quality-control inspections. In addition, such parts need extensive machining to achieve the necessary surface finish and size requirements, a step that adds as much as 80% to the final cost of the disks.

By contrast, Rothman and Bowen find that up to 86% of disks made from chemically synthesized silicon carbide powder, which has a much finer particle size and more uniform chemical composition, meet quality-control standards. The disks also can be produced much closer to their final shape, so they require less machining. Such chemically synthesized powders are more expensive; however, Rothman and Bowen conclude that the benefits of using chemically synthesized starting powders could overcome a nearly 10-fold increase in powder cost to produce disks at competitive costs.

High-quality silica glass made by the sol-gel method—one of the major approaches to chemical processing of ceramics—is actually less expensive than similar glass made by conventional high-temperature processes. Asahi Glass Co. of Japan produces silica glass fibers by this method and sells them at half the



Wei-Heng Shih (left) and Ilhan A. Aksay of the department of materials science and engineering of the University of Washington use a rheometer to characterize the stress-strain behavior of sol-gels used in chemical processing of ceramics

cost of conventionally produced fibers. In a number of other applications—including electronic ceramics, such as thin ferroelectric films, and ultrafilters, such as alumina membranes—materials costs are so small, compared with labor, overhead, and other production costs, that they are not deterring application of chemical processing approaches.

There are two main processes for controlling ultrastructure—sol-gel processing and colloidal processing. In sol-gel processing, an intermediate phase is a gelatinlike solid called a gel.

In one type of sol-gel processing—called colloidal—a stable dispersion of solid particles with diameters in the range of 1 to 100 nm is formed in a liquid. Because of the size of the particles this is a colloidal dispersion, and it is called a sol. When the viscosity of this sol increases sufficiently, usually through the partial loss of its liquid phase, it becomes a rigid gel.

In alkoxide sol-gels, the sol is composed of alkoxide precursors that hydrolyze and polymerize to form the gel. By varying the chemical conditions under which the precursor is polymerized, structures can form that vary from lacy branched polymers to dense particulates.

Sol-gel processing can be used to make many ceramic and glass multicomponent systems using metal alkoxides, other organometallic compounds, or soluble salts. Mixing these precursors while they are dispersed in a liquid results in excellent homogeneity. New materials can be synthesized and the composition limits of current materials extended, often at lower temperatures than are required for solid-state reactions.

Ceramics with very close to the desired final shape, even those that have internal cavities, can be fabricated by casting sol-gels into molds near room temperature and sintering them at temperatures near 1150 °C. Jean-Luc R. Nogues of Geltech Inc., Alachua, Fla., for example, has used this approach to make precision optical components that come out of their molds within 10 μ m of their desired final dimensions.

Any system that contains particles with dimensions between 1 and 1000 nm is a colloid, whether or not it forms a gel. The second type of ultrastructure processing—colloidal processing—begins by synthesizing uniform particles in this size range with well-defined composition and shape. Then, by use of colloidal chemistry, the interactions of the particles are regulated to form dense, uniform compacts that can be sintered into dense ceramics without cracking or excessive shrinking.

Sol-gel optical components

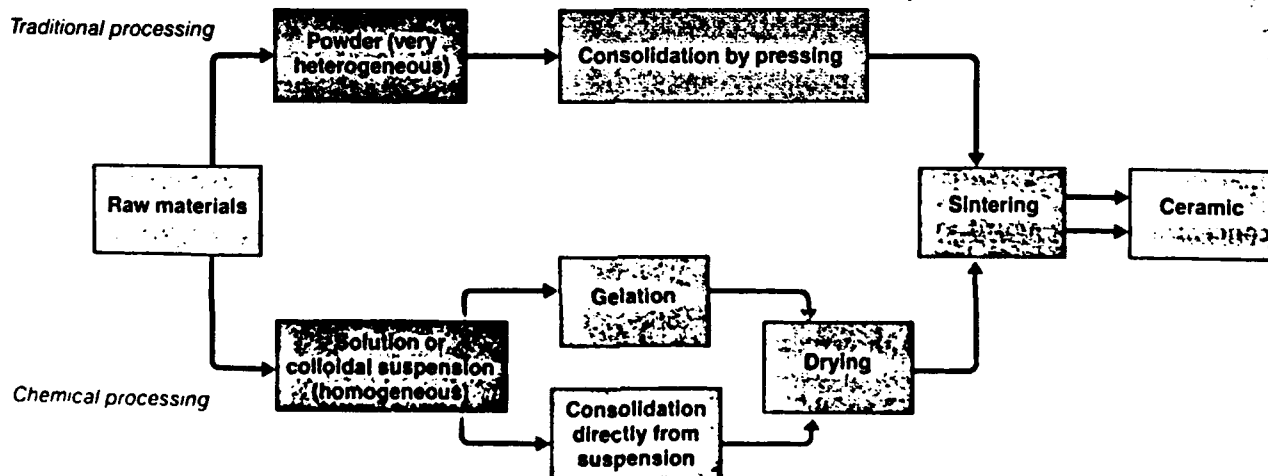
Most research on producing glass and crystalline ceramics from sol-gels produces powders, fibers, and films. For the most part, the stresses that occur during drying cannot be controlled well enough to produce larger structures, such as monoliths.

However, Larry L. Hench and his colleagues at the advanced materials research center at the University of Florida and Robert D. Shoup of Corning Glass Works each have developed sol-gel processes to make large, crack-free silica glass components for optical equipment.

Silica is preferred for many optical applications because of its low coefficient of thermal expansion; transparency in the ultraviolet, visible, and near-infrared electromagnetic spectrum; and high optical homogeneity. It is used in lenses, laser mirrors, and components for intercavity laser optics such as prisms and windows. Present methods of manufacturing fused silica for optics can result in high levels of impurities, particularly high-valence cations—such as iron and aluminum—and hydroxyl and chloride anions. These impurities limit the homogeneity and transparency of the glass, so that it is difficult to manufacture homogeneous optics with diameters as large as 3 to 4 inches.

Hench makes silica glasses by an alkoxide sol-gel process in which he hydrolyzes tetramethyl orthosili-

Chemical processing uses pure homogeneous materials and controls their consolidation



cate. By adjusting the rate of hydrolysis in comparison with the rate of condensation, he can control the pore size distribution in the gel. His dried alkoxide gels have totally interconnected pores averaging 1.5 nm in diameter. Gels with pores that are all this small and the same size are optically transparent.

Because the ultrastructure of the gels is uniform, they can be sintered at the relatively low temperature of 1150 °C. By comparison, fused quartz is processed at temperatures greater than 2000 °C and colloidal sol-gel silica at about 1710 °C. The lower temperature processing has important advantages. Competing chemical reactions are minimized and the glass picks up fewer atmospheric contaminants. In addition, silica glass, like most ceramics, expands when it's heated, which limits how close to its final shape it can be cast. Internal cavities, for instance, can disappear if the expansion that occurs during processing is too great.

Densification of Hensch's gels into the final ceramic takes place almost entirely by decreasing the connectivity of the pore network, and this process is very sensitive to pore size. Since there is no pore growth, alkoxide-derived monoliths remain optically transparent throughout processing. The complete processing cycle takes eight to 10 days.

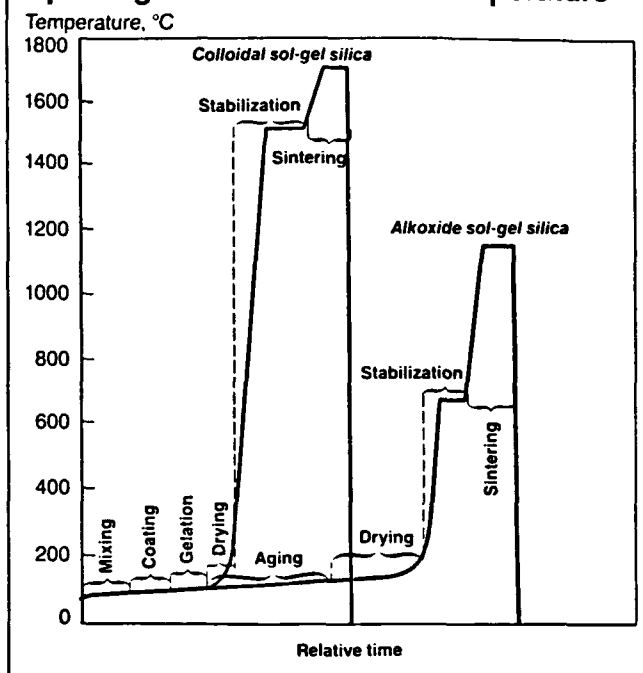
Shoup's process forms a gel from a colloidal suspension containing both potassium silicate and silica. By choosing the proper ratio of the two in the presence of formamide, he produces pore diameters ranging from 200 to 250 nm in rigid silica gels. These larger pores give the gels less uniform optical properties than those produced from alkoxide sol-gels. Total density is achieved after 30 minutes at 1500 °C, but high-quality optical silica requires processing at 1710 to 1720 °C because nucleation of crystals of an unwanted structural form of silica (cristobalite) occurs below this narrow temperature range and deformation occurs above it.

The physical, optical, and thermal properties of optical monoliths made of completely densified sol-gel silica derived from alkoxides are superior to those of monoliths made any other way and are nearly as good as the finest silica optical fibers. Hydroxyl impurities are almost eliminated—the hydroxyl content is 1 ppm—and high-valence cation impurities are also very low compared with fused silica and fused quartz.

These alkoxide-derived silica glasses are transparent over much of the UV and infrared regions. Quantum mechanical calculations by Jon West of the University of Florida and collaborators indicate that the greater transmission in the UV of these glasses is due to their lower alkali and radical hydroxyl content.

Silica glasses derived from sol-gels have a lower coefficient of thermal expansion than fused silica. This property, combined with the ability to control pore size during processing, enables reproducible fabrication of large and complex optical parts. For example, they can be used to make lightweight mirrors that have a support structure known as a faceplate and a honeycomb backing cast with the mirror as a single piece. These three components have to be made separately and then joined in fused silica mirrors. Such

Alkoxide sol-gel silica process produces optical glass at much lower temperature



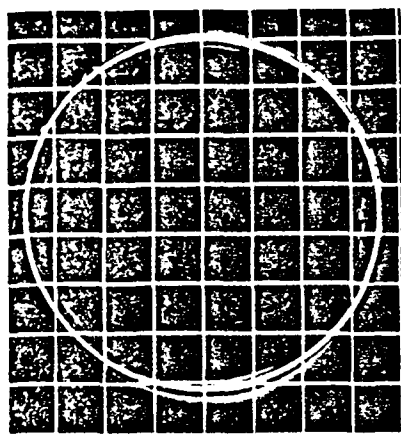
multicomponent mirror systems are necessary for highly sensitive optical systems used in spacecraft that cannot tolerate distortions caused by temperature changes.

Sol-gel silica glasses have also started to demonstrate their future importance in UV holography and precision optical imaging. One example is Fabry-Perot etalons, which are optical elements with highly parallel surfaces used for frequency tuning in laser cavities. Resonant frequencies of light emitted from a laser that span a range of about 10,000 MHz are called a single line. A single mode, consisting of a much narrower range of closely spaced frequencies (about 5 MHz) can be selected from the single line by a Fabry-Perot etalon.

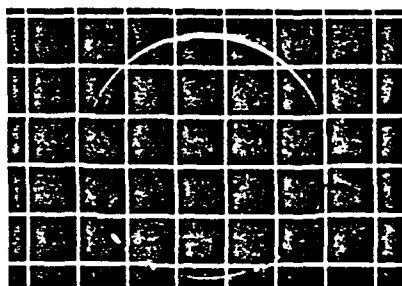
Current etalons for argon lasers are made of coated, fused silica. Their single-line to single-mode conversion efficiency is 35 to 50%; that is, the laser loses from half to nearly two thirds of its power in this conversion. Nicholas Phillips of the department of physics, Loughborough University of Technology in Leicestershire, U.K., finds that uncoated etalons made from Hensch's densified alkoxide-derived glass give 85 to 90% conversion efficiency, a twofold improvement.

Sol-gel processing also can make important contributions in the newly emerging area of nonlinear optics. When a material is subjected to the intense light of a laser pulse, it undergoes effects that can be used to switch a device, such as a directional coupler used in telecommunications, from a low to a high optical transmission state. An optical waveguide, in the form of an optical fiber or a film, confines the propagation of light to one or two directions, thereby increasing

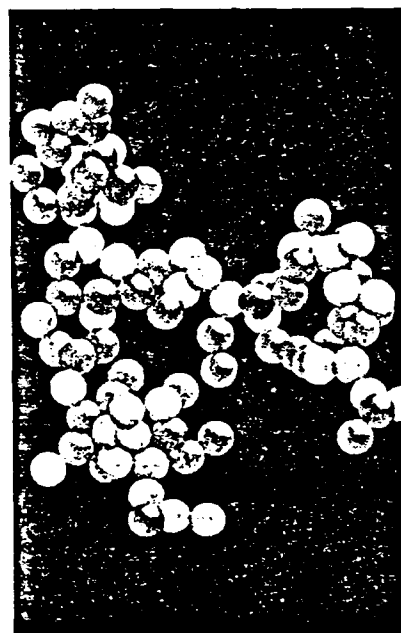
Alkoxide sol-gel process produces large, high-quality silica glass optical discs



Silica glass discs made by the alkoxide sol-gel process display excellent transparency and lack of distortion. The disc shown above is the gel silica after drying at 180 °C, which removes all liquids. A small amount of alkoxide precursor remains in the gel, giving it



its yellowish cast. The gel contains an interconnected network of pores averaging 1.5 nm—or about four silica molecules—in diameter. Further processing to produce poreless glass reduces the size of the disc (above) 50% without forming cracks. Grid lines are 1.4 cm apart. Molecular model (right) shows the silica molecules (the spheres) in the gel. The spaces between the molecules are pores.



the effective intensity of a light beam. Consequently, optical switching in a waveguide can occur at a much lower light level and can use a smaller laser.

Glass fibers or films make excellent optical waveguides because the optical loss in glass is very low. Unfortunately, the nonlinear optical response of glass is weak. In 1989, Paras N. Prasad of the State University of New York, Buffalo, and Frank E. Karasz of the University of Massachusetts demonstrated a sol-gel-processed, low optical-loss waveguide made of a composite of a conjugated polymer and silica glass. The high optical nonlinearity and rapid response time of the composite are due to the polymer and its excellent optical quality to the silica glass.

The polymer Prasad and Karasz use is poly-*p*-phenylenevinylene (PPV). Instead of impregnating the polymer into a porous, gel-derived glass, they dissolve a PPV precursor, poly(*p*-xylene- α -dimethylsulfonium chloride), with tetramethoxysilane silica sol and a drying agent such as formic acid in methanol. Films of the mixture are cast on a glass substrate and treated at 130 °C to consolidate the sol. Then the PPV precursor is polymerized at 200 °C in a thermal elimination reaction that produces hydrochloric acid, which catalyzes formation of a sol-gel and gelation. The composite is densified during this process without high temperature and without cracking.

The effective π -conjugation for the polymer in the composite is comparable to that of pure PPV, and this electron distribution is responsible for the large optical nonlinearity of PPV. Optical losses that would be high in the polymer alone are low in the composite, so that the researchers were able to propagate light of 1.06- μ m wavelength in their initial attempt. The non-

linear optical response time of the composite is also extremely fast, shorter than 100 femtoseconds. This combination of properties holds promise for use in very fast all-optical switching devices. Using this composite, such devices could operate at lower power than is now possible with any material.

Sol-gel electronic ceramics

Another important group of multicomponent ceramics that are amenable to formation by sol-gel techniques is electronic ceramics. Transparent ferroelectric films—including lithium niobate, lead lanthanum zirconium titanate (known as PLZT), and strontium barium niobate—have been deposited on substrates using the alkoxide sol-gel process. Ferroelectric ceramics are nonlinear dielectric materials that can maintain a charge separation (dipoles) in the absence of an applied voltage. Essential in many current electronics applications, such as capacitor chips, ferroelectric ceramics may find use as capacitor films in integrated semiconductors. The ability of these films to modulate optical birefringence in an electric field is also being studied as a way to store information.

David A. Payne and his students in the materials science and engineering department at the University of Illinois have developed PLZT and lithium niobate films that can be deposited on silicon and gallium arsenide substrates. Shin-ichi Hirano, professor of applied chemistry at Nagoya University, Japan, has synthesized lithium niobate and $\text{Li}(\text{Nb,Ta})\text{O}_3$ films at temperatures as low as 250 °C by controlled hydrolysis of bimetallic alkoxide solutions. Hydrolysis of a typical mixture of single-metal alkoxides in solution results in an unhomogeneous material because differ-

ent metal alkoxides hydrolyze at very different rates. Single-metal hydroxides are also less soluble than lithium niobium alkoxide in the organic solvents usually used in these reactions. Incorporating both lithium and niobium (or lithium and tantalum) into the alkoxide precursor also ensures a stoichiometric ratio of these metals in the final oxide.

Using this method, Hirano can grow lithium niobate on sapphire substrates so that the crystallographic planes in the growing ceramic orient in a specific direction. However, when he grows these films on silicon, the crystallites are randomly oriented.

John D. Mackenzie and coworkers of the materials science and engineering department of the University of California, Los Angeles, have synthesized high-quality transparent films of ferroelectric strontium barium niobate, $(\text{Sr}_x\text{Ba}_{1-x})\text{Nb}_2\text{O}_6$, from strontium, barium, and niobium ethoxides prepared in ethanol. The synthesis requires water-free conditions so that no hydrolysis occurs before the coating stage. The system is refluxed to adjust the viscosity for coating 700-nm films on silicon wafers that have either (100) or (111) orientation. The ferroelectric phase forms by crystallization of amorphous phases derived from sol-gel solutions at temperatures ranging from 500 to 900 °C. This

temperature is as much as 50% lower than that needed to produce the same material by conventional processing. Well-defined hysteresis loops approximating those characteristic of single-crystal ferroelectrics are obtained in these films, perhaps because they are very pure and their crystallites have the preferred orientation.

Mackenzie, Payne, and other researchers, such as Robert E. Newnham of Pennsylvania State University, are demonstrating that ceramics made by chemical processing techniques retain their nonlinear electrical properties even when the crystallites are very small. Sintered ferroelectrics and piezoelectrics available before the 1980s lost their nonlinear electrical properties when their grain size was less than 1000 nm, presumably because of interference from heterogeneities at the grain boundaries. Newnham has shown that chemically synthesized ceramic ferroelectrics retain these properties down to 100 nm, and Mackenzie's strontium barium niobate films show strong ferroelectricity even though the crystallites are only 20 to 30 nm in diameter.

Chemical forming of ceramic superconductors

The recently discovered oxide ceramic superconductors show promise of revolutionizing many technologies by eliminating electrical resistance at temperatures that can be maintained during practical operation. A major problem with these materials for many applications, however, is that they are difficult to fabricate into useful forms. Many research teams have made superconducting thin films that can be used in electronic devices and sensors. But other envisioned uses, such as in motors and generators, need strong and flexible materials that can easily be fabricated into wires, fibers, and bulk shapes.

Superconducting wires have been made in the laboratory by several techniques, including oxidation of metallic alloy wires, powder consolidation, and molding a plastic mixture of superconducting powder that is then sintered and annealed. Sol-gels, too, have been used to draw superconducting fibers of $\text{YBa}_2\text{Cu}_3\text{O}_{7-x}$, as long as 200 cm by an international research team headed by Mackenzie at UCLA, Jacques Livage at the Université de Paris VI (Pierre et Marie Curie), and Adrian Wright at the University of Reading, U.K. Their accomplishment is particularly impressive since the solubility of yttrium, barium, and copper alkoxides is extremely low in many organic solvents, making the sol-gel route a difficult way to prepare these fibers. In addition, the salt precursors normally used to make sol-gels produce a solution that is not viscous enough to spin fibers.

The researchers overcome these problems by using covalent precursors in a modified sol-gel method that produces thermoplastic gels that are compatible with fiber-spinning technology. They dissolve yttrium, barium, and copper ethoxides in diethylenetriamine and acetic acid, forming a homogeneous solution with the appropriate 1:2:3 stoichiometry for the three metals. Heating makes the solution almost rigid, with a viscosity of about 10^6 poise.



Paras N. Prasad of the State University of New York, Buffalo, uses colliding-pulse, mode-locked laser system to study the ultrafast nonlinear response of a waveguide he and his colleagues have made of a glass-polymer composite made by the alkoxide sol-gel process. Their composite combines the large optical nonlinearity of poly-p-phenylenevinylene with the low optical loss of silica glass to make a nonlinear waveguide for applications such as all-optical switching

Photo by Rob McElroy

The viscosity of this thermoplastic gel decreases as it is reheated to increasing temperature. Fibers can be drawn from the gel when its viscosity ranges from 2 to 1000 poise at 60 to 150 °C. The researchers believe the gel has a main chain consisting of repeating units of diethylenetriamine and copper linked by coordination bonding. The yttrium and barium form side chains via alkoxide bridges from the main-chain copper atoms. Such a linear structure would be compatible with spinnability and fiber formation, unlike a gel consisting of three-dimensional, crosslinked molecules.

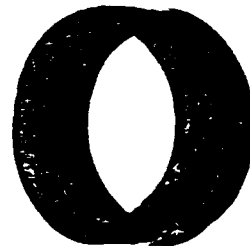
The drawn fiber is heated at 250 °C in air for one hour, fired at 500 °C in argon, fired again at 950 °C for 12 hours in an oxygen atmosphere, and slowly cooled to room temperature. This treatment produces grains of 1000 to 2000 nm in an orthorhombic 1-2-3 phase without minor phases. The superconducting properties of these fibers compare well with the best materials produced so far by any method. Their superconducting transition begins at 91 K and their zero-resistance temperature is 84 K. The increase in demagnetization with cooling, called the Meissner effect, occurs sharply below 91 K, indicating a narrow temperature transition in resistivity.

Mackenzie and Haixing Zheng at UCLA have also made machinable, complex shapes of superconducting $\text{Bi}_4\text{Sr}_3\text{Ca}_3\text{Cu}_4\text{O}_{16}$ by crystallizing the material from a previously formed glass. In their glass-ceramic process, bismuth, calcium, strontium, and copper oxides are mixed and melted, and the viscous melt is cast and quenched to form a glass. Carefully controlled heating converts this glass to a crystalline ceramic with less than 1% of its volume occupied by pores. This synthesis demonstrates that a combination of metal oxides useful in superconductors can be melted into a glass without adding glass-forming compounds, such as silica or boric oxide, that would dilute the superconductivity of the crystalline ceramic.

Other desirable chemical developments occur in this synthesis. Slow cooling causes the crystallites to form with their high-current-density *ab* plane preferentially oriented along the longitudinal plane of rods or fibers. The glass-ceramic method also permits uniform introduction of dopants, such as phosphorus pentoxide and lead oxide, that can control the development of the superconducting phase. These dopants affect the transformation between amorphous and crystalline phases, although their exact role is not well understood. The dopants also control the fluidity of the melt, so that tapes, fibers, films, and intricate shapes such as rings can be produced.

Preparing ceramic superconductors in bulk form will require powders that are sinterable into dense compacts of single-phase superconducting material at low temperatures without forming extraneous phases at the grain boundaries that could adversely affect the critical current. For orthorhombic $\text{YBa}_2\text{Cu}_3\text{O}_{7-x}$, one of the most troublesome of these grain boundary contaminants is barium carbonate. Most of the published synthetic routes to $\text{YBa}_2\text{Cu}_3\text{O}_{7-x}$ use barium carbonate as a starting material. Even in those that

Glass-ceramic method makes machinable superconductor



The high-temperature superconductor $\text{Bi}_4\text{Sr}_3\text{Ca}_3\text{Cu}_4\text{O}_{16}$ can be made into rods, plates, and more intricate shapes, such as rings. The material, which is first formed and shaped as a glass and then crystallized, is also machinable. Holes and even an internal spiral can be cut into it without fracturing it. The process produces a crystalline material with less than 1% of its volume occupied by pores. Its tensile strength—



→ 5 mm ←

nearly 100 megaPascals—is one of the best for ceramic superconductors. Mechanical weakness caused by high porosity has been a problem in ceramic superconductors produced by other methods.

don't, residual organic starting materials will react with barium to form the carbonate.

Harold S. Horowitz and coworkers at Du Pont have used chemical ultrastructure processing to produce ceramic precursors that avoid barium carbonate formation and can be synthesized into ceramics at temperatures as low as 650 °C. The precursors include aqueous hyponitrites and hydrated oxides derived from the hydrolysis of organometallic solutions. They can be converted to tetragonal 1-2-3 material at temperatures of 650 to 700 °C. For example, controlled hydrolysis of homogeneous tetrahydrofuran solutions containing yttrium and barium isopropoxides and copper dibutylamine produces a material that can be oxidized at 300 °C and then heated to 700 °C in argon to decompose the remaining precursors. Subsequent annealing at 400 °C in oxygen converts the tetragonal 1-2-3 form to the superconducting orthorhombic form with the correct stoichiometry.

The powder consists of agglomerates of lightly sintered primary particles, 100 to 500 nm in size. The grain boundaries are clean and smooth, with no evidence of amorphous layers or impurities. The superconducting transition for this material begins at about 85 K, as measured by magnetic susceptibility in the powders. Because the particles are so small, they are

only weakly diamagnetic. Unfortunately, higher temperature processing may be needed to improve this important superconducting property.

Polyimides and other organic polymer films are used as thermal blankets and protective coatings on the space shuttle and other spacecraft that travel in low-Earth orbit. In flight, the films, as well as structural adhesives and matrix resins, are seriously degraded by the atomic oxygen they encounter. Because of the orbital velocity of the spacecraft, sandblasting by these oxygen atoms quickly erodes away the polymers.

This problem has been overcome by chemistry professor James E. McGrath of Virginia Polytechnic Institute & State University and his colleagues using a blend of poly(siloxane imide)-segmented copolymers with the ladder polymer, polybenzimidazole. These two polymers recently have been discovered to be miscible, although the polysiloxane microphase gradually separates from the polyimide in the blend as a result of the vast difference in solubility of these components. Because of its low surface energy, the siloxane preferentially migrates to the film surface. There atomic oxygen converts it to ceramic silica, which protects the film from further degradation. This protective silicate surface may regenerate if it somehow becomes eroded, since the siloxane component of the blend probably continues to migrate to the outer surface, where it can re-form the silicate barrier. The siloxane is anchored to the polyimide film by covalent bonds. Simple homopolymer siloxane coatings can provide short-term protection, but when these films crack, new polymer is not available to re-form the coating.

A chemical strategy for powder processing

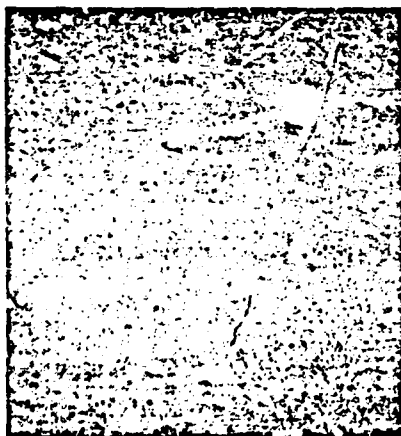
Structural ceramics cannot be used in their present state because of their lack of uniformity. Many of the strength-limiting microstructural heterogeneities in ceramics formed by powder compaction and sintering originate as heterogeneities in the powder itself. Frederick F. Lange of the materials department of the University of California, Santa Barbara, finds that producing compacts with high packing densities and uniformly sized pores requires starting with uniformly sized particles or with particles of several known sizes that can be interdispersed in a controlled way.

Chemists are also addressing these crucial problems in ceramic powder processing by developing chemical procedures to make homogeneous, nanometer-sized powders as well as reproducible, uniform dispersions of particles of several different sizes. In addition, they are applying physical chemistry principles to show how colloidal powder suspension techniques can produce high-density ceramics without undesirable agglomerate formation.

For example, Egon Matijević and his group in the chemistry department at Clarkson University have developed several procedures to make reproducible dispersions of a large number of inorganic colloids without heterogeneities. They use homogeneous precipitation, chemical reactions in aerosols, and crystallization from gels to develop simple, versatile methods that allow them to make amorphous or crystalline ceramics containing more than one cation or anion.

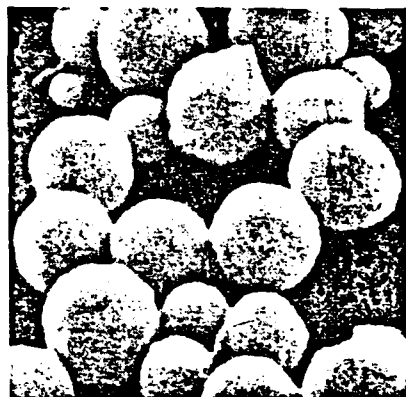
Building on Matijević's work, Bowen, Wendall E. Rhine, and coworkers at MIT began in the early 1980s

Ceramic silica coating protects polymer against oxygen-caused erosion



Atomic oxygen erodes away polyimide and other organic polymer films that are used as thermal blankets and protective coatings on the space shuttle and other spacecraft that orbit Earth at relatively low altitudes where the atom is present. Scanning electron micrograph at left shows initial smooth surface of Kapton polyimide protective blanket before oxygen exposure, magnified 6600 times. The pitting and material loss caused by impact with atomic oxygen is apparent in the center micrograph. The film on the right also has been exposed to atomic oxygen but it has retained its integrity. This film, developed by James E. McGrath and colleagues at Virginia Polytechnic Institute and State University, is a blend of 25% polybenzimidazole and 75% poly(siloxane imide)-segmented copolymers. Its siloxane component continuously migrates to the film's surface, where reaction with atomic oxygen converts it to a protective silica ceramic coating.

Chemical synthesis controls shape and composition of powders for making ceramics



Spheres, flowerlike crystals, and thin needles are among the shapes of zinc oxide crystals that can be produced by chemical synthesis. Such precise control of both the composition and shape of ceramic starting materials is an important advantage of chemical synthesis. Zinc oxide crystals are used to make ceramic varistors. The spheres are made by heating zinc nitrate-triethylamine solutions to 70 °C. The prismatic clusters form from zinc nitrate-ammonium hydroxide solutions heated to 90 °C. The needles form from zinc nitrate-ammonium hydroxide solutions at very high pH, heated to 154 °C.

to develop chemical processes to synthesize discrete, submicrometer, uniformly sized particles. They make oxide powders of silicon, titanium, zinc, and zirconium by hydrolyzing dilute alcohol solutions of the corresponding metal alkoxides under a nitrogen atmosphere.

Controlling these reactions to produce multicomponent powders—such as BaTiO_3 , a ferroelectric material, or $2\text{MgO} \cdot 2\text{Al}_2\text{O}_3 \cdot 5\text{SiO}_2$, a dielectric used in ceramic microelectronic packaging—is harder since each metal alkoxide hydrolyzes at a different rate. One way to control the composition and shape of such multicomponent oxide powders, developed by Anne B. Hardy at MIT, is to hydrolyze the alkoxides within emulsion droplets. Each droplet acts as a microreactor, controlling both the shape and the composition of the particles produced within it. The concept is similar to the suspension polymerization methods used by polymer chemists to synthesize spherical polymer beads.

Hardy emulsifies alkoxide mixtures in a nonaqueous polar solvent, such as propylene carbonate. Adding water hydrolyzes the alkoxides. If the hydrolysis is complete before the droplet breaks, the particles will be spherical. Particle size can be controlled to a certain extent by the method used to form the emulsion. Mechanical agitation produces large particles (20 to 50 μm) and large size distribution. By contrast, emulsions formed using ultrasonic energy produce submicrometer particles with a much narrower size distribution. Hardy has used the technique to prepare submicrometer powders of the multicomponent systems Al_2O_3 - TiO_2 , ZrO_2 - Al_2O_3 , and Y_2O_3 - Al_2O_3 .

This approach also has been combined with sol-gel techniques by emulsifying sols in an organic solvent and gelling each droplet to convert it to a ceramic

particle. Superconducting cuprates, yttrium-aluminum garnet, and ytterbium zirconate have been prepared this way.

Lange is investigating what size particles should be synthesized to make the best ceramics. Using polymer spheres to model ceramic powders, he finds that identical, nanometer-sized spheres can be packed into a periodic, multilayered arrangement only over a very small domain of about 10 μm . Heating causes cracks to open at the boundaries of these domains. He suggests that chemists should investigate what particle size distributions will produce densely packed compacts in some disordered arrangement. The idea would be to minimize the volume of the compact occupied by pores above a certain critical size, those that are the source of cracks.

Ilhan A. Aksay of the department of materials science and engineering at the University of Washington has shown that uniformly sized particles never form a compact in which more than 70% of the total volume is occupied by the particles. How powders that contain particles of two distinctly different size ranges pack is being investigated in several laboratories, including those at MIT and Clarkson.

Colloidal processing of ceramics

Ceramic powders consisting of submicron-sized particles require colloidal processing if they are to form suspensions that are highly concentrated yet sufficiently fluid so that, on the one hand, they can be processed into near-net-shape compacts, and, on the other, they do not form undesirable agglomerates. Theoretical and experimental research over the past six years by Aksay and his associates Wan and Wei-

Heng Shih and Ryoichi Kikuchi at the University of Washington has shown the importance of this approach, which was not previously recognized. Their studies of the dispersion and stability of micron and submicron particles in suspension and of how such suspensions consolidate are an excellent example of the creative application of physical chemical principles to ceramics processing.

These researchers began by developing a classic phase diagram to treat all aspects of phase stability in colloidal systems. If colloids contained only one type of particle, one-component equilibrium phase diagrams—like those familiar in atomic systems—could be used to describe the transitions from a stable suspension to the consolidated state.

When colloidal fluids consolidate, however, particles cluster to form networks that display several levels of organization. Particles clump together to form clusters that come together to form larger clusters. Large clusters clump together into even larger clusters called agglomerates. These agglomerates are nonequilibrium systems and Aksay suggested nonequilibrium phase diagrams to describe them.

These phase diagrams clearly show that two concepts are important: For repulsive particles, minimizing the thickness of surface modifiers, such as polyelectrolytes and block copolymers, adsorbed on the particles allows the particles to pack densely by modifying the charge on the particles. For attractive particles, thicker layers of "lubricating" surfactants allow low-density, fractal clusters to repack into higher density clusters. Generally, higher packing density allows the ceramic to be produced closer to the final shape of the object being fabricated. It also minimizes processing defects. As a result very highly concentrated colloidal solids (greater than 60% by volume) can be prepared from particles smaller than 1 μm .

However, particles less than 100 nm in size form suspensions in which only 25 to 30% of the volume is occupied by the particles. These low-density gels and microemulsions shrink dramatically during drying, causing cracking and incomplete sintering. A current research challenge is to find chemical methods to modify the interactions of these smaller particles so that they can be densely packed, thereby reducing shrinkage and cracking problems. Such high-density suspensions could then be converted into high-density ceramics at much lower temperatures than are needed in conventional pressing and sintering methods.

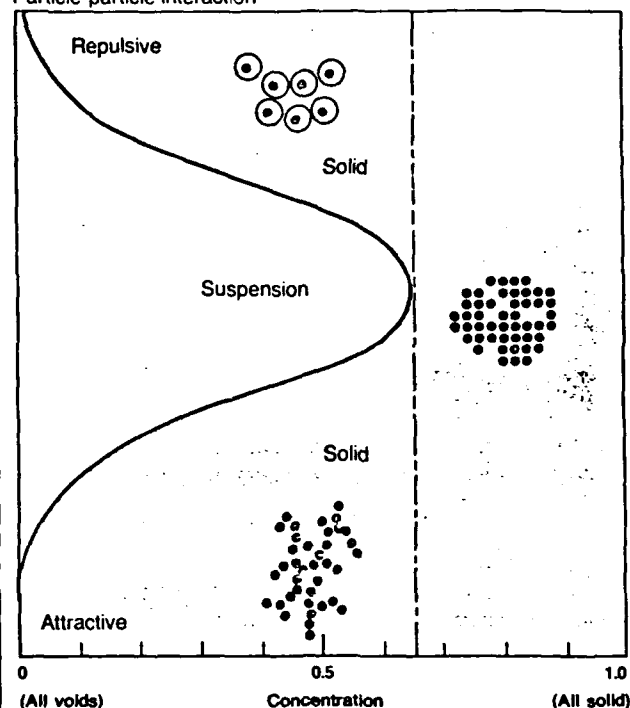
New ceramic and ceramic-metal composites

New composites with novel combinations of properties also are being made based on principles developed by Aksay and his coworkers. One of these is a boron carbide-aluminum ceramic-metal (cermet) composite, which combines both the toughness of aluminum and the strength of boron carbide ceramic in a single material.

The toughest, strongest cermet made so far is tungsten carbide-cobalt, but its high density of 14.3 g per cc restricts its use to cutting tools. Boron carbide-aluminum is more than five times lighter. However,

Nonequilibrium phase diagram highlights role of particle-particle interactions

Particle-particle interaction



In colloidal processing of ceramics, highly repulsive particles, at the top of the diagram, will pack together no more tightly than their hydrodynamic radii will allow (shown here as circles around each particle). Highly attractive particles, at the bottom of the diagram, clump together into low-density, fractal clusters. The tightest particle packing, in which 64 to 70% of the volume is filled by the particles, requires moderate particle-particle interactions. Repulsive interactions can be lessened by coating the particles with surface modifiers, such as polyelectrolytes and block copolymers. Particle attractions can be reduced by coating particles with lubricating surfactants.

processing this material is plagued with problems of poor wetting, unwanted chemical reactions, and densification. For example, to process a cermet, the metal must wet the ceramic, but at 1150 °C, where aluminum wets boron carbide, capillary action draws molten aluminum between the grains of boron carbide, filling small pores but leaving large ones only partially filled. These unfilled spaces serve as origins for cracks.

Aksay consolidates a homogeneous, colloidal suspension of boron carbide powder by sedimentation into a high-density (greater than 60% by volume) cake. The cake is partially sintered at 2200 °C into a solid boron carbide sponge in which all the pores are the same size. Molten aluminum at 1100 °C will fill all these pores by capillary action. The process produces a fully dense, boron carbide-aluminum cermet with a homogeneously distributed, three-dimensional

Sol-gel processing eliminates amorphous regions from mullite



Conventional ceramic processing of mullite, $3\text{Al}_2\text{O}_3 \cdot 2\text{SiO}_2$, a high-temperature ceramic and optical material, traps amorphous silica-rich phases within the mullite grains; such a phase is shown in the transmission electron micrograph at left. The orderly crystalline mullite lattice can be seen to the right of the amorphous region. These amorphous regions absorb infrared light in the 4- to 5- μm region, where mullite is otherwise transparent. Such glassy regions also form at the grain boundaries, where they cause deformation at high temperatures.

Mullite crystallites (center and right micrographs) made by sol-gel processing, are free of these amorphous regions. Well-developed crystallites, labeled A, B, and C (center), form, each about 150 nm wide. At right is an atomic-scale micrograph of the grain boundary between crystallites B and C, which shows that even it is free of amorphous regions.

microstructure of boron carbide and aluminum phases. High-resolution electron microscopy reveals an interfacial structure free of any detrimental phases.

Lange, working with colleagues at Rockwell International Science Center, has laid the foundation for a new field that might be called composite engineering by using colloidal processing and agglomerate control to increase the resistance of ceramics to brittle fracture. They work with yttria-containing zirconia-alumina composites, which are promising advanced ceramics because of their high-temperature stability. These are transformation-toughened ceramics—their resistance to fracturing has been increased by a process that rapidly transforms their crystal structure near a propagating crack. The researchers find that colloidal processing does not reintroduce heterogeneities into these materials once they have been eliminated from the powders. The processing breaks apart agglomerates. Each processing step repeats this breakup of agglomerates and incrementally strengthens the composite.

Designing ceramics at the nanometer scale

Aksay and Mehmet Sarikaya of the University of Washington, along with Barbara J. Tarasevich of Battelle Pacific Northwest Laboratories, have applied colloidal processing principles to mullite, $3\text{Al}_2\text{O}_3 \cdot 2\text{SiO}_2$, a promising material for high-temperature applications, such as engine components, either alone or as part of a ceramic composite. Mullite does not lose its strength even at temperatures above 1500 °C, unlike other high-performance materials like silicon nitride. However, conventional ceramic processing of mullite re-

quires heating to 1650 °C to achieve a fully dense state. During this process, amorphous silica forms at grain boundaries, causing the material to deform (creep) at high temperatures. Pockets of silica-rich phases—less than 10 nm in size—also form within mullite grains owing to the lack of control of particle clustering. This silica-rich phase makes mullite less useful as an optical material because it absorbs infrared light in the 4- to 5- μm range.

The researchers use nanometer-sized amorphous gel particles to produce monolithic gels that can be sintered into transparent mullite with 98% of the material's theoretical maximum density at 1250 °C and atmospheric pressure. The essential requirement in this synthesis is keeping the material homogeneous on the nanometer scale. Particles of aluminum hydroxide, about 15 nm in size, are used as the alumina source, and the controlled hydrolysis of tetraethoxysilane around these particles forms the silica portion of the material. Viscous deformation of silica at temperatures of about 1250 °C causes rapid densification. The material is then crystallized into mullite.

This chemical processing technique eliminates the inter- and intragranular silica inclusions that can diminish mullite's mechanical and optical properties. Tests by Robert F. Davis of North Carolina State University show the material to be more resistant to creep than silicon carbide at 1500 °C. Its transparency to infrared radiation means that it can also be used for optical components used in the 3- to 5- μm infrared region.

Mullite synthesis is an example of making maximally homogeneous high-performance ceramics by sol-gel

processing. The same process has been used by Rustum Roy and Sridhar Komarney at the materials research laboratory of Pennsylvania State University to introduce heterogeneity—rather than homogeneity—on the nanometer scale into ceramic composites. They call these materials nanocomposites. Roy and Komarney mix two sols, each with the same liquid phase but a different solid component, to form a diphasic gel that is sintered into a ceramic containing two or more heterogeneous phases. These phases fill domains 1 to 10 nm in size and vary from one another in their chemical composition, crystal structure, or both.

The researchers have used the method to make a high-temperature ceramic $\text{Ca}_{0.5}\text{Sr}_{0.5}\text{Zr}_2\text{P}_6\text{O}_{24}$ that does not expand when heated from 0 °C to at least 500 °C. The individual domains either expand or contract during heating, but these effects cancel one another over the entire ceramic. The two components of this nanocomposite are calcium zirconium phosphate and strontium zirconium phosphate.

Nanocomposites also can be designed to have multifunctional properties. For example, the Penn State researchers have combined sodium zirconium phosphate and yttrium iron garnet to make a high-temperature-stable nanocomposite that has low thermal expansion (from the sodium zirconium phosphate) and is magnetic (from the yttrium iron garnet). Combining $\text{CaZr}_2\text{P}_6\text{O}_{24}$ and magnesium oxide in a nanocomposite produces a material with zero thermal expansion and a melting point of 1700 °C.

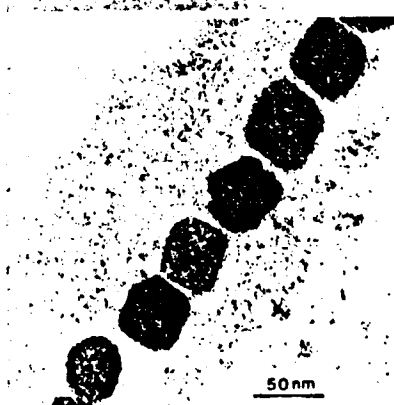
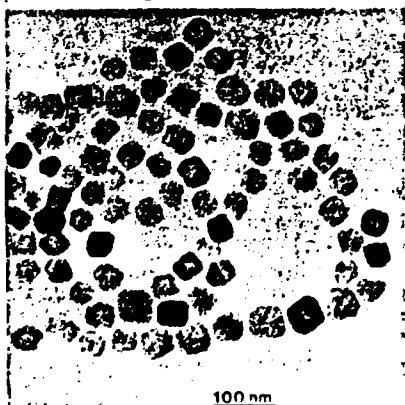
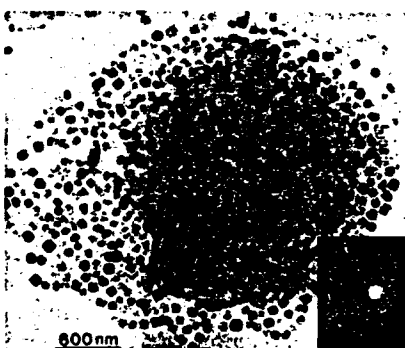
Novel classes of materials that combine organic and inorganic functionalities at the 1- to 10-nm level have been developed by Donald R. Uhlmann at the University of Arizona and Helmut Schmidt of the Fraunhofer-Institut Silicaforschung in Würzburg, West Germany. The Arizona group has incorporated a wide range of preformed organic polymers—including polydimethylsiloxane, polybutadiene, polystyrene, and poly(methyl methacrylate)—into an inorganic silica network during sol-gel polymerization to make materials that they call polycerams. Schmidt calls his nanocomposites ormosils. These organic-inorganic nanocomposites have exceptional relaxation behavior. For example, even though they form gels with 5% or less of their volume as solids, when the solvent is removed from these gels, they simply collapse without cracking.

Nonoxide ceramic powders

Organometallic research continues to find new precursors for nonoxide ceramics. In addition to the traditional silicon compounds, precursors now include metals and intermetallic systems containing germanium, aluminum, boron, hafnium, tantalum, titanium, and zirconium. However, it is still difficult to obtain high ceramic yields with the correct stoichiometry using these materials.

Recently, Leonard V. Interrante of the chemistry department at Rensselaer Polytechnic Institute synthesized an organometallic ceramic precursor $[\text{H}_2\text{Si-CH}_2]_n$ that can be converted with 97% efficiency to

Cell-free synthesis duplicates magnetite crystals made in bacteria



A cell-free system containing an isolate from the bacterium *Aquaspirillum magnetotacticum* produces magnetite crystals about 50 nm in diameter (shown far left at two magnifications) that are virtually identical to the ones produced by the intact bacterium (shown left, also at two magnifications). These particles are quite different than those produced by microemulsions or precipitation. They are larger, denser, and form single crystals that respond more strongly to a magnetic field. The reason seems to be that they are surrounded by a membrane coating 0.5 to 2.0 nm thick. This coating resembles surfactant coatings used to reduce agglomerate formation and allow denser particle packing in some colloidal suspensions.

the high-temperature ceramic silicon carbide. If aluminum nitride, which fits well into the silicon carbide lattice, is incorporated into the ceramic, the several phase transformations between 1400 and 2200 °C in silicon carbide are stabilized, thereby preventing grains from growing too large.

It is difficult to prepare homogeneous silicon carbide solid solutions with aluminum nitride at temperatures lower than 2300 °C by traditional ceramic processing. Interrante uses two different copolyolysis methods in which homogeneous mixtures of organoaluminum amides and either a vinylic polysilane or a polycarbosilane are converted to a homogeneous crystalline silicon carbide-aluminum nitride solid solution at temperatures below 1600 °C. Two distinct types of particles are produced with 3:1 and 10:1 silicon:aluminum ratios.

Bioprocessing of ceramics

Living organisms produce ceramic materials by processes that are often more controlled than synthetic methods and are true examples of ultrastructure processing. The underlying principles of nature's processing methods are not well understood and are being investigated by only a few laboratories. Understanding the nucleation and growth of biocrystals is the first step to biomimetic processing of ceramics.

Microbiologist James T. Staley in the school of medicine at the University of Washington, along with Daniel M. Dabbs, Sarikaya, and Aksay in the materials science and engineering department there, is investigating the formation and crystallization of nanometer-sized magnetite particles in the freshwater magnetotactic bacterium *Aquaspirillum magnetotacticum*. They use an isolate from the bacterium to produce an assembly of magnetite particles and membrane called a magnetosome.

Synthetic magnetite particles produced by microemulsions or precipitation are smaller—10 to 20 nm—than those of bacterially produced magnetite and have a looser crystalline structure. Bacterial magnetite particles are single crystals, 30 to 50 nm in size, without defects, and they respond more strongly to a magnetic field.

Bacterially produced magnetite particles form clusters that are more closely packed than the porous structures formed by nanometer-sized particles in synthetic ceramics. Particles in the biological clusters are separated from one another by about 0.5 to 2.0 nm, a distance similar to that in synthetic ceramics made from nanometer-sized particles that are covered with surfactants. Instead of surfactants, however, the particles are covered by the magnetosome membrane, which remains intact as the particles pack together. All of these biosynthetic advantages are maintained in the researchers' cell-free system.

Other biosynthesized particles also are being actively studied. Janos H. Fendler of Syracuse University and C. T. Dameron of the University of Utah, with co-workers there and at AT&T Bell Laboratories, have produced semiconductor crystallites of cadmium sulfide that range in size from about 2 nm up to a few

tens of nanometers. Dameron induces yeasts to grow the crystallites by culturing them in the presence of cadmium salt. These particles are particularly interesting because they are so small that they show quantum effects that make their optical properties different from those of bulk crystals.

Ceramists concerned with micromechanics, property characterization, and fabrication need to team up with chemists to produce a viable advanced ceramic technology for the U.S., since the ideal properties they seek in materials can only be realized through innovative processing. The field offers rich opportunities for chemists, chemical engineers, biological scientists, and physicists; and I expect scientists and engineers in these disciplines to be increasingly attracted to it. □

Donald R. Ulrich is a senior program manager with the directorate of chemical and atmospheric sciences of the Air Force Office of Scientific Research. He has helped to establish and manage major national and international research programs in the chemical processing of ceramics, ceramic ultrastructure, sol-gel processing, nonlinear optical polymers, ordered polymers, molecular composites, polymer alloys, and multifunctional materials.



Ulrich received B.S., M.S., and Ph.D. degrees in ceramic engineering with a minor in chemistry from Rutgers, the state university of New Jersey. Following postdoctoral study in electrical engineering at the University of Minnesota, he held research and management positions at the National Aeronautics & Space Administration's Langley Research Center and with General Electric before joining the Air Force Office of Scientific Research in 1975.

Ulrich was awarded the 1988 Strategic Defense Award and Gold Medal by the American Defense Preparedness Association. He has coedited 12 books, published 45 papers, and has five patents. Along with service on many other national committees on science and technology policy, he has served as chairman of the subcommittee on monitoring of emerging technologies for the Secretary of Defense's Committee on National Security & Technology Transfer. Following the recommendations of that subcommittee, Department of Defense policy now calls for unrestricted dissemination of DOD-sponsored basic research data obtained at universities and in industry and of applied research data obtained at universities.

Reprints of this C&EN special report will be available in black and white at \$5.00 per copy. For 10 or more copies, \$3.00 per copy. Send requests to: Distribution, Room 210, American Chemical Society, 1155—16th St., N.W., Washington, D.C. 20036. On orders of \$20 or less, please send check or money order with request.

Heeding the Call of the Wild

Drawn by the engineering brilliance embodied in biological materials, a growing number of researchers and entrepreneurs are getting into the business of biomimicking

IF NATURE COULD FILE PATENTS ON THE miraculous materials it has devised, materials scientist Joseph Cappello and his fledgling San Diego company, Protein Polymer Technologies, Inc., might end up paying out a lot of royalties. Biology has two prior claims on the company's very first product—an adhesive for gluing living cells to Petri dishes and other surfaces. The adhesive, which mates a molecular motif from spider's silk with one from a common blood-plasma protein that binds living cells to one another, could make lab technicians' lives a lot easier, Cappello believes. And he isn't alone in his debt to nature. A biology-savvy community of materials scientists is pirating its ideas from the living world—so much so that if species other than our own could demand intellectual tribute, a host of academic and corporate researchers would have to start crediting their best inspirations to mollusks, insects, and even rodents.

Some members of the tribe—known as biomimetic researchers—are unabashedly striving to reverse-engineer the ancient biochemical secrets that enable marine mussels to make some of the strongest adhesives in all of the oceans. Others are attempting to mimic the chemical and engineering virtuosity embodied in the tough, hard shells of abalones. Still others are filching ideas about making lightweight composite materials from beetle exoskeletons. "Nature has these wonderful solutions and exquisite structures that are far beyond anything we have now," remarks Michael T. Marron, molecular biology program manager in the Office of Naval Research (ONR), which has funded biomimetic materials research since the mid-1980s.

Not every materials scientist is sanguine that the lessons of biology can be translated to high-volume industrial processes (see box on p. 968). But Marron and his peers have dedicated themselves to proving the skeptics wrong. They hope to push the performance envelope of materials—creating, say, more capable armor, extra-durable textiles, or lightweight composite materials for advanced aircraft—by imitating the molecular makeup, microscopic architecture, and manufacturing processes of biological materials.

As biomimetic researchers see it, much of their basic R&D has been done for them—

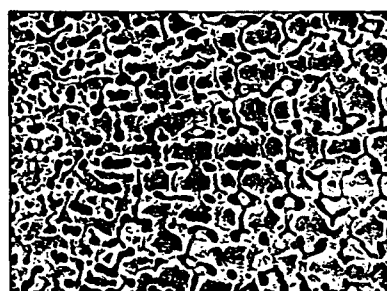
by the process of natural selection. "Nature has been developing materials for hundreds of millions of years," remarks Frederick L. Hedberg, program manager at the Air Force Office of Scientific Research (AFOSR), which oversees a modest biotechnology initiative that includes about \$500,000 for a handful of projects, among them

the development of paint-stripping enzymes, marine adhesives, and aircraft materials based on biological models. Over the eons, evolutionary selection pressure has put millions of biological materials themes to the test, leading to today's long catalogue of durable, strong, fracture-resistant, elastic, energy-absorbing, lubricating, self-repairing, self-assembling materials. Inferior materials went the way of unsuccessful species, notes George Haritos, associate director of AFOSR.

In that vast catalogue of biological materials, researchers have identified a common theme: They all reflect exquisitely precise control over composition and structure at every level, from atomic and molecular components through intermediate structures such as fibers and crystals on up to visible objects such as tendons, bones, and skin. That multilevel control is a skill that materials scientists are eager to acquire. "Learning from these complicated hierarchical material systems is the goal," explains chemist Eric Baer of Case Western Reserve University.

As an example, Baer cites collagen, a protein-based material found in connective tissue, tendon, tooth, and bone. Collagen fibers are structured rather like cables made up of bunches of twisted wire strands, with each strand a protein molecule. Thanks to that structure, they are strong, flexible, and tough, since the breakage of individual strands or bunches leaves the structure as a whole intact. Materials scientists could build better properties into their products by imitating that sort of microscopic hierarchy, Baer says.

He isn't preaching slavish imitation, however. Biomimickry most often involves borrowing nature's design principles but execut-



Crystal power. The porous, intricate structure of a sea urchin spine is actually a single crystal of calcite.

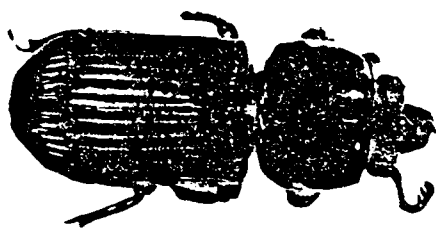
ing them in quite different materials (see opposite page). Stephen Gundersen of the University of Dayton Research Institute, for example, has been trying to imitate the multilayer construction that toughens the cuticle of the bess beetle, a biological composite turned up by one of Gundersen's colleagues during a literature search. But the

resulting biomimetic materials—possible prototypes for strong, failure-resistant, and lightweight aircraft composites—would be made of decidedly unbiological materials such as epoxy resin and carbon fibers. Similarly, Paul Calvert and his colleagues at the University of Arizona are using synthetic ceramics and polymers to mimic the intricate architecture of mineral and protein found in rat's tooth.

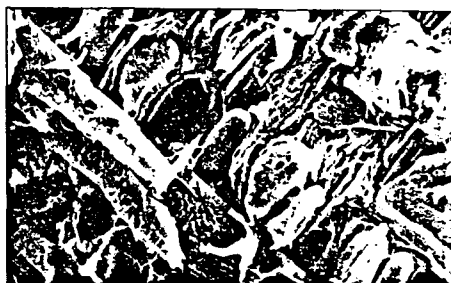
Translating such natural microstructures into lab-made materials, Gundersen, Calvert, and other biomimickers are finding, takes painstaking work. Standard laboratory techniques for making materials are ill-suited to giving researchers the kind of molecule-to-macromaterials control that results in something like collagen or insect cuticle. In making a material as simple as calcite (a form of calcium carbonate), for example, chemists and sea creatures couldn't be further apart at the moment. Chemists make calcite—the stuff of chalk and over-the-counter antacid pills—by precipitating it in bulk from a solution. The ions crystallize willy-nilly, most often into simple cubes. In sea urchins, a favorite object lesson for biomineralization researchers, calcite crystallization takes place within individual cells, which control the process to produce crystals with extremely intricate architectures: Witness the urchins' arrays of predator-detering spines, each spine a single calcite crystal.

And that inspires biomimickers to learn not just what nature has done but how it does it, notes Stephen Mann, a chemist at the University of Bath who studies how organic structures resembling cell membranes can serve as precise templates for forming minerals. Mann, Ilhan Aksay and Mehmet Sarikaya

Biomimetic Materials and Their Natural Models



Sturdy as a VW bug? A bess beetle goes through life armored with an exoskeleton consisting of a protein matrix riddled with layers of chitin fibers, as shown in an electron micrograph (*center*).



Gundersen, et al.

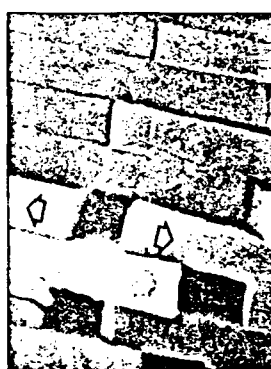


The chitin layers are criss-crossed like the reinforcing plies in an old tire. The structure inspired a strong, lightweight composite (*right*) of epoxy polymer matrix with carbon reinforcing fibers.

Abalone architecture. In the tough inner layer of its shell (*center right*), an abalone lays down calcium carbonate crystals in a bricklike pattern with a mortar of organic polymers such as chitin. The resulting material is not only strong but also fracture resistant, since a fissure is forced to take a tortuous path through the layered structure. The synthetic analogue (*far right*) consists of multiple layers made of a boron-carbide/polypropylene mixture alternating with thinner layers of polypropylene.



Animals Animals



M. Sankaya, et al.



I. Aksay et al.

Animals Animals



Calvert, et al.

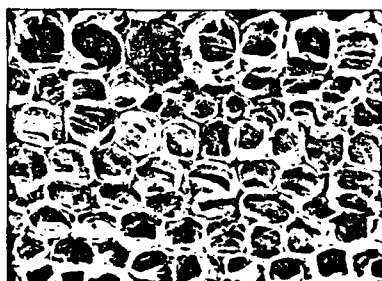


Rodent dentistry. Rats can gnaw through cans thanks to their tough, wear-resistant teeth. The secret lies in crossed rods of hydroxyapatite (a calcium compound that is also the main mineral in bone) embedded in

collagen, a biological polymer. The structure (*center*), has inspired a biomimetic material in which elongated particles of the mineral titania (TiO_2) are distributed through a polymer matrix (*right*).



Artificial wood grain. The cellular structure of Douglas fir wood (*right*) serves as a mold for depositing the ceramic precursor tetraethoxysilane. Water already within the cellulose of the cell walls hydrolyzes the precursor into a ceramic. Heating the preparation to 800 C gets rid of the cell material, leaving behind a cellular ceramic (*far right*)—strong but lighter than the monolithic material.



Aksay, F. Kaynan, Weyenhaeuser Corp.



of the University of Washington, and others have been learning how to draw crystal precursors into tiny sacs or sheets made of phospholipids, the same kind of molecules that make up the membranes of living cells. The membranes serve as templates or, as Aksay prefers to call them, "nanoscale reaction vessels," for crystal growth. These scientists ultimately hope to use collections of such crystal-growing templates for controlling the size and shape of ceramic crystals and organizing them into technologically important forms—"elaborately structured ceramics, finely powdered catalysts, or single crystals of unusual shapes for electronic devices" are some of the possibilities Mann lists.

An important bonus, says Mann, is the fact that these tiny crystal factories work at normal temperatures and pressures. Indeed, that's typical for materials manufacturing modeled on biological processes. In contrast to the harsh conditions and toxic effluents of human manufacturing, living creatures make their own high-performance materials in aqueous environments, at low temperatures,

and under physiologically friendly conditions. As a result, Calvert points out, biomimetic material making could lead to more environmentally sound manufacturing methods.

Still, the minuscule reaction vessels in which living things make the hard parts of their anatomies often cook too slowly for the purposes of modern industry, says Dan Urry, a University of Alabama materials scientist whose 10 years of work with protein-based polymers led to his founding of Bioelastics Research, Ltd., in Birmingham 2 years ago. "The clam makes its shell over a long period of time," he points out. So after discovering the rules by which animals slowly make bones, teeth, shells, and spines, biomimetic ceramic researchers need to learn ways of speeding up these biomineralization processes, he says. But Calvert suggests a simple remedy: using a feed solution more concentrated than the seawater from which marine animals extract the building blocks for their ceramics.

Researchers trying to harness biological polymer-making methods may face fewer hurdles in trying to scale up to industrial

production, notes synthetic chemist David Tirrell of the University of Massachusetts. For one thing, organisms, especially when working en masse, can churn out natural polymers such as proteins at a good clip. For another, the path has been smoothed by biotechnology researchers, who are already engineering bacteria to produce proteins. Now Tirrell and others are harnessing bacteria to make artificial materials—specialized biomimetic polymers. Equipped with genes for the chemical units of the novel materials, the bacteria act as minuscule polymer factories, working in parallel by the billions.

Two early fruits of this strategy are Protein Polymer Technologies' cell adhesion product and the candidate products of Urry's fledgling company. Urry and his colleagues are developing a series of epithelium-like materials with a molecular structure partially mimicking the elastin proteins found in blood vessels, lungs, and other tissues that repeatedly stretch and relax. The Navy is interested in trying out such materials as resorbable surgical implants; by providing a compliant layer between a patient's tissues, the implants might prevent the painful and sometimes dangerous "surgical adhesions" that often form after an operation.

The small scale of these ventures emphasizes how far research and development on biomimetic materials still has to go. For now, many researchers are driven more by the thrill of uncovering and trying to imitate the exquisite match between biological form and function than by the lure of the market. "These are early days yet," Mann stresses.

And like any field in its infancy, this one faces threats to its future. For example, Marron of the ONR fears industry may not be willing to face development periods that could last 5 years or more, poor prospects for short-term gains, and the lack of any guarantee that biomimetic products will ever catch on in a marketplace raised on conventional synthetic materials.

Marron and like-minded scientists are biased, of course, but they see the potential payoffs of their work as more than making up for such uncertainties. Pursued to its limit, the most enthusiastic of the tribe will argue, the approach could even expand the definition of materials beyond the inert substances the word now conjures. Julian Vincent, an expert in biological materials at the University of Reading, puts it this way: "If some of the techniques of nature could be exploited, self-designing, self-adjusting, and self-repairing structures could be developed." Vincent and his fellow biomimetic researchers will have to pull off heroic feats to justify this dream, but if they do, they will have imitated not just the structures but the very dynamism of living material.

■ IVAN AMATO

No Easy Lessons in Nature

A researcher's role in life might be described as pushing the bounds of optimism. That doesn't mean, however, that the materials scientists who are trying to imitate the products and processes of nature think their task will be simple (see main text). But their efforts to be pragmatic strike Rustum Roy, a veteran materials scientist at Pennsylvania State University who is known for his outspokenness, as pollyannaish. When it comes to the potential payoffs of biomimetic research, Roy also pushes the bounds—of pessimism. "Mimicking nature has the same chance as a snowball in hell," Roy told *Science*.

In a memo sent earlier this year to funding agencies—including the National Science Foundation, the Office of Naval Research, and the Air Force Office of Scientific Research (AFOSR)—and in other documents that have circulated throughout the materials science community, Roy has blasted the field. Exaggerated claims about the potential for mimicking biological materials and the technological promise it holds, he warns, can distort national goals for materials research.

Roy was prompted to write his memo by a research report and accompanying commentary that appeared in *Nature* on 24 January. He claimed the work—a biologically inspired experiment in which cadmium sulfide crystals were precipitated within a synthetic matrix—duplicated (without crediting) earlier studies published by him and others. The memo stressed that biomimetic materials researchers should scour the literature so as not to neglect crediting earlier researchers—a plea his fellow materials scientists mostly welcome. But Roy went on to question the concept of biomimetic materials as a whole.

As his complaint about credit shows, Roy himself has not been immune to the lure of biomimicking; in his ceramics research he has sometimes sought to duplicate natural mineralization processes. But those attempts, he says, taught him that the mild conditions biology uses—which enthusiasts tout as an added benefit of the biomimetic strategy—just don't allow materials to be synthesized fast enough for industrial purposes.

Many biomimickers acknowledge the need to find ways to accelerate natural processes, but they think it's too early to be discouraged. Besides, says AFOSR associate director George Haritos, "Nothing ventured, nothing gained."

■ I.A.



Rustum Roy

THE NEW ALCHEMY

HOW SCIENCE IS MOLDING MOLECULES INTO MIRACLE MATERIALS



It isn't exactly *Terminator 2*, whose "mimetic polyalloy" villain melts and recomposes as it stalks its hapless victims. But in a lab in Evanston, Ill.,

a version of this Hollywood fantasy—more modest, but then it's real—is being brought to life. Using new modeling software that incorporates a wealth of knowledge from the exploding field of materials research, Gregory B. Olson, a Northwestern University professor, is designing entirely new substances, atom by atom. Olson and a group of students are hot on the trail of custom-made ceramic superconductors and ultrahigh-strength plastics, but alloys are their top priority. They already have one success, a mixture of atoms from five metals so precise that finding it by trial and error might have required "a few zillion" attempts. The resulting extra-tough steel is being tested for bearings in space-shuttle engine turbo pumps, which now must be rebuilt after every flight.

Materials have always influenced the basic fabric of life. The Stone, Bronze, and Iron Ages marked key periods when humans fashioned materials into new tools that vastly improved their lot. So it is with the latest—and most sweeping—revolution in materials science. Using ultraprecise new technologies, researchers are probing worlds far tinier than the submicroscopic realm of viruses. Like voyeurs peeping into a particularly raucous party, they are peering into the world of atoms and unlocking the secrets of how they interact. Then, using technology developed primarily to deal with the rapidly decreasing dimensions of microelectronics, modern-day alchemists are rearranging molecules—and even atoms—to assemble novel substances from scratch.

Often, the most commercial results of this wizardry are, like Olson's steel, offshoots of existing materials. But researchers are also probing the unknown.

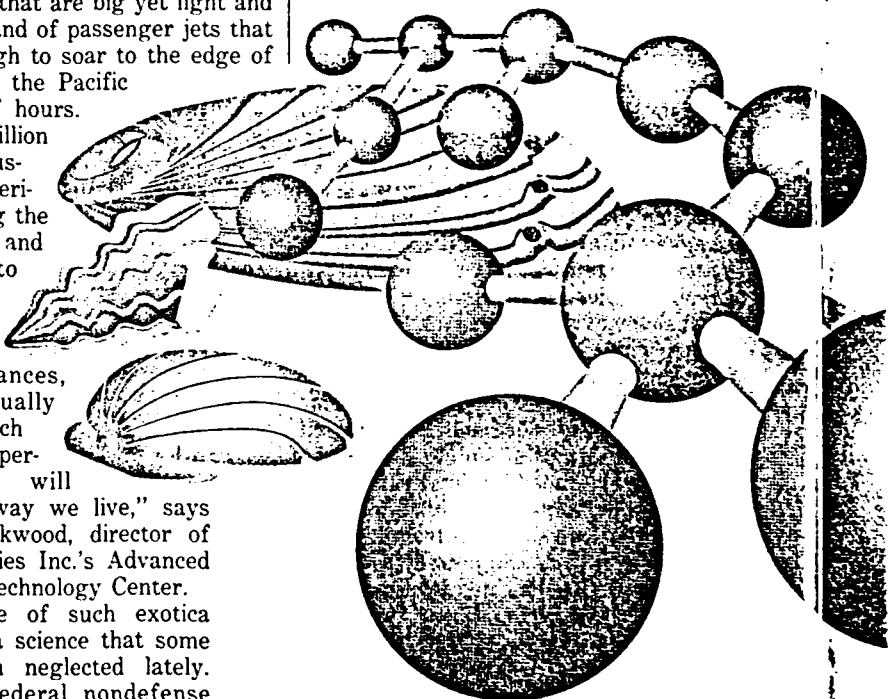
They're making "aerogels," airy silicon concoctions that far outperform the best insulators; ceramics pliable enough for use in car or jet engines; and composites embedded with artificial "nerves" and "muscles" that let them respond to stress almost as a living thing would. With such substances in mind, scientists dream of cars that are big yet light and fuel-efficient, and of passenger jets that are light enough to soar to the edge of space and hop the Pacific in a couple of hours.

In the \$300 billion electronics industry, new materials are pushing the speed of chips and computers to the edge of physical limits.

These advances, leading eventually to products such as handheld supercomputers, will "change the way we live," says Harry F. Lockwood, director of GTE Laboratories Inc.'s Advanced Components Technology Center.

The promise of such exotica should boost a science that some say has been neglected lately. Since 1980, federal nondefense support for materials R&D has fallen 17% in real dollars. Industry support has plummeted, too, experts add, while Germany and Japan, among others, are pumping money into the field. A 1989 report by the National Research Council found that America's competitive position in metals and ceramics is declining vis-à-vis Japan's and that Germany and Britain have caught up. To stay in the game, says the Materials Research Society, a trade group, U.S. government and industry need to add \$1.25 billion to the \$3 billion a year they now spend on materials R&D.

Confronted with losing ground in a \$148 billion world market, the usually laissez-faire Bush Administration seems abnormally concerned. In April, David L. Huber, acting executive director of the National Critical Materials Council, announced an Administration materials-research initiative. The White House



BIOMIMETICS

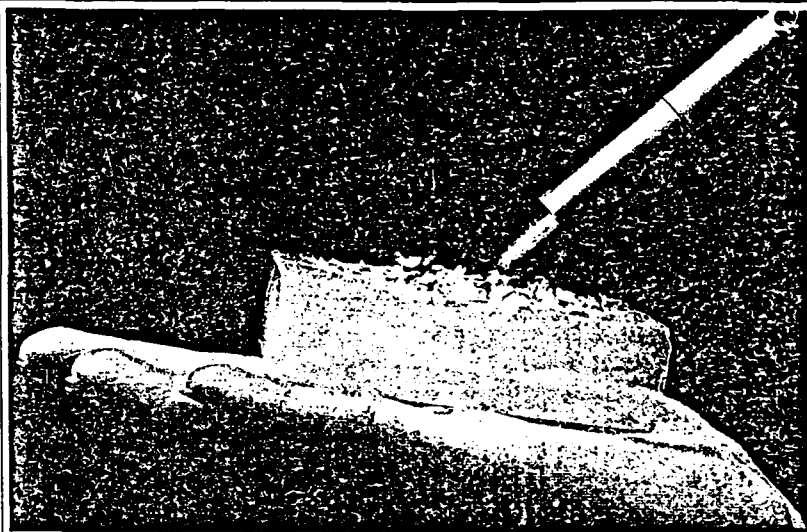
Nature provides the molecular architecture for some of the most interesting new materials. The abalone shell is an excellent example of a ceramic composite made mainly from a simple material—chalk. Its relatively high strength comes from the unique way in which its mole-

cules are arranged, in a brick-and-mortar pattern with a natural polymer acting as the glue between the chalk 'bricks.' Using higher-tech materials but enlisting the abalone as a model, researchers have synthesized an impact-resistant tank armor that's twice as tough as any man-made ceramic and more effective than today's armor.

Other to in sho rial The luti hov test

Office of Science & Technology Policy, with which Huber's group is affiliated, wants to add "hundreds of millions in new and reprogrammed dollars" for materials research, probably in the 1993 federal budget. And Huber wants to sharpen R&D priorities: "It's not clear that we are doing all we should with the money we have," he says.

He is trying to reignite a movement whose roots reach back to the 1960s, when researchers began large-scale production of molecules that nature overlooked. The result was an explosion in synthetics that revolutionized industries such as packaging, homebuilding, and textiles. Today, athletes use carbon-fiber-reinforced golf clubs, polypropylene sweat-suits that draw sweat away from the body, and waterproof jackets that "breathe." Scientists know so much about how the chemical structure of a polymer—a chain of repeating molecules—dictates its function that researchers can sit down at computers and noodle together materials with the de-



SMOKE SCREEN: SUPERLIGHT AEROGELS MAKE EXCELLENT INSULATORS

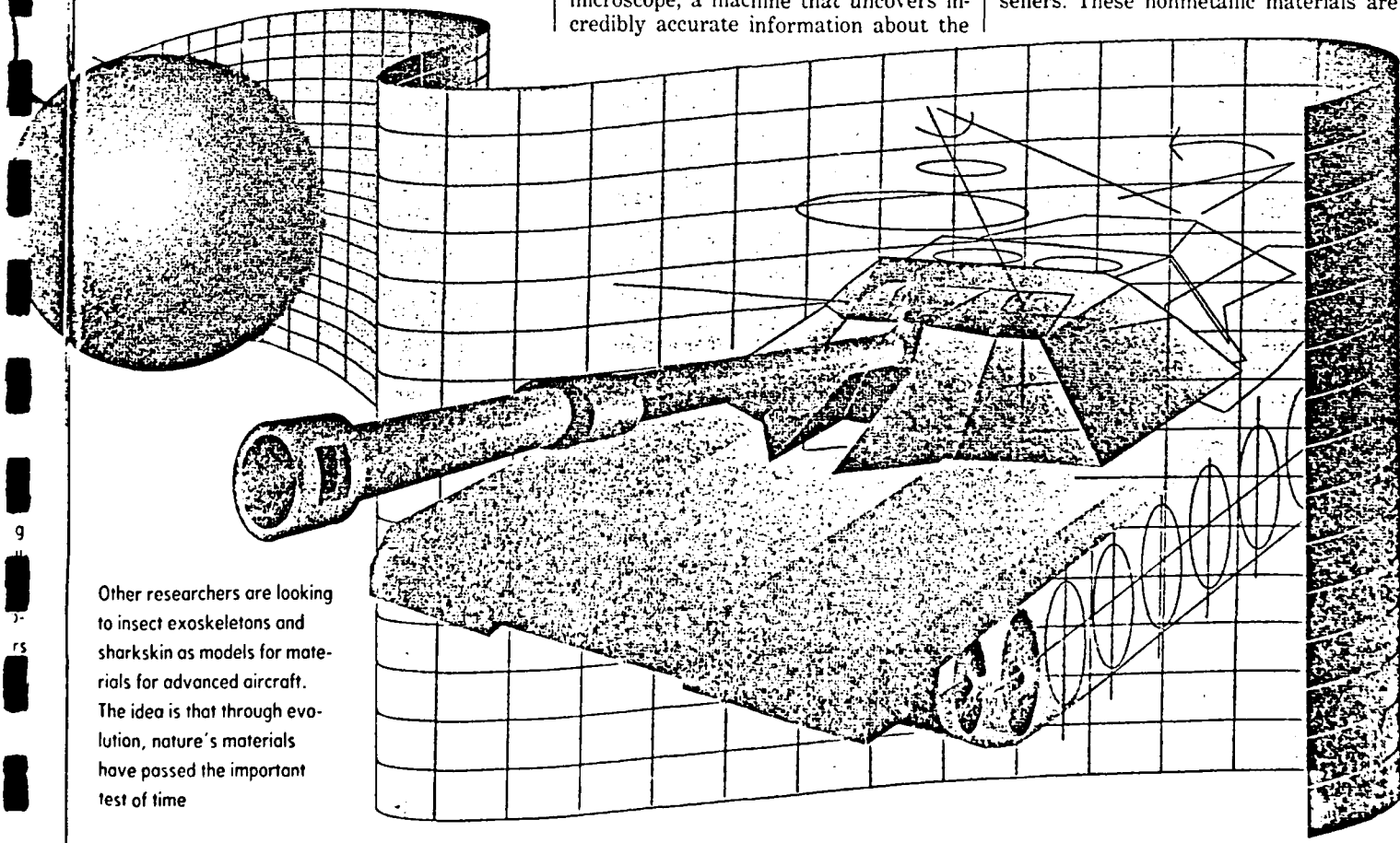
sired qualities. This means that "instead of 10-year development cycles" for finished products, "we'll see results in 3 to 5 years," says Donald P. Knechtges, vice-president for marketing at B.F. Goodrich Co.'s Geon Div. in Cleveland.

The most dramatic advances have come in electronics (page 54). To meet the increasing demand for improved performance in storing and processing data, researchers are working harder than ever on techniques and equipment to shrink silicon circuitry. One of the newest tools is the scanning-tunneling microscope, a machine that uncovers incredibly accurate information about the

positions of individual atoms on surfaces. Couple the STM with advances in computer modeling, and "we can model how molecules place themselves on a substrate without doing exhaustive hunt-and-peck experiments," says Frank Fradin, associate director of physical sciences at Argonne National Laboratory, near Chicago. Now, scientists are using these same tools and insights to fashion materials to improve everything from planes to bridges to artificial body parts.

ENGINEERED MATERIALS These alchemists follow a less greedy pursuit than the Merlins of old, who sought to turn lead into gold. In its most practical form, the new alchemy seeks to devise better versions of structural materials—the metals, composites, and ceramics that permeate everyday life. A modest-sounding endeavor, it's nonetheless likely to produce vast riches. In a decade, Japanese industry alone expects to be using \$90 billion a year worth of such products.

Ceramics will be one of the hottest sellers. These nonmetallic materials are



Other researchers are looking to insect exoskeletons and sharkskin as models for materials for advanced aircraft. The idea is that through evolution, nature's materials have passed the important test of time

ENGINEERED MATERIALS

These are variations on the metals, plastics, composites, and ceramics that already are used in large quantities in industries as diverse as aero-

space, autos, and construction. Now, scientists are engineering into these materials such high-performance properties as increased strength and stiffness, lighter weight, and higher temperature resistance. Some exam-

ples include superstrong, corrosion-resistant alloys and flexible ceramics that can be molded into engine parts. Improved structural materials hold the greatest promise for near-term profits

superstrong and can withstand extreme heat, holding out the promise of hotter burning, more efficient engines needed for jets and low-polluting cars. But ceramics are brittle, which limits their use. Now, by adding small amounts of polymers or fiber "whiskers," researchers are developing much more ductile varieties. "If you can remove their deficiencies, you can open ceramics to a wide, wide range of applications," says Richard W. Siegel, an Argonne researcher. That could include everything from lighter, more durable engine parts to flexible superconducting wire and tougher cutting tools.

Metal alloys are getting a face-lift, too. For instance, a 15-year, \$6 billion initiative jointly funded by the U.S. defense agencies, NASA, and seven jet-engine makers aims to double the thrust of aircraft engines by the year 2003 without increasing their size or weight. "Today's titanium alloys and nickel alloys don't have the necessary strength or temperature capabilities, and they're too heavy," says James S. Petty, manager for the project at Wright Paterson Air Force Base in Dayton, Ohio. But by using new alloys, Petty's team is nearing its first-step goal of a 30% increase in the ratio of engine thrust to weight, plus a 20% gain in fuel efficiency. These improvements will show up in the new stealth fighter's engines, to be built by Pratt & Whitney.

One obstacle has been finding key engine-parts materials that can withstand temperatures of up to 800°F,

the point at which more of the oxygen entering an engine combines with fuel, creating greater efficiency. Titanium, a traditional jet-engine metal, will burn up at that temperature, says Petty. So, his researchers are looking to so-called intermetallics—mixtures that go beyond chemical bonding by intertwining differing atoms within the same crystal structure. Made of titanium and aluminum, or of nickel and aluminum, intermetallics are superlight and can withstand temperatures up to 1,400°F. Adding ceramic fibers to these creates composites that are three times as strong, by weight, as current alloys used in jet engines, Petty adds.

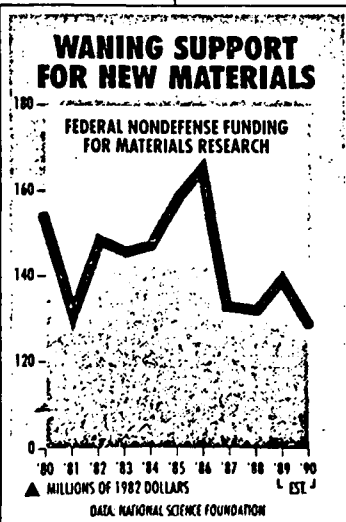
ATOMSCOPIC MATERIALS Improved structural materials may be the most practical products of the new research. But, not content with mere variations, the most aggressive new alchemists are flirting with creation—developing entire new classes of materials. These will foster big advances in electronics and elsewhere. Argonne's Siegel, for example, is forming clusters of atoms, called crystalline grains, into superdense ceramics or metals. In these "nanophase materials," each crystal is less than 100 nanometers, or billionths of a meter, across. That is smaller than most viruses.

The individual grains of most metals or ceramics

consist of millions or

billions of atoms. But the grains that make up nanophase materials contain just a few thousand. After these grains are squeezed, under pressure, into a solid material, they exhibit remarkable properties. Siegel's superdense ceramics can be bent and molded like plastics and extruded or formed into a final shape without the shrinkage normally typical of ceramics. Nanophase versions of metals such as copper or palladium are five times as strong as their larger-grained counterparts. Siegel is also fashioning nanophase composites—combining tiny crystals of ceramics with metals—and he is working on forming unusual metallic alloys. "There are astounding opportunities," he says.

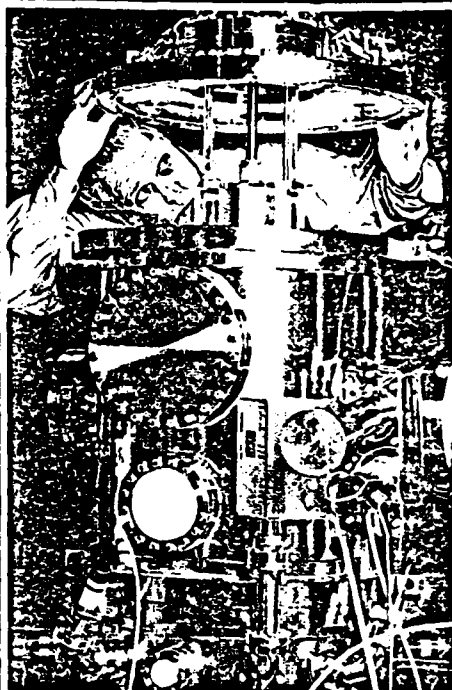
Scientists aren't sure why nanophase materials act as they do, but Siegel says that the size of the crystalline grains plays a big role. Nanophase metals, for example, are so strong because it requires a lot of energy to force cracks among the close-knit grains. For research purposes, Siegel's group usually makes only penny-size disks of nanophase materials. But, he says, "there's nothing in the process that prevents it from being scaled up." In late 1989, in fact, Siegel helped found a company to commercialize the Argonne work. Called Nanophase Technologies Corp., it is making up to several grams of the materials per hour. "I suspect within a year we'll be at the kilogram-per-hour stage," he says. The first use for nanophase



materials will be in electronics—ceramic chips and optical devices—and in making catalysts to drive chemical reactions.

The Japanese, meanwhile, are hot on the trail of designer compounds called functionally gradient materials (FGMs). These combos of ordinarily incompatible materials—metal and ceramics—remain stable over perhaps a 1,000-degree range of temperature and withstand searing heat—more than 3,000F. That would make them useful for everything from lining space planes to making turbine blades for nuclear power plants. Researchers have known that a “sandwich” of metals and ceramics could provide unusual heat resistance and elasticity. But the sandwich usually peels apart under thermal or mechanical stress.

To avoid that, the Japanese use techniques with names such as chemical vapor deposition and particle injection to lay down multiple, ultrathin layers that gradually transform a material from 100% metal to a 50-50 mixture to 100% ceramic. This eliminates the sharp boundary where the ceramic ends and the metal begins. So, the new material stays together. Japan's Science & Technology Agency first advanced the notion of FGMs as a basic research project in 1986. Already, steelmakers NKK and Nippon Steel have taken up the challenge, as has Toshiba Ceramics. “If it is a good idea, money flows in that direction,” says Toshikazu Ishii, deputy director of the STA's office of material science and technology.



IN ARGONNE'S NANOPHASE LAB: CERAMICS THAT BEND AND SUPERSTRONG METALS

SMART MATERIALS As impressive as all this sounds, for some engineers the new alchemy implies the metaphysical. They want to impart the ultimate property: a crude sort of intelligence that infuses materials with artificial “nerves” and “muscles.” Because these altered ceramics and composites sense changes in their environment and then react accordingly, they are called smart materials.

At Michigan State University, for example, Mukesh V. Gandhi and Brian Thompson are working on an adaptive helicopter rotor that can sense turbulence and stiffen in response. The Air Force is sponsoring work on

a smart ceramic for the leading edge of airplane wings: It would adjust its shape to achieve maximum lift under changing conditions and thus improve fuel efficiency and safety. And Robert E. Newnham, professor of solid state science at Pennsylvania State University, is developing a “stealthy” material for submarine hulls that flexes to change shape and reduce underwater turbulence. That would help a sub escape detection by underwater listening systems.

One key to making materials “smart” is to imbed in them nonmechanical materials that change their shape or physical state without using moving parts. Electro-rheological fluids are one such family: They change from a liquid to a solid milliseconds after a small electric current is applied. By scattering these fluids throughout a ceramic, Gandhi and Thompson can dampen vibration in their rotor. Sensors on the outside of it pick up damage or turbulence, then send a signal to stiffen the rotor blades.

In a variation on this concept, Craig A. Rogers, director of Virginia Polytechnic Institute's Center for Intelligent Materials Systems & Structures, adds wires of nickel-titanium alloy to the graphite-reinforced composites used in everything from aircraft to tennis rackets. The nickel-titanium alloy is one of a family of so-called shape-memory metals—they remember their shape when heated. Rogers says that normally, graphite-reinforced epoxy loses half its stiffness when the temperature goes over 300F—not a pleasant prospect in a high-performance airplane wing. But “with the memory fibers, the graphite epoxy increases its stiffness at the higher temperatures,” he says. When heated, as in flight, the fibers try to return to their remembered shape, adding energy to the material. The resulting composite is more than 10 times as stiff at high temperatures as those used in aircraft now.

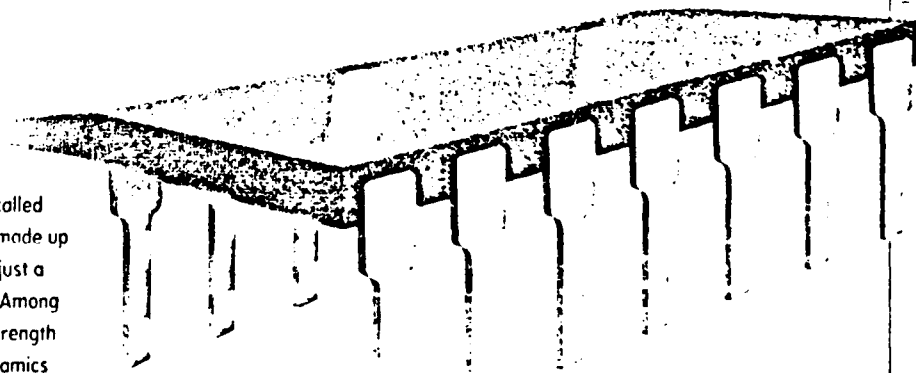
BIOMIMETICS Attempts to imitate life are at the foundation, too, of biomimetics, perhaps the most revolutionary new materials approach. For this, scientists look to nature for inspiration, to materials as



ATOMSCOPIC MATERIALS

Using techniques developed in the race to make smaller, faster semiconductors, scientists are rearranging atoms into novel substances. By layering thin films of different elements—some just an atom or two thick—researchers can design in superconductivity or high strength. They also

are working with so-called nanophase materials made up of grains that contain just a few thousand atoms. Among the results are high-strength metals and pliable ceramics



varied as abalone shell, snake skin, and insect exoskeletons. They start from the view that Mother Nature offers the supreme models: "As far as we know, her failures are extinct," says Lieutenant Colonel George A. Haritos, associate director of the Air Force Office of Scientific Research (AFOSR). "We are mimicking the best she can offer."

For instance, Ilhan A. Askay, professor of materials science and engineering at the University of Washington, was intrigued by the shell of the abalone—a flattened, ear-shaped mollusk shell made from calcium carbonate, or common chalk—that is hard to break even if a

breathe through it, insulates it, and provides all kinds of sensing devices." A multifunctional skin that removes heat and senses damage would be particularly useful for the aerospace plane.

The exoskeleton is also resilient. "It is designed to absorb enormous amounts of energy in relative terms before it breaks down," says Haritos. Such a quality is important because one of the biggest barriers to using composite materials in aircraft wings is concern that the composite will fail catastrophically after suffering limited damage. In the beetle, nature has designed in damage control. Conventional composites are re-

implicated in the destruction of the ozone layer. A Swedish company, Airglass, is trying to drum up interest in using them in insulated windows.

These and other discoveries may mark the 90s as the golden age for materials science. With new federal support, the U.S. could regain some of its edge. But money is just part of the equation, says Argonne's Fradin. In Japan, companies, not academic or government labs, form the cutting edge: Nearly 75% of funding for materials work in Japan comes from industry, vs. half in the U.S.

The challenge, in short, is to envision products from promising technologies.

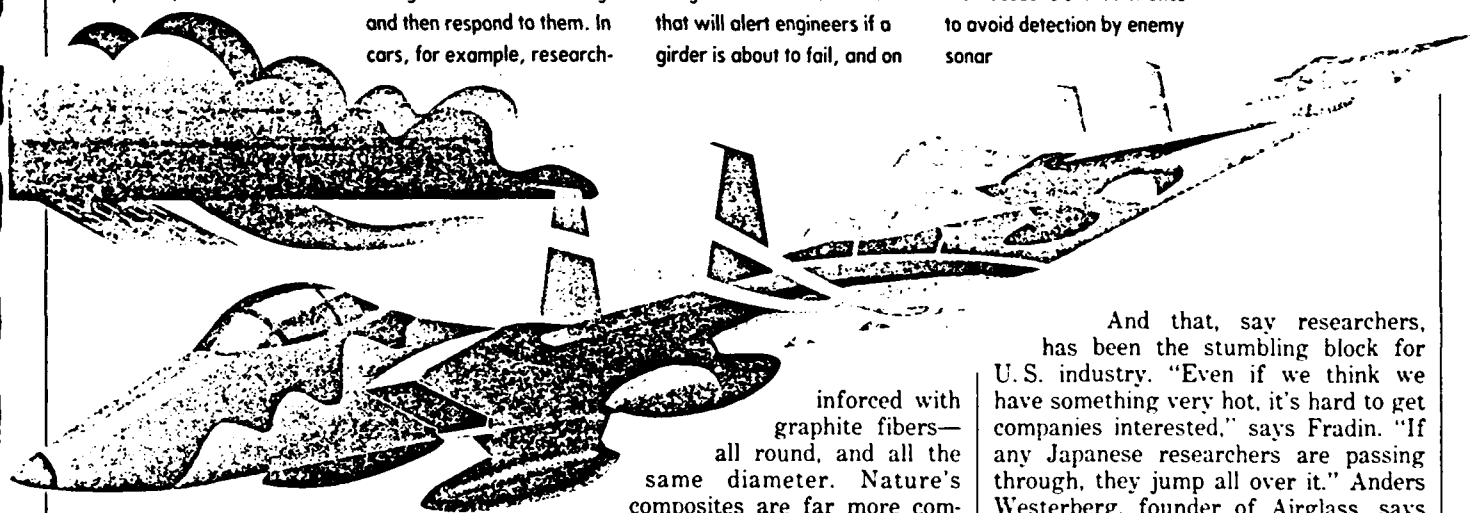
SMART MATERIALS

Usually metals, ceramics, or composites, these are embed-

ded with sensors and actuators that give them some of the characteristics of living things. They can sense changes in their surroundings and then respond to them. In cars, for example, research-

ers have already developed smart suspension systems that dampen vibration. They are also working on smart bridges laden with sensors that will alert engineers if a girder is about to fail, and on

helicopter rotors that stiffen in response to turbulence. The military envisions smart submarine hulls that can alter their acoustic characteristics to avoid detection by enemy sonar



300-lb. beachcomber steps on it.

When viewed under an electron microscope, the shell represented a near-perfect imitation, so to speak, of a ceramic composite. Using higher-tech materials but enlisting the abalone as a model for arranging the molecules, Askay has synthesized an impact-resistant tank armor that's twice as tough as the man-made ceramics now used. The U.S. Army is testing his armor at Lawrence Livermore National Laboratory in California.

One of the systems AFOSR researcher Fred L. Hedberg sees benefiting from biomimetics is the proposed national aerospace plane, which would enter low orbit during its two-hour trip from New York to Tokyo. It would carry a much greater load than the space shuttle, but to reach the right speed and altitude, it must weigh less. That's where biomimetics comes in, says Hedberg, who has studied the strong yet lightweight exoskeleton of the horned beetle. "When nature builds a protective coating for an insect, it also permits the animal to

be inforced with graphite fibers—all round, and all the same diameter. Nature's composites are far more complex, made from intertwining fibers that often themselves are composites. And the fibers vary in shape from round to extreme oval. "This complex structure is something man is just now experimenting with," says Haritos. "But it is the wave of the future."

With an explosion in the number of new materials coming out of labs, it isn't clear yet what all the uses might be. Take carbon 60—a new form of carbon synthesized in bulk just two years ago. The 60 carbon atoms of this substance are organized in a soccer-ball shape reminiscent of R. Buckminster Fuller's geodesic domes. Called "buckyballs," they may be used for lubricants, high-temperature superconductors, or as the foundation for new plastics. Aerogels, developed at Lawrence Livermore last year, have enormous potential. Often called "frozen smoke," they incorporate superior insulating abilities in one of the world's lightest known solids. Livermore researchers envision them replacing foam insulation, whose manufacture is

And that, say researchers, has been the stumbling block for U.S. industry. "Even if we think we have something very hot, it's hard to get companies interested," says Fradin. "If any Japanese researchers are passing through, they jump all over it." Anders Westerberg, founder of Airglass, says the U.S. and European companies he has approached in search of \$7 million for a commercial-scale aerogel plant have held back, concerned about how long it will take to turn a profit. But four or five Japanese companies are interested. And "when I tell them it will take several years to see any kind of payback, they say that's O.K."

Ultimately, the impact of designer materials research will be strikingly evident in the world around us. Faster trains, stronger buildings, and more lifelike artificial limbs will all carry the mark of the modern-day alchemist. New materials will also play an integral role in solving some of society's most pressing problems, from cleaning up the environment to reducing energy consumption. All in all, it's an even better goal than transforming lead into gold.

By Naomi Freundlich in New York, with Neil Gross in Tokyo, John Carey in Washington, and Robert D. Hof in San Francisco

Continued on page 54

CREATING CHIPS AN ATOM AT A TIME

Tiny 'nanosandwiches' grown in crystals will put a supercomputer's power in the palm of your hand



Visitors to Praveen Chaudhari's lab used to stop in their tracks, perplexed by the scene before them: Candles gleamed alongside the exotic equip-

ment used to explore materials and structures for tomorrow's chips. "People would think we were praying," muses Chaudhari, a senior IBM scientist. But the candles had a down-to-earth purpose. His team was experimenting with semiconductor wires so tiny that the friction of a person moving through the air generated enough static electricity to zap the circuits. The candles solved that. Soot particles from their flames discharged the air, protecting the "nano-electronic" devices.

Nanoelectronics is the watchword of the coming revolution in semiconductors. Chipmakers are entering a realm where transistors will be too tiny to "print" on silicon. Instead, they'll be "grown" in the material, as clusters of atoms. These devices will be measured in nanometers, or billionths of a meter. A fat human hair is 10,000 nanometers in diameter. The wires Chaudhari worked on a decade ago were 10 nanometers wide.

BIG LEAP. Today, at key research centers in the U.S., Japan, and Europe, scientists are thinking even smaller. They talk in angstroms, or tenths of a nanometer, and they're making materials and devices by piling up elements in layers as thin as two angstroms—just a single atom thick. Tinier transistors can be packed more closely, which means more powerful circuits that run faster. So, when these technologies are perfected, they'll bring quantum

leaps in performance to all things that use chips, from computers and cars to satellites and appliances. A shirt-pocket supercomputer may be in the cards, as well as memory chips that hold a library.

The industry is going all out to make this happen. For the first 25 years after the integrated circuit was invented in 1959, the number of transistors per chip doubled every other year. Had auto makers done as well, "a Rolls-Royce would cost \$3 and get 100 million miles to the gallon," jokes George H. Heilmeier, president of Bell Communications Research Inc. (Bellcore). Since 1985, though, the growth rate for transistor counts has slipped a bit, according to market watcher Dataquest Inc., and it's headed lower. So chipmakers are turning to basic physics to keep the shrinking act going for another 25 years.

Today's chip technology is based on bulk materials: The thinnest wires on the fastest chips are thousands of atoms

across. But the day is coming—three chip generations from now—when bulk properties won't be able to cut it. The first dynamic random-access memories (DRAMs) of the next century won't be feasible without big breakthroughs. The reason: Below dimensions of 0.2 microns, or 200 nanometers, conventional transistors will be too minuscule to offset the dire effects of "quantum tunneling." A phenomenon of quantum physics, tunneling occurs when electrons squirt right through solid matter and electrical barriers that, in bulk materials, are usually impassable. A 100-nanometer transistor would leak so many electrons when switched off, and release so few when turned on, that it wouldn't be reliable.

"We are moving into a size range where we have to reexplore the physics involved in semiconductor devices," says Richard D. Skinner, president of consultant Integrated Circuit Engineering Corp. And that means devising technologies to harness quantum mechanics.

Quantum transistors will be so tiny as to verge on the ethereal. And their switching speeds would, in theory, be 1,000 times as fast as anything around now. Building such critters, says Arno A. Penzias, vice-president for research at AT&T Bell Laboratories, will require radically new production methods that can "create semiconductor structures atom by atom." How this might be done in factories is anyone's guess. But the tools will have to be very precise. G. Dan Hutcheson, president of

consultant VLSI Research Inc., notes that in quantum electronics, "a variation of just one or two atoms can make a drastic difference." In fact, Bell Labs has found that clusters of 13 silicon atoms behave so differently from clusters of



IBM researcher Praveen Chaudhari burns candles in his lab to clear from the air traces of static electricity that could zap his nanoelectronic devices.

any other size that "Silicon-13" is almost a distinct element. "We're still trying to find out why," says Mark Jarrold, a Bell Labs researcher.

A technique called band-gap engineering looks like the best way to harness quantum electronics. Band gap is physics-speak for the energy difference, or gap, that separates the electrons in an atom's outermost orbit, or band, from those in the next lower band. So, the band gap is the amount of energy that an electron must absorb to make a quantum jump to the highest orbit, where it's in a position to conduct electrical signals.

ADDING OOMPH. Electrons by nature prefer to occupy the lowest possible energy band. So, scientists theorized, electron tunneling could be regulated by exploiting this tendency. The idea is to sandwich an ultrathin layer of a relatively good conductor between another material that's not so hot: gallium arsenide, say, between sheets of gallium aluminum arsenide. The good conductor's outermost electrons have less energy than those orbiting the other compound's atoms. As a result, the inner layer's electrons are trapped, unable to muster enough oomph to muscle past the higher-energy electrons of the surrounding atoms—unless outside energy, such as a switching signal, is applied.

Scientists dubbed such hypothetical structures "quantum wells" and started dowsing for them in the 1960s, spearheaded by Bell Labs and IBM. But before they could slap nanosandwiches together, they had to identify the best pairings of materials and develop new methods for laying down ultrathin films. Finding the right recipes is critical because a chip must be a perfect crystal. When two elements are combined, each material's crystalline lattice, or arrangement of atoms, must match up exactly. Otherwise, the composite crystal's "superlattice" will contain structural flaws that can render a chip useless.

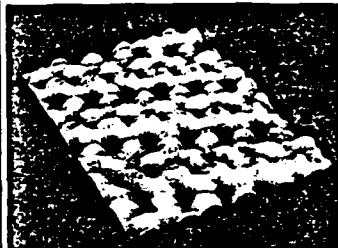
Keeping tight reins on crystal growth requires some of the most esoteric machinery ever built. Take molecular-beam epitaxy (MBE). An MBE system creates the highest vacuum on earth. That's so molecules of air won't affect the atoms ejected by a sophisticated spray gun that is so precise it can "paint" wafers with successive coats of material that may be no more than a single atom thick. While the U.S. pioneered such techniques, Japan's consummate engineers are now

at the cutting edge of some equipment. Fujitsu Laboratories Ltd., for instance, is experimenting with an innovative pulse-jet epitaxy (PJE) system that can produce gallium-based superlattice crystals with superior electrical properties.

Still, it was a U.S. team that finally turned a quantum well into the first working quantum transistor. In the summer of 1988, Texas Instruments Inc. researchers led by Robert T. Bate discovered how to make a quantum well switch on and off. The trick is tickling the middle layer with a current of just the right voltage while pulsing it at just the right frequency. Suddenly, the band-gap barriers topple, and electrons zip across the inner layer—so fast that it's hard to measure the transistor's switching speed. Roughly, it's 5 femtoseconds, or quadrillionths of a second. By comparison, it takes light, traveling at 186,000 miles per second, some 200 femtoseconds to traverse the period at the end of this sentence.

More recently, these tools and techniques have yielded what may be the biggest breakthrough yet: silicon-based materials with features similar to those of gallium arsenide, once considered the chip material of the future. That wasn't supposed to happen. Band-gap engineering is possible only in semiconductors made from two materials, and they must be essentially identical crystals. Silicon's nearest cousin is germanium—not a close match. But nearly a decade ago, Bernard S. Meyerson, an IBM physicist, decided to give it a whirl. "Rule No. 1 in this business is never bet on what somebody can't do," he says. What he found is that silicon alloys containing 5% to 10% germanium are sufficiently elastic to grow into defect-free crystals. "By getting the dimensional control down to the atomic level," says Meyerson, "you can do pretty amazing things."

The first transistors fabricated with Meyerson's hybrid clocked in more than a year ago with a switching speed of 75 gigahertz, or 75 billion on/off cycles per second. That's nearly double silicon's previous record of 40 gigahertz



SEEING ATOMS

Scientists got their first clear look at individual atoms—shown here in a germanium semiconductor crystal—after IBM invented the scanning tunneling microscope.

and far above the 45-gigahertz level where silicon—as supposed to top out. Switching speeds continue to improve, though Meyerson won't say by how much. But even the initial mark provides so much new latitude that gallium arsenide may never replace silicon, declares John A. Armstrong, IBM's vice-president for science and technology. For chipmakers, that's sweet music. Changing over

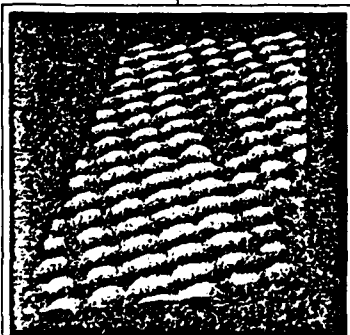
to gallium arsenide would cost a bundle and mean that three decades of know-how would get scrapped.

Every major chipmaker has now launched silicon-germanium projects. Still, researchers have barely dented the mix of technologies needed to build quantum-effect chips. Today's chief challenge is to find a way of connecting thousands of quantum transistors in an integrated circuit. Printed-metal connections won't do. Even if the wires could be slimmed down vastly, they might melt, since resistance in metal conductors rises rapidly as size diminishes.

WISPY LINES. So, researchers are looking to band-gap engineering to fashion quantum wires. Scientists at Tokyo Institute of Technology and Stuttgart University use pinpoint beams of electrons or ions to scribe wispy lines in semiconductors. Then, a better conductor is deposited in the channel and masked with the original material. That's how Bellcore produced the first quantum-wire laser last year. Its gallium arsenide core had a cross-section only 30 atoms high by 300 atoms wide. Yet many scientists consider that too bulky. Learning to grow finer quantum wires in the crystal, along with quantum transistors, is one focus of research at facilities such as the Center for Quantized Electronic Structures, established in 1989 at the University of California at Santa Barbara. And Japan's Ministry of International Trade & Industry is launching a 10-year nanotech initiative that it hopes will be supported by dozens of companies to the tune of \$100 million or more.

When it all comes together, the wonders of nanoelectronics should dwarf today's digital marvels. "Because we are learning how atoms carry on and how that affects properties," says Simon Ramo, retired co-founder of TRW Inc., computers and other high-tech gadgets will no longer be limited by nature's materials. And chipmakers may soon make their wildest material dreams come true.

By Otis Port in New York



SPORTING DEFECTS

Imperfections in a semiconductor crystal, such as grain boundaries, dislocations, and other defects, can impede the flow of electrons and reduce the efficiency of the device.

RESEARCH

Biomimetics: Creating Materials From Nature's Blueprints

BY ROBIN EISNER

In order to design a 21st-century, impact-resistant substance, materials scientist Mehmet Sarikaya of the University of Washington in Seattle finds inspiration in a 500-million-year-old feat of evolution—the shell of a present-day mollusk, the abalone.

Following blueprints drawn from analysis of the microarchitecture of the shell, Sarikaya and colleague Ilhan Aksay have manufactured a prototype material that mimics the shell's laminar, protection-providing structure.

Sarikaya is one of growing number of materials researchers involved in biomimicking, or biomimetics—the study of the structure and function of biological materials and systems as models for materials design. According to materials scientist Aksay, also from the University of Washington, about 500 scientists in the United States are involved in some aspect of biomimicking, although they might not identify their specialty as such.

What they have in common is looking at nature as a guide to create the materials for the new machines, fabrics, and shelters of the next century. While biomimicking, per se, represents a small part of the federal government's current resurgence of interest in materials research, these scientists see their approach as crucial to the national technology development effort and as a source of opportunities for collaborations involving academic, industrial, and government scientists in disciplines as diverse as botany, aerospace, and condensed-matter physics.

Proponents of biomimetics say there are numerous economic, environmental, and scientific advantages to be gleaned from their approach to materials design. Sarikaya says that when the time comes to actually develop materials based on the biomimetic paradigm, around 15 to 20 years from now, "we will most likely use raw materials that are cheaper; energy costs will be lower, since many of the processes in nature take place at room temperature; and, to some extent, these materials we make will be biodegradable."

But the material, based on the shell, that Sarikaya and Aksay created in their laboratory at the University of Washington—a carbon, boron, and aluminum mixture—is not as tough or strong as they believe it can be. Although their new material is better than a similar substance composed of these elements, it is still not as good as the shell in these parameters.

Sarikaya and Aksay's material tested 1.3 times tougher and stronger than the standard carbon, boron, and aluminum mixture. But the shell's protein-and-calcium-carbonate-layered structure has hundred-fold superiority to the strength and toughness of its standard of comparison, calcium carbonate—the inorganic

salt that makes up 98 percent of the shell—alone. Since the scientists cannot directly measure their new material against the shell for these characteristics, because it would be like comparing apples and oranges, they must compare these magnitudes of difference. They are still off by at least a factor of 10.

To increase the toughness and strength of their biomimetics-produced material, they think they will have to make the component layers of their substance thinner. The mollusk somehow exudes its protein in a layer that is two hundred-millionths of a meter thick and places it upon a five ten-millionths of a meter layer of calcium carbonate. The University of Washington group can achieve thicknesses only on the order of a hundred-thousandth of a meter. Eventually, though, the group expects to overcome this limitation by layering both biologic and synthetic materials during manufacture.

According to researchers working in this area, the collaborations that are necessary for biomimetics to be successful will generate advances



Sarikaya looks to a 500-million-year-old feat of evolution, a mollusk, in designing a 21st-century material.

SIGNIFICANT PAPERS IN BIOMIMETICS

• J. Currey, "Biological Composites," *Journal of Materials Education*, 9(1-2):118-296, 1987.

• E. Baer, A. Hiltner, H.D. Keith, "Hierarchical Structure in Polymeric Materials," *Science*, 235:1015-22, 1987.

• L. Addadi, S. Weiner, "Interaction between Acidic Proteins and Crystals: Stereochemical Requirements in Biomineralization," *Proceedings of the National Academy of Sciences*, 82:4110-14, 1985.

• S. Mann, et al., "Controlled Crystallization of CaCO_3 Under Stearic Acid Monolayers," *Nature*, 334:692-95, 1989.

for all the scientific disciplines concerned. Biologists, for example, will ask more fundamental questions about the nature of the organisms and systems they study in order to answer the questions that the chemists, physicists, and engineers pose when they do materials design. "Biologists and technologists are finally coming to the realization that there is something to be gained by seriously working together," says Stephen Wainwright, a mechanical biologist at Duke University. Sarikaya adds: "There is no way a materials scientist will be able to do it on his or her own."

Armutur Srinivasan, aerospace engineer at United Technologies in Hartford, Conn., and coeditor of *Biomimetics*, a journal that Plenum Press in New York expects to launch in the spring of 1992, says biomimetics will spawn new kinds of sci-

tific instruments and approaches to materials manufacturing. "To truly understand materials in nature, we have to see them in their living state," he says. "Most of the measurements we make are unnatural, based on dead material. This field offers opportunities to design machines that can monitor life better. And once we understand how materials are made in living systems, we can then mimic the processes artificially and efficiently."

Wainwright says that biological materials and systems are multifunctional, adaptive, nonlinear, complex, and, in general, just "weird and wonderful" compared to somewhat simplistic synthetically created materials. Bone, for example, is far more complicated than metals, according to Srinivasan, and possesses remarkable abilities of structural adaptation to external loading. Bone differs not only from animal to animal, but also from place to place within the same animal. It changes over time, and under various loading conditions.

Wainwright says biomimetics is the single most exciting thing in science he has experienced in his life. "And I am turning 60 this year," he says. Since biological form and function will be the key to materials design, Wainwright feels that descriptive biology, the study of the structure of biological systems, will overcome its current poor reputation as a dead, 19th-century science. "It's going to take a lot of morphologists [descriptive biologists] out of the ivory tower of basic research into the area of applied research. It will open many doors for them," he says.

But the main disadvantage of this kind of research is related to its very advantage: Most biological systems operate at room temperature and

pressure, and often in aqueous environments that aren't good for, say, aerospace or extreme applications. "Jet engine parts function at 2,000°F," says Srinivasan. "The challenge for materials scientists is to learn from biological systems and modify the chemistry so we can benefit. Some people think we cannot do it."

Another concern of biomimetics is that too much publicity about the field will arouse unrealistic expectations of quick success by governmental, academic, and industrial research grant providers. "If they expect results and they don't happen, they will get disenchanted, cut back on funding, and hurt the people really interested in the field," says Aksay, who, along with Sarikaya, organized a three-day conference in Seattle in April on "Design and Processing of Materials by Biomimicking," sponsored by the Air Force Office of Scientific Research.

"But this field will only reach maturity after many years of work," Aksay says. He worries that the field could suffer the same problems that superconductivity did. "Publicity will make people expect products to be rolling out of the manufacturing plant in the next four to five years. But the real scientists know it takes much longer than that."

Aksay's concern is timely. Biomimicking is part of a larger effort among U.S. scientists and policymakers to develop a strong, economically competitive materials research program in the U.S. This past April, after many high-level meetings and a National Research Council report, the Office of Science and Technology Policy (OSTP) in the White House announced its plan to coordinate and make new monies available for materials research in the country.

All the agencies that have a stake in this initiative, which will be administered by the OSTP's Federal Coordinating Council on Science, Engineering and Technology (FCCSET), are in the process of providing their budgetary and scientific input to this executive-level office. Analogous multiagency initiatives currently administered by FCCSET

coordinate high-performance computing and education in the U.S.

For materials, "each agency is driven by different needs," says Aksay. "The Department of Energy, for example, is concerned about environmentally conscious materials processing. They are looking for materials and processes that are energy-conserving, nonpolluting, and recyclable. The Department of Defense, on the other hand, is interested in materials for weapons and for the Air Force. They are interested in airplanes that can lift off without a runway. The Navy wants materials that will protect their ships from corrosion. The National Institutes of Health want biomaterials that have medical applications."

Although the OSTP materials program will be included in the president's 1993 budget, the National Science Foundation has gotten a jump start in this initiative in the agency's 1992 budget. According to Jim Brown, division director of molecular biosciences at NSF, the agency expects an additional \$25 million for materials research in 1992 over its 1991 allocation of \$59 million. Of that new money, some \$7 million to \$9 million is slated for biomimicking-related research. In late March, the foundation sent out letters announcing the funds to 5,000 scientists. "We hoped to generate the development of collaborations for eventual proposal submissions," says Brown.

The same day that the OSTP made its announcement, the two senators from New Mexico, Democrat Jeff Bingaman and Republican Pete Domenici, introduced the Advanced Synthesis, Processing and Commercialization Act, which would provide \$475 million over the next five years for materials research partnerships among industry, academia, and federal laboratories. The bill allots an additional \$474 million for university-based efforts exclusively.

In late June, the Technology and Competitiveness Subcommittee of the House Committee on Science, Space, and Technology held a hearing focusing on ways to beef up materials science in the U.S. Among the issues the committee discussed with leaders in materials research were the status of materials technology, the consequences of foreign domination in this field, the question of involvement of federal labs in joint ventures with industry, and whether regulatory and safety concerns are impeding the development and commercialization of materials in the U.S.

Says a staffer on the subcommittee: "Materials are essential for the economic viability and competitiveness of American industry. If the U.S. loses out on this, which is the cornerstone for numerous other industries in the U.S., we are in trouble." And according to materials scientist Aksay, biomimicking will play a critical role in keeping America's edge.

Robert W. Cahn

Clearly, the urge to scale up is now widespread. For example, the straight evaporation method has been developed to the point where useful nanostructured metallic films can be deposited on a silicon substrate and aerosol clusters can be directed to form conducting strips no

FIG. 1 Fracture toughness versus fracture strength (normalized with respect to density) of the nacre section of abalone shell compared with several high-technology ceramic and cermet materials. (After Sarikaya *et al.*.)

NATURE · VOL 348 · 29 NOVEMBER 1990

RÉSUMÉ

To the point

ALTHOUGH conventionally regarded as point sources of charge, electrons may, according to some theories of high-energy physics, acquire an electric dipole — equivalent to a separation of charge. But new experiments have failed to detect any such dipole. The theories have been developed to explain a fundamental asymmetry — termed charge-parity violation — inherent in the weak nuclear force. Although different theories predict different values for the electron's dipole, it is expected to be vanishingly small. Using a 600-fold amplification of the dipole's value expected from relativistic effects in atomic tantalum, K. Abdullah *et al.* (*Phys. Rev. Lett.* **65**, 2342–2350; 1990) have sought, unsuccessfully, to find its imprint on this element's spectrum. The value the authors derive ($-2.78 \pm 8.3 \times 10^{-27}$ e cm (compare water's 3.9×10^{-33} e cm) rules out more recent models invoking the increasingly popular 'Higgs boson' to explain charge-parity violation. But a further improvement of ten orders of magnitude is needed in the accuracy before all mechanisms for this asymmetry are tested.

Quasi-stable

SOME quasicrystals may be more stable than periodic crystals, claims Z. Olami (*Phys. Rev. Lett.* **65**, 2559–2562; 1990). Quasicrystals have no long-range periodicity yet give sharp diffraction patterns with 'forbidden' symmetries (tenfold, for example, suggesting a quasiperiodic lattice of icosahedral symmetry). The first quasicrystals discovered, alloys of aluminium and manganese, were formed by rapid quenching, implying that they were being trapped in an uncomfortable, metastable configuration that would prefer to relax to a more stable, regular crystalline form. But by summing up interatomic interactions throughout the respective lattices, Olami finds that a monatomic face-centred icosahedral phase can be energetically more favourable than the most obvious periodic alternatives, such as body- and face-centred cubic arrays. So forming quasicrystals may prove easier than expected.

Face to face

FOLLOWING the positive identification of the skull of Wolfgang Amadeus Mozart last year, a group led by P.-F. Puech has used forensic techniques to recreate his face (*L'Information Dentaire* **22**, 2003–2008; 1990). The skull was exhumed in 1801, since when it has been kept in the Mozarteum in Salzburg. Reconstructing the face involves using clay to build up layers of soft tissue on a cast of the cranium. The nose is difficult to include because it depends on cartilage, but its dimensions can be calculated from the size and position of the nasal aperture — only the ears are impossible to reconstruct.

now*, a B₂C/Al laminar composite has been made, following the abalone model, and proves to have outstanding properties (Fig. 1).

By no means was the conference limited to applications. Fundamental scientific issues were also much aired: for example, the nature of the intercrystalline boundary regions in nanostructured materials. Whereas high-resolution electron microscopy (G. Thomas and R. Siegel, Argonne National Laboratory) and Raman spectroscopy of nanocrystalline CO₂ (ref. 7) indicate a normal, atomically narrow grain-boundary structure. Mössbauer studies (Gleiter; B. Fultz, California Institute of Technology), electrochemical measurements (R. Kirchheim, Max-Planck-Institut für Metallforschung, Stuttgart, Germany), density and diffusion measurements (Gleiter) and calorimetry indicate that boundaries are more disordered and have a lower local density than conventional boundaries. The curiously sluggish grain growth already cited may be linked with this. Fultz and coworkers' Mössbauer data for a nanostructured Cr-Fe alloy can be accurately analysed to yield an estimated boundary width of about 1 nm; after grain growth, the boundary signal of course diminishes. The issue is still very much open; it may be that the structure depends sensitively on the nature of the misorientation and varies from boundary to boundary.

Several excellent papers were devoted to the characteristic clusters themselves. S. Riley (Argonne National Laboratory) showed how precise measurements of NH₃ uptake could be used to identify the exact geometrical form of size-separated metal clusters, Ni and Co in particular, because NH₃ attaches itself only to atoms standing proud of the surface, for instance at icosahedral vertices. X. Miao and P. Marquis (Birmingham University) showed how pH control and the combination of two differently sized populations (of alumina and silica) allowed them to create stable combined colloid particles of the two compounds which then sinter more easily.

Magnetic studies of both elementary and multicomponent nanoclusters, as well as metallic multilayers, reveal curious combinations of ferromagnetic, anti-ferromagnetic and superparamagnetic behaviour, as well as anomalous easy magnetization directions. In this connection, a highlight of the conference was H. Warlimont's report on recent developments by G. Herzer in his laboratory (Vakuumschmelze, Hanau, Germany) of an innovation first reported by Yoshizawa *et al.*¹ Certain metallic glasses containing Fe, Si and B have excellent soft magnetic properties and are currently used as transformer laminations. Yoshizawa and coworkers found that if Nb and (crucially) Cu are added to this glass and it is then

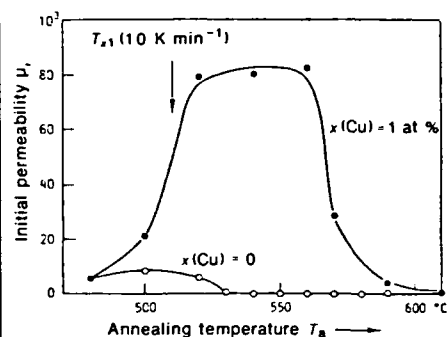


FIG. 2 Initial permeability, μ_i , of Fe_{74.5-x}Cu_xNb₃Si_{13.5}B₃ alloys, initially glassy (with $x=0$ and $x=1$), as a function of annealing temperature, T_a , for a constant 1-h annealing time. T_{x1} is the first crystallization temperature. (After G. Herzer and Warlimont.)

crystallized in the right way, a giant magnetic permeability can be attained, comparable with that of permalloy.

Herzer and Warlimont's results (Fig. 2) show that 1 atomic per cent of copper has a spectacular effect. It turns out that the annealed glass (provided it is not heated at too high a temperature) consists of nanocrystalline, ferromagnetic Fe₂Si phase separated by films of residual glass, rich in B and Cu, which is either nonmagnetic or has weaker magnetism. The residual glass crystallizes above 600 °C. Herzer and Warlimont analysed the magnetic properties of such a structure.

Nanocrystalline ferromagnetic particles are single-domain (Gleiter in a recent review² cites very new evidence to this effect), and the ferromagnetic exchange interaction then overtrumps the effects of magnetocrystalline anisotropy in the nanograins and constrains the magnetization vector to be parallel to that in a neighbouring grain, irrespective of easy directions of magnetization. At a critical grain size, this results in very low coercivity and high permeability, as observed: here the critical dimension is around 35 nm. This Cu-bearing alloy has also a very low magnetostriction and the hysteresis loop shape can be shaped by magnetic annealing. This kind of nanostructured magnetic dispersion in a residual glass, by analogy with the 'superstrong' dispersions cited above, might perhaps be termed a 'super-magnet' — nanostructural researchers are predisposed to superlatives. □

Robert W. Cahn is in the Department of Materials Science and Metallurgy, University of Cambridge, Pembroke Street, Cambridge CB2 3QZ, UK.

- Andres, R.P. *et al.* *J. Mater. Res.* **4**, 704–736 (1989).
- Kratschmer, W., Lamb, L.D., Fostiropoulos, K. & Huffman, D.R. *Nature* **347**, 354–358 (1990).
- Marcus, M.A. *Acta Metall.* **27**, 893–902 (1979).
- Louat, N.P. *Acta Metall.* **33**, 59–69 (1985).
- Wakai, F. *et al.* *Nature* **344**, 421–423 (1990).
- Sarikaya, M., Gunnison, K.E., Yasrebi, M. & Aksay, I.A. *Mat. Res. Soc. Symp. Proc.* **174**, 109–116 (1990).
- Melendres, C.A. *et al.* *J. Mater. Res.* **4**, 1246–1250 (1990).
- Yoshizawa, Y., Oguma, S. & Yamauchi, K. *J. appl. Phys.* **64**, 6044 (1988).
- Gleiter, H. *Prog. Mater. Sci.* **33**, 1 (1990).

Tinkering with Glass and Ceramic Structures

Advances in the venerable technique of sol-gel processing are producing new materials with previously unobtainable properties

THE WIZARDS OF MATERIALS SCIENCE have come up with many surprises lately. Take the advances they have been making in sol-gel technology, a time-honored way of producing glasses and ceramics. For more than 100 years, the materials made by this technology have found a wide variety of applications. They have been used, for example, for making insulating seals for electronic and aerospace equipment and as antireflection coatings for the windows of the Bauhaus-style "glass box" office buildings that dominate city skylines.

But the potential of the old technology is far from exhausted. Material scientists have recently used it to produce brand-new glasses and ceramics that cannot be made otherwise. These range from the aryl-gels, a type of glass that can be made so porous that 1 gram can have as much surface area as three tennis courts, to "nanocomposites," whose extremely small dimensions give them new properties, such as increased hardness, not seen in the more usual formulations.

And this isn't just alchemy for its own sake. The new materials may help solve our toxic waste problems, prove invaluable to the petrochemical industry, and provide ultrapure, high strength advanced materials for the aerospace industry.

The aryl-gels are among the most advanced of these new materials. They are being developed in the laboratories of materials scientist Owen Webster of the Du Pont Company in Wilmington, Delaware, and his cross-country collaborators, chemists Kenneth Shea and Douglas Loy at the University of California, Irvine.

Regular glass is made of plain silica, with the silicon and oxygen atoms irregularly arranged to produce an amorphous solid. But the Irvine and Du Pont workers came up with the idea of introducing organic spacers, particularly aromatic rings (aryl groups) such as phenylene, at regular intervals between the silicate molecules. Loy compares the resulting aryl-gels to molecular Tinkertoys, "because a variety of aryl spacers of different lengths can be used to build new materials."

Shea, Loy, and Webster begin by joining organic silicate compounds called silanes to a desired aryl group by means of a Grignard

reaction, a standard condensation reaction of organic chemistry. This produces a monomer, the simple building block that will next be polymerized to make the gels themselves. When one of the monomer materials is dissolved in the solvent ethanol and treated with aqueous acid or base, it polymerizes, Loy explains. Within a few hours, the solution gels, giving it a consistency similar to that of the familiar dessert, Jello. "At this stage, the aryl-gels behave more like glass, even ringing when lightly tapped," Loy says. After aging for 48 hours, the aryl-gels are dried under a vacuum to remove the solvent, leaving behind a porous network that resembles lightweight, brittle glass.

And the aryl spacers—the rods of the Tinkertoy—make the glasses very porous indeed. Just one gram of an aryl-gel can have a total surface area of 9000 square feet—more than that of three tennis courts. Moreover, the researchers have a degree of control over the pore size, which depends partly on the spacers used. Longer spacers tend to create larger pores in the aryl-gels and short spacers smaller pores, allowing pore diameters to be tailored to a specified molecular size, although

Molecular Tinkertoy. Aryl-gels (B) have organic spacers (bars) that make them much more porous than ordinary glass (A).

the drying time also influences pore size. If aryl-gels are dried quickly, the pores shrink, causing the gels to lose as much as 70 to 90% of their volume.

Rapid drying can also cause the gels to fragment. This may sound disastrous, but it isn't. Fragment the gels and you have a powder, perfect for some applications, for use as starting materials for making other ceramics, for example. And then there's chromatography.

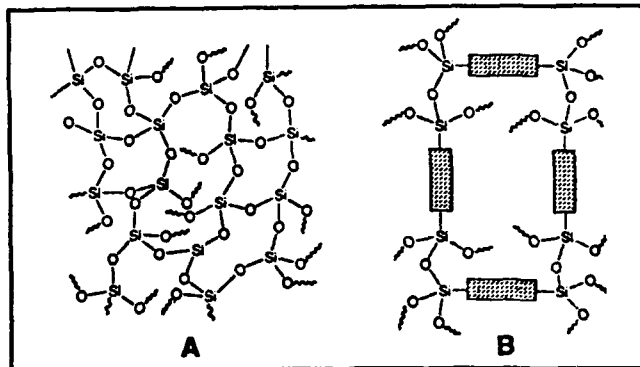
The beauty of these Tinkertoys is that their high porosity makes them extremely well suited for use as "molecular sieves," chromatographic adsorbents that separate

mixtures of molecules by size. And the ability to control the pore size means that they can be custom-designed according to the specifications that a researcher wants. For this application, the gels have to be ground to a powder anyway.

In addition to their high molecular surface area and microporosity, the new materials have yet another advantage as chromatographic adsorbents: they are stable at temperatures of up to 500°C. That property has caught the eye of the oil industry, as none of the chromatographic adsorbents it currently uses can withstand temperatures that high. "We've had several calls from the oil industry asking about their potential uses in gas purification," Loy says.

And the aryl-gels, thanks to their organic spacers, can fluoresce—absorb light at 1 wavelength and emit it at another. This may make them ideal for another application, as laser dyes. Current lasers cannot emit light at all desired wavelengths. Although this problem can be solved by incorporating appropriate liquid dyes into the laser setup, aryl-gels may have several advantages over liquids. The gels are easier to transport and store and may also last longer than liquids. In addition, they should simplify laser design by eliminating the pumps needed to circulate liquid dyes.

So why aren't aryl-gels sweeping the marketplace? Their major limitation is their production cost, which currently runs several times higher than the cost of making traditional glasses and ceramics. The latter



Kenneth Shea and Douglas Loy

are often produced from cheap and readily available starting materials, such as sand, whereas the starting materials for the aryl-gels have to be made synthetically. The Irvine and Du Pont team is confident, however, that it can develop economical ways of producing the large quantities of aryl-gels needed for industrial application.

Meanwhile, researchers at other labs are making their own advances in sol-gel technology. For example, chemist Jeff Brinker and his colleagues at Sandia National Laboratory in Albuquerque, New Mexico, have

developed a way to use sol-gel technology to make thin films at room temperature. The method is applicable, Brinker says, "to anything that you can make glass with." That includes the aryl-gels, although the Sandia team hasn't used them so far, as well as commonplace starting materials such as silica and alumina. The advantage of the thin films is that they don't shrink and crack the way the gels are likely to do when made in bulk.

To make a thin film, Brinker first dissolves an inorganic polymer in a solvent and concentrates the solution. Then the item to be coated, which can be made of plastic, glass, metal, ceramic, or other material, is dipped into the solution and slowly withdrawn at a constant rate. Maintaining the constant rate is important because otherwise the film will be uneven. Typical coatings at Sandia have been between 100 and 500 nanometers thick and up to 10 feet long, but, Brinker says, "They can be scaled to any length you want."

One of the main benefits of making thin films by Sandia's sol-gel method is that the films can be layered, one on top of another. "At the molecular level, the thin films resemble tumbleweeds," Brinker explains. "They each have highly porous interiors but cannot penetrate each other. They pile up rather like tumbleweeds pile up against a fence." The total thickness of all the layers can be no greater than about 500 nanometers, however, because around that point the materials begin to crack.

The most obvious application for such thin films would be as protective coatings for microelectrical components and for metals subject to corrosion. But it is possible that their most valuable application will not be as a coating but in making chemical sensors and membranes for separating molecules of different sizes.

Layered films can be constructed so that the outer layer has very tiny pores that allow some molecules to enter the film while keeping larger molecules out. The pores of the inner layer can be much larger, big enough to incorporate ion exchange sites for holding on to any molecules that have entered the porous maze or for housing chemical reactants that could serve as detectors for the trapped molecules.

Such layered films might be used both to monitor and clean up the toxic pollutants in waste streams from chemical processes. The Sandia group has so far focused on membranes that can trap and analyze inorganic chemicals, such as the heavy metals in electroplating effluents, but it should ultimately be possible, Brinker says, to construct layered membranes that can sense virtually anything.

Rustum Roy, at Pennsylvania State University in University Park, is spearheading research into perhaps the most exotic phase of sol-gel technology: the making of the ultrathin films he calls nanocomposites. These nanocomposites vary in thickness from 1 to 100 nanometers, just thinner than the thinnest gels at Sandia. At nanometer



Fluorescent glass. Chemist Douglas Loy examines one of his group's aryl-gels, which is glowing under fluorescent light.

dimensions, matter begins to take on new properties (also see *Science*, 5 January, p. 26). Metals may be harder than normal, for example, or ceramics more ductile.

But thinness is not even the major distinction between Roy's films and those of other investigators. The Penn State researcher's advance is to combine two different compounds to produce heterogeneous materials, a breakthrough in sol-gel processing.

To make the heterogeneous composites, a

It should ultimately be possible to construct layered membranes that can sense virtually anything.

noncrystalline clay mineral, such as thorium silicate, is ground to an exceedingly fine powder and hydrolyzed to form a gel. The gel is then seeded with very tiny crystals of a crystalline material, such as the mineral huttonite. As a result, the entire gel takes on a crystalline structure, in this case that of huttonite, as opposed to the amorphous

structure it would have otherwise had.

As a result, Roy says, ceramics, polymers, metals, and semiconductors can be mixed in any combination, thereby yielding a vast array of potential new materials. Moreover, nanocomposites can be processed at much lower temperatures than more conventional mixtures of the same bulk composition, and therefore can be produced at a lower cost.

Other benefits of nanocomposites include their strength, which increases fivefold as sizes decrease from 100 to 20 nanometers. "Some scientists have even reported nanocomposites that are harder than diamonds. They are made of crystalline diamonds in a semicrystalline diamond mixture, but the scientific community is still skeptical," Roy says.

The optical properties of nanocomposites may also change. For example, when chemists at the N.E.C. Corporation's Materials Development Center in Tokyo embedded a luminescent material in a nanocomposite, its light output was ten times brighter than normal. Already, Roy says, about 50 companies have applied for patents based upon nanocomposite technology in ceramic processing.

Additional nanocomposites are being investigated by Ilhan A. Aksay of the University of Washington in Seattle. He has produced a new form of mullite, a rare aluminum silicate. Mullite is extremely heat-resistant, retaining its chemical identity and physical shape when subjected to high temperatures. That makes it useful as engine components and for other high-temperature industrial applications, but also makes it difficult to process. Production of ordinary mullite requires temperatures as high as 1650°C, and the resulting material is not homogeneous, as it contains pockets of amorphous silica.

But Aksay's sol-gel method, which uses a controlled hydrolysis of tetraethoxysilane around particles of aluminum hydroxide to guide the mullite formation, deforms the silica portion of this mixture at 1250°C, causing it to become dense quickly and then to crystallize into a homogeneous, transparent material. That opens up a potential new application for the ceramic as lenses that are transparent to infrared light with wavelengths between 3 and 5 micrometers, a range for which good lenses had not previously been available.

The new advances in sol-gel processing are producing a wealth of novel materials with previously inaccessible applications. The technology should be good for another 100 years. ■ GAIL FINLAYSON-DUTTON

Gail Finlayson-Dutton is a free-lance writer based in Westminster, California.